Stony Brook University

Heavy Ion Collisions from AdS/CFT correspondence

A Dissertation Presented

by

Shu Lin

to

The Graduate School

in Partial Fulfillment of the Requirements

for the Degree of

Doctor of Philosophy

in

Physics

Stony Brook University

May 2010

Stony Brook University

The Graduate School

Shu Lin

We, the dissertation committee for the above candidate for the Doctor of Philosophy degree, hereby recommend acceptance of this dissertation.

Edward Shuryak - Dissertation Advisor
Distinguished Professor, Department of Physics and Astronomy

Martin Roček - Chairperson of Defense
Professor, Department of Physics and Astronomy

Tom Hemmick
Professor, Department of Physics and Astronomy

Dmitri Kharzeev
Senior Scientist, Brookhaven National Laboratory

This dissertation is accepted by the Graduate School.

Lawrence Martin
Dean of the Graduate School

Abstract of the Dissertation

Heavy Ion Collisions from AdS/CFT correspondence

by

Shu Lin

Doctor of Philosophy

in

Physics

Stony Brook University

2010

It is now believed that heavy ion collisions have produced a state of strongly coupled quark gluon plasma. The strong coupling of the fields make the perturbative field theoretical calculation less reliable. The gauge/gravity duality has recently emerged as a powerful tool allowing us to study the dynamics of the gauge fields at strong coupling. Many novel features of strongly coupled gauge fields have been revealed in recent studies via the duality. In this dissertation, I will focus on an important aspect in heavy ion collisions: the equilibration of matter and formation of quark gluon plasma.

While linearized Einstein equation encodes dynamics near equilibrium, e.g quasi-normal mode, the thermalization of matter far from equilibrium necessarilly involves strong gravity behavior. I will first use a gravitational collapse model, which is dual to thermalization process of the quark gluon plasma. The spectral densities of stress energy tensor are studied and found to show universal behavior as the thermalization is approached. Then I will also describe a

model of gravitational shock wave collision, which mimics the relativistic nucleus collisions. The shock wave model allows us to find the apparent horizon, its area giving a lower bound to the entropy production as a function of the impact parameter. An critical impact parameter is observed, beyond which no thermalization is possible. I will finally comment on the equivalence between the collisions of sourced shock wave and sourceless shock wave.

Contents

List of Figures

List of Tables

Acknowledgements

I would like to express my great gratitude to Prof. Edward Shuryak, without whose directions the dissertation is not possible. The most important thing I have learned from him during the PhD period is how physics should be pursued. Physics should always be in the first place rather than a collection of formulas, which I believe will truly meaningful to my future career. I would also like to thank Prof. Derek Teaney, Prof. Ismail Zahed, Prof. Jacobus Verbaarschot, Prof. Thomas Kuo, Prof. Venugopalan, Prof. Yuri Kovchegov for their numerous helps on the dissertation as well as broadening my knowledge in physics. I also benefit from countless discussions with postdocs Misha Lublinsky and Claudia Ratti, graduate students Kevin Dusling, Keun-young Kim, Jinfeng Liao, Clint Young, Stanislav Srednyak, Jorge Casalderrey-Solana, Peng Dai, Yu-tin Huang, Sung-tae Cho, Huan Dong, Juhee Hong et al. Finally I would like to thank my families, who constantly support and encourage my pursuit of science throughout my entire graduate period.

Chapter 1

Introduction

1.1 Heavy Ion Collisions

It is believed that collisions of heavy nucleus with sufficient high energy are able to liberate quarks and gluons from nucleons, resulting in a novel state of matter called "Quark Gluon Plasma". The exploration of this matter, which is close to the primordial matter produced shortly after the Big Bang, is one of the main purpose of heavy ion collisions.

In the past few years, experiments in Relativistic Heavy Ion Collider at Brookhaven National Laboratory have discovered fascinating properties of the matter. Confirmation of the matter being produced can be found in observable like nuclear modification factor. The nuclear modification factor measures ratio between particles produces in heavy ion collisions and the counterpart in proton collisions, with the latter properly scaled by the number of binary collisions. This quantity for various particle species is found to deviate significant from unity, showing the effect of the matter as a medium. The existence of the medium is further supported by more concrete phenomena such as jet quenching and collective flow. The former fits nicely into the picture one jet from a pair gets absorbed by the medium as it penetrate through it. The latter is a natural realization of the fluid behavior of the matter.

It is by now widely believed that the QGP is strongly coupled. One of the main evidence is the early thermalization as suggested by successful application of hydrodynamics in the study of phenomenology of heavy ion collisions. Although "Quantum Chromo-Dynamics" has been established as the fundamental theory for strong interaction, it is only tractable in weak coupling regime, where perturbative calculation can be trusted. "Lattice Gauge Theory" allows one to go beyond weak coupling regime, however, one is restricted to stationary quantities. This is because Lattice gauge theory is formulated

in Euclidean space, with Euclidean time being the inverse temperature. The usual time is trade off for temperature. This makes the study of dynamical aspects within lattice gauge theory extremely hard. Also, the so called sign problem prohibits the lattice study of QCD at finite fermionic density. On the other hand, effective field theory and model study of QCD often suffer from their limited applicable domain. A theoretical tool, which is well tractable is always desirable for the description of real world experiments. The AdS/CFT correspondence(or the gauge/gravity duality) proposed by Maldacena, and developed further by Witten, Gubser, Klebanov and Polyakov[1–3] has become a promising candidate.

1.2 AdS/CFT correspondence(Gauge/Gravity duality)

The AdS/CFT correspondence originally emerged from string theory. It is a specific realization of 't Hooft's old idea of holographic principle [4], which states that the description of a volume of space can be thought of as encoded on a boundary to the region. It is a duality between the type II B superstring theory in the near horizon limit of $D3$ branes background and $\mathcal{N}=4$ supersymmetric Yang-Mills gauge theory in the worldvolume of the branes. One way leading to the correspondence is a low energy limit argument. Consider a stack of D-branes carrying mass and Ramond-Ramond charge in ten dimensional spacetime, they will form a black hole. Due to the gravitational red-shift phenomenon, finite energy excitations emanated from the horizon will have very low energy as appears to an observer at infinity. On the other hand, the low energy limit can be realized as a small string length scale limit with string coupling fixed. In this limit, all massive open string excitations of the D-branes are not relevant, with the physics governed by only the massless worldvolume field theory of the D-brane. In case of coincident $D3$ brane, the near horizon limit of the gravity background is given by $AdS_5 \times S^5$. The worldvolume theory is $\mathcal{N}=4$ supersymmetric Yang-Mills gauge theory, which is a conformal field theory. As a result of the above argument, a correspondence is obtained between the string theory in $AdS_5 \times S^5$ background and a conformal field theory in Minkowski space.

Two sets of parameters in both theories are identified:

$$\frac{g_{YM}^2}{4\pi} = g_s, \ \sqrt{g_{YM}^2 N} = \frac{L^2}{\alpha'} \tag{1.1}$$

where g_{YM} and N are the Yang-Mills coupling and number of colors on the gauge theory side. g_s and α' is the string coupling and string length scale on the string theory side. L is the radius of AdS_5 space and S^5. A particular interesting limit is $g_s \ll 1$ and $\frac{L^2}{\alpha'} \gg 1$. Small string coupling allows us to ignore the string loop correction, leaving us with a classical string theory. When the AdS radius is much greater than the string length scale, all the curvature corrections are suppressed. The classical string theory is further simplified to a classical super gravity theory. This double limit translates to the gauge theory as large color number $N \gg 1$ and strong 't Hooft coupling $\lambda \equiv g_{YM}^2 N \gg 1$. By virtue of the duality, one can understand the properties of gauge theory in strong coupling regime by studying classical SUGRA problem in AdS background. Over the past ten years since the discovery of AdS/CFT, applications of it have been made in many different areas of physics, such as nuclear physics, condensed matter physics and black hole physics, with vast promising results.

1.3 Motivations

In heavy ion collisions, one of the main open questions is the equilibration of matter and the formation of quark gluon plasma. Hydrodynamical simulations have suggested a short thermalization time. A theoretical understanding of the mechanism is by all means desirable to confirm this observation.

The study of gauge fields near equilibrium has a long history. Satisfactory understanding of the thermalization has been achieved both at weak and strong coupling regime. At weak coupling, particle distribution function is believed to give reasonable approximation of the system. The evolution of the distribution function is described by Boltzmann equation. The transport coefficients of Boltzmann equation are to be provided by the microscopic theory and have already been computed in perturbative field theory. At strong coupling, gauge fields in equilibrium is dual to an AdS black hole background according to AdS/CFT correspondence. Near equilibrium dynamics has been nicely understood via "Quasi Normal Mode" of the black hole, which characterizes the dissipative modes of he gauge fields. For gauge fields far away from equilibrium, the weak coupling description in terms of particle distribution becomes questionable. Improvement can be made by including distribution of particle correlations, which together with particle distribution satisfy BBGKY hierarchy equation. While the counterpart is missing in strong coupling regime. In particular, I am interested in how the matter equilibrates starting from the initial coherent nucleus before collisions. It is worth mentioning the very problem is also an active pursuit with "Glasma" model in weak coupling domain.

The model is aimed at joining the initial "Color Glass Condensate" of the nucleus to the formation of "Quark Gluon Plasma". Despite of the smallness of the coupling, the problem is actually nonperturbative due to the large field of the nucleus.

In this dissertation, I will focus on the dynamics of gauge fields at strong coupling by application of AdS/CFT correspondence, with an emphasis on the equilibration of matter and formation of quark gluon plasma. It is nevertheless to be cautious that the dual theory of string theory is still not too close to QCD, which is not a supersymmetric theory. Also the number of colors and coupling in QCD is not infinitely large as is usually treated in the duality. A review of these issues can be found in [6]. I will assume, however, the approximation of QCD by supersymmetric theory does capture the main features of QCD in the regime of interest.

1.4 Outline of the dissertation

The bulk of the dissertation is a collection of the works done with my advisor Edward Shuryak (from Chapter 2 to 6). Chapter 7 is based on a recent work with Yuri Kovchegov. It is structured as follows: I will start by introducing a gravity dual to heavy ion collisions in Chapter 2. The process after the collisions is modelled by the falling of various stringy objects (to be referred to as debris) in the AdS background. The debris will merge and eventually form black hole during the falling, corresponding to the thermalization of gauge theory. we studied the geodesic equations of the debris, from which a generic feature of the falling at asymptotic time will be found. The effect of these falling debris will be visible when their backreaction to the AdS background is included. The restoration of the backreaction requires solving linearized Einstein equation with debris acting as the source. The metric correction to AdS background can be used to obtain stress energy tensor of the gauge theory according to AdS/CFT prescription. We developed and illustrated the method by examples of stationary stringy objects in Chapter 3. Then we generalized and applied the method to dynamical debris in Chapter 4.

Although linearized Einstein equation can give us results on near equilibrium phenomena e.g.hydrodynamical relaxation, it is expected to miss the features of black hole formation, which is of our main interest for its relevancy to gauge theory thermalization. Therefore we switched to a gravitational collapse model in Chapter 5. The model is composed of a homogeneous shell separating an AdS Schwarzschild metric and a pure AdS metric. It is a specific realization of plasma in the evolution to equilibrium on the gauge theory side. The falling of the shell as well as the gravitational wave crossing the

shell will be studied by Israel Junction condition. We extracted from the behavior of the gravitational wave the retarded correlator of stress energy tensor using AdS/CFT prescription. The associated spectral density corresponding to different stage of equilibration shows a universal behavior as the plasma thermalizes.

Chapter 6 will be devoted to the study of a novel type of critical behavior in heavy ion collisions, which is a transition between matter being able to equilibrate and failing to reach equilibrium. We modelled heavy ion collisions by a collision of gravitational shock waves in AdS space. The apparent horizon can be constructed from past infinity to the moment of the collision. The area of apparent horizon can serve as an estimate for the entropy production in gauge theory. We found in this setting the existence of critical impact parameter, beyond which apparent horizon cannot be found, meaning the gauge theory should fail to thermalize. We discussed the limitation of this approach and suggested a slightly different model, which incorporates saturation scale. We will analyzed the model in details in Chapter 7 and compare it with a sourceless shock wave model. We demonstrated an equivalence between the two models as the saturation scale vanishes.

The last Chapter will summarize the main results of the dissertation and discuss some of the on-going efforts to explore the gravitational interaction between the shock waves after the collision, which will shed more light on the physics of equilibration of strongly coupled gauge theory.

Chapter 2

Falling of stringy debris

2.1 Introduction

The AdS/CFT correspondence [1–3] is a duality of the conformal (CFT) $\mathcal{N}$=4 supersymmetric Yang-Mills theory and string theory in 5d Anti-de-Sitter space (AdS_5). Multiple papers use this fascinating theoretical tool, in a regime in which the gauge theory is in a strong coupling regime while string part is in weak coupling – the classical SUGRA regime. The equilibrium finite temperature version of this correspondence, using a black-hole background, was suggested by Witten [5]. Applications of this version of correspondence to properties of strongly coupled high-T phase of QCD are very actively pursued: we will briefly review those in the next subsection.

The aims of this series of works are however quite different: instead of focusing on equilibrium thermal matter, we hope to develop a gravity dual framework to time-dependent process of high energy collisions. We will not assume equilibration or use macroscopic variables like temperature or hydrodynamic flows: we hope to be able to understand how they naturally appear for collisions of large systems. Instead we focus on motion of strings in AdS_5 in this work, and, in the second one, on "holograms" which an observer will see in our world – the AdS_5 boundary – as a function of time.

Since this is the first paper of the series, we decided to start with rather extensive introduction, which describes similar works and summaries our current understanding of the subject.

2.1.1 Strongly coupled Quark-Gluon Plasma

It is well known that non-perturbative properties of the QCD vacuum phase – confinement and chiral symmetry breaking – are absent above some

critical temperature, where matter is in the so called Quark-Gluon Plasma (QGP) phase. Although at high T one naturally expects the QGP to be in a weakly coupled regime, it has been conjectured recently [8] that at least at $T = (1-2)T_c$ – known as the RHIC domain – it is closer to a 'strongly coupled' regime (sQGP).

This was a significant "paradigm shift" in the field, and various directions toward the understanding of sQGP constitute a mainstream of the field. Basically there are two competing options: one, based on electric-magnetic duality [9], relates small viscosity and diffusion of sQGP to presence of magnetic monopoles and predicts that it will disappear at T away from critical region. Another – based on AdS/CFT – relates it to "quasiconformal behavior" of QGP at $T > 2T_c$. A comparison between experimental results from RHIC ($T = (1-2)T_c$) with those at LHC (higher T) will hopefully shed light on it in near future.

Let us only mention some important developments related to the latter approach, AdS/CFT. In a static finite-T setting with AdS-black hole metric [2] the study started with classic results on bulk thermodynamics [10] and transport coefficients [11]: those works provided the first exciting results, showing that while the Equation of State can be quite close to that of weakly coupled plasma, the transport properties can differ from them by orders of magnitude. Then attention focused on high energy jet quenching, with the result that a heavy quark pulls a string obtaining a calculable shape and has a calculable drag force. It turns out that AdS/CFT provided results for the drag force [14] and heavy quark diffusion [13], which are also related by the Einstein relation. For a recent brief summary see e.g. [15]: it is sufficient to mention here that all these results seem to be in much better agreement with what is seen phenomenologically in heavy-ion collisions at RHIC than their weak-coupling counterparts.

Further development of the jet quenching problem was related to the question *where does the lost energy go?*. In a hydrodynamical context it was suggested that the so called "conical flow" [16] of matter should develop, induced by a heavy charge moving in a strongly coupled plasma. The "hologram" of the dragging string has to be calculated to see that: this task was recently performed by Princeton and Seattle groups [17, 18], which indeed recovered the conical flow picture, in a stunning detail.

2.1.2 Gravity dual for heavy Ion collisions

The results mentioned above are all obtained using static AdS-black hole metric. Although for a macroscopically large and slowly expanding fireball one should be able to use matter properties calculated in a static regime, one may

also wander whether the AdS/CFT in time-dependent setting will be able to provide new insights into when exactly the thermo and hydrodynamics become applicable in a real-time expanding fireball, and what exactly corrections to the usual macroscopic treatment will appear.

The questions of non-equilibrium corrections are not only long standing and challenging theoretical problems, they are of significant practical importance. It is enough to mention that while viscosity to entropy ratio is believed to be limited by the AdS/CFT value from below [12]

$$\frac{\eta}{s} > \frac{1}{4\pi} \tag{2.1}$$

recent hydrodynamical studies by three groups [19] have concluded that the experimental data on the so called elliptic flow can only be reproduced if this ratio is at the very limit or even smaller! (For a possible way out of this dilemma, see e.g. [20].)

In [21], the high energy collision was formulated in the gravity dual language. It was later argued by Giddings [22] that strong gravity effect played an important role in high energy collision. One particular picture proposed in that paper is the formation and melting of black hole in the AdS background.

Heavy ion collision consists of multiple high energy collisions. A new ingredient is the creation/thermalization and further evolution of the fireball. In [23] (SSZ below) Sin, Shuryak and Zahed suggested a time-dependent scenario, in which the gravity dual to an expanding/cooling fireball is a black hole *departing* from the boundary. A specific solution they discussed in the paper was a "hologram" on a brane departing from a static black hole, which corresponds to a spherically symmetric (Big-Bang-like) solution with a decreasing T . SSZ also proposed few other idealized settings, with d-dimensional stretching, corresponding for d=1 to a collision of two infinite thin walls and subsequent Bjorken rapidity-independent expansion[24], with 2d and 3d corresponding to cylindrical and spherical relativistic collapsing walls, but have not provide gravity solutions for them.

Janik and Peschanski[25] (below referred to as JP) have addressed the simplest 1+1 dimensional scaling (or Bjorken) hydrodynamical solution. In this case the time and longitudinal coordinate x_1 are substituted by the proper time and spatial rapidity variables

$$\tau = \sqrt{t^2 - x_1^2}, \;\; y = \frac{1}{2} log(\frac{t - x_1}{t + x_1}) \tag{2.2}$$

and the solution does not dependent on y, but only the proper time τ.

Instead of solving Einstein equations with certain source, they applied an

inverse logic: using expected hydrodynamical solution as a boundary condition, they extrapolated it into the bulk. JP found an *asymptotic* (large-time) solution for the "stretching" AdS-BH. As expected, it indeed possesses a singularity moving away from the AdS boundary $z_{singularity} \sim \tau^{1/3}$. A very important feature of the leading-order in time JP solution is that while their presumed horizon is stretching in one direction and contracting in others, to the *leading order* two effects compensate each other and keep the *total horizon area constant*. This was already conjectured by SSZ, that a time-dependent gravity dual should lead to late-time entropy conservation (a well known feature of hydrodynamical explosions), but (to our knowledge) JP were the first to related the horizon area to entropy outside static solutions. We will discuss a bit more this solution and use it in section 2.4.1.

Further discussion of the next subleading (next power of inverse time) terms has been made by Sin and Nakamura [26] (below SN) who identified corrections to the JP solution with the viscosity effects. Terms of higher order have been subsequently studied as well [27] and also a simpler problem in 1+1 dimension *without* transverse dimensions was solved by Kajantie et al [28]. More recently it was argued in [29] that the expansion of JP solution is inconsistent beyond the first few orders. Thus one may naturaly(at least in our view) ask the following questions: What is the nature of this singularity? Where exactly is the "trapped surface"? What is the metric behind this singularity? Is there any matter object as an alternative to the singularity?

Unlike all the papers, we will not adopt the "inverse logic" and will not be looking for the solutions which would generate a pre-assumed hydrodynamical flow at the boundary. Instead we will focus on the formation stage, whether black hole is or is not formed, and will *calculate* the (time-dependent) stress tensor on the boundary, whether it is hydro-type on not.

2.1.3 Hadron collisions in QCD, the Lund model and the "Color Glass"

Rather early in development of QCD, when the notion of confinement and electric flux tubes – known also as the QCD strings – were invented in 1970's, B.Andersen and collaborators [30] developed what gets to be known as the Lund model of hadronic collisions. Its main idea is that during short time of passage of one hadron through another, the strings can get reconnected, and therefore with certain probability some strings become connected to color charges in two different hadrons. Those strings get stretched longitudinally and then break up into parts, making secondary mesons and (with smaller probability) baryons. Many variants of string-based models were developed

based on the Lund model, and some descendant –like PYTHIA – remains popular "event generator" used by nuclear/high energy physicist till today.

If there are several string stretched, it is usually assumed that both their interaction and influence on breaking is negligible.

However if one either considers very high energy collisions, when a single hadron should be viewed as being made of many color charges (partons), or heavy ion collision, a different asymptotic picture has been proposed. McLerran and Venugopalan [32] argued that instead of multiple string the fields produced should be considered as classical gauge fields –known as Color Glass model – and their subsequent evolution be derived from solution of classical Yang-Mills equation [33]. They suggested this regime is true at very high parton density, when the effective coupling is weak. Accepting the Color Glass picture as a correct asymptotic for very high parton density and large saturation scale $Q_s \to \infty$, one still wanders what should happen in the case of intermediate scale $Q_s \sim .3 - 1.5\, GeV$.

Recent developments of the so called AdS/QCD proposed a view that this interval of scales in QCD constitute a "strong coupling window". In particular, Brodsky and Teramond [31] have argued that the power scaling observed for large number of exclusive processes is not due to perturbative QCD (as suggested originally in 1970's) but to a strong coupling regime with near-constant coupling (quasi-conformal regime). Polchinski and Strassler [21] have shown that in spite of exponential string amplitudes one does get power laws scaling for exclusive processes, due to convolution (integration over the z variable) with the power tails of hadronic wave functions. One of us proposed a scenario [34] for AdS/QCD in which there are two domains, with weak and strong coupling. The gauge coupling rapidly rises at the "domain wall" associated with instantons. Such approach looks now natural in comparison to what happens in heavy ion/finite T QCD, where we do know now that at comparable parton densities the system indeed is in a strong coupling regime.

2.1.4 The goals of this series of papers

In short, it is to study self-consistently the collision process in AdS/CFT. For hadronic collisions we basically follow QCD-string-inspired (Lund) picture of the collision. While QCD phenomenology focused on "string breaking", in AdS/CFT setting we will have instead their "falling" (departure from the boundary, or our world) into the IR.

In this paper we will study in detail motion of "debris" – massless and massive particles and open strings, and membranes – in AdS_5. In the second paper we will calculate the corresponding "holograms" of these objects – the stress tensor of matter created on the boundary. Although "debris" fly away

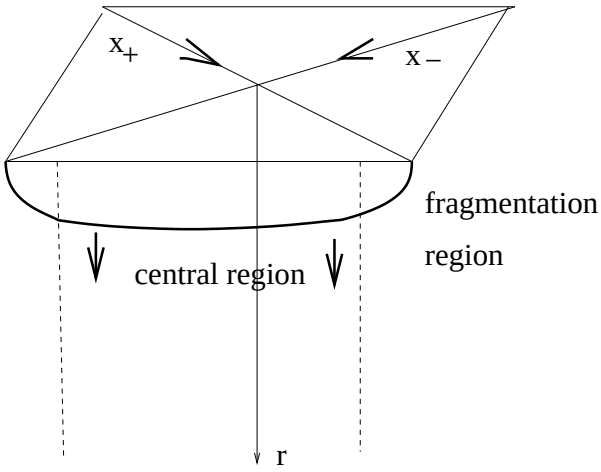

Figure 2.1: Schematic view of the collision setting. The classical heavy charges move along directions $x_\pm$ and collide at the origin. String snapping leads to longitudinally stretched strings (wide black line) which are also extended into the 5-th coordinate r toward the AdS center at $r = 0$. The heavy charges move on the plane $r = \infty$

in 5-th dimension, the usual energy and momenta are conserved in our world, and those "holograms" describe a flow of matter outward from the collision point. As we mentioned already, this can be viewed as a strongly-coupled version of Color Glass, put in the realm of $\mathcal{N}$=4 SYM theory.

We hope in subsequent works to go beyond the linearized gravity and follow nonlinear effects leading to a gravitational collapse of debris and formation of trapped surfaces. This would be dual to information loss (entropy production) and appearance of equilibration.

2.2 The setting

One important suggestion made by SSZ is that heavy ion collisions posses "some internal high momentum scale", usually called $Q_{saturation}$, related to high density of color charges in boosted heavy ions. In order to model it more simply, we now propose substitute energetic light quarks by heavy ones, with the mass M_Q of heavy fundamental quarks Q introduced into AdS/CFT via D_7 brane. As soon as M_Q is at the scale of $Q_{saturation}$, it makes little dynamical difference: but in the AdS/CFT language treatment of heavy quarks is simpler, as they are sources of classical strings. (This simplifying feature has been put to heavy use in treatment of the heavy quark jet quenching [14].)

We will further assume that heavy quarks have no dynamics of their own,

as they are moving along straight lines

$$x_\pm = x_1 \pm vt \tag{2.3}$$

with constant velocity v, both before and after the collisions, see Fig.2.1. If so, there is no conventional gluonic radiation on the brane or gravitational radiation from them in the bulk, as there is no acceleration.

The dynamical objects we will focus on are classical strings, ending at these heavy quarks and propagating in the bulk (for metrics changing from AdS to JP-like one). We will study which solutions exist as a function of collision rapidity and whether they are stable or not: we will conclude that at sufficiently large $v > v_c$ these strings basically go into free fall toward the AdS center.

The next step is to consider not a single pair of charges (a single stretching string), but many. One limit is a pair of colliding "walls of matter", containing multiple heavy quarks. For simplicity, think of these two walls as CP mirror images of each other, made of colorless "dipoles". "Snapping" of their string at the collision leads to multiple strings, all of which being stretched longitudinally.

We then argue that many such strings combined could be considered as a thin singular sheet of matter, referred to below as "membrane". It is then gravitationally collapsing under its own weight. (Note an important distinction between a membrane and a "true brane": since the former has only energy-momentum but lacks the RR charges and consequent Coulomb repulsion, it cannot "levitate" like branes, and simply falls under gravity.)

It has been shown by Israel [35] how a gravitational collapse of a thin layer of matter can be described via two different discontinuous *vacuum* solutions of the Einstein equation without matter ($T_{\mu\nu} = 0$). Self-consistency of the solution is then reached by fulfilling covariant *junction conditions*, resulting in membrane equation of motion.

The issue of self-consistency will not be addressed in this work: we will discuss below falling of various objects – particles and open strings, as well as 3+1 membranes – ignoring for now the effect of their own weight on the metric. The proposed evolution of the system is explained schematically in Fig2.2. Part (a) of it shows some snapshots of this surface, at some early time and then at a later stage. The horizontal direction is the collision direction x_1 while the one along the circles represent any of the two other transverse directions x_2, x_3 (on which no dependence is expected). The radial direction r in part (b) is the 5-th AdS radial direction, a distance from the AdS center. Since the "membrane" is being stretched in x_1 (linearly in time), it has to retreat in r and become a thinner cylinder, just as a stretching soap film will

do in a similar setting.

At this point we would like to emphasize a close analogy, as well as differences, with the jet quenching problem. One studied first a single falling string governed by simple Nambu-Goto action and the overall metric. The complicated picture of matter flow is then recovered using weak (linearized) gravity. One difference is that in a jet quenching problem the string is stationary (in the charge frame) while in our case it is not. Furthermore, we will discuss also multiple strings, which may form another singular object – the *membrane*. Also the metric in our problem is first considered to be just AdS, but eventually it will be non-trivially affected by the membrane's own weight. If so, one should no longer use the linearized gravity but solve Einstein equations in its full nonlinear form.

Needless to say, this is a very difficult task, amenable to analytic treatment only if some drastic simplifications are made. A scenario outlined in Fig2.2(a) would have metric dependent on 3 variables: time, longitudinal direction and the AdS radial one, t, x_1, r. We thus propose a further simplification of the problem: changing variables to proper time and spatial rapidity (2.2) we would look for y-independent solutions, corresponding to purely cylindrical part of the membrane in the middle of Fig2.2(a), ignoring the curved "fragmentation" regions. With only two variables, τ, r one has a problem of similar level of complexity as the one addressed by Israel[1], for a spherical gravitational collapse.

Further clarification of the proposed scenario is shown in Fig.2.2(b), displaying a trajectory of the membrane $r(\tau)$. During the first stage of the process the "debris" of a collision in a bulk – the closed and open strings – are accelerated by the AdS gravity and fall into the 5-th dimension till they reach the relativistic velocity $v \approx 1$ (stage 2)). If there be only one object falling, its gravity being negligible compared to overall gravity of the N branes at the AdS center and they would simply continue their relativistic fall. However large number of them have enough mass to create a horizon which suddenly slows down the membrane (as a distance observer sees it[2]): at stage 3 the membrane is trailing the receding horizon (the dashed line).

If we would discuss pure AdS/CFT theory this would be the end of the story: but in other more QCD-like setting one can have an additional potential which will stop membrane because of existence of a stationary "deconfinement" horizon. If so, the system reaches a "mixed phase" era with stationary horizon

[1]Except that in Israel's problem of non-stretching black hole the horizon is stationary, while in our case it is moving.

[2]As usual for a gravitational collapse, in a co-moving frame the horizon is not important and is crossed, which is not important for us to follow in this work.

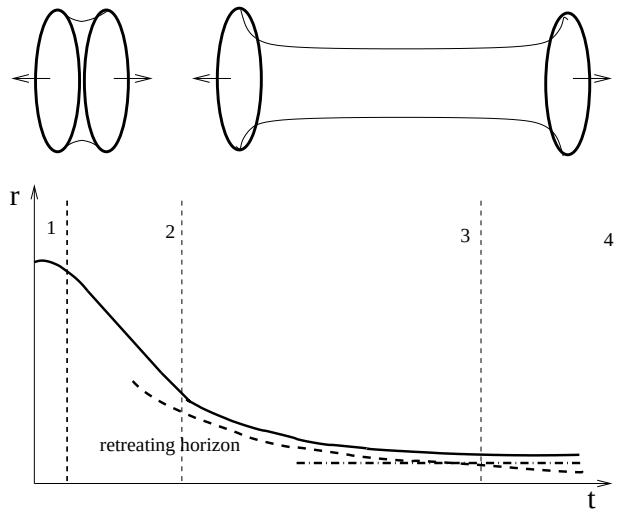

Figure 2.2: (a=upper) Two snapshot of the membrane shapes, at different time moments. See text for explanation of the coordinates. (b=lower)Schematic view of the four periods in gravity dual solution in which falling objects are (1) accelerated into the 5-th dimension r till they reach a relativistic velocity $v \approx 1$, then (2) continue their relativistic fall till (3) breaking near the retreating horizon.

and fixed T, similar to static fireball discussed by Aharoni et al [36] except that in our setting the longitudinal stretching continues.

The trajectory of the collapsing matter sheet should be such as to provide a consistent solution to Einstein equations, combining the JP-like vacuum solution outside the falling sheet, with the "stretching AdS" inside it.

The paper is structured as follows. In the next section we solve equation of motion for different objects falling in AdS. We start with massless and massive particles in subsection 2.3.1.

The main part of this work is study of the open strings, being stretched between two departing charges. We derive analytically the so called *scaling* (factorisable) solution in section 2.3.2. Similar solutions have been used previously in connection to anomalous dimensions of "kinks". New part is discussion of the limits for its existence and stability.

We then find more general non-factorisable solutions in section 2.3.3 which can only be obtained numerically. We find that in proper time -spatial rapidity coordinates τ, y we use those basically becomes "rectangular" , with a nearly free-falling rapidity-independent part. We conclude this section with results for falling membranes. The next section starts with an introduction to the issue of "stretching black holes" in section 2.4.1, and concludes with section 2.4.2 in which we show that all objects considered above are approaching

the (retreating) horizon in a very universal fashion. We conclude with some discussion and outlook in section 2.5.

In the second paper of the series we will calculate back reaction of gravity, by solving linearized Einstein equations and obtaining stress tensor on the boundary ("holograms") for some of these falling objects.

2.3 Objects falling in AdS_5

The collisions creates a lot of "debris" in form of various excitations. Since we would like to follow the collision in the bulk, we naturally have to think of them in terms of string theory. Thus there are the following types of objects: (i) massless and massive particles; (ii) open strings, with ends at the receding walls; (iii) membrane. The "open string" category is naturally split into "mesons" with both ends on the *same* wall, and "stretched strings", with both ends attached to different walls and moving in the opposite direction. We will consider a set of multiple strings copied many times in transverse dimensions x_2, x_3 as a 3-d membrane. The validity of this approximation will be explained later.

2.3.1 Falling particles

As is usually done in this kind of problems, the AdS radius is inverted, so that a coordinate $z = 1/r$ is used instead of r. The AdS boundary is thus at $z = 0$ and "falling" objects move away from it toward infinity. The $AdS_5 \times S^5$ metric in such coordinates is

$$ds^2 = \frac{R^2}{z^2}(d\vec{x}^2 - dt^2 + dz^2) + R^2\, d\Omega_5^2 \tag{2.4}$$

where the last term, related to angles of S^5 is of no importance in this work. We choose to work in τ, y coordinates mentioned above (2.2). The metric is translated into the following form:

$$ds^2 = \frac{R^2}{z^2}(-d\tau^2 + \tau^2 dy^2 + dz^2) \tag{2.5}$$

where we ignore the transverse coordinates and the S_5 part.

One feature of AdS_5 metric is its boost invariance, the importance of which will be seen later. Let us assume particles move with constant spatial rapidity y, so the trajectory can be described by $z(\tau)$. Massless particles move along

the geodesics with zero interval $ds^2 = 0$ which in the metric (2.5) simply means $z = \tau$.

Massive falling objects were already discussed in [39], but here we present it in a different form, more closely resembling much more nontrivial ones in the next sections. Using the coordinate time τ one simply write down the interval as an action for a particle moving in the 5-th direction of

$$S \sim \int d\tau \frac{\sqrt{1-\dot{z}(\tau)^2}}{z(\tau)} \tag{2.6}$$

where the non-trivial trace of the AdS metric is z in the denominator. This leads to well known EOM

$$\ddot{z}(\tau) = \frac{1-\dot{z}(\tau)^2}{z(\tau)} \tag{2.7}$$

Nonrelativistically, one can neglect $\dot{z}(\tau)$ and think thus about a motion in a logarithmic potential well[3]. Ultrarelativistically, one finds instead that as $\dot{z}(\tau) \to 1$ the acceleration goes to zero, as needed. Thus, in the standard coordinates, very little seems to happen after the particle reaches ultrarelativistic regime: it runs forever toward $z \to \infty$ with speed of light. But this is a (well known) illusion due to relativistic time slowing: in its own proper time, the particle continue to accelerate and reaches the AdS center in finite proper time.

This EOM is easily integrated yielding

$$z(\tau) = \sqrt{\tau^2 + v_0 z_0 \tau + z_0^2} \tag{2.8}$$

2.3.2 Falling open strings: the scaling solution

After this little warm-up, let us consider motion of the open strings. Its action is that by Nambu-Goto, and if one ignores two transverse coordinates x_2, x_3 and uses as two internal coordinates the t, x (time and longitudinal coordinate) the string is described by by one function of two variables $z(x,t)$. The corresponding string action is then

$$S = -\frac{R^2}{2\pi\alpha'} \int dt \int \frac{dx}{z^2} \sqrt{1 + (\frac{\partial z}{\partial x})^2 - (\frac{\partial z}{\partial t})^2} \tag{2.9}$$

[3]The reader may ask why we don't refer to conserved energy, which will make this much simpler: the reason is the next section would not have this avenue open for us.

Note that only one term, the time derivative, is different from long-used static action used in [37] for static calculation of the inter-charge potential. The boundary conditions would be $z = 0$ at two rays $x = \pm vt$, the world lines of the heavy quarks.(The boost invariance of the AdS_5 metric allows us to work in a frame where the open string endpoints move with opposite velocities)

Translating into the τ, y language, the boundary conditions are now determined at fixed $y = \pm Y$ where $v = tanhY$ and Y is the rapidity of the heavy quarks (colliding walls). by doing so, we transfer time dependence from the boundary conditions into the equations themselves. The corresponding action is now

$$S = -\frac{R^2}{2\pi\alpha'}\int \frac{\tau d\tau dy}{z^2}\sqrt{1-\left(\frac{\partial z}{\partial \tau}\right)^2+\frac{\left(\frac{\partial z}{\partial y}\right)^2}{\tau^2}} \tag{2.10}$$

Before solving the corresponding equation in full, we will first discuss "scaling" solutions in the separable form

$$z(\tau, y) = \frac{\tau}{f(y)} \tag{2.11}$$

suggested by conformal properties of the theory. Such solutions were known in literature [38], in Euclidean context, they were used for AdS/CFT calculation of the anomalous dimensions of "kinks" on the Wilson lines (of which our produced pair of charges is one).

The scaling ansatz leads to a simple action

$$S = -\frac{R^2}{2\pi\alpha'}\int \frac{d\tau dy}{\tau}\sqrt{f'^2+f^4-f^2} \tag{2.12}$$

Using the fact that y does not appear in the action, there is a conserved "energy"

$$\frac{V}{\sqrt{f'^2+V}} = E \tag{2.13}$$

with the "potential" $V = f^4 - f^2$, and thus the derivative of the function f can be readily obtained

$$f' = \frac{\sqrt{V(V-E^2)}}{E} \tag{2.14}$$

Note that the function f decreases from infinity on the boundaries to its lowest

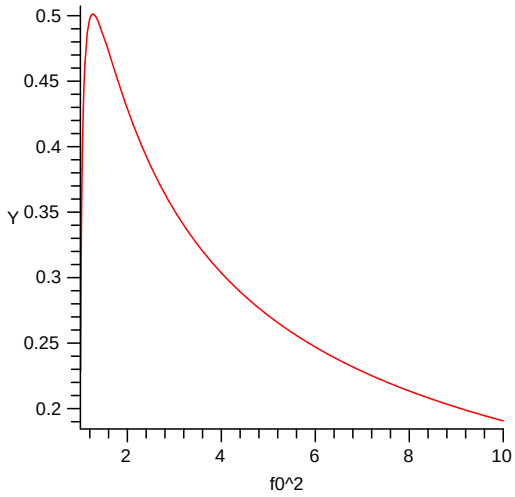

Figure 2.3: Rapidity of the collision $Y = arctanh(v)$ vs f_0^2. The maximum gives a critical rapidity Y_c. For $Y < Y_c$, two f_0^2 are possible, corresponding two string configurations. For $Y = Y_c$,only one f_0^2 is possible. The region $Y > Y_c$ cannot be reached

value at the middle of the string which we will call f_0, so $f > f_0$. At $f = f_0$ the derivative vanishes, so (2.14) provides also a simple equation $f_0^4 - f_0^2 - E^2 = 0$ relating E to f_0.

Integration of (2.14) gives the following solution

$$y = f_0 \sqrt{\frac{(f_0^2-1)}{2f_0^2-1}} F\left(\sqrt{\frac{f^2-f_0^2}{f^2-1}}, \frac{f_0}{\sqrt{2f_0^2-1}}\right) - \frac{1}{f_0}\sqrt{\frac{(f_0^2-1)^3}{(2f_0^2-1)}} \Pi\left(\sqrt{\frac{f^2-f_0^2}{f^2-1}}, \frac{1}{f_0^2}, \frac{f_0}{\sqrt{2f_0^2-1}}\right) \tag{2.15}$$

where F and Π are elliptic integral of the first and the third kind. f_0^2 depends on collision rapidity $Y = arctanh(v)$ via the boundary condition at $f(Y) = \infty$, as shown in Fig. 2.3.

The existence of a maximum means that there are no scaling solutions when the rapidity Y is larger than some critical value, while if the quarks move on the boundary slower that the critical rapidity, there are *two* solutions.

In order to characterize the solutions, it is useful to introduce "effective

potential" for two separating quarks for each scaling solution, defined as instantaneous energy $U = \Delta S/\Delta t$, where ΔS is action given by the area of the string world sheet, Δt is the time interval. U needs to be regulated, which is obtained by subtracting the Wilson loop corresponding to two non-interacting moving quarks. In other words, we calculate the subtracted area:

$$\begin{aligned} S_{reg} &= -\frac{R^2}{2\pi\alpha'}\int\frac{dt}{t}\int dy\sqrt{f'^2+V} - \int_0^\infty df \\ &= -\frac{R^2}{2\pi\alpha'}\int\frac{dt}{t}\left(\int_{f_0}^\infty df\sqrt{\frac{V}{V-E^2}} - \int_0^\infty df\right) \end{aligned} \tag{2.16}$$

The second term corresponds to $f' = \infty$, precisely the straight string going in z direction, which is AdS solution for a moving quark. Note that we have switched to t,y coordinates, which does not change the form of the string action (2.12). With this prescription, we calculated U for solutions in both branches, which are compared in Fig. 2.4. The solution with the lower potential has a chance to be the stable one, while the higher potential one (with large f_0, or longer string) must be metastable.

Let us now comment on the *small* v limit of the scaling solution. At large separation (realized at late time) the quarks can be considered as quasi-static. At small v, or large f_0^2, the effective potential can be simplified to the following form

$$\begin{aligned} dS_{reg}/dt &= -\frac{R^2}{2\pi\alpha'}\int df\left(\sqrt{\frac{V}{V-E^2}}-1\right)/t \\ &= -\frac{R^2}{2\pi\alpha'}\left(-0.5991\,\sqrt{f_0} - 0.1780\,\frac{1}{f_0}\right)\frac{2v}{L} \end{aligned} \tag{2.17}$$

and relate more simply the velocity and f_0

$$v = \frac{0.5991}{f_0} - \frac{0.03115}{{f_0}^3} \tag{2.18}$$

Combining (2.17) and (2.18), we obtain the effective potential for small velocity and large separation to be

$$V = 0.2285\,\frac{(1+0.6830\,v^2)\,\sqrt{g^2\,N}}{L} \tag{2.19}$$

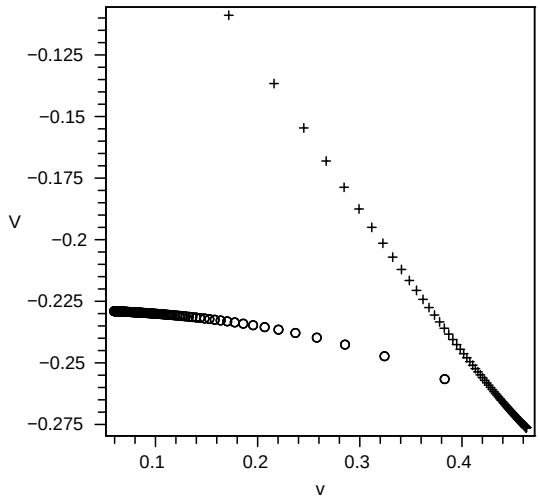

Figure 2.4: the potential V as a function of v for different branches of solution. circles for large-f_0^2 branch, crosses for small-f_0^2 branch V is plotted in unit of $\sqrt{g^2\,N}/L$ The potential from the large f_0^2 branch is lower than that from small f_0^2 branch

The coefficient in front (the leading term at $v \to 0$) coincides with the well known coefficient of static Maldacena potential.

The second term is thus the velocity-dependent "Ampere's law" $O(v^2)$ correction to it. We are not aware of any other previous calculation of this term, except for the paper by Zahed and one of us [40] in which, based on resummation of ladder diagrams via Bethe-Salpeter eqn, the result was that the velocity dependence is

$$U(v)/U(v=0) = \sqrt{1-\vec{v}_1\vec{v}_2} \approx 1 + .5v^2 + ... \tag{2.20}$$

It is close but not the same[4].

Both branches of the scaling solution was also confirmed by solving the equation numerically, starting from the middle point and scanning all values of f_0.

The applicability of the scaling solution for a particular Y depends of course not only on availability of a solution, but also on its *stability* i.e. how does the scaling solution evolve with time(τ), given some perturbation at initial time.

[4]The situation in which two charges move in the same direction is just a Lorentz boosted static solution: in this case a square root of v in the Lorentz factor is of course obvious.

Denoting scaling solution $g_s(y) = \frac{1}{f(y)}$ and perturbation as

$$z(\tau, y) = \tau g(\tau, y) \qquad g(\tau, y) = g_s(y) + \delta g(\tau, y) \tag{2.21}$$

we want to know whether the perturbation will grow or decay with time. The EOM for $g(\tau, y)$

$$\begin{aligned}
&-2 - \tau^3 g(\frac{\partial g}{\partial \tau})^3 + 2\tau g(\frac{\partial g}{\partial y})^2 \frac{\partial g}{\partial \tau} - 2\tau g^2 \frac{\partial g}{\partial y}\frac{\partial^2 g}{\partial \tau \partial y} + \\
&\tau^2 g(\frac{\partial g}{\partial y})^2 \frac{\partial^2 g}{\partial \tau^2} + 2\tau \frac{\partial^2 g}{\partial y^2} g^2 \frac{\partial g}{\partial \tau} + \tau^2 \frac{\partial^2 g}{\partial y^2} g(\frac{\partial g}{\partial \tau})^2 - 2\frac{\partial g}{\partial y} - g^4 \\
&-\frac{\partial^2 g}{\partial y^2} g^2 + 7\tau g \frac{\partial g}{\partial \tau} - 3\tau g^3 \frac{\partial g}{\partial \tau} - 3\tau^2 g^2 (\frac{\partial g}{\partial \tau})^2 + \tau^2 g \frac{\partial^2 g}{\partial \tau^2} \\
&+3g^2 + 2\tau^2 (\frac{\partial g}{\partial \tau})^2 + \frac{\partial^2 g}{\partial y^2} g^3 - 2\tau^2 g \frac{\partial g}{\partial y}\frac{\partial g}{\partial \tau}\frac{\partial^2 g}{\partial \tau \partial y} = 0
\end{aligned} \tag{2.22}$$

can be used by plugging (2.21) in (2.22), and keeping only term linear in $\delta g(\tau, y)$(consider only sufficient small perturbation), we obtain the following linearized EOM for the perturbation:

$$\left[A + B\frac{\partial}{\partial \tau} + C\frac{\partial}{\partial y} + D\frac{\partial^2}{\partial \tau \partial y} + E\frac{\partial^2}{\partial \tau^2} + F\frac{\partial^2}{\partial y^2}\right] \delta g(\tau, y) = 0 \tag{2.23}$$

with

$$\begin{aligned}
A &= g_s'' g_s^2 + 6g_s - 4g_s^3 - g_s'' \\
B &= \tau(2g_s g_s'^2 + 2g_s'' g_s^2 + 7g_s - 3g_s^3) \\
C &= -4g_s' \\
D &= -\tau(2g_s^2 g_s') \\
E &= \tau^2(g_s g_s'^2 + g_s) \\
F &= g_s^3 - g_s
\end{aligned} \tag{2.24}$$

define $\tilde{\tau} = ln\tau$ as our time, the EOM simplifies to:

$$\left[\tilde{A} + \tilde{B}\frac{\partial}{\partial \tilde{\tau}} + \tilde{C}\frac{\partial}{\partial y} + \tilde{D}\frac{\partial^2}{\partial \tilde{\tau} \partial y} + \tilde{E}\frac{\partial^2}{\partial \tilde{\tau}^2} + \tilde{F}\frac{\partial^2}{\partial y^2}\right] \delta g(\tau, y) = 0 \tag{2.25}$$

with

$$\tilde{A} = A, \tilde{B} = B - E, \tilde{C} = C, \tilde{D} = D, \tilde{E} = E, \tilde{F} = F \tag{2.26}$$

(To make it easier to get all these functions one can approximate scaling solution $g_s(y)$ with some parameterizations: we found that $(\frac{g_s}{g_s(0)})^3 + (\frac{y}{Y})^n = 1$ fits all the scaling solution very well.)

We need to seek eigenfunction $\delta g(\tau, y) = e^{\lambda\tilde{\tau}}\psi(y)$ satisfying (2.25) and boundary condition $\psi(y = \pm Y) = 0$ In general, out of many eigenvalues λ we should be interested in those with positive real part, which will allow us to conclude when the solution is unstable.

The eigenfunction results in the following EOM:

$$\left[C_0 + C_1\frac{\partial}{\partial y} + C_2\frac{\partial^2}{\partial y^2}\right]\psi(y) = 0 \tag{2.27}$$

with

$$\begin{aligned}
C_0 &= \lambda^2 g_s(g_s'^2 + 1) + \lambda(g_s g_s'^2 + 6g_s + 2g_s^2 g_s'' - 3g_s^3) + 3g_s'' g_s^2 + 6g_s - 4g_s^3 - g_s'' \\
C_1 &= -2g_s'(\lambda g_s^2 + 2) \\
C_2 &= g_s(g_s^2 - 1)
\end{aligned}$$

Due to the symmetry $y \leftrightarrow -y$ of the problem, we can solve it in the positive-y region, with boundary condition $\psi(Y) = 0$,$\psi'(0) = 0$. To solve this Schrodinger-like eqn, we use the iterative method. Starting on one boundary with $\psi'(0) = 0$,$\psi(0) = 1$, the second condition only affects the normalization of $\psi(y)$. With some initial value of λ, we can obtain the $\psi(Y)$ from the EOM. then we variate the value such that $\psi(Y)$ converge to 0. The resulting λ gives the eigenvalue. Without much difficulty, we found the following set of eigenvalue for different Y, shown in Table.2.1. We also plot the eigenvalue λ in the complex plane Fig.2.5. The evolution trend of this set of eigenvalues suggests that the transition from stable to unstable occurs at Y_m inside .22-.27 interval, which is way below the critical value $Y \sim .5$ above which there were no scaling solutions at all. This shows that we essentially lose the scaling solution to instability for $Y > Y_m$: we were not able to tighten this limits any further.

In summary, the scaling solution exist only for sufficiently small rapidities $Y < Y_c \sim 0.5$. Furthermore, we were able to verify that it is classically unstable already for $Y > Y_m \approx 1/4$. Therefore solutions other than the scaling one is need for large rapidity, which is more important for our purpose.

Table 2.1: one set of eigenvalue for different rapidity

$\lambda(10^{-2})$	4.2+94.8i	3.3+126.7i	2.8+157.5i	2.0+188.5i
Y	0.48	0.45	0.42	0.40
$\lambda(10^{-2})$	1.2+222.1i	0.78+265.7i	0.38+299.5i	0.12+346.4i
Y	0.37	0.33	0.30	0.27
$\lambda(10^{-2})$	-0.27+404.2i	-0.63+492.9i	-0.80+569.8i	
Y	0.24	0.21	0.18	

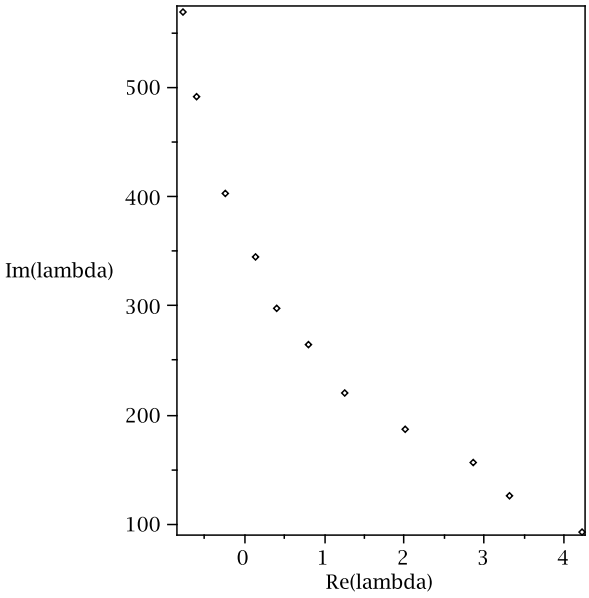

Figure 2.5: The evolution of eigenvalue λ from Y=0.48 to 0.18 in the complex plane

2.3.3 Falling strings: the non-scaling solutions

In this section we study generic solutions outside the scaling ansatz. But before we do so, let us explain qualitatively why such solution must fail as the rapidity of the collision grows. The scaling solution, in which τ and y dependences factorize, means that one tries to enforce a particular stable profile to a string. But as the rapidity gap $2Y$ between the walls grows, we so-to-say try to build wider and wider "suspension bridge" out of the string: it is going to break under its weight at some point.

We again use $z(\tau, y) = \tau g(\tau, y)$ and EOM (2.22). The boundary condition is $g(\tau, y = \pm Y) = 0$. Due to the symmetry of the problem, it is sufficient to solve the dynamics of half of the string, with initial condition $g(\tau, Y) = 0$ and $\frac{\partial g}{\partial y}(\tau, 0) = 0$.

However there are two potential problems in (2.22). (i)the y derivative diverges on the boundary. (ii)the PDE is highly nonlinear and will show self-focusing of energy at certain "corners", as we will see. These make it difficult to obtain a well-behaved numerical solution [5], and to improve the performance of Maple PDE solver we used function $h(\tau, y) = g(\tau, y)^n$ as dynamical variable, with properly chosen integer power n so that the y derivative is finite on the boundary.

Fig.2.6 shows the dynamics of the string with $Y = 0.6$. We start from the initial condition $(\frac{g(1,y)}{0.88})^3 + (\frac{y}{Y})^3 = 1$ and $\frac{\partial g}{\partial \tau}(1, y) = 0$. We chose the initial time $\tau = 1$ to avoid the singularity at $\tau = 0$. $n = 6$ is used in solving the PDE. As time grows, the string profile approach a rectangular shape with sharper and sharper turn at the "corners". Based on the numerical solution, we infer that in the τ, y coordinates, any point of the string other than the boundary will ultimately become free falling when time is sufficient large. This can be supported by the following qualitative argument. Any tiny piece of string experiences the AdS effective gravity and the drag from his neighbors. Since in the non-scaling solution, the whole string keeps falling, it is natural to expect any point of the string approach the speed of light asymptotically, end up with a rectangular profile. Therefore, we conclude the edge of the profile is not important asymptotically. It can be well approximated by a flat profile in y, which will be studied in the next section.

2.3.4 Falling strings and membrane in AdS_5

The falling string can be considered as a solution at the center of the generic case considered above in the large rapidity limit of the ends $Y \to \infty$. which makes z y-independent. Ignoring all derivatives over y in the EOM above one gets an ODE problem with the following eqn:

$$-2\,\tau + \dot{z}\,z - \dot{z}^3 z + \tau\,\ddot{z}\,z + 2\,\dot{z}^2\tau = 0 \tag{2.28}$$

which is similar but not identical to that of a falling massive object (2.7): the difference comes from dimensionality of the object: $1/z^2$ in the action (instead of $1/z$), because the string action is a 2-dimensional integral. It is now explicitly depending on τ: there is no integral of motion but one can straightforwardly solve the EOM for different initial conditions numerically. We found at large τ, g tends to 1. Therefore we show in this extreme case

[5] Similar problems have been encountered by previous studies of jet quenching, and another way to deal with them, proposed in Herzog et al [14], takes advantage of the re-parametrization invariance to fine tune the performance of PDE solver.

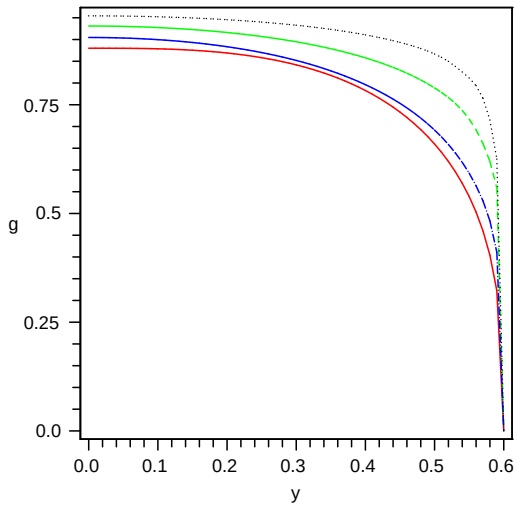

Figure 2.6: The dynamics of the string(half) $g(\tau, y)$ with $y = 0.6$. The profiles from the innermost to the outermost correspond to $\tau = 1$(solid red),$\tau = 2$(dotted blue),$\tau = 4$(dashed green), $\tau = 8$(dot-dashed black).

that the asymptotic solution is again $z \sim \tau$

Summarizing the falling of all string objects, they have a universal asymptotic behavior $z \sim \tau$. Therefore we may model the falling particles/open strings by a membrane, which is made of multiple strings and is flat in x_2, x_3 and y coordinates

The coefficient in its DBI action, the membrane tension, is now proportional to the density of charges in the colliding walls, and thus can be very large. This fact would mean that the membrane should eventually be considered heavy enough, so that its weight would affect the metric itself. Since in this work we would not attempt to solve this problem yet, we treat the membrane as a test body falling in external AdS metric. In this case the value of its tension does not matter, and the action is very similar to Nambu-Goto string action except of the different power of z (now $1/z^4$)

$$S \sim \int \tau d\tau dy dx_2 dx_3 \frac{\sqrt{1 - (\frac{\partial z}{\partial \tau})^2}}{z^4} \tag{2.29}$$

We parametrize the membrane with τ,y,x_2,x_3, and z-coordinate is a function of τ only, $z = z(\tau)$. The EOM is readily obtained, it is similar to the

y-independent string case (coefficients 2 change to 4 in two terms):

$$\dot{z}z - \dot{z}^3 z + 4\tau\dot{z}^2 + \tau\ddot{z}z - 4\tau = 0 \tag{2.30}$$

Its asymptotic solution is again $z \sim \tau$.

2.4 Near-horizon "braking"

2.4.1 Stretching black holes

The JP solution we will now discuss addresses the first case, d=1. The main feature of the JP solution is that these two variables enter the metric via one specific combination

$$v = \frac{z}{\tau^\gamma} \tag{2.31}$$

which simplifies Einstein's eqns and leads to a solution. JP have found that only for one particular power $\gamma = 1/3$ there is no singularity at the horizon in one of the invariants – the square of the 4-index Riemann curvature, and argued that thus this solution should be preferred on this ground.

However it is not clear what the physical meaning and significance of this singularity may be, in general. Furthermore, in the "membrane scenario" proposed in this work the JP-like metric only extends from the AdS boundary till the falling membrane, while the would-be singularity is in the second domain, where this solution is not supposed to be used at all. It is, so to say, a "mirage behind the mirror", singular or not does not matter.

There is another reason why this particular power should be selected: only in $\gamma = 1/3$ case such that the total area of the horizon (3d object normal to time and z) is *time independent*: the factor τ (from stretching y_1) is canceled by the factor $1/z^3$ from contracting z. Thus, this stretching solution is area-preserving, and thus potentially dual to the entropy-conserving adiabatically expanding fireball.

The specific form of the JP metric is

$$ds^2 = -\frac{(1 - v^4\frac{e_0}{3})^2}{(1 + v^4\frac{e_0}{3})}\frac{d\tau^2}{z^2} + (1 + v^4\frac{e_0}{3})\frac{\tau^2 dy^2 + dx_\perp^2}{z^2} + \frac{dz^2}{z^2} \tag{2.32}$$

The horizon determined from $g_{\tau\tau}(v) = 0$ is at $v_h = (\frac{3}{e_0})^{1/4}$, thus it is moving away from $z = 0$ (the AdS boundary) as needed. The 4-th power of v is related to the fact that its expansion near $z = 0$ to the 4-th order is responsible for the stress tensor as observed on the boundary, which was tuned to correspond to

the Bjorken boost invariant solution of ideal hydrodynamics [24]: the starting point for JP.

This metric provides an asymptotic (large τ) solution to the Einstein eqns

$$R_{\mu\nu} - (R/2)g_{\mu\nu} - 6g_{\mu\nu} = \kappa T_{\mu\nu} \tag{2.33}$$

After this metric is substituted to the l.h.s. one finds that all terms of the "natural" order of magnitude $O(\tau^{-2/3})$ cancel out, with only the higher order terms remaining. More specifically, we found that only the terms $T_{\mu\nu} \sim 1/\tau^2$ are present, with rather compact expressions such as

$$\tau^2 T_{\tau\tau} = -\frac{4v}{(3+v)^2} \tag{2.34}$$

$$\tau^2 T_{zz} = -\frac{4v^2}{(3+v)(v-3)^2} \tag{2.35}$$

$$\tau^2 T_{yy} = (-4/9)\frac{v(4v^2-15v-63)}{(v-3)^3} \tag{2.36}$$

Please note that those terms are not only subleading at large τ but also are much simpler than all the terms which had canceled out. Also note that there is a significant singularity at the horizon ($v = 3$ in these units) in this stress tensor, which is again irrelevant because this metric is not supposed to be used there.

2.4.2 Objects approaching the horizon

Before we discuss the JP metric, let us remind the reader how this approach works in the usual black holes with the Schwartzschild metric: it will be needed to emphasize the difference between them.

Massless particle falling radially in the Schwartzschild metric satisfies the $ds^2 = 0$ eqn, which is

$$(\frac{dr}{dt})^2 = (1 - \frac{r_h}{r})^2 \tag{2.37}$$

leading to exponentially fast "freezeout",

$$(r - r_h) \sim exp(-t/r_h) \tag{2.38}$$

The same is also true for other objects, of course.

We use the following rescaled coordinates:

$$z \to c\,z, \tau \to c\,\tau, y \to y, x_\perp \to c\,x_\perp$$

with $c = (\frac{3}{e_0})^{\frac{3}{8}}$. The resultant metric is

$$ds^2 = -\frac{\left(1-\frac{z^4}{\tau^{4/3}}\right)^2}{1+\frac{z^4}{\tau^{4/3}}}\frac{d\tau^2}{z^2} + \left(1+\frac{z^4}{\tau^{4/3}}\right)\frac{\tau^2 dy^2 + dx_\perp^2}{z^2} + \frac{dz^2}{z^2} \tag{2.39}$$

The massless particle moves according to $ds^2 = 0$, which in JP metric is

$$\frac{dz}{d\tau} = \frac{1-\frac{z^4}{\tau^{4/3}}}{\sqrt{1+\frac{z^4}{\tau^{4/3}}}} \tag{2.40}$$

We have assumed that the particle always starts from outside the horizon: $z < \tau^{\frac{1}{3}}$ This EOM is solved numerically for different initial conditions.(From here on, we always use $\tau = 10$ as initial time for numerical solution, since the metric (2.39) is valid asymptoticly $\tau >> 1$)

To obtain the analytical form of the asymptotic behavior, we define:

$$u = \frac{z^4}{\tau^{\frac{4}{3}}} \tag{2.41}$$

and the EOM becomes

$$\frac{1-u}{\sqrt{1+u}} = \frac{1}{4}\frac{\dot{u}\,\tau^{1/3}}{u^{3/4}} + \frac{1}{3}\frac{u^{1/4}}{\tau^{2/3}} \tag{2.42}$$

Note $u \to 1$ as $\tau \to \infty$. Assuming the second term dominates the first term on the RHS, we obtain the asymptotic form $u = 1 - \frac{\sqrt{2}}{3}\,\tau^{2/3}$, which confirms our assumption. In terms of z and τ, we have:

$$z = \tau^{1/3}\left(1 - \frac{1}{6\sqrt{2}}\,\tau^{-2/3}\right) \tag{2.43}$$

For massive particle, the action is given by $S = m\int ds$. Similarly we focus on the case that particle moves in a trajectory with constant y and $x_\perp$: EOM follows from variation on action. Let $z = \tau^{1/3}\,f$, then the function f needs to satisfy the following eqn:

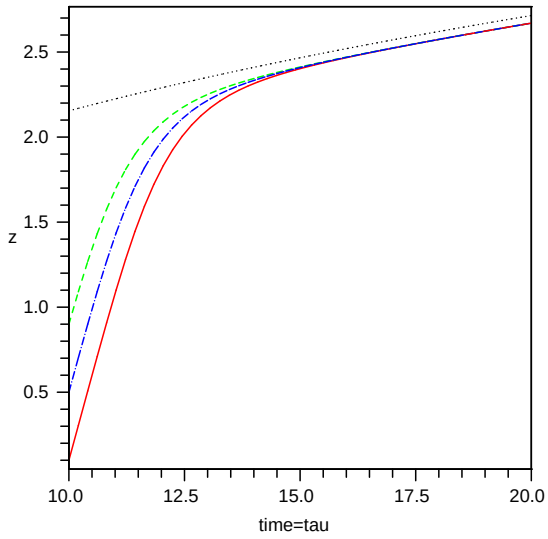

Figure 2.7: trajectories of massless particles, with initial z coordinates: z(10)=0.1(solid red) z(10)=0.5(dash-dotted blue) z(10)=0.9(dashed green) The horizon is also plotted(dotted black) for comparison. The trajectories of the massless particles approach each other asymptotically, but does not seem to approach the moving horizon.

$$
\begin{aligned}
&-27\tau^2 f^{16}\dot{f}^2 - 6\tau f^{17}\dot{f} + 18\tau^2 f^8\dot{f}^2 - 108\tau^2 f^{12}\dot{f}^2 - 6f^{14} \\
&+4f^{10} + 54\tau f^5\dot{f} - 54\tau f^{13}\dot{f} + 12\tau f\dot{f} + 108\tau^2 f^4\dot{f}^2 - 6\tau f^9\dot{f} \\
&+6f^6 - 3f^{18} + 9\tau^2 f^{17}\ddot{f} + 9\tau^2 f\ddot{f} - 9\tau^{4/3} - 18\tau^2 f^9\ddot{f} \\
&-126\tau^{4/3} f^{12} + 9\tau^{4/3} f^{20} + 27\tau^{4/3} f^{16} - 27\tau^{4/3} f^4 + 126\tau^{4/3} f^8 \\
&-f^2 + 9\tau^2\dot{f}^2 = 0
\end{aligned} \tag{2.44}
$$

It is again solved numerically, with initial conditions satisfying $z_0 < \tau_0^{1/3}$ and $\dot{z}(\tau_0) < \frac{1-\frac{{z_0}^4}{{\tau_0}^{4/3}}}{\sqrt{1+\frac{{z_0}^4}{{\tau_0}^{4/3}}}}$. Note that free falling massive object will move with speed of light asymptotically. We expect (2.43) to be the asymptotic solution. By plugging (2.43) in (2.44), we get the RHS: $\frac{8}{3}\tau^{-4/3}$, which tends to zero as τ grows

Furthermore, we compare numerical solution with the asymptotic solution in Fig.2.8. The two solutions agree well at large τ. This confirms (2.43) is the correct asymptotic solution.

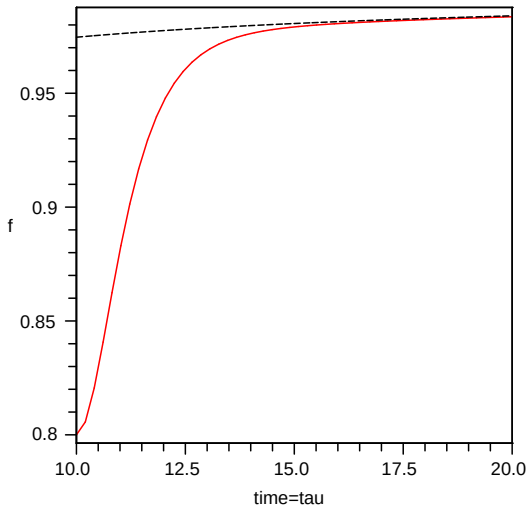

Figure 2.8: trajectory of massive particles starting with $f = 0.8$ and $\dot{f} = 0$.(solid red) at $\tau = 10$. The trajectory is indistinguishable from the asymptotic solution(dashed black) at $\tau \sim 15$

To study the falling string, we first parameterize the string by $z = z(\tau, y)$. Instead of solving it this form. We recall our experience with non-scaling solution in AdS space. At large enough τ, the edge of the string will be less important, with most part of the string falling freely. Therefore we ignore the y dependence of z: $z = z(\tau)$

Defining $f = \frac{z}{\tau^{1/3}}$, The EOM follows straightforwardly from the Nambu-Goto action with the metric (2.39). It is a quite lengthy expression, which we choose not to show here.

We expect the same asymptotic solution (2.43). By plugging (2.43) in the EOM, we get the RHS: $-\frac{95\sqrt{2}}{12}\tau^{-2/3}$, which tends to zero as τ grows. Fig.2.9 compares numerical solution with the asymptotic solution, which confirms it is the correct asymptotic solution.

Now we proceed to our final case, a *membrane* falling in JP metric. Let $z(\tau, y, x_2, x_3) = \tau^{1/3} f(\tau)$: the EOM is again quite lengthy and not shown here.

We have solved it with a number of initial conditions and found that all extra terms are subleading near horizon, so this EOM gives the same asymptotic solution as the other cases, namely $f = 1 - (\frac{1}{6\sqrt{2}})\tau^{-2/3}$.

The numerical solutions are displayed in Fig.2.10, which confirm the asymptotic solution.

We found that in all cases studied – massless and massive particles, string

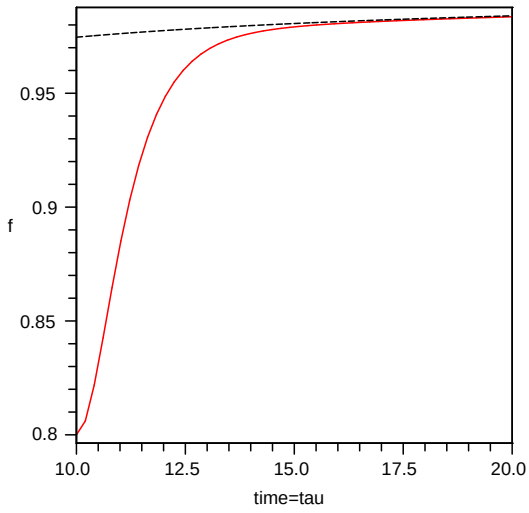

Figure 2.9: trajectory of string with initial condition $f = 0.8$ and $\dot{f} = 0$(solid red) at $\tau = 10$. The trajectory is indistinguishable from the asymptotic solution(dashed black) at $\tau \sim 15$

and membranes – their late time behavior can be approximated by the same asymptotic solution

$$(z - z_h(\tau)) \sim [-\frac{1}{6\sqrt{2}}\tau^{-1/3} + ...] \tag{2.45}$$

2.5 Summary

This is the first paper of the series, devoted to quantitative formulation of the "gravity dual" to high energy collisions of macroscopically large bodies (heavy ions). In it we have formulated the setting in which the problem is simplified sufficiently to be solvable.

Its central idea is that various "debris" from a collisions, in form of massless and massive particles or "stretching" open strings, all fall toward the AdS center. Although qualitatively such falling may look quite similar, the equations of motion and solutions are different for different objects. The main result of this work is a systematic demonstration of this statement in detail, both for initial time (when the underlying metric is supposed to be close to AdS) and at the late times (when the metric is close to JP solution). As we will see in

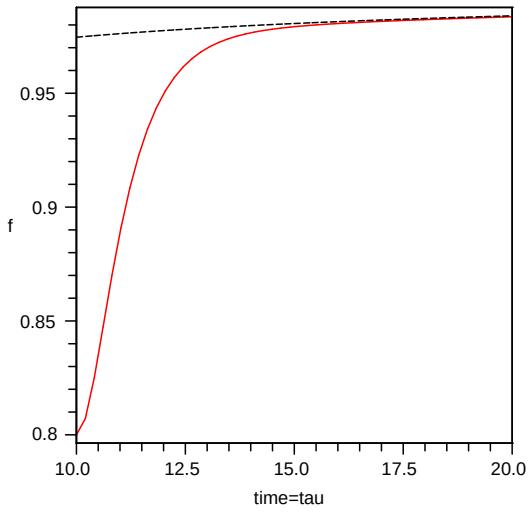

Figure 2.10: trajectory of membrane with initial condition $f = 0.8$ and $\dot{f} = 0$(solid red) at $\tau = 10$. The trajectory is indistinguishable from the asymptotic solution(dashed black) at $\tau \sim 15$

subsequent papers later, small differences in "falling" leads to quite different "holograms" in form of stress tensor at the boundary.

One possible solution can be to unify all such "debris" as a single massive "membrane", falling under its own weight. As shown first by Israel [35] long ago, in such case one can greatly simplify the gravitational aspect of the problem, using two different solutions of the sourceless Einstein equations inside both space-time domains, appropriately matched at the hyper surface made by the world-volume of the membrane. Two solutions are subject to "junction conditions" providing new EOM for the membrane itself. We will discuss those issues elsewhere.

Let us now point out few more specific results of this work. In the study of longitudinally stretched strings we have found that "scaling" solutions used previously for determination of "kink"'s anomalous dimensions are not at all adequate in Minkowski time. We found that while for wall rapidity $Y > Y_{max} \approx 1/2$ these solutions are absent, and there are two of them for smaller Y. We further studied stability of the solutions and have proven that at least for $Y > Y_c \sim 1/4$ they indeed are unstable.

Our main finding for generic non-scaling solutions (which come from numerical solutions of PDEs) is that while at small velocity of stretching there is the so called scaling solution, generically at high stretching one gets instead

asymptotic approach to a "rectangular" solution, consisting basically of two near-vertical strings and freely falling horizontal part.

Another result which was not expected is that although all types of objects – massless and massive particles as well as open strings and membranes – approach the JP horizon in the same universal way. Unlike in the textbook case of the Schwartzschild metric, this approach does not happen exponentially but only as a power $\tau^{-2/3}$ of time. Note that this power is the same as appears in subleading terms, ignored by JP at late time. It remains a challenge to find an appropriate vacuum solution to Einstein equation complementing the late-time JP metric.

Chapter 3

Hologram of static stringy objects

3.1 Introduction

AdS/CFT correspondence [1–3] relates conformal $\mathcal{N}$=4 supersymmetric Yang-Mills theory (CFT) with string theory in $AdS_5 \times S_5$ space-time. Large number of colors $N \to \infty$ and 't Hooft coupling $\lambda = g^2_{YM} N \to \infty$ further lead to the classical supergravity regime (weak coupling) for the latter, putting the CFT into a strong coupling regime. In the decade since its invention, this correspondence became an indispensable theoretical tool, providing multiple interesting results about a strongly coupled regime of $\mathcal{N}$=4 supersymmetric gauge theory.

Among the earliest were calculation of the energy of a static electric dipole [37], based on a shape of "pending string" held at the AdS boundary at the positions of two static fundamental quarks, separated by distance L. For further reference we will need the EOM of the string[1]

$$x_z = -\frac{z^2}{\sqrt{z_m^4 - z^4}} \tag{3.1}$$

where z_m is the maximal string extension into z direction. We will also use notation $L/2 = x_m \approx 0.60 z_m$.

[1]Which is not the second order equation coming from the Lagrangian but the first (energy) integral of it. The eqn(3.1) represents half of the string, the other half is obtained by reflection $x \leftrightarrow -x$.

The resulting potential

$$E = -\frac{4\pi^2 \left(g_{YM}^2 N\right)^{\frac{1}{2}}}{\Gamma\left(\frac{1}{4}\right)^4 L} \tag{3.2}$$

has the famous factor $\sqrt{\lambda}$ (instead of λ in the weak coupling Coulomb law. Soon this calculation was extended to include magnetic objects (monopoles and dyons) by Minahan [41], which can be viewed as an endpoints of the appropriate D_1 branes on the boundary. We will continue to discuss puzzles related with the dipoles in the next subsection.

Naively one may interpret this answer by thinking of a strongly coupled vacuum as a dielectric medium, with a dielectric constant given by the ratio of the strong coupling result to the zero order Coulomb[2]: potential

$$\epsilon = \frac{V_{Coulomb}}{V_{Maldacena}} = \frac{\sqrt{\lambda}\Gamma(1/4)^4}{8\pi^3} \approx .636\sqrt{\lambda} \tag{3.3}$$

Although in a very qualitative sense this idea is not wrong, it is certainly not literally true. A proof of that are the calculations to be reported below, which shows that the stress tensor distribution in space is very different from that in weak coupling. Of course, this is to be expected, as the strongly coupled vacuum recieves nonperturbative modification from the fields, leading to a nonlinear response.

Now, a decade later, there is a spike of activity of using AdS/CFT to understand properties of the deconfined phase of QCD, known as Quark-Gluon Plasma (QGP) [7]. A number of phenomenological considerations lead to a conjecture [8] that QGP to be in a 'strongly coupled' regime (sQGP) at temperatures not too high above the deconfinement temperature $T = (1-2)T_c$. It is in this domain where RHIC experiments at Brookhaven found a "perfect liquid" properties of sQGP. Among AdS/CFT-based works devoted to it are calculations of the energy loss [14] and stress tensor imprint [17] of the moving objects in thermal CFT plasma. Those are quite spectacular, providing in particular a compete picture justifying another hydrodynamical phenomenon, a "conical flow" in Mach direction around the jet.

Lattice studies of sQGP have also indicated features indicative of a strong coupling regime. Those most relevant for this work obviously are studies of static charge pairs (electric or magnetic). Large deviation from a perturba-

[2]We remind the reader that we include in it exchange due to scalars. It is equal to that from gauge field exchange for quark-antiquark pair, while for two quarks they have the opposite signs and cancel out.

tive picture of a screened Coulombic potential are observed at T above the deconfinement transition T_c. More specifically, many features at $T > 1.5Tc$ suggest a "quasi-conformal" regime, in which all dimensional quantities (e.g. normalized energy density ϵ/T^4) show weak T-dependence.

(Even larger deviations from perturbative approach – the Debye-screened charges – are seen for static dipoles at $T_c < T < 1.5T_c$. Here the entropy and potential energy associated with the string has very large part, linearly growing with distance in some range, see e.g. [42]. The question whether flux tubes – remnants of confining strings – can continue to exist in a plasma phase was recently studied in [43].)

More generally, the dynamics of electric and magnetic gauge fields in a strongly coupled plasma remains very poorly understood. In particular, it has been suggested that sQGP contains large component of magnetically charged quasiparticles – monopoles and dyons, see [9, 44]. Studies of the energy distribution in plasma induced by static dipoles have been extensively done at zero temperature, demonstrating existence of quantum confining string: unfortunately similar calculations at $T > T_c$ are not yet available. One may wander whether the deconfined QCD-like theories in those regimes are or are not similar to the vacuum of $\mathcal{N}$=4 Gauge Theory at strong coupling.

These ideas motivated our present calculation, in which we calculate stress tensor "imprint" of static dipoles in AdS/CFT. A simple diagrammatic picture of what is calculated is provide by Fig.3.2. Apart of the solutions themselves, to be given below in different regimes, there are few particular issues which would like to investigate:
(i) How the dipole is seen at large distances $r \to \infty$? What is the power of distance and its angular distribution? Can it be related to expected behavior of electric and scalar fields?
(ii) What is the field near one of the charges? Can a non-singular part corresponding to the fields of a second charge and polarization cloud be identified?
(iii) Is there a visible remnant of the Matsubara string, or a picture rather is of two polarization clouds? In particular, what is the r.m.s. transverse size $\sqrt{< y_\perp^2 >}$ at $|y| = 0$ (the middle point)?
(iv) We will also consider an electric-magnetic pair: our main interest in that is to see if there is some nontrivial features related with electric-magnetic field interaction.

3.1.1 Strongly coupled versus weakly coupled dipoles

One issue discussed in literature (after AdS/CFT potentials been calculated) was whether some kind of diagram resummation can get the reduction[3] of the coefficient, from $\sim \lambda$ to $\sim \sqrt{\lambda}$. Semenoff and Zarembo[45] have found that one can do so using ladder diagrams[4]. Shuryak and Zahed [47] have noticed that such ladder diagrams in a strongly coupled regime imply a very short correlation time between colors of both charges

$$\delta t \sim L/\lambda^{1/4} \tag{3.4}$$

which will be crucial for understanding of the large-distance field below.

The "imprint" of the pending string on the boundary was first addressed by Callan and Guijosa [46], who had calculated an "image" due to scalar (dilaton) field propagating in the bulk. The boundary operator associated with a dilaton is trF^2. Our work is very close to theirs, except that we calculate much more cumbersome graviton propagation instead of a scalar one, to get the boundary stress tensor.

Their main results was a distribution of scalar density at large distances from a dipole $r \gg L$ (i) has the form

$$trF^2(r) \sim L^3/r^7 \tag{3.5}$$

and (ii) is spherically symmetric. Both are very different from what one finds for the shape of the electric field of a weakly coupled electric dipole, which has (i) power 6 and (ii) has a characteristic dipole energy distribution $(3cos^2(\theta)+1)$ (θ is polar angle from a dipole direction). Our calculation to be reported also will show power 7 but will have more complicated angular distribution.

The reason why the power is 7 rather than 6 was explained by Klebanov,Maldacena and Thorn [48]. Imagine Euclidean time and perturbative diagram, in which perturbative field of each charge can be written as a time integral over a propagator, from a world line of a charge to an observation point: it produces power 6. The nontrivial point is that in strongly coupled regime color time correlation [47] mentioned above require both charges to emit quanta at the *same* time; this changes a double time integral into a single one, adding one more power of the distance.

[3] We remind the reader that we discuss $\lambda \gg 1$ regime.

[4] Which is exact for a round Wilson loop, approximate for rectangular ones.

3.2 Solving the linearized Einstein equations in AdS_5

As is clear from Introduction, the source of gravity in our problem are strings extended into the AdS space. Naturally those are considered to be weak sources, so we will linearize the Einstein equations (with $\Lambda = 6$)

$$R_{\mu\nu} - \frac{1}{2}Rg_{\mu\nu} + \Lambda g_{\mu\nu} = -\kappa^2 T_{\mu\nu} \tag{3.6}$$

(3.6) and solve for small deviations from the unperturbed AdS_5 metric.

We choose to start with another form of (3.6):

$$R_{\mu\nu} + \left(\Lambda - \frac{-\kappa^2 T - \Lambda d}{2-d} g_{\mu\nu}\right) = -\kappa^2 T_{\mu\nu} \tag{3.7}$$

with $d = 5$ Linearizion of the above gives:

$$\delta R_{\mu\nu} - 4\delta g_{\mu\nu} = \delta S_{\mu\nu} \tag{3.8}$$

where $\delta S_{\mu\nu} = -\kappa^2 \left(\delta T_{\mu\nu} - \frac{\delta T}{3} g_{\mu\nu}\right)$

We denote weak gravity perturbation as $\delta g_{\mu\nu} = h_{\mu\nu}$ and use an axial gauge in which the following components vanish $h_{z\mu} = 0$ ($\mu = z, t, x^1, x^2, x^3$). We use the usual Poincare coordinates for the AdS metric:

$$ds^2 = \frac{-dt^2 + d\vec{x}^2 + dz^2}{z^2} \tag{3.9}$$

and set the AdS radius L_{ADS} to 1[5].

Expressing the modifications of curvature $\delta R_{\mu\nu}$ in terms of $h_{\mu\nu}$, (see Appendix.8 for a brief derivation) we get the following equations

$$\frac{1}{2}h_{,z,z} - \frac{1}{2z}h_{,z} = \delta S_{zz} \tag{3.10}$$

$$\frac{1}{2}\left(h_{,m} - h_m\right)_{,z} = \delta S_{zm} \tag{3.11}$$

$$\frac{1}{2}\Box h_{mn} - 2h_{mn} + \frac{z}{2}h_{mn,z} - \frac{1}{2}\left(h_{m,n} + h_{n,m}\right) + \frac{1}{2}\left(h_{,m,n} - \Gamma^z_{mn}h_{,z}\right) = \delta S_{mn} \tag{3.12}$$

[5]Factors of L_{ADS} can be easily reinstated by dimensional analysis.

where we have defined $h = g^{\lambda\sigma}h_{\lambda\sigma}$, $h_m = g^{\lambda\sigma}h_{\lambda m,\sigma}$, $\Box = z^2\left(-\partial_t^2 + \partial_{\vec{x}}^2 + \partial_z^2\right)$, and from now on latin indices stand for 4 boundary coordinates $(m, n = t, x^1, x^2, x^3)$.

We could in principle solve for h from (3.10), the result of which can help to solve for h_m from (3.11). Finally solve for h_{mn} with h,h_m plugged in (3.12). However, we choose to do it in a slightly different way: As (3.11) is first order in z, it is only a constraint equation. With the boundary condition: $h_{mn} = 0$(thus $h = 0$,$h_m = 0$) at $z = 0$, we obtain

$$h_m = h_{,m} - 2\int_0^z \delta S_{zm} dz \tag{3.13}$$

(3.10) is second order in z, but it gives also a constraint when combined with (3.12): Denoting (m, n) as the mn component of (3.12), $-(t, t) + \Sigma_i (x^i, x^i)$ gives:

$$\frac{1}{2}h_{,z,z} - \frac{7}{2z}h_{,z} = -\delta S_{tt} + \Sigma_i \delta S_{x^i x^i} - 2\int \left(-\delta S_{zt,t} + \Sigma_i \delta S_{zx^i,x^i}\right) dz \tag{3.14}$$

Combining (3.10) and (3.14), we obtain the solution for h

$$h = \frac{1}{3}\int_0^z dz \cdot z\left[\delta S_{zz} + \delta S_{tt} - \Sigma_i \delta S_{x^i x^i} + 2\int_0^z dz\left(-\delta S_{zt,t} + \Sigma_i \delta S_{zx^i,x^i}\right)\right] \tag{3.15}$$

With h obtained from (3.15) and h_m eliminated, (3.12) becomes a closed eqn for remaining components:

$$\frac{1}{2}\Box h_{mn} - 2h_{mn} + \frac{z}{2}h_{mn,z} = s_{mn} \tag{3.16}$$

where a "generalized source" is $s_{mn} = \delta S_{mn} - \int_0^z \left(\delta S_{zm,n} + \delta S_{zn,m}\right) dz + \frac{1}{2}h_{,m,n} + \frac{1}{2}\Gamma^z_{mn}h_{,z}$

The source terms created by the string are obtained from the Nambu-Goto action of the string in a standard way

$$\begin{aligned} S_{NG} &= -\frac{1}{2\pi\alpha'}\int d^2\sigma \int d^5x\sqrt{-detg}\delta^{(5)}\left(x - X\left(\sigma\right)\right) \\ \delta T^{\mu\nu} &= \frac{2\delta S_{NG}}{\sqrt{-G}\delta G_{\mu\nu}} \\ &= \frac{-1}{\sqrt{-G}2\pi\alpha'}\int d^2\sigma\delta^{(5)}\left(x - X\left(\sigma\right)\right)\partial_\alpha X^\mu \partial_\beta X^\nu g^{\beta\alpha} \end{aligned} \tag{3.17}$$

here we use $G_{\mu\nu}$ and $g_{\alpha\beta}$ to denote AdS metric and induced metric respectively.

The string world sheet can be described by

$$x^1 = x\left(t, z\right), \; x^2 = x^3 = 0 \tag{3.18}$$

The resulting source is as follows (we use the order of coordinate indices in the following 5-d matrices as t, z, x^1, x^2, x^3 and all absent entries are zeros)

$$\delta S_{\mu\nu} = \frac{-\kappa^2 z}{2\pi\alpha'}\delta\left(x^1 - x\right)\delta\left(x^2\right)\delta\left(x^3\right)\frac{1}{\sqrt{1+x_z^2-x_t^2}}$$
$$\begin{pmatrix} \frac{2x_t^2+x_z^2+1}{3} & x_t x_z & -x_t & & \\ x_t x_z & \frac{x_t^2+2x_z^2-1}{3} & -x_z & & \\ -x_t & -x_z & \frac{x_t^2-x_z^2+2}{3} & & \\ & & & -\frac{2(x_t^2-x_z^2-1)}{3} & \\ & & & & -\frac{2(x_t^2-x_z^2-1)}{3} \end{pmatrix} \tag{3.19}$$

With (3.16),(3.15) and (3.19), we can solve for h_{mn}, provided any explicit profile of the string. We will do this for three different string profiles separately in the following sections, and extract the corresponding stress tensors.

3.3 The stress tensor of a static quark

As a warm up, we will start with the case of a straight string, which corresponds to a single quark in $\mathcal{N}$=4 SYM. The string profile is simply $x\left(t, z\right) = 0$. Substitute in (3.19), we obtain:

$$\delta S_{\mu\nu} = \frac{-\kappa^2 z}{2\pi\alpha'}\delta\left(x^1\right)\delta\left(x^2\right)\delta\left(x^3\right)\begin{pmatrix} \frac{1}{3} & & & & \\ & -\frac{1}{3} & & & \\ & & \frac{2}{3} & & \\ & & & \frac{2}{3} & \\ & & & & \frac{2}{3} \end{pmatrix} \tag{3.20}$$

Static source leads to the metric perturbation h_{mn} which is time-independent. Performing a Fourier transform $h_{mn}^k = \int h_{mn} e^{i\vec{k}\vec{x}} d^3x$ we convert the PDE (3.16) to an ODE:

$$\frac{1}{2}z^2\left(h_{mn,z,z}^k - k^2 h_{mn}^k\right) - 2h_{mn}^k + \frac{z}{2}h_{mn,z}^k = s_{mn}^k \tag{3.21}$$

An upper index k will be used below to indicate a Fourier transformed quantity. $S_{\mu\nu}^k$ is just $S_{\mu\nu}$ without delta functions. h^k and $s_{\mu\nu}^k$ have simple forms

displayed as follows:

$$h^k = -\frac{2}{9}\frac{-\kappa^2}{2\pi\alpha'}z^3 \tag{3.22}$$

$$s^k_{mn} = \frac{-\kappa^2}{2\pi\alpha'}\left[\begin{pmatrix} \frac{2}{3} & & & \\ & \frac{1}{3} & & \\ & & \frac{1}{3} & \\ & & & \frac{1}{3} \end{pmatrix} z + \begin{pmatrix} 0 & & \\ & & \\ & & k_m k_n \end{pmatrix} \frac{z^3}{9}\right] \tag{3.23}$$

The equation is Bessel type and can be dealt with using a Green function built out of such functions. Instead we consider a more general equation with arbitrary power of z in the source

$$\frac{1}{2}z^2\left(h^k_{mn,z,z} - k^2 h^k_{mn}\right) - 2h^k_{mn} + \frac{z}{2}h^k_{mn,z} = c_n z^n \tag{3.24}$$

which is directly solvable in terms of Meijer-G funcion and hypergeometric function:

$$\begin{aligned} h^k_{mn} = I_2(kz)\left(C_2 + G^{2,1}_{1,3}\left(\frac{k^2z^2}{4}\Big|^{1}_{\frac{n}{2}+1,\frac{n}{2}-1,0}\right)\frac{2^{n-1}}{k^n}\right) \\ + K_2(kz)\left(C_1 \, {}_{-1}F_2\left(\begin{matrix}\frac{n}{2}+1 \\ \frac{n}{2}+2,3\end{matrix}\Big|\frac{k^2z^2}{4}\right)\frac{k^2 z^{n+2}}{4n+8}\right) \end{aligned} \tag{3.25}$$

The constants C_1 and C_2 are to be fixed by boundary conditions. One of the condition is the metric perturbation vanishes at AdS boundary, i.e. $h^k_{mn} = 0$ at $z = 0$, which fixes $C_1 = 0$. The other boundary condition proposed in [72] for thermal AdS is incoming metric perturbation at the horizon. However in our case, we need a different boundary condition due to the absence of horizon in AdS. Since h^k grows as z^3 in the present case, while h^k_{mn} show possible exponential growth at large z. It is natural to propose no exponential growth at $z = \infty$ as the boundary condition.

At large z, only the first term containing $I_2(kz)$ is dominant, the boundary condition becomes:

$$C_2 + \frac{2^{n-1}}{k^n}G^{2,1}_{1,3}\left(\frac{k^2z^2}{4}\Big|^{1}_{\frac{n}{2}+1,\frac{n}{2}-1,0}\right) = 0 \tag{3.26}$$

The asymptotic of Meijer-G function ($z \to \infty$) gives:

$$G^{2,1}_{1,3}\left(\frac{k^2z^2}{4}\Big|^{1}_{\frac{n}{2}+1,\frac{n}{2}-1,0}\right) \to \Gamma\left(\frac{n}{2}+1\right)\Gamma\left(\frac{n}{2}-1\right) \tag{3.27}$$

which finally fixes $C_2 = -\frac{c_n 2^{n-1}}{k^n}\Gamma\left(\frac{n}{2}+1\right)\Gamma\left(\frac{n}{2}-1\right)$. Applying it to our source $s_{mn} = c_1 z + c_3 z^3$, where c_1 and c_3 are matrix-valued (the indices are suppressed here), we have $C_2 = \frac{\pi}{k}c_1 - \frac{3\pi}{k^3}c_3$

The stress tensor of the corresponding boundary CFT is proportional to the coefficient of z^2 term, [6] which we denote as Q_{mn} throughout this paper, in small z expansion of h_{mn}. The precise relation can be obtained from (36) of [17], which in our case is simply (with $L_{ADS} = 1$):

$$T_{mn} = \frac{2}{\kappa^2} Q_{mn} \tag{3.28}$$

Note $G^{2,1}_{1,3}\left(\frac{k^2z^2}{4}\Big|^{1}_{\frac{n}{2}+1,\frac{n}{2}-1,0}\right)$ and ${}_1F_2\left(\begin{matrix}\frac{n}{2}+1\\ \frac{n}{2}+2,3\end{matrix}\Big|\frac{k^2z^2}{4}\right) z^{n+2}$ contains only odd power of z for odd n, thus does not contribute to Q_{mn}. We have

$$Q_{mn} = \frac{1}{8}k^2 C_2 \tag{3.29}$$

Reinstate the factor L^2_{ADS}, together with the relation $\frac{L^2_{ADS}}{\alpha'} = \sqrt{\lambda}$, we have the final stress tensor:

$$T^k_{mn} = \frac{-\sqrt{\lambda}}{\pi}\frac{k^2}{8}\left[\begin{pmatrix}\frac{2}{3} & & & \\ & \frac{1}{3} & & \\ & & \frac{1}{3} & \\ & & & \frac{1}{3}\end{pmatrix}\frac{\pi}{k} - \begin{pmatrix}0 & & & \\ & & & \\ & & k_m k_n & \\ & & & \end{pmatrix}\frac{\pi}{3k^3}\right] \tag{3.30}$$

It is easy to verify the stress tensor above is traceless $T_{mn}\eta^{mn} = 0$, which is a consequence of conformal invariance. It also satisfies the conservation of energy and momentum $k^m T_{mn} = 0$. In doing inverse Fourier transform, we find the k-integrals are not well-defined. One trick is to introduce a regulator e^{-ak} $(a > 0)$ to the integral, and take the limit $a \to 0$ in the final answer. We end up with the following result:

$$T_{mn} = \frac{-\sqrt{\lambda}}{\pi}\frac{1}{8\pi}\left[-\frac{2}{3r^4}\begin{pmatrix}1 & & & \\ & 1 & & \\ & & 1 & \\ & & & 1\end{pmatrix} + \begin{pmatrix}0 & & & \\ & & & \\ & & y_m y_n & \\ & & & \end{pmatrix}\frac{4}{3r^6}\right] \tag{3.31}$$

[6] We remind the reader that unperturbed metric has $1/z^2$ and thus the relative smallness is $O(z^4)$ fitting the dimension of the stress tensor.

where r is the distance from the quark. The $\frac{1}{r^4}$ power is obvious by dimension. Let us recall the result obtained in [46][7]

$$\begin{aligned}\mathcal{O}_{F^2} &= \frac{1}{4g_{YM}^2} trF^2 + \cdots = \frac{1}{2g_{YM}^2} tr(-E^2 + B^2) + \cdots \\ &= \frac{1}{32\pi^2}\frac{\sqrt{\lambda}}{r^4}\end{aligned} \tag{3.32}$$

While in our case, the T_{00} component gives

$$\begin{aligned}T_{00} &= \frac{1}{2g_{YM}^2} tr(E^2 + B^2) + \cdots \\ &= \frac{1}{12\pi^2}\frac{\sqrt{\lambda}}{r^4}\end{aligned} \tag{3.33}$$

In both (3.32) and (3.33), the dots represent contributions from scalars and gluinoes. If we assume the magnetic field is not present, the difference in the two operators implies significant contribution are received from the scalars and gluinoes.

3.4 The stress tensor image of static electric dipole

Now we turn to the Maldacena's pending string, the ends of which attached to a quark and antiquark, corresponding to a static electric dipole. The string profile $x(z)$ is double-valued. We use $\pm x(z)$ $(x(z) > 0)$ to denote two halves of the string. The EOM can be integrated to give $x(z)$ in terms of elliptic integrals. We will not refer to explicit form until the end of the calculation.

The source term and its Fourier transformed version are a bit complicated:

$$\begin{aligned}\delta S_{\mu\nu} = &\frac{-\kappa^2 z}{2\pi\alpha'}\delta\left(x^1 - x(z)\right)\delta\left(x^2\right)\delta\left(x^3\right)\frac{1}{\sqrt{1+x_z^2}} \\ &\begin{pmatrix} \frac{x_z^2+1}{3} & & & & \\ & \frac{2x_z^2-1}{3} & -x_z & & \\ & -x_z & \frac{-x_z^2+2}{3} & & \\ & & & \frac{2x_z^2+2}{3} & \\ & & & & \frac{2x_z^2+2}{3} \end{pmatrix} + (x \to -x)\end{aligned} \tag{3.34}$$

[7]There is a typo in eqn (23) of the paper. We quote the corrected expression

$$\delta S^k_{\mu\nu} = \frac{-\kappa^2 z}{2\pi\alpha'}\frac{2}{\sqrt{1+x_z^2}}\Bigg[\begin{pmatrix} \frac{x_z^2+1}{3} & & & & \\ & \frac{2x_z^2-1}{3} & & & \\ & & \frac{-x_z^2+2}{3} & & \\ & & & \frac{2x_z^2+2}{3} & \\ & & & & \frac{2x_z^2+2}{3} \end{pmatrix}\cos(k_1 x)$$
$$+\begin{pmatrix} 0 & 0 & 0 & & \\ 0 & 0 & -x_z & & \\ 0 & -x_z & 0 & & \\ & & & 0 & 0 \\ & & & 0 & 0 \end{pmatrix} i\sin(k_1 x)\Bigg] \tag{3.35}$$

It is understood that the source term vanishes for $z > z_m$. (3.15) and (3.16) gives:

$$h(z < z_m) = \frac{1}{3}\frac{-\kappa^2}{2\pi\alpha'}F(z) \tag{3.36}$$
$$h(z > z_m) = \frac{1}{3}\frac{-\kappa^2}{2\pi\alpha'}\left(F(z_m) + \frac{1}{2}(z^2 - z_m^2)G(z_m)\right) \tag{3.37}$$

$$s^k_{mn}(z < z_m) = \frac{-\kappa^2}{2\pi\alpha'}\Bigg[\frac{1}{3}E_1(z)\begin{pmatrix} 1 & & & \\ & -1 & & \\ & & 2 & \\ & & & 2 \end{pmatrix} + \frac{1}{3}E_2(z)\begin{pmatrix} 1 & & & \\ & -1 & & \\ & & 2 & \\ & & & 2 \end{pmatrix}$$
$$+H(z)\begin{pmatrix} 0 & & & \\ & 2k_1 & k_2 & k_3 \\ & k_2 & & \\ & k_3 & & \end{pmatrix} - \frac{1}{3}F(z)\begin{pmatrix} 0 & & & \\ & \frac{k_m k_n}{2} & & \\ & & & \end{pmatrix} + \frac{F'(z)}{6z}\begin{pmatrix} -1 & & & \\ & 1 & & \\ & & 1 & \\ & & & 1 \end{pmatrix}\Bigg] \tag{3.38}$$

$$s^k_{mn}(z > z_m) = \frac{-\kappa^2}{2\pi\alpha'}\Bigg[H(z_m)\begin{pmatrix} 0 & & & \\ & 2k_1 & k_2 & k_3 \\ & k_2 & & \\ & k_3 & & \end{pmatrix} - \frac{1}{3}\left(F(z_m) + \frac{1}{2}(z^2 - z_m^2)G(z_m)\right)$$
$$\begin{pmatrix} 0 & & & \\ & \frac{k_m k_n}{2} & & \\ & & & \end{pmatrix} + \frac{G(z_m)}{6}\begin{pmatrix} -1 & & & \\ & 1 & & \\ & & 1 & \\ & & & 1 \end{pmatrix}\Bigg] \tag{3.39}$$

with

$$
\begin{aligned}
E_1(z) &= \frac{2z}{\sqrt{1+x_z^2}} x_z^2 \cos(k_1 x) \\
E_2(z) &= \frac{2z}{\sqrt{1+x_z^2}} \cos(k_1 x) \\
F(z) &= \int_0^z \frac{-4\cos(k_1 x)}{\sqrt{1+x_z^2}} z^2 dz + \int_0^z dz \left(z \int_0^z \frac{-4\sin(k_1 x)}{\sqrt{1+x_z^2}} z k_1 x_z dz \right) \\
G(z_m) &= \int_0^{z_m} \frac{-4\sin(k_1 x)}{\sqrt{1+x_z^2}} z k_1 x_z dz \\
H(z) &= \int_0^z \frac{2z\sin(k_1 x)}{\sqrt{1+x_z^2}} x_z dz
\end{aligned} \tag{3.40}
$$

With the explicit expression of s^k_{mn}, we can build the general solution to (3.16):

$$
\begin{aligned}
h^k_{mn} &= I_2(kz)C_2 + K_2(kz)C_1 + 2\big[I_2(kz)\int_{z_m}^z \frac{s^k_{mn}(z)K_2(kz)}{z} dz \\
&- K_2(kz)\int_{z_m}^z \frac{s^k_{mn}(z)I_2(kz)}{z} dz\big]
\end{aligned} \tag{3.41}
$$

At large z, no exponential growth condition requires $C_2 + 2\int_{z_m}^{\infty} \frac{s^k_{mn}(z)K_2(kz)}{z} dz = 0$. The convergence of the integral is ensured by $K_2(kz)$ in the integrand. At small z, $s^k_{mn} \sim O(z)$ while $I_2(kz) \sim O(z^2)$ the integral containing $I_2(kz)$ is finite as z approaches 0, therefore the boundary condition gives: $C_1 - 2\int_{z_m}^0 \frac{s^k_{mn}(z)I_2(kz)}{z} dz = 0$.

In order to extract the stress tensor, we need to collect z^2 terms. It is helpful to write down the series expansion of the two integrals

$$
\int_{z_m}^z \frac{s^k_{mn}(z)I_2(kz)}{z} dz = a_0 + a_1 z + \cdots \tag{3.42}
$$

$$
\int_{z_m}^z \frac{s^k_{mn}(z)K_2(kz)}{z} dz = \frac{b_{-1}}{z} + b_0 + \cdots \tag{3.43}
$$

The coefficient of z^2 is given by: $Q_{mn} = \frac{1}{8}k^2 C_2 + \frac{k^2}{4} b_0$. Note C_1 does not appear in the expression We may also write it as

$$
Q^k_{mn} = -\frac{k^2}{4}\int_{z_m}^{\infty} \frac{s^k_{mn}(z)K_2(kz)}{z} dz + \frac{k^2}{4}\lim_{\epsilon\to 0}\left(\int_{z_m}^{\epsilon} \frac{s^k_{mn}K_2(kz)}{z} dz - \frac{b_{-1}}{\epsilon}\right) \tag{3.44}
$$

We could proceed in momentum space. However it turns out to be much easier and illustrating to do inverse Fourier transform and continue in configuration space from now on.

A nice property of Fourier transform is $\mathcal{F}^{-1}(F(k)G(k)) = \int f(x)g(y-x)dx$. Identifying the source dependent s^k_{mn} as $F(k)$, the inverse Fourier transform of which gives $f(x)$. Correspondingly, each $G(k)$ is transformed to $g(y-x)$. The latter can be interpreted as a propagator from a point on the source x to a point on the boundary y. With this in mind, we define the following propagator:

$$P_s(\vec{y}-\vec{x}) = \frac{1}{(2\pi)^3}\int k^2 K_2(kz)e^{-i\vec{k}\vec{x}}d^3k = \frac{15}{4\pi}\frac{z^2}{(z^2+r^2)^{\frac{7}{2}}} \tag{3.45}$$

Let us take a moment to worry about the term involving b_{-1}. By analyzing small z behavior of s_{mn} and $I_2(kz)$, we find $b_{-1} = \frac{\#}{k^2}$. Inverse Fourier transform of $\frac{k^2}{4}b_{-1}$ is not well-defined. Again we introduce the same regulator e^{-ak} as in the previous section. We find a vanishing result after taking the limit $a \to 0$ [8]

Finally, we can write the stress tensor in a very short form:

$$\begin{aligned} Q_{mn} &= -\frac{1}{4}\int_{z_m}^{\infty} dz \int \frac{s_{mn}(z,\vec{x})P_s(\vec{y}-\vec{x})}{z}d^3x \\ &+\frac{1}{4}\int_{z_m}^{0} dz \int \frac{s_{mn}(z,\vec{x})P_s(\vec{y}-\vec{x})}{z}d^3x \end{aligned} \tag{3.46}$$

Before proceeding with the calculation, we would like to make few general comments: (i) The trace of the stress tensor is given by the coefficient of z^4 term of h. From (3.36), we find that $h \sim F(z)$ at small z does *not* contain z^4 term, therefore we expect the final stress tensor to be *traceless*, which is also required by conformal invariance. (ii) The divergence of the stress tensor $\partial_\lambda T_{\lambda m}$ turns out to be the the coefficient of z^4 term of h_m. From (3.13) and (3.36) we conclude $\partial_\lambda T_{\lambda m} = \frac{\sqrt{\lambda}}{\pi}\frac{1}{2z_m^2}\left(\delta(x^1-x_m)-\delta(x^1+x_m)\right)\delta(x^2)\delta(x^3)\delta_{m1}$. The divergence is non-vanishing only for $m = x^1$ at the end points of the string where the quark and antiquark are placed. It corresponds to a pair of antiparallel forces which hold quark and antiquark, preventing them from falling onto each other. This will be another general condition to be satisfied by the stress tensor.

[8] this may seems problematic. Actually the same regularization can also be applied to $K_2(kz)$ if we first expand it in series of k. The non-vanishing terms match those obtained from series expansion of propagator P_s in r

3.4.1 Far field

With (3.46) at hand, we first calculate the stress tensor in region far from the dipole. The inverse Fourier transforms of s_{mn} are linear combinations of those of E_1, E_2, F, G, H. Such terms as $k_m H$ can be replaced by $i\partial_{x_m} H = -i\overleftarrow{\partial}_{x_m} H = i\overleftarrow{\partial}_{y_m}$. In the first identity, we use partial integration so that the derivative only acts on the propagators (we indicate this with a left arrow on top of the derivative). The second identity is due to $P_s = P_s(\vec{y}-\vec{x})$. Similarly, $k_m k_n F \to -\overleftarrow{\partial}_{x_m}\overleftarrow{\partial}_{x_n} F \to -\overleftarrow{\partial}_{y_m}\overleftarrow{\partial}_{y_n} F$

We list the back-transformed result of E_1, E_2, F, G, H here:

$$E_1 = \frac{z^5}{z_m^2\sqrt{z_m^4 - z^4}}\delta(x^2)\delta(x^3)\delta(x^1 - x(z)) + (x^1 \to -x^1) \tag{3.47}$$

$$E_2 = \frac{z\sqrt{z_m^4 - z^4}}{z_m^2}\delta(x^2)\delta(x^3)\delta(x^1 - x(z)) + (x^1 \to -x^1) \tag{3.48}$$

$$F = \frac{4}{z_m^2}\delta(x^2)\delta(x^3)\frac{-(z^2 - z_1^2)(z_m^4 - 3z_1^4)}{4z_1^2}\theta(z - z_1) + (x^1 \to -x^1) \tag{3.49}$$

$$G = \frac{4}{z_m^2}\delta(x^2)\delta(x^3)\Big[- \frac{z_m^4 - 3z_1^4}{2z_1^2}\theta(z - z_1) + \frac{z_m^4 - z_1^4}{2z_1}\delta(z - z_1)\Big]$$
$$+(x^1 \to -x^1) \tag{3.50}$$

$$H = -\frac{1}{z_m^2}\delta(x^2)\delta(x^3)\frac{z_1\sqrt{z_m^4 - z_1^4}}{i}\theta(z - z_1) - (x^1 \to -x^1) \tag{3.51}$$

with $z_1 = z_1(x^1)\,(0 < x^1 < x_m)$, the inverse function of $x(z)$. Contribution from negative x^1 is included in the second term for each function. Note E_1, E_2, F, G are symmetric in x^1, while H is antisymmetric.

In order to obtain the far field stress tensor, we need to perform a large $|y|$ expansion of the stress tensor. Note the y-dependence enters the stress tensor via the propagator, we can do a large $|y|$ expansion on the propagator in the second term since $z < z_m \ll |y|$. While for the first integral, z extending to infinity, we need to do the integral first before a valid expansion is possible. Fortunately this time the source has very simple z-dependence: $s_{mn}(z) = \# + \#z^2$. The rest of the calculation is straight forward. After collecting all terms, we find the first nontrivial result appears at the order $\frac{1}{|y|^7}$. The power again agree with the result of trF^2 obtained in [46]. We list the stress tensor as follows (up to the order $\frac{1}{|y|^7}$):

$$T_{00} = \frac{1}{4}\frac{-\sqrt{\lambda}}{\pi}\frac{15}{4\pi}\left[\frac{a_G(7y_1^2 - y^2)}{12|y|^9} + \left(\frac{a_{E1}}{3} + \frac{a_{E2}}{3} + \frac{a_F}{6}\right)\frac{1}{|y|^7}\right] \tag{3.52}$$

$$T_{0m} = 0 \tag{3.53}$$

$$T_{mn} = \frac{1}{4}\frac{-\sqrt{\lambda}}{\pi}\frac{15}{4\pi}\left[\left(-7a_H + \frac{7}{6}a_G\right)\begin{pmatrix} 2y_1 & y_2 & y_3 \\ y_2 & & \\ y_3 & & \end{pmatrix}\frac{y_1}{|y|^9} + \frac{2}{3}\left(a_{E1} + a_{E2}\right)\delta_{mn}\frac{1}{|y|^7}\right.$$
$$\left. - \left(a_{E1} + \frac{a_G}{6} - 2a_H\right)\begin{pmatrix} 1 & 0 & 0 \\ 0 & & \\ 0 & & \end{pmatrix}\frac{1}{|y|^7} - \left(\frac{7a_F}{6} - \frac{7a_G}{12}\right)\frac{y_m y_n}{|y|^9} - \frac{21a_G}{4}\frac{y_m y_n y_1^2}{|y|^{11}}\right] \tag{3.54}$$

with

$$a_G = 2\int_0^{x_m} G(z_m)\left(x^1\right)^2 dx^1 = -0.7189 z_m^3$$
$$a_F = 2\int_0^{x_m} F(z_m) dx^1 = -0.9585 z_m^3$$
$$a_H = 2\int_0^{x_m} H(z_m) x^1 dx^1 = 0.1797 z_m^3$$
$$a_{E1} = \int_{z_m}^0 E_1(z) dz = -0.7189 z_m^3$$
$$a_{E2} = \int_{z_m}^0 E_2(z) dz = -0.4793 z_m^3$$

We can verifiy explicitly that the stress tensor is traceless and divergence-free at this order.

Now we proceed to analysis of the results, describing which features are general and should be expected and which of them are qualitatively new.

A vanishing energy flux (Poynting vector) $T_{0m} = 0$ is related with zero magnetic field expected for static electric configuration. Indeed, a time reversal would change the sign of the magnetic field and the Poynting vector, but leaves the problem invariant.

Having said that, we by no means imply that the only field in question is the electric field. Indeed, vacuum polarization should include all other fields of the theory, and perturbatively we know that all color fields of the theory – gluinoes and scalars – should contribute, to charge polarization density as well

as to the energy we calculate. However, a very simplistic view of the scalars[9] based on $(\partial_\mu \phi)^2$ Lagrangian would produce the same distributions as a vector field, since that can be viewed as just generated by another scalar field A_0.

The obvious point of comparison is stress tensor distribution for a perturbative dipole. Its electric field

$$E_m(y) = (\frac{g^2}{4\pi}) \left(\frac{y_m - (L/2)e_m}{|y_m - (L/2)e_m|^3} - \frac{y_m + (L/2)e_m}{|y_m + (L/2)e_m|^3} \right) \tag{3.55}$$

leads to stress tensor which is at large distances $\sim L^2/y^6$. The result we obtain is $\sim L^3/r^7$: the difference is due to the a phenomenon of "short-time-color-locking" [47, 48] we already discussed in the Introduction. Perhaps another way to explain it is to say that a scalar density, induced by a dipole, is large in all the volume $\sim L^3$.

Let us now comment on the angular distribution. Perturbative dipole field at large distances contains the first power of the dipole vector: thus its angular momentum is 1. Energy density constructed out of this field, obviously has only angular momenta 2 and 0, or powers of $cos^n(\theta)$ with $n = 0, 2$. Stress tensor also contains such components, but also terms of the type $T_{mn} \sim y_m y_n (\vec{L}\vec{y})^2$. Looking at our result we find that indeed *no other* angular structures appeared. This is to be expected, as electric field is still the only vector field of the theory. The angular distribution of the far field energy is compared to the perturbative result in Fig.3.1: although there is tendency to a more spherical distribution (like obtained for scalar density [46]), the peaks in the dipole directions are still there.

One more simple case to discuss is the stress tensor on a line connecting the charges: by symmetry transverse component of the field $\vec{E}_\perp = 0$ and only E_x remains. The Maxwellian tensor then should satisfy $T_{22} = T_{33} = -T_{11} = T_{00}$: and the result we obtain does not satisfy it. We thus see once again, that gluino and scalar parts of the stress tensor *must* contribute to the far field asymptotic in question.

3.4.2 A field near one charge

Next we would like to study the stress tensor near one of the charge. For this purpose, we make a shift of variables $y_1 \to y_1 + x_m$, $y_2 \to y_2$, $y_3 \to y_3$, and consider small $|y|$ behavior of the stress tensor.

It is clear from the single charge result(3.31) the stress tensor will blow up as $|y| \to 0$, so to the leading order in $|y|$, we may focus on its divergent part

[9] Ignoring quartic terms with commutators of various flavor components.

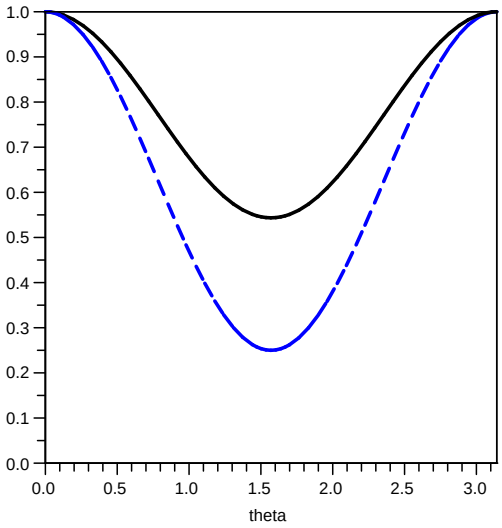

Figure 3.1: (Color online) The far field energy distribution in polar angle $\theta(cos(\theta) = y_1/|y|)$, normalized at zero angle. Solid (black) line is our result, compared to the perturbative result $(3cos^2 + 1)/4$ given by the dashed (blue) line.

only.

Let us recall the basic expression for the stress tensor:

$$Q_{mn} = -\frac{1}{4}\int_{z_m}^{\infty} dz \int \frac{s_{mn}(z,\vec{x})P_s(\vec{y}-\vec{x})}{z} d^3x$$
$$+\frac{1}{4}\int_{z_m}^{0} dz \int \frac{s_{mn}(z,\vec{x})P_s(\vec{y}-\vec{x})}{z} d^3x \qquad (3.56)$$

As $|y| \to 0$, the first term is finite($z > z_m$), which we ignore as discussed above. While the propagator in the second term $P_s = \frac{15}{4\pi}\frac{z^2}{(z^2+r^2)^{\frac{7}{2}}}$ contains a singularity at $z = 0$, $r = 0$, which leads to a possible divergence in stress tensor(unless the source provide enough powers of z). We can also claim the divergence is from integration at small z. Since the integral involving s_{mn} and P_s cannot be done analytically, a careful analysis is needed to obtain the leading terms in Laurent expansion of the stress tensor.

We first use the common factor $\delta(x^2)\delta(x^3)$ in the source to simplify the

propagator:

$$r^2 = (y_1 + x_m - x^1)^2 + (y_2 - x^2)^2 + (y_3 - x^3)^2 = (y_1 - \Delta x)^2 + y_2^2 + y_3^2$$
$$= r_0^2 - 2y_1\Delta x + \Delta x^2$$

with $r_0^2 = y_1^2 + y_2^2 + y_3^2$, $\Delta x = x^1 - x_m$. Then the propagator can be expanded in Δx^1:

$$P_s = \frac{15}{4\pi}\left(\frac{z^2}{(z^2 + r_0^2)^{\frac{7}{2}}} - 7\frac{z^3}{(z^2 + r_0^2)^{\frac{9}{2}}}y_1\Delta x^1 + \cdots\right) \tag{3.57}$$

Note the leading term of the propagator does not depend on x^1, x^2, x^3. A similar trick is used as in the case of far field: $k_m = -i\overleftarrow{\partial}_{x_m} = i\overleftarrow{\partial}_{y_m}$. The second identity is due to $P_s = P_s(\vec{y} - \vec{x})$. If only the leading order result of the stress tensor is needed, we perform the x-integral with the source, keeping the smallest power in z(As we argued before smaller power of z corresponds to larger term in expansion of the stress tensor):

$$\int E_1 d^3x \sim \frac{z^5}{z_m^4}$$
$$\int E_2 d^3x \sim z$$
$$\int F d^3x \sim -z_m^2 \int (z^2 - z_1^2)\theta(z - z_1)dx^1 = -\frac{2}{3}z^3$$
$$\int \frac{F'}{z} d^3x \sim -2z_m^2 \frac{z}{z_1^2}\theta(z - z_1)dx^1 = -2z$$
$$\int -iH d^3x \sim z_1\theta(z - z_1)dx^1 = \frac{z^4}{4z_m^2}$$

Convolute the above results with the leading order propagator, we find they give the following divergence:

$$E_1 \to ln(r_0)$$
$$E_2, \frac{F'}{z} \to \frac{1}{r_0^4}$$
$$F \to \frac{1}{r_0^2}$$
$$iH \to \frac{1}{r_0}$$

Therefore the leading order result is given by $E_2, \frac{F'}{z}$ and F. The last also give $\frac{1}{r_0^4}$ when combined with the double derivatives in the coefficient. Collecting all the contributions, we find the leading near field contribution, which is of course precisely the stress tensor of a single charge (3.31)

$$T^{LO}_{mn} = \frac{-\sqrt{\lambda}}{\pi}\frac{1}{8\pi}\left[-\frac{2}{3r_0^4}\begin{pmatrix}1 & & & \\ & 1 & & \\ & & 1 & \\ & & & 1\end{pmatrix} + \begin{pmatrix}0 & & & \\ & & & \\ & & y_m y_n & \\ & & & \end{pmatrix}\frac{4}{3r_0^6}\right] \tag{3.58}$$

The aim now is to extend the analysis to the next order correction to (3.58). Note the correction from the source will give at least $O(z^4)$ correction, while that from the propagator is of $O(\Delta x^1) \sim z_1^3 \sim z^3$, with an additional $z^2 + r_0^2$ in the denominator. As a result, we can keep the leading order source but care about the correction from the propagator when necessary. Finally we find the next order correction to the stress tensor is from the LO source $E_2, F, \frac{F'}{z}$ convoluted with the NLO correction to the propagator $-7\frac{z^3}{(z^2+r_0^2)^{\frac{9}{2}}}y_1\Delta x^1$, as well as the leading result from iH. We display the correction to the near field as follows:

$$T^{NLO}_{mn} = \frac{-\sqrt{\lambda}}{\pi}\frac{1}{12\pi}\frac{1}{z_m^2}\left[\frac{y_1}{6r_0^3}\begin{pmatrix}5 & & & \\ & 8 & & \\ & & 8 & \\ & & & 8\end{pmatrix} - \begin{pmatrix}0 & & & \\ & 2y_1 & y_2 & y_3 \\ & y_2 & & \\ & y_3 & & \end{pmatrix}\frac{4}{3r_0^3}\right.$$
$$\left. - \begin{pmatrix}0 & & & \\ & & & \\ & & y_m y_n & \\ & & & \end{pmatrix}\frac{y_1}{2r_0^5}\right] \tag{3.59}$$

We can also verify the stress tensor at this order is traceless and divergence-free.

Let us now analyze the results and compare it with expectations. In general one can expect that close to the charge there is a singular electric field $E^{sing} \sim 1/r_0^2$ plus a finite field induced by all other charges.

$$E_i E_j \approx E_i^{sing} E_j^{sing} + E_i^{sing} E_j^{reg} + E_j^{sing} E_i^{reg} + ... \tag{3.60}$$

The scalar field in weak coupling add the same distributions.

If the vacuum would be a simple dielectric, both the singular and regular field would be just free fields times the dielectric constant (3.3), and the relative correction be the same. Let us see whether this idea works or not. In weak

coupling[10] the correction to T_{00} is $1-2(y_1 r)/L^2$ while our strong coupling result gives

$$\frac{T_{00}}{T_{00}^{LO}} = 1 - \frac{(y_1 r)}{z_m^2} \approx 1 - 0.34\frac{2(y_1 r)}{L^2} \tag{3.61}$$

The sign and the structure of the local field is the same, while the magnitude is additionally reduced by about a factor 1/3. What we learn from this comparison, once again, is that although a strongly coupled vacuum of the theory works as a polarizable dielectric qualitatively, this is not true literally.

3.4.3 Is there a visible trace of the string?

Another interesting question is the transverse distribution of energy. In particular we calculate the r.m.s.: $\sqrt{< y_2^2 >} = \left(\frac{\int T_{00} y_2^2 dy_2}{\int T_{00} dy_2}|_{y_1=y_3=0}\right)^{\frac{1}{2}}$, which characterizes the transverse energy distribution on the middle plane between the quark-antiquark pair.

$$\begin{aligned} T_{00} \sim Q_{00} &= \frac{1}{4}\int_{\infty}^{0} dz \int \frac{s_{00}(z,\vec{x}) P_s(\vec{y}-\vec{x})}{z} d^3x \\ s_{00}(z<z_m) &\sim \frac{E_1(z)}{3} + \frac{E_2(z)}{3} - \frac{F'(z)}{6z} \\ s_{00}(z>z_m) &\sim -\frac{G(z_m)}{6} \end{aligned} \tag{3.62}$$

Note y-dependence enters only through the propagator P_s, we can do the y_2 integral with the propagator first, then convolute the result with the source s_{00}. The rest of the calculation is straight forward. We will skip the details and only give the result: $\sqrt{< y_2^2 >} \approx 0.41 z_m$, while half the size of the dipole is $\frac{L}{2} \approx 0.60 z_m$. The r.m.s. is about $\frac{1}{3}$ of the dipole size, smaller than the perturbative result $\sqrt{< y_2^2 >} = \frac{L}{2}$.

In order to make the trace of string clear, we would like to rewrite (3.46) in a more physical form. This is done by defining: $s^h_{mn} = s_{mn} - S_{mn}$, then we

[10] There are both gauge and scalar fields, but distributions they produced in zeroth order are the same.

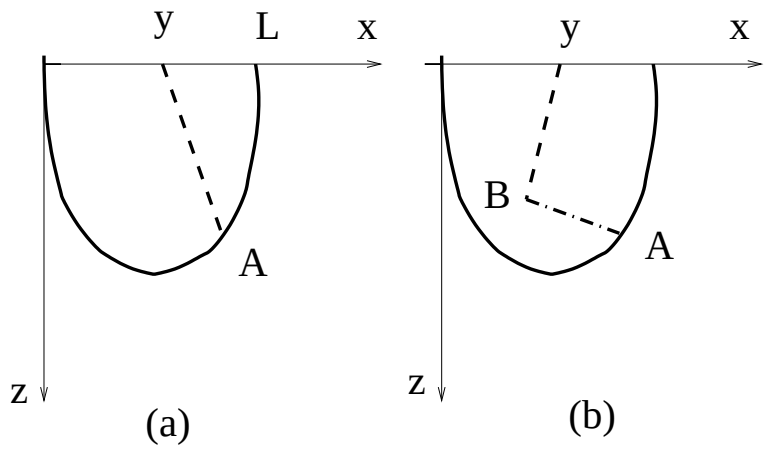

Figure 3.2: (color online) Schematic demonstration of the pending string and the propagators of stress tensor. The source is at the point A integrated over string, it either (a) goes directly to the observation point y via bulk-to-boundary propagates(dashed line) , or (b) first transforms to s^h_{mn} in some other point B via bulk-to-bulk propagator(dash-dotted line), then goes to the observation point

have

$$Q_{mn} = -\frac{1}{4}\int_0^\infty dz \int \frac{S_{mn}(z,\vec{x})P_s(\vec{y}-\vec{x})}{z} d^3x$$
$$-\frac{1}{4}\int_0^\infty dz \int \frac{s^h_{mn}(z,\vec{x})P_s(\vec{y}-\vec{x})}{z} d^3x \tag{3.63}$$

The first piece is sourced by the original string S_{mn}, while the second piece corresponds to contribution from s^h_{mn}. Since the latter is obtained from $S_{\mu\nu}$ via (3.15) and (3.13). The transform from $S_{\mu\nu}$ to s^h_{mn} can be interpreted as a bulk-to-bulk propagator, which is then attached to the bulk-to-boundary propagator P_s to contribute to the stress tensor. We schematically illustrate the two contributions in Fig.3.2

We use the component T_{00} as an example to study the relative contribution from the two pieces:

$$
\begin{aligned}
Q^1_{00} &= -\frac{1}{4}\int_0^\infty dz \int \frac{S_{mn}(z,\vec{x})P_s(\vec{y}-\vec{x})}{z} d^3x \\
&= \frac{-1}{6}\int_0^{z_m} \frac{z\left(\frac{z^5}{z_m^2\sqrt{z_m^4-z^4}} + \frac{z\sqrt{z_m^4-z^4}}{z_m^2}\right)}{(z^2+x(z)^2)^{\frac{7}{2}}} \qquad (3.64) \\
Q^2_{00} &= -\frac{1}{4}\int_0^\infty dz \int \frac{s^h_{mn}(z,\vec{x})P_s(\vec{y}-\vec{x})}{z} d^3x \\
&= \frac{-1}{6}\int_0^\infty dz \int_0^{x_m} dx^1 \frac{z_m^4-3z_1^4}{z_1^2}\theta(z-z_1)\frac{z}{(z^2+(x^1)^2)^{\frac{7}{2}}} \\
&= \frac{-1}{6}\int_0^{z_m} \frac{z_m^4-3z_1^4}{\sqrt{z_m^4-z_1^4}z_m^2}\frac{1}{5(z_1^2+x^1(z_1)^2)^{\frac{5}{2}}} \qquad (3.65)
\end{aligned}
$$

We plot the integrands of (3.64) in Fig.3.3. All three curves have a peak at $z = z_m$, which is due to geometry of the string. However the peaks are square root singularities of geometric origin, which do not contribute significantly to the integral and the finial T_{00}. Instead the latter receives significant contribution from integration of all values of z.

3.5 A field of electric-magnetic dipole

It is also interesting to consider the stress tensor of an quark and monopole, in which case both electric and magnetic fields are obviously present. The string profile of the electric-magnetic dipole is obtained by Minahan[41]. It consists of a $(1,0)$ and a $(0,1)$ string, attached to the quark and monopole at $z=0$ respectively, and a $(1,1)$ string extending from $z=\infty$. The three string attach to each other at $z=z_0$, forming a Y-junction. With a suitable choice of coordinate, we can describe the $(1,1)$ string by $x^1=0$, and describe the $(1,0)$ string and $(0,1)$ string profile by $x^1 = x(z_{m1},z) > 0$ and $x^1 = -x(z_{m2},z) < 0$, where z_{m1}, z_{m2} are parameters of the string profile $x(z)$. $x(z_m,z)$ satisfies $x_z = -\frac{z^2}{\sqrt{z_m^4-z^4}}$. The parameters given by [41] are:

$$
\begin{aligned}
z_{m1} &= z_0\alpha_1 \qquad (3.66) \\
z_{m2} &= z_0\alpha_2 \qquad (3.67) \\
\alpha_1 &= \left(\frac{1+t^2}{t^2}\right)^{\frac{1}{4}} \quad \alpha_2 = \left(1+t^2\right)^{\frac{1}{4}}
\end{aligned}
$$

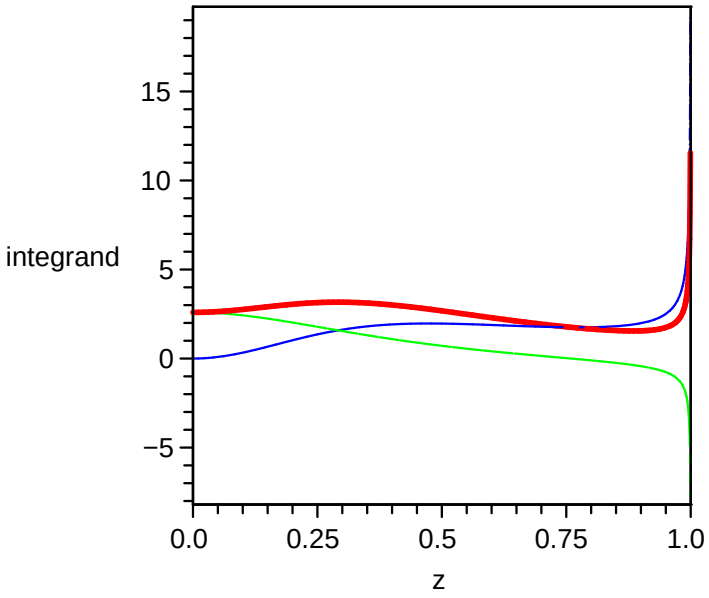

Figure 3.3: (color online) The integrands of the z integral along the string for Q^1_{00}(blue dotted),Q^2_{00} (green dashed) and their sum(red solid), with $z_m = 1$

where $t = \frac{1}{g}$, g is the string coupling.

The action of a (p, q) string is given by:

$$S_{NG} = -\frac{\sqrt{p^2 + q^2 t^2}}{2\pi\alpha'} \int d^2\sigma \sqrt{-detg} \tag{3.68}$$

The $\delta S_{\mu\nu}$ following from the action is:

$$\delta S_{\mu\nu}(z<z_0)=\frac{-\kappa^2 z}{2\pi\alpha'}\delta(x^1-x(z_{m1},z))\delta(x^2)\delta(x^3)\frac{1}{\sqrt{1+x_z^2}}$$
$$\begin{pmatrix}\frac{x_z(z_{m1},z)^2+1}{3} & & & & \\ & \frac{2x_z(z_{m1},z)^2-1}{3} & -x_z(z_{m1},z) & & \\ & -x_z(z_{m1},z) & \frac{-x_z(z_{m1},z)^2+2}{3} & & \\ & & & \frac{2x_z(z_{m1},z)^2+2}{3} & \\ & & & & \frac{2x_z(z_{m1},z)^2+2}{3}\end{pmatrix}$$
$$+\left(x(z_{m1},z)\to -x(z_{m2},z)\right)t$$
$$\delta S_{\mu\nu}(z>z_0)=\frac{-\kappa^2 z}{2\pi\alpha'}\delta(x^1)\delta(x^2)\delta(x^3)\begin{pmatrix}\frac{1}{3} & & & & \\ & -\frac{1}{3} & & & \\ & & \frac{2}{3} & & \\ & & & \frac{2}{3} & \\ & & & & \frac{2}{3}\end{pmatrix}\sqrt{1+t^2} \quad (3.69)$$

We are not going to elaborate the calculation in any detail, as the same procedures for the electric dipole's case apply. The far-field answer is

$$T_{mn}=\frac{-\sqrt{\lambda}}{\pi}\frac{1}{8\pi}\left[-\frac{2}{3|y|^4}\begin{pmatrix}1 & & \\ & 1 & \\ & & 1\end{pmatrix}+\begin{pmatrix}0 & & \\ & y_m y_n & \\ & & \end{pmatrix}\frac{4}{3|y|^6}\right]\sqrt{1+t^2} \quad (3.70)$$

Different from the case of electric dipole, in which the leading total charge term drops out, the leading order now is $\frac{1}{|y|^4}$. The result is proportional to $\sqrt{\lambda(1+t^2)}=\sqrt{N(g_{YM}^2+(4\pi)^2/g_{YM}^2)}$, in good agreement with electric-magnetic duality[11] of the problem. This shows the electric-magnetic dipole looks like a dyon to distant observer.

Perturbatively one expect no correlation between electric and magnetic charges, and the answer proportional to a sum $N(g_{YM}^2/4\pi+4\pi/g_{YM}^2)$, *without* a square root. The reason a common square root appears can again be traced to color correlation time by Shuryak and Zahed: for example they have also shown that Coulomb, spin-spin and spin-orbit forces are also united into one common square root [40].

For the near field, we recall the calculation of the previous section. the LO

[11] We remind the reader that Dirac condition in this theory is simply that magnetic charge is the inverse of the electric one.

stress tensor near the quark(monopole) is again the same as that of a single quark(monopole). the NLO stress tensor only depend on the profile of the string attached to the quark(monopole). Therefore, we can obtain the stress tensor by the substitution: $z_m \to z_{m1}$(quark), $z_m \to z_{m2}$(monopole). We display the NLO near field result for the quark and monopole in (3.71),(3.72).

$$T_{mn} = \frac{-\sqrt{\lambda}}{\pi}\frac{1}{12\pi}\frac{1}{z_{m1}^2}\Bigg[\frac{y_1}{6r_0^3}\begin{pmatrix}5 & & & \\ & 8 & & \\ & & 8 & \\ & & & 8\end{pmatrix} - \begin{pmatrix}0 & & & \\ & 2y_1 & y_2 & y_3 \\ & y_2 & & \\ & y_3 & & \end{pmatrix}\frac{4}{3r_0^3}$$
$$- \begin{pmatrix}0 & & \\ & & \\ & y_m y_n & \end{pmatrix}\frac{y_1}{2r_0^5}\Bigg] \tag{3.71}$$

$$T_{mn} = \frac{-\sqrt{\lambda}}{\pi}\frac{1}{12\pi}\frac{t}{z_{m2}^2}\Bigg[-\frac{y_1}{6r_0^3}\begin{pmatrix}5 & & & \\ & 8 & & \\ & & 8 & \\ & & & 8\end{pmatrix} + \begin{pmatrix}0 & & & \\ & 2y_1 & y_2 & y_3 \\ & y_2 & & \\ & y_3 & & \end{pmatrix}\frac{4}{3r_0^3}$$
$$+ \begin{pmatrix}0 & & \\ & & \\ & y_m y_n & \end{pmatrix}\frac{y_1}{2r_0^5}\Bigg] \tag{3.72}$$

The result at NLO suggests the impact of a monopole to the quark is the same as an antiquark at some distance away. The precise relation between the quark-monopole distance L_{QM} and quark-antiquark distance $L_{Q\bar{Q}}$ can be estimated. $L_{Q\bar{Q}}$ should be chosen such that z_m reproduce z_{m1} for L_{QM}. (2.6) and (3.2) of [41] gives:

$$
\begin{aligned}
L_{Q\bar{Q}} &= 2z_m \int_1^\infty \frac{dy}{y^2\sqrt{y^4-1}} \\
L_{QM} &= z_0 \left(\alpha_1 \int_{\alpha_1}^\infty \frac{dy}{y^2\sqrt{y^4-1}} + \alpha_2 \int_{\alpha_2}^\infty \frac{dy}{y^2\sqrt{y^4-1}} \right) \\
&\approx z_0 \alpha_1 \int_1^\infty \frac{dy}{y^2\sqrt{y^4-1}} \\
&= \frac{1}{2} L_{Q\bar{Q}}
\end{aligned} \tag{3.73}
$$

where the approximation is due to the limit $g \to 0,\ t \to \infty$. The result shows that in the above limit, the quark feels the monopole like an antiquark at twice the distance. Similarly, the monopole feels the quark at a distance L like an antimonopole $\frac{2\alpha_2}{\alpha_1} L = \frac{2}{\sqrt{g}} L$ away.

Finally, let us address the ussue of the angular momentum and Poynting vector. Perturbative charge-monopole pair has at a generic point electric and magnetic fields crossing at some angle, thus producing a nonzero Poynting vector $T_{0m} \neq 0$. In fact its direction is rotating around the line connecting charges, leading to nonzero angular momentum of the field. In fact the Dirac quantization condition is known to be directly related to quantization of this angular momentum.

However, in our setting with Minahan's solution this effect is entirely absent and there is no anular momentum or Poynting vector, $T_{0m} = 0$. This can be traced directly to the expression (3.70) for the source which has no such component. In gravity setting the energy-momentum of the Minahan string construction does not care about direction of the magnetic flux, and the problem is again static and t-reflection symmetric.

Perhaps the way to remedy the situation is to start with a different classical *rotating* string, with some nonzero angular momentum, which value is to be tuned to fit the Dirac condition. If we will be able to make progress along this line, we will report it elswhere[12].

3.6 Summary and outlook

The main results of this work are general expressions for the stress tensor induced by objects in the AdS bulk (3.31),(3.52),(3.58),(3.59), (3.70),(3.71),(3.72).

[12]We thank Andrei Parnachev and Jinfeng Liao for helpful discussions of this issue.

In general, we found that two components of gravity perturbation – the trace of the metric h and its tensor part $h_{\mu\nu}$ – have different equations and Green functions. Although h itself on the boundary does not have $O(z^4)$ corrections or induced stress tensor (as follows from conformal symmetry of the boundary theory), two components are intermixed in curved background and thus h (incorporated into a "generalized source") leads to physical effects including the stress tensor.

General formulae are then used for static electric and electric-magnetic dipoles, as important examples. Confidence in the results come from checking all of them for tracelessness and energy-momentum conservation. We worked out the far field asymptotic, as well as an expressions for the field near one of the charges.

The far distance asymptotic of the stress tensor is $\sim L^3/r^7$, the same as in previous calculation [46] for dim-4 scalar density, the angular distribution is different. We found that although all angular structures are as expected from perturbative analysis for dipoles, the coefficients (and angular distribution of stress tensor) are quite different from the weak coupling limit. The same is found for the near-field domain. It means although a naive idea of strongly coupled vacuum acting as a dielectric qualitatively is holding, quantitatively it definitely fails.

We also found that on the boundary there seems to be no visible trace of a string. In fact even in between the two charges (e.g. at $y_1 = 0$) the dominant contribution still comes from "vertical" parts of the string rather than its "horizontal" part directly beneath the observation point. The distribution looks like two distorted polarization clouds about two charges, instead of a string-like object.

This conclusion is relevant for interpretation of string-like entity which seems to appear via linear part in static dipole potentials on the lattice at T just above deconfinement for QCD-like theories. We think those are due to some flux tubes. Their formation is due to phenomena which needs more specific ingredients than just a strong coupling regime. Let us further conjecture that the distributions we calculated from AdS/CFT should instead be similar to those in QCD-like theories in a "quasi-conformal regime", at temperatures not too close to deconfinement, $T > 1.5Tc$. This is the region in which flux tube effects are gone, the potentials become a screened-Coulomb type and thermodynamical observables are about constant when divided by appropriate powers of T. This conjecture will be tested directly in forthcoming lattice calculations.

As an outlook for this work we have in mind, we would like to work out stress tensor imprints of dynamical (rather than static) objects. In particular,

those are "debris" created in high energy heavy ion collisions, see [23] for a basic picture and to our previous paper [54] in which we formulated the picture and calculated trajectories of different types of objects falling into AdS bulk. We hope then elucidate the process of black hole formation, out of those "debris" and see whether the stress tensor imprints would be approaching hydrodynamical solutions, which were so successful for the description [8] of RHIC data.

Chapter 4

Hologram of the debris

4.1 Introduction

This is the second paper of the series, and the first one [54] (to be referred to as [I] below) had rather extensive introduction. Therefore we just briefly reiterate here what are the main goals of this study.

Holographic description of $\mathcal{N}$ =4 SYM theory in strong coupling regime can be achieved via AdS/CFT correspondence[1–3], which relates it to string theory in $AdS_5 \times S^5$ space, in classical supergravity regime. Large number of applications use this tool to study properties of strongly coupled Quark-Gluon plasma: but most of them are done in a static setting, with fixed temperature via Witten's AdS black hole metric.

High energy hadronic collisions in QCD are very difficult problems. They are time-dependent and include non-equilibrium physics (only collisions of heavy ions can be approximated by hydrodynamics and locally equilibrated QGP). On top of that they involve different scales and different coupling regimes. Pure phenomenological approaches were developed long ago, such as e.g. Lund model [30] which are based on a picture of QCD strings stretched by departing partons. More recent approach – known as the Color Glass picture – was proposed by McLerran and Venugopalan [32] who argued that since fluctuations high energy collisions lead to large local color charges (in the transverse plane) they would lead to production of strong color fields. Those are treated by classical Yang-Mills eqn in a *weak coupling* regime.

Arguments suggested recently put forward a view that QCD has certain "strong coupling window". In particular, Brodsky and Teramond [31] have argued that the power scaling observed for large number of exclusive processes is not due to perturbative QCD (as suggested originally in 1970's) but to a strong coupling regime in which the running is absent and quasi-comformal regime

sets in. Polchinski and Strassler [21] have shown that in spite of exponential string amplitudes one does get power laws scaling for exclusive processes, due to convolution (integration over the z variable) with the power tails of hadronic wave functions. One of us proposed a scenario [34] for AdS/QCD in which there are two domains, with weak and strong coupling. The gauge coupling rapidly rises at the "domain wall" associated with instantons. Pion diffractive dissociation is a process where a switch and weak coupling domains are observed: and cross section behavior is consistent with Polchinski-Strassler expression and expected coupling change. Last but not least, such approach looks now natural in comparison to what happens in heavy ion/finite T QCD, where we do know now that at comparable parton densities the system indeed is in a strong coupling regime.

Accepting the Color Glass picture as an asymptotic for very high parton density and large saturation scale $Q_s \to \infty$, one should ask what should happen in the case of saturation scale falling to intermediate momenta $Q_s \sim .3 - 1.5\, GeV$ associated with "strongly coupled window". This is the issue we address in this work, using the AdS/CFT correspondence in its time-dependent version, as a tool to describe the evolution of the system.

The setting has been discussed in [I], where we extensively studied how exactly the "debris" produced in a collision – closed or open strings – are falling under gravity force into IR (the AdS throat). In this work we do the next technical step and calculate the back reaction of gravity by solving the linearized Einstein eqns for metric pertubations, deducing the space-time dependence of the stress tensor $T_{\mu\nu}(x)$ of excited matter observed on the boundary.

The general setting is in fact rather similar to the Lund model: except that strings are departing from our world ($z = 0$ boundary) rather than breaking. Technically our work is a development along a line actively pursued by many authors. In particular, it can be considered a continuation of our recent work [56] in which we calculated static (time-independent) stress tensor associated with Maldacena's static dipole. It is also similar to recent AdS/CFT calculations of a hydrodynamical "conical flow" from quenching jet in QGP [17, 18]: in this case the picture is static in the moving quark frame. To our knowledge, our work is the first attempt to solve a fully time-dependent problem in this context.

The process we describe resembles what happens in heavy ion collisions, but with very important distiction. In the setting of this paper we treat "debris" as small pertubation, solving linearized Einstein eqns in pure AdS_5 background. Therefore there is no black hole and/or temperature in this work, and our "mini-explosion" produce matter which is not equilibrated and the resulting stress tensor cannot be parameterized hydrodynamically.

To get all that one needs to proceed to nonlinear gravity and a non-linear process of black hole formation: the problem which we hope to attack elsewhere.

4.2 Solving Linearized Einstein equation

We want to solve linearized Einstein equation in AdS_5 background in Poincare coordinates, with standard background metrics

$$ds^2 = \frac{-dt^2 + d\vec{x}^2 + dz^2}{z^2} + h_{\mu\nu} \tag{4.1}$$

An axial gauge is chosen for metric perturbation, so $h_{z\mu} = 0$

The linearized Einstein equation are well known and the tactics used in its solution are discussed in [56]: the present case is only different by appearence of time derivatives. We put it into the form

$$\frac{1}{2}\Box h_{mn} - 2h_{mn} + \frac{z}{2}h_{mn,z} = s_{mn} \tag{4.2}$$

where $\Box = z^2\left(-\partial_t^2 + \partial_{\vec{x}}^2 + \partial_z^2\right)$, the indices are 0-3 and the r.h.s. is the generalized source

$$s_{mn} = \delta S_{mn} - \int_0^z \left(\delta S_{zm,n} + \delta S_{zn,m}\right) dz + \frac{1}{2}h_{,m,n} + \frac{1}{2}\Gamma^z_{mn}h_{,z} \tag{4.3}$$

containing not only the stress tensor of the source

$$S_{\mu\nu} = -\kappa^2(T_{\mu\nu} - \frac{T}{3}g_{\mu\nu}) \tag{4.4}$$

but also the following combinations of perturbation metric which can be easily found from the eqns:

$$h = \frac{1}{3}\int_0^z dz \cdot z\left[\delta S_{zz} + \delta S_{tt} - \Sigma_i \delta S_{x^i x^i} + 2\int_0^z dz\left(-\delta S_{zt,t} + \Sigma_i \delta S_{zx^i,x^i}\right)\right]$$

The source term for different objects is standard, obtained via variation of their action (the Nambu-Goto action for the string and point particle action

for the stone) over the metric

$$S_{NG} = -\frac{1}{2\pi\alpha'}\int d^2\sigma\sqrt{-detg_{ind}}\int d^5x\delta^{(5)}\left(x - X\left(\sigma\right)\right)$$

$$T^{\mu\nu} = -\frac{2\delta S_{NG}}{\sqrt{-g}\delta g_{\mu\nu}}$$

$$= \frac{1}{\sqrt{-g}2\pi\alpha'}\int d^2\sigma\delta^{(5)}\left(x - X\left(\sigma\right)\right)\partial_\alpha X^\mu\partial_\beta X^\nu g^{\beta\alpha}_{ind} \tag{4.5}$$

$$S_m = m\int d^5x\delta^{(5)}(x - X(s))\int ds\sqrt{-g_{\mu\nu}\frac{dx^\mu}{ds}\frac{dx^\nu}{ds}}$$

$$T^{\mu\nu} = -\frac{m}{\sqrt{-g}}\int ds\delta^{(5)}(x - X(s))\frac{\frac{dx^\mu}{ds}\frac{dx^\nu}{ds}}{\sqrt{-g_{\mu\nu}\frac{dx^\mu}{ds}\frac{dx^\nu}{ds}}} \tag{4.6}$$

here $g_{\mu\nu}$ and $g_{ind,\alpha\beta}$ denote the AdS metric and the induced metric on the string worldsheet, respectively.

In the next section we find an expression for Green's function, which will provide h_{mn} for any given source s_{mn}. We will then exctract an expression for the coefficient of the z^2 term in Taylor series of h_{mn} at the boundary, which by the rules of AdS/CFT correspondence gives us the boundary stress tensor.

4.3 The Green's function for the linearized gravity in AdS_5

The Green's function we need satisfies the following eqn:

$$\frac{z^2}{2}(\partial_z^2 - \partial_t^2 + \partial_{\vec{x}}^2)G(z,z') - 2G(z,z') + \frac{z}{2}\partial_z G(z,z') =$$
$$\delta(z - z')\delta(t - t')\delta^{(3)}(x - x') \tag{4.7}$$

and the solution to (4.2) is then given by $h_{mn}(z) = \int G(z,z')s_{mn}(z')dz'$. Thus $G(z,z')$ should satisfy the same boundary condition as $h(z)$. Fourier transforming 4-dim part of (4.7), we have z- dependent eqn

$$\frac{z^2}{2}(\partial_z^2 + \omega^2 - k^2)G(z,z') - 2G(z,z') + \frac{z}{2}\partial_z G(z,z') = \delta(z - z') \tag{4.8}$$

where $G^k(z,z') = \int G(z,z')e^{-i\omega t + i\vec{k}\vec{x}}dtd^3x$

(4.8) can be solved in terms of Bessel functions: For $|\omega| > k$, the solution is a linear combination of Bessel functions of the first and second kind. We

impose the following boundary condition: at $z = 0$, $G(z, z') = 0(h(z) = 0)$, at $z \to \infty$, $G(z, z')(h(z))$ contains outgoing wave only, i.e. the wave propagates from the source to infinity[1]. The solution is composed of two homogeneous solutions:

$$G(z, z') = \begin{cases} AJ_2(\lambda z) & z < z' \\ B(J_2(\lambda z) - isgn(\omega)Y_2(\lambda z)) & z > z' \end{cases} \tag{4.9}$$

with $\lambda = \sqrt{\omega^2 - k^2}$, A, B is fixed by matching the function itself and its first derivative at $z = z'$:

$$\begin{cases} A = \frac{\pi isgn(\omega)}{z'}(J_2(\lambda z') - isgn(\omega)Y_2(\lambda z')) \\ B = \frac{\pi isgn(\omega)}{z'}J_2(\lambda z') \end{cases} \tag{4.10}$$

For $k > |\omega|$, the solution can be built from Modified Bessel function. We choose the no exponential growth boundary condition at $z \to \infty$[56]. The solution is given by:

$$G(z, z') = \begin{cases} CI_2(\tilde{\lambda} z) & z < z' \\ DK_2(\tilde{\lambda} z) & z > z' \end{cases} \tag{4.11}$$

with $\tilde{\lambda} = \sqrt{k^2 - \omega^2}$

$$\begin{cases} C = \frac{-2K_2(\tilde{\lambda} z')}{z'} \\ D = \frac{-2I_2(\tilde{\lambda} z')}{z'} \end{cases} \tag{4.12}$$

It turns out the solution can be organized in a compact form using properties of Bessel function:

$$G(z, z') = \begin{cases} -\frac{2}{z'}I_2(i\lambda z_<)K_2(i\lambda z_>) & \omega > 0, |\omega| > k \\ -\frac{2}{z'}I_2(-i\lambda z_<)K_2(-i\lambda z_>) & \omega < 0, |\omega| > k \\ -\frac{2}{z'}I_2(\tilde{\lambda} z_<)K_2(\tilde{\lambda} z_>) & |\omega| < k \end{cases} \tag{4.13}$$

where $z_< = min(z, z')$ $z_> = max(z, z')$

Doing the inverse Fourier transform: $\frac{1}{(2\pi)^4}\int G^k(z, z')e^{i\omega t - i\vec{k}\vec{x}}d\omega d^3k$, we obtain a retarded propagator for the metric: (See Appendix.8 for the evaluation

[1]the same boundary condition is used in [72] as a limiting case of thermal AdS background

of the integral, a retarded propagator for scalar field was found in [39])

$$P_R = \frac{12iz}{(2\pi)^2}\left[\frac{1}{(t^2-r^2-z^2+i\epsilon)^4} - \frac{1}{(t^2-r^2-z^2-i\epsilon)^4}\right]\theta(t-r) \quad (4.14)$$

Several comments of the propagator are in order: (i)The theta function implies the propagator acts inside the lightcone $t^2 - r^2 = z^2 > 0$ and moreover is retarded $t > r > 0$, which we indicate by the subscript R. It is also consistent with the outgoing boundary condition. Note that the propagator is also Lorentz invariant. (ii)The propagator relates the z^2 coefficient of metric perturbation Q_{mn} and the source s_{mn} in the following way(assuming $s_{mn}(z)$ does not contain z^0 and z^2 terms): $Q_{mn}(t', x') = \int P_R(t'-t, x'-x, z)s_{mn}(z, t, x)dzdtd^3x$ The primed and unprimed coordinates correspond to boundary and bulk respectively. (iii)The propagator is dynamical. For static source, one can perform the t-integral to obtain a static propagator, which agrees with the one obtained in [56].

4.4 The stress tensor of a falling open string

We want to study the stress tensor by a falling string. A scaling string profile is obtained in [I] for a separating quark- antiquark pair, provided the separating velocity is not too large: $v < 0.6$. We briefly recall the scaling solution. The quark(antiquark) moves along the trajectory $x = \pm vt$. The string profile is given by:

$$\begin{aligned} z &= \frac{\tau}{f(y)} \\ y &= f_0\sqrt{\frac{f_0^2-1}{2f_0^2-1}}F\left(\sqrt{\frac{f^2-f_0^2}{f^2-1}}, \frac{f_0}{\sqrt{2f_0^2-1}}\right) \\ &-\frac{1}{f_0}\sqrt{\frac{(f_0^2-1)^3}{2f_0^2-1}}\Pi\left(\sqrt{\frac{f^2-f_0^2}{f^2-1}}, \frac{1}{f_0^2}, \frac{f_0}{\sqrt{2f_0^2-1}}\right) \end{aligned} \quad (4.15)$$

τ and y are proper time and space-time rapidity. The $y = Y$ limit of (4.15) relates the parameter f_0 and the quark rapidity $Y = arctanh(v)$. It is also very useful to write down the EOM of $f(y)$:

$$f' = \frac{\sqrt{V(V-E^2)}}{E} \quad (4.16)$$

with $V = f^4 - f^2$, $f_0^4 - f_0^2 - E^2 = 0$.

We want the source term due to the scaling string. It is convenient to switch to a different parametrization:

$$z = z\left(t, x\right) \ , x_\perp = 0 \tag{4.17}$$

where x and $x_\perp$ represent longitudinal and transverse coordinates respectively. The above parametrization leads directly to

$$S_{\mu\nu} = -\frac{1}{3}\frac{\kappa^2 z}{2\pi\alpha'}\delta\left(z-\bar{z}\right)\delta\left(x^2\right)\delta\left(x^3\right)\frac{1}{\sqrt{1-z_t^2+z_x^2}}\cdot$$
$$\begin{pmatrix} 1+2z_t^2+z_x^2 & 3z_t z_x & -3z_t & & \\ 3z_t z_x & z_t^2+2z_x^2-1 & -3z_x & & \\ -3z_t & -3z_x & 2+z_t^2-z_x^2 & & \\ & & & 2(1-z_t^2+z_x^2) & \\ & & & & 2(1-z_t^2+z_x^2) \end{pmatrix} \tag{4.18}$$

(In the matrices here and below we only show the nonzero enties: the adopted order of coordinate indices is t, z, x^1, x^2, x^3.) With the help of string EOM, (15) of [48], h can be expressed in a very compact form:

$$h = -\frac{2}{3}\frac{\kappa^2}{2\pi\alpha'}\delta\left(x^2\right)\delta\left(x^3\right)\frac{z_t^2-z_x^2+2}{\sqrt{1-z_t^2+z_x^2}}\frac{1}{2}(z^2-\bar{z}^2)\theta(z-\bar{z})$$

We also record the generalized source for later reference:

$$
\begin{aligned}
s_{mn} = \frac{1}{3}\frac{-\kappa^2}{2\pi\alpha'}\delta(x^2)\delta(x^3)\Bigg[& \frac{\bar{z}}{\sqrt{1-z_t^2+z_x^2}}\delta(z-\bar{z}) \times \\
& \begin{pmatrix} 1+2z_t^2+z_x^2 & 3z_tz_x & & \\ 3z_tz_x & z_t^2+2z_x^2-1 & & \\ & & 2(1-z_t^2+z_x^2) & \\ & & & 2(1-z_t^2+z_x^2) \end{pmatrix} \\
& + \begin{pmatrix} 2\partial_t & \partial_x & \partial_{x_2} & \partial_{x_3} \\ \partial_x & & & \\ \partial_{x_2} & & & \\ \partial_{x_3} & & & \end{pmatrix} \frac{3\bar{z}z_t}{\sqrt{1-z_t^2+z_x^2}}\theta(z-\bar{z}) \\
& + \begin{pmatrix} & \partial_t & & \\ \partial_t & 2\partial_x & \partial_{x_2} & \partial_{x_3} \\ & \partial_{x_2} & & \\ & \partial_{x_3} & & \end{pmatrix} \frac{3\bar{z}z_x}{\sqrt{1-z_t^2+z_x^2}}\theta(z-\bar{z}) \\
& + \begin{pmatrix} \partial_t^2 & \partial_t\partial_x & \partial_t\partial_{x_2} & \partial_t\partial_{x_3} \\ \partial_t\partial_x & \partial_x^2 & \partial_x\partial_{x_2} & \partial_x\partial_{x_3} \\ \partial_t\partial_{x_2} & \partial_x\partial_{x_2} & \partial_{x_2}^2 & \partial_{x_2}\partial_{x_3} \\ \partial_t\partial_{x_3} & \partial_x\partial_{x_3} & \partial_{x_2}\partial_{x_3} & \partial_{x_3}^2 \end{pmatrix} \frac{z_t^2-z_x^2+2}{\sqrt{1-z_t^2+z_x^2}} \times \\
& \frac{1}{2}(z^2-\bar{z}^2)\theta(z-\bar{z}) + \begin{pmatrix} -1 & & & \\ & 1 & & \\ & & 1 & \\ & & & 1 \end{pmatrix} \frac{z_t^2-z_x^2+2}{\sqrt{1-z_t^2+z_x^2}} \times \\
& \theta(z-\bar{z})\Bigg]
\end{aligned}
\tag{4.19}
$$

With the source now at hand, we proceed to the calculation of stress tensor. We use similar substitutions as before: $\overrightarrow{\partial}_x = -\overleftarrow{\partial}_x = \overleftarrow{\partial}'_x$. Performing the derivative explicitly, we find the z-integral and $x_\perp$-integral can be done easily. We arrive at the following result:

$$
\begin{aligned}
Q_{mn} = \frac{1}{3}\frac{-\kappa^2}{2\pi\alpha'}\int dtdx\Bigg[&\frac{\bar{z}^2}{\sqrt{1-z_t^2+z_x^2}}P \\
&\begin{pmatrix} 1+2z_t^2+z_x^2 & 3z_tz_x & & & \\ 3z_tz_x & z_t^2+2z_x^2-1 & & & \\ & & 2(1-z_t^2+z_x^2) & & \\ & & & 2(1-z_t^2+z_x^2) & \end{pmatrix} + \\
&\frac{3\bar{z}z_t}{\sqrt{1-z_t^2+z_x^2}}P\begin{pmatrix} 2(t'-t) & -(x'-x) & -x_2' & -x_3' \\ -(x'-x) & & & \\ -x_2' & & & \\ -x_3' & & & \end{pmatrix} + \\
&\frac{3\bar{z}z_x}{\sqrt{1-z_t^2+z_x^2}}P\begin{pmatrix} & t'-t & & \\ t'-t & -2(x'-x) & -x_2' & -x_3' \\ & -x_2' & & \\ & -x_3' & & \end{pmatrix} + \\
&\frac{z_t^2-z_x^2+2}{\sqrt{1-z_t^2+z_x^2}}P\begin{pmatrix} (t'-t)^2 & -(t'-t)(x'-x) & -(t'-t)x_2' & -(t'-t)x_3' \\ -(t'-t)(x'-x) & (x'-x)^2 & (x'-x)x_2' & (x'-x)x_3' \\ -(t'-t)x_2' & (x'-x)x_2' & x_2'^2 & x_2'x_3' \\ -(t'-t)x_3' & (x'-x)x_3' & x_2'x_3' & x_3'^2 \end{pmatrix}\Bigg]
\end{aligned}
\tag{4.20}
$$

with

$$
\begin{aligned}
P &= \frac{12i}{(2\pi)^2}\Bigg[\frac{1}{((t'-t)^2-(x'-x)^2-x_\perp'^2-\bar{z}^2+i\epsilon)^4} \\
&-\frac{1}{((t'-t)^2-(x'-x)^2-x_\perp'^2-\bar{z}^2-i\epsilon)^4}\Bigg] \\
&\equiv \frac{12i}{(2\pi)^2}\frac{\pm 1}{((t'-t)^2-(x'-x)^2-x_\perp'^2-\bar{z}^2\pm i\epsilon)^4}\theta(t'-t)
\end{aligned}
\tag{4.21}
$$

which is just the integrated propagator. The four matrices in the expression above we will refer to later as I,II,III,IV, respectively.

Here we replaced the theta function of P_R by $\theta(t'-t)$. It is justified since the $\pm i\epsilon$ prescription encodes derivatives of the delta function, and the theta function picks up only one pole of the propagator.

In order to plugin the scaling solution for the string, we return to τ, y coordinates:

$$z_t = \frac{chy}{f} + \frac{shyf'}{f^2}$$
$$z_x = -\frac{shy}{f} - \frac{chyf'}{f^2}$$
$$\int dtdx = \int \tau d\tau dy$$

The source together with the integration measure has one of the following simple τ-dependence: τ, τ^2, τ^3. The propagator now is

$$\begin{aligned} P &= \frac{12i}{(2\pi)^2} \frac{\pm\theta(\tau' - \tau)}{((1 - \frac{1}{f^2})\tau^2 + \tau'^2 - 2\tau\tau' ch(y - y') - x'^2_\perp \pm i\epsilon)^4} \\ &= \frac{12i}{(2\pi)^2} \frac{\pm 1}{((1 - \frac{1}{f^2})(\tau - \tau_+)(\tau - \tau_-) \pm i\epsilon)^4} \theta(\tau' - \tau) \end{aligned} \tag{4.22}$$

with

$$\tau_\pm = \frac{\tau' ch(y' - y) \pm \sqrt{\tau'^2 ch^2(y' - y) - (\tau'^2 - x'^2_\perp)(1 - \frac{1}{f^2})}}{1 - \frac{1}{f^2}} \tag{4.23}$$

This propagator as a function of τ contains two fourth order poles, so the τ-integral is calculated by the residue theorem. Note that the theta function picks up only one pole at $\tau = \tau_-$. Since our τ-integral extends from zero to infinity, we must have a positive τ_- in order to have a nonvanishing result, which requires $\tau'^2 - x'^2_\perp = t'^2 - r'^2 > 0$, precisely the condition that the observer must stay inside the lightcone. Since the quark and the antiquark are emerging from the space-time origin, the stress tensor is indeed expected to vanish outside the lightcone.

Completed the τ integral and replacing $\frac{1}{3}\frac{-\kappa^2}{2\pi\alpha'}$ by $\frac{-\sqrt{\lambda}}{3\pi}$, we convert Q_{mn} to the boundary stress tensor T_{mn} (compare [56]). We thus get our final result

$$
\begin{aligned}
T_{mn} = \frac{-\sqrt{\lambda}}{3\pi}\int_{-Y}^{Y} dy \Bigg[& \frac{1}{f^2\sqrt{1-z_t^2+z_x^2}} A \\
& \begin{pmatrix} 1+2z_t^2+z_x^2 & 3z_t z_x & & \\ 3z_t z_x & z_t^2+2z_x^2-1 & & \\ & & 2(1-z_t^2+z_x^2) & \\ & & & 2(1-z_t^2+z_x^2) \end{pmatrix} \\
& - \frac{3z_t B}{f\sqrt{1-z_t^2+z_x^2}} \begin{pmatrix} -2t' & x' & x_2' & x_3' \\ x' & & & \\ x_2' & & & \\ x_3' & & & \end{pmatrix} + \frac{3z_t A}{f\sqrt{1-z_t^2+z_x^2}} \begin{pmatrix} -2chy & shy & 0 & 0 \\ shy & & & \\ 0 & & & \\ 0 & & & \end{pmatrix} \\
& - \frac{3z_x B}{f\sqrt{1-z_t^2+z_x^2}} \begin{pmatrix} & -t' & & \\ -t' & 2x' & x_2' & x_3' \\ & x_2' & & \\ & x_3' & & \end{pmatrix} + \frac{3z_x A}{f\sqrt{1-z_t^2+z_x^2}} \begin{pmatrix} & -chy & & \\ -chy & 2shy & 0 & 0 \\ & 0 & & \\ & 0 & & \end{pmatrix} \\
& + \frac{z_t^2-z_x^2+2}{\sqrt{1-z_t^2+z_x^2}} C \begin{pmatrix} t'^2 & -t'x' & -t'x_2' & -t'x_3' \\ -t'x' & x'^2 & x'x_2' & x'x_3' \\ -t'x_2' & x'x_2' & x_2'^2 & x_2'x_3' \\ -t'x_3' & x'x_3' & x_2'x_3' & x_3'^2 \end{pmatrix} + \frac{z_t^2-z_x^2+2}{\sqrt{1-z_t^2+z_x^2}} B \times \\
& \begin{pmatrix} -2t'chy & t'shy+x'chy & x_2'chy & x_3'chy \\ t'shy+x'chy & -2x'shy & -x_2'shy & -x_3'shy \\ x_2'chy & -x_2'shy & & \\ x_3'chy & -x_3'shy & & \end{pmatrix} + \frac{z_t^2-z_x^2+2}{\sqrt{1-z_t^2+z_x^2}} A \\
& \begin{pmatrix} chy^2 & -chyshy & & \\ -chyshy & shy^2 & & \\ & & & \\ & & & \end{pmatrix} \Bigg]
\end{aligned}
\tag{4.24}
$$

with

$$
\begin{aligned}
A &= \frac{1}{(1-\frac{1}{f^2})^4} \frac{{\tau_+}^3 + 9{\tau_+}^2\tau_- + 9\tau_+{\tau_-}^2 + {\tau_-}^3}{(\tau_+-\tau_-)^7} \\
B &= \frac{4}{(1-\frac{1}{f^2})^4} \frac{{\tau_+}^2 + 3\tau_+\tau_- + {\tau_-}^2}{(\tau_+-\tau_-)^7} \\
C &= \frac{10}{(1-\frac{1}{f^2})^4} \frac{\tau_+ + \tau_-}{(\tau_+-\tau_-)^7}
\end{aligned}
$$

4.4.1 A field near one charge

We first consider the stress tensor close to the quark. Note the quark moves with velocity v, the observer should also move in order to stay close to the quark. Thus it is convenient to switch to rest coordinate of the moving quark, yet we still stay in the rest frame of the system. The rest coordinates of the quark, indicated by a tilde, relates the original coordinates in the following way:

$$\begin{aligned}
\tilde{t} &= chYt' - shYx' \\
\tilde{x} &= chYx' - shYt' \\
\tilde{x}_2 &= x'_2 \\
\tilde{x}_3 &= x'_3
\end{aligned} \tag{4.25}$$

We expect to obtain the field by the quark only, provided we are sufficient close to the quark, which corresponds to the limit $\tilde{t} \gg \tilde{r}$, $\tilde{r} \equiv \sqrt{\tilde{x}^2 + \tilde{x}_2^2 + \tilde{x}_3^2} \to 0$. Comparing the string profile for the stretching dipole with that for a single quark, we claim the leading order field near the quark receives contribution from the quark end of the string, which corresponds to the integration of y near $y = Y$ in (4.24). If we instead do the integral in f with $dy = \frac{df}{f'}$, we may only focus on large f integration.

Note $f' \sim \frac{f^4}{E}$ $y - Y \sim \frac{1}{f^3}$. To the leading order, we can simplfy replace y by Y, which leads to the following relations:

$$\begin{aligned}
&\tau_+ - \tau_- = \frac{2\sqrt{\tilde{t}^2 - (1 - \frac{1}{f^2})(\tilde{t}^2 - \tilde{r}^2)}}{1 - \frac{1}{f^2}} \\
&{\tau_+}^3 + 9{\tau_+}^2\tau_- + 9\tau_+{\tau_-}^2 + {\tau_-}^3 = \frac{8\tilde{t}^3}{(1 - \frac{1}{f^2})^3} + \\
&\frac{12(\tilde{t}^2 - \tilde{r}^2)\tilde{t}}{(1 - \frac{1}{f^2})^2} \\
&{\tau_+}^2 + 3\tau_+\tau_- + {\tau_-}^2 = \frac{4\tilde{t}^2}{(1 - \frac{1}{f^2})^2} + \frac{\tilde{t}^2 - \tilde{r}^2}{1 - \frac{1}{f^2}} \\
&\tau_+ + \tau_- = \frac{2\tilde{t}}{1 - \frac{1}{f^2}}
\end{aligned} \tag{4.26}$$

Performing the f integral near ∞, and take the limit $\tilde{t} \gg \tilde{r}$, $\tilde{r} \to 0$, which

is essentially a small $\tilde{r}$ expansion, we find the leading order field given by source I and IV diverges as $O(\frac{1}{\tilde{r}^4})$, while source II and III only yield subleading contribution $O(\frac{1}{\tilde{r}^2})$. We display the LO field near the quark as follows:

$$T_{mn} = \frac{2\sqrt{\lambda}}{\pi^2}\Bigg[\begin{pmatrix} 1+2\gamma^2\beta^2 & -2\gamma^2\beta & & \\ -2\gamma^2\beta & -1+2\gamma^2 & & \\ & & 1 & \\ & & & 1 \end{pmatrix}\frac{1}{24\tilde{r}^4} - \begin{pmatrix} \gamma^2\beta^2\tilde{x}^2 & -\gamma^2\beta\tilde{x}^2 & -\gamma\beta\tilde{x}\tilde{x}_2 & -\gamma\beta\tilde{x}\tilde{x}_3 \\ -\gamma^2\beta\tilde{x}^2 & \gamma^2\tilde{x}^2 & \gamma\tilde{x}\tilde{x}_2 & \gamma\tilde{x}\tilde{x}_3 \\ -\gamma\beta\tilde{x}\tilde{x}_2 & \gamma\tilde{x}\tilde{x}_2 & \tilde{x}_2^2 & \tilde{x}_2\tilde{x}_2 \\ -\gamma\beta\tilde{x}\tilde{x}_3 & \gamma\tilde{x}\tilde{x}_3 & \tilde{x}_2\tilde{x}_3 & \tilde{x}_3^2 \end{pmatrix}\frac{1}{12\tilde{r}^6}\Bigg] \tag{4.27}$$

with $\gamma = chY$, $\gamma\beta = shY$.

This does not look very nice at first glance, actually it is just the stress tensor of a static quark boosted to a frame moving with velocity $-v$. It is clearly traceless and divergence-free. We confirm that the LO field near the quark contains contribution from the quark only.

Next we would like to extend the result to NLO to include the effect of the antiquark. Note there are two possible corrections relevant for NLO: correction to the source $\Delta y = y - Y = \frac{\Delta f}{f'} = \frac{E}{3f^3}$, thus $chy = chY + shY\Delta y$, $shy = shY + chY\Delta y$. The other is correction to the propagator(we refer to the two

terms in the expansion as P_4 and P_5):

$$
\begin{aligned}
P &= \frac{12i}{(2\pi)^2}\frac{\pm\theta(\tau'-\tau)}{((1-\frac{1}{f^2})\tau^2+\tau'^2-2\tau\tau' ch(y-y')-x_\perp'^2\pm i\epsilon)^4} \\
&= \frac{12i}{(2\pi)^2}\Bigg[\frac{\pm 1}{((1-\frac{1}{f^2})\tau^2+\tau'^2-2\tau\tau' ch(y'-Y)-x_\perp'^2\pm i\epsilon)^4} \\
&+\frac{\pm 1}{((1-\frac{1}{f^2})\tau^2+\tau'^2-2\tau\tau' ch(y'-Y)-x_\perp'^2\pm i\epsilon)^5}\times \\
&(-8\tau\tau' sh(y'-Y)\Delta y)+\cdots\Bigg]\theta(\tau'-\tau) \\
&= \frac{12i}{(2\pi)^2}\Big[\frac{\pm 1}{((1-\frac{1}{f^2})\tau^2+\tau'^2-2\tau\tau' ch(y'-Y)-x_\perp'^2\pm i\epsilon)^4} \\
&+\frac{\pm 1}{((1-\frac{1}{f^2})\tau^2+\tau'^2-2\tau\tau' ch(y'-Y)-x_\perp'^2\pm i\epsilon)^5}(\frac{8E\tau\tilde{x}}{3f^3}) \\
&+\cdots\Big]\theta(\tau'-\tau) \\
&\equiv P_4+P_5+\cdots
\end{aligned}
\tag{4.28}
$$

After relatively lengthy calculation and comparison we find that the NLO correction is composed of three pieces: the first one is source II and III convoluted with P_4, the second correspond to source IV and P_4, and the third one comes from the convolusion of source I and P_5. Collecting all of them, we find the following result:

$$
\begin{aligned}
T_{mn} = \frac{2\sqrt{\lambda E}}{\pi^2}\Bigg[&-\begin{pmatrix} 5+13\gamma^2\beta^2 & -13\gamma^2\beta & & \\ -13\gamma^2\beta & -5+13\gamma^2 & & \\ & & 8 & \\ & & & 8 \end{pmatrix}\frac{\tilde{x}}{144\tilde{r}^3\tilde{t}^2} \\
&+\begin{pmatrix} \gamma^2\beta^2\tilde{x}^2 & -\gamma^2\beta\tilde{x}^2 & -\gamma\beta\tilde{x}\tilde{x}_2 & -\gamma\beta\tilde{x}\tilde{x}_3 \\ -\gamma^2\beta\tilde{x}^2 & \gamma^2\tilde{x}^2 & \gamma\tilde{x}\tilde{x}_2 & \gamma\tilde{x}\tilde{x}_3 \\ -\gamma\beta\tilde{x}\tilde{x}_2 & \gamma\tilde{x}\tilde{x}_2 & \tilde{x}_2^2 & \tilde{x}_2\tilde{x}_3 \\ -\gamma\beta\tilde{x}\tilde{x}_3 & \gamma\tilde{x}\tilde{x}_3 & \tilde{x}_2\tilde{x}_3 & \tilde{x}_3^2 \end{pmatrix}\frac{\tilde{x}}{48\tilde{r}^5\tilde{t}^2} \\
&+\begin{pmatrix} 2\gamma^2\beta^2\tilde{x} & -2\gamma^2\beta\tilde{x} & -\gamma\beta\tilde{x}_2 & -\gamma\beta\tilde{x}_3 \\ -2\gamma^2\beta\tilde{x} & 2\gamma^2\tilde{x} & \gamma\tilde{x}_2 & \gamma\tilde{x}_3 \\ -\gamma\beta\tilde{x}_2 & \gamma\tilde{x}_2 & & \\ -\gamma\beta\tilde{x}_3 & \gamma\tilde{x}_3 & & \end{pmatrix}\frac{1}{18\tilde{r}^3\tilde{t}^2}\Bigg]
\end{aligned}
\tag{4.29}
$$

We had found with satisfaction that this result is indeed traceless and divergence-

free (to order $O(\frac{1}{\tilde{r}^3})$).

After this result is boosted to a frame moving with velocity $+v$, it reproduces the NLO field near the quark of a static dipole with the identification $\frac{E}{\tilde{t}^2} \to \frac{1}{z_m^2} \approx \frac{1.2^2}{L^2}$($L$ is the quark-antiquark seperation). It confirms that close to one charge it is not important to this accuracy what the other charge is doing. In fact in the quasi-static limit $v \to 0$, $\frac{E}{\tilde{t}^2} \approx \frac{1.2^2}{4v^2\tilde{t}^2} = \frac{1.2^2}{\tilde{L}^2}$, where $\tilde{L}$ is the quark-antiquark seperation at time $\tilde{t}$.

4.4.2 The slow-moving limit

Since the stretching string solution depends on only one parameter v, the ends velocity, which is bounded from above by the critical velocity. One interesting limit in which calculations can be pushed a step further is $v \to 0$, which correspond to slow motion. In practice, it corresponds to expantion of the stress tensor in inverse powers of f_0.

We start with considering the large f_0 limit of (4.24). Define $\eta = \frac{f}{f_0}$ $\eta \geqslant 1$ such that the range of η is independent from f_0. The large f_0 expansion of y is a little complicated:

$$\begin{aligned} y &= \frac{1}{2}\sqrt{f_0^4 - f_0^2}\left[\frac{2F(\frac{f^2-f_0^2}{f^2-1}, \frac{f_0^2}{2f_0^2-1})}{\sqrt{2f_0^2-1}} - \frac{2(f_0^2-1)\Pi(\frac{f^2-f_0^2}{f^2-1}, \frac{1}{f_0^2}, \frac{f_0^2}{2f_0^2-1})}{\sqrt{2f_0^2-1}f_0^2}\right] \\ &= \frac{-F(\frac{\sqrt{\eta^2-1}}{\eta}, \frac{\sqrt{2}}{2}) + 2E(\frac{\sqrt{\eta^2-1}}{\eta}, \frac{\sqrt{2}}{2})}{\sqrt{2}f_0} + O(\frac{1}{f_0^3}) \\ &\equiv \frac{G(\eta)}{f_0} + O(\frac{1}{f_0^3}) \end{aligned} \tag{4.30}$$

With the asymptotic expansion of y and f_0, we are ready to proceed to the stress tensor. It seems at first glance the leading order is of $O(\frac{1}{f_0})$, given by source IV. Actually the prefactor, which is an integral of η vanishes. The order $O(\frac{1}{f_0^2})$ does not contribute either due to the symmetry $y \leftrightarrow -y$. Finally we have to extend the calculation to order $O(\frac{1}{f_0^3})$. Expand all the relevant quantity in f_0, and keep the order $O(\frac{1}{f_0^3})$ in the result of stress tensor. It is a quite lengthy but straight forward calculation. The result is displayed as follows(we have omitted the prime in boundary coordinates):

$$
\begin{aligned}
T_{tt} &= \frac{2\sqrt{\lambda}}{f_0^3\pi^2}\frac{2t}{r^9}\big[(10a+5e_1+5e_2)r^2t^2+45e_1x^2r^2-35e_1t^2x^2-(9e_2+2f\\
&+6a-24c+7e_1)r^4\big]\\
T_{tx} &= \frac{2\sqrt{\lambda}}{f_0^3\pi^2}\frac{2x}{r^9}\big[(45e_1+15e_2-90d-30c)r^2t^2+15e_1x^2r^2-105e_1t^2x^2\\
&-(3e_2+7e_1+2f-6c-18d)r^4\big]\\
T_{tx_i} &= \frac{2\sqrt{\lambda}}{f_0^3\pi^2}\frac{2x_i}{r^9}\big[(15e_2+15e_1-30c)r^2t^2-105e_1t^2x^2+15e_1x^2r^2\big]\\
T_{xx} &= \frac{2\sqrt{\lambda}}{f_0^3\pi^2}\frac{2t}{r^{11}}\big[(20a-30b+10e_1-60d)r^4t^2+(-12a+18b-6e_1+36d)r^6\\
&+(420d-175e_1-35e_2)r^2t^2x^2\\
&+(-180d+15e_2+65e_1+10f)x^2r^4\\
&+315e_1x^4t^2-105e_1x^4r^2\big]\\
T_{xx_i} &= \frac{2\sqrt{\lambda}}{f_0^3\pi^2}\frac{10txx_i}{r^{11}}\big[(42d-21e_1-7e_2)t^2r^2-21e_1x^2r^2+63e_1t^2x^2\big]\\
T_{x_ix_j} &= \frac{2\sqrt{\lambda}}{f_0^3\pi^2}\frac{8t}{r^7}(5at^2-3ar^2)\delta_{ij}-\frac{2\sqrt{\lambda}}{f_0^3\pi^2}\frac{10tx_ix_j}{r^{11}}\big[(7e_1+7e_2)r^2t^2-\\
&(3e_2+e_1+2f)r^4+21e_1x^2r^2\\
&-63e_1x^2t^2\big]
\end{aligned}
\tag{4.31}
$$

with

$$
\begin{aligned}
r &= \sqrt{x^2 + x_2^2 + x_3^2} \\
a &= \int_1^\infty \frac{1}{\eta^2\sqrt{\eta^4-1}} d\eta = 0.5991 \\
b &= \int_1^\infty \frac{1}{\eta^6\sqrt{\eta^4-1}} d\eta = 0.3594 \\
c &= \int_1^\infty (\frac{1}{\eta} + G(\eta)\sqrt{\eta^4-1}) \frac{1}{\eta^5\sqrt{\eta^4-1}} d\eta = 0.4493 \\
d &= \int_1^\infty \frac{G(\eta)}{\eta^5} d\eta = 0.0899 \\
e_1 &= \int_1^\infty \frac{3-\eta^4}{\eta^4\sqrt{\eta^4-1}} G(\eta)^2 d\eta = -0.1797 \\
e_2 &= \int_1^\infty \frac{3-\eta^4}{\eta^6\sqrt{\eta^4-1}} d\eta = 0.4793 \\
f &= \int_1^\infty \frac{-5\eta^4+6\eta^2+9}{2\sqrt{\eta^4-1}(\eta^2+1)\eta^6} d\eta = 0.7189
\end{aligned}
\tag{4.32}
$$

Several comments about the result are in order: (i)the result applies for arbitrary point on the boundary, i.e.general t, x, x_2, x_3, provided the point lies inside the lightcone. The discontinuity of the stress tensor on the lightcone is a consequence of the discontinuity in source at $t = 0$ (ii)trace and divergence of the stress tensor vanish for any points away from the trajectory of the dipole ends, which is of course implicitly assumed in our calculation. (iii)If we consider the limit $t \gg r$, which amounts to keeping only the highest power of t. Recalling the quasi-static limit: $\frac{t^3}{f_0^3} \sim (\frac{vt}{0.6})^3 = (\frac{L}{1.2})^3$, where L is the dipole size at time t. While for the case of static dipole: $z_m^3 = (\frac{L}{1.2})^3$, we find the stretching dipole result agrees with static dipole in the double limits: $v \to 0$,$t \gg r$. The numerical factors matches as well. (vi)the agreement of quasi-static result and NLO near field with those of static dipole by the simple identification: $L = 2vt$ seems to suggest that the vacuum-quark(antiquark) interaction is instantaneous.

We plot the energy density T^{00} and the momentum density (energy flow) T^{0i} as a function of the spatial coordinates at three different times in Fig.4.1 and Fig.4.2, respectively. We observe that although the shape of energy distribution becomes more alongated with time, reflecting changing shape of the

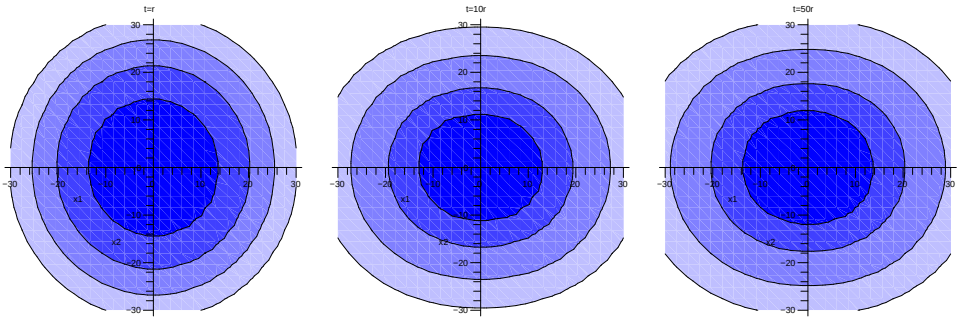

Figure 4.1: (color online) The contours of energy density T^{00}, in unit of $\frac{2\sqrt{\lambda}}{f_0^3\pi^2}$, in $x_1 - x_2$ plane at different time. The three plots are made for $t = r$, $t = 10r$ and $t = 50r$ from top to bottom. Note the quark/antiquark is at $x_1 = \pm vt$. In the slow moving limit, they are nearly at the origin. The magnitude of T^{00} is represented by the color, with darker color corresponding to greater magnitude. As time increases, the shape of the contours gets elongated along x_1 axis

string, the shape of the momentum flows seems to stay the same, with an interesting "eight" shape or forward-backward depletion. Small arrows display the direction of the energy flow. Although they overall show outgoing explosion away from the origin (the collision point), one can also see some "cumulative" flow with jets converging along the collision axes.

4.5 The energy density of matter in comoving frame and freezeout

It is illuminating to ask if the stress tensor we obtained can or cannot be described by some hydrodynamical flow. The latter is widely used in describing heavy ion collisions [51, 52]. More precisely, the question is if our stress tensor (4.31) is that of a flowing ideal liquid

$$T_{\mu\nu} = (\epsilon + p)u_\mu u_\nu + p g_{\mu\nu} \tag{4.33}$$

where u_μ is the 4-velocity of the liquid and ϵ and p are the energy density and the pressure. (Tracelessness would of course demand that $\epsilon = 3p$) It is not difficult to show that this is *not* the case: the structure of our answer is richer than this simple form.

Nevertheless, it is still possible to define a "comoving frame" of matter at any point, in which the (boosted) momentum density T'_{0i} vanishes. The

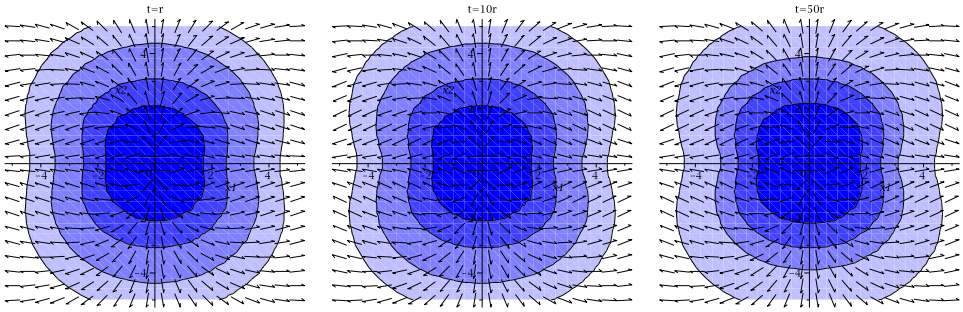

Figure 4.2: (color online)The contours of momentum density T^{0i}, in unit of $\frac{2\sqrt{\lambda}}{f_0^3\pi^2}$, in $x_1 - x_2$ plane at different time. The three plots are made for $t = r$, $t = 10r$ and $t = 50r$ from top to bottom. Note the quark/antiquark is at $x_1 = \pm vt$. In the slow moving limit, they are nearly at the origin. The magnitude is represented by color, with darker color corresponding to greater magnitude. The direction of the momentum density is indicated by normalized arrows

(boosted) local value T'_{00} component is the energy density in such a comoving frame, which we denote by ϵ like for a liquid. We use the contour of ϵ to define the freezeout surface.

However the (boosted) local values of other spatial componets are in general unrelated and can be viewed as "anistropic pressure" of non-equilibrium matter. Needless to say, it remains unknown what combinations of fundamental fields of the $\mathcal{N}$=4 theory – the gauge one, the fermion or the scalars – participate in this flow of produced matter: to learn that one should do "holography" for many more operators on the boundary.

Recall that the stress tensor in different frames are related by $T'_{\alpha\beta} = S^\mu_\alpha S^\nu_\beta T_{\mu\nu}$ where $S^\mu_\alpha = \frac{\partial x^\mu}{\partial x^\alpha}$ are Lorentz boost matrix. The primed quantities correspond to new frame. Therefore the aim is to find such boost which kills all the $(0, i)$ components.

In practice, it is achieved numerically by the following recipe:

We pick up any point inside the lightcone, calculate the eigenvalue and associate eigenvectors of the corresponding stress tensor matrix. Out of the four eigenvalues, one is selected to be the local energy density based on its eigenvector(See Appendix.8 for a short explanation). Fig.4.3 is a surface plot of ϵ profile in spatial coordinate. The plot is made for $t = 1$. It shows a nearly spherical shape for contour with large r and an elongated shape for contour with small r. By virtue of conformality of the setting, this translates to the following: At early time the local energy density contour is nearly spherical and at late time it gets elongated along x_1 axis.

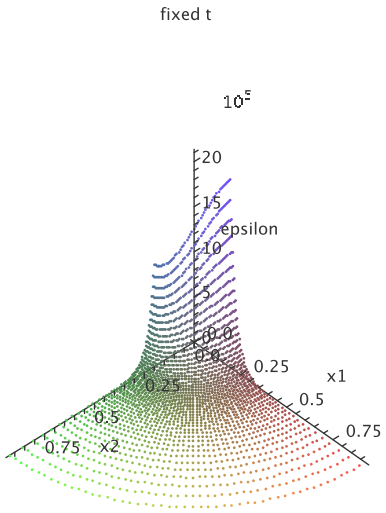

Figure 4.3: (color online)The profile of ϵ, in unit of $\frac{2\sqrt{\lambda}}{f_0^3\pi^2}$, at $t = 1$ with $r \approx 0.2 - 1$. The evolution of the shape of contour, i.e. the freezeout surface is contained in this plot. The contours with large r(small ϵ) are nearly spherical while the contours with small r(large ϵ) are elongated along x_1 axis

4.6 The stress tensor of multiple strings

A simple extension of what is done above is to consider many collidng quark-antiquark pairs uniformly distributed in the transverse plane. Every pair with the same transverse coordinate is connected with a string. Let's assume quark and antiquark only interact pairwise, which in the dual picture means the strings do not interact with each other. As a result, the overall stress tensor induced by the mutiple strings, in the linearized approximation simply amounts to integrating (4.31) over the transverse coordinates. Note in order to preserve causality, the integral is done for $0 < x_\perp^2 = r^2 - x^2 < t^2 - x^2$ We display the result as follows(we omit a factor of transverse string density, which does not alter space-time dependence of the stress tensor):

$$
\begin{aligned}
T_{tt} &= \frac{8\sqrt{\lambda}}{f_0^3\pi}\Big[-4e_1\frac{x^2}{t^4}+(\frac{4}{3}e_1+\frac{2}{3}f+2e_2-8c)\frac{1}{t^2}\\
&+(\frac{20}{3}e_1-\frac{2}{3}f+8c-3e_2-2a)\frac{t}{x^3}+(e_2+2a-4e_1)\frac{t^3}{x^5}\Big]\\
T_{tx} &= \frac{8\sqrt{\lambda}}{f_0^3\pi}\Big[12e_1\frac{x^3}{t^5}+(\frac{-20}{3}e_1+4c+12d+\frac{2}{3}f-2e_2)\frac{x}{t^3}+\\
&(\frac{2}{3}e_1+2c-\frac{2}{3}f-e_2+6d)\frac{1}{x^2}+(-6c-6e_1-18d+3e_2)\frac{t^2}{x^4}\Big]\\
T_{tx_i} &= 0\\
T_{xx} &= \frac{8\sqrt{\lambda}}{f_0^3\pi}\Big[-20e_1\frac{x^4}{t^6}+(12e_1+2e_2-2f-24d)\frac{x^2}{t^4}\\
&+(6b-4a-4e_1+3e_2-24d+2f)\frac{t}{x^3}+(12e_1-6b+48d\\
&+4a-5e_2)\frac{t^3}{x^5}\Big]\\
T_{xx_i} &= 0\\
T_{x_ix_j} &= \frac{8\sqrt{\lambda}}{f_0^3\pi}\Big[10e_1\frac{x^4}{t^6}+(f-e_2-14e_1)\frac{x^2}{t^4}\\
&+(e_2-\frac{5}{3}f+\frac{8}{3}e_1)\frac{1}{t^2}+(-4a+e_2+\frac{2}{3}f-\frac{8}{3}e_1)\frac{t}{x^3}+(4a\\
&-e_2+4e_1)\frac{t^3}{x^5}\Big]
\end{aligned}
\tag{4.34}
$$

We plot the energy density profiles in Fig.4.4.

4.7 Summary and discussion

The main objective of this paper was to calculate a "hologramm" of the falling open string, which has ends attached to heavy quarks moving with constant velocities $\pm v$. After an appropriate tool – Green function for time-dependent linearized Einstein equation – was constructed, and stress tensor of the string calculated, a convolution of the two gave us the stress tensor of an "explosion" seen by an observer at the AdS boundary. Apart of analytical results in different limits, we have given pictures of the time evolution of the energy density and the Poynting vector in Figs.4.1, 4.2. In short, our main finding is that it looks like an explosion, with matter "fireball" expanding from

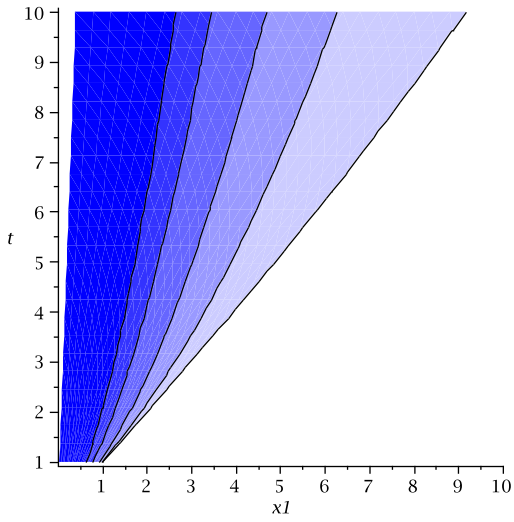

Figure 4.4: (color online)The contours of energy density, in unit of $\frac{8\sqrt{\lambda}}{f_0^3\pi}$, as a function of t and x_1. The magnitude is represented by color, with darker color corresponding to greater magnitude.

the collision point, but a non-hydrodynamical explosion, in which fluid cannot be assigned temperature or entropy.

What can be a physical significance and applications of these results?

Literally, they describe energy/momentum flow following a collision of say two heavy-quark mesons in a strongly coupled $\mathcal{N}$=4 gauge theory). It would then be instructive to compare these results with those in a weakly coupled regime of the same theory, in which the appropriate calculation would be perturbative radiation of massless gluons and scalars. Those are well known to produce dipole radiation at small velocities and bremmstrahlung cones (or "jets") in forward and backward directions. In QCD perturbative radiation is affected by confinement effects as well as the presence of light fermions: thus formation of QCD strings and their breaking by light quark pair production. All of it is well modeled by QCD "event generators", one of which – the Lund model – we mentioned in the Introduction.

So, why one would be interested in a strongly-coupled version of the "event generator"? One reason can be methodical: to better understand the difference between strongly coupled conformal regime and confining theories, as far as jet physics is concerned. It has been studied in literature that hypothetical "hidden valleys theories" which may be found at LHC [55] are strongly coupled: so there is some nonzero (but tiny) chance that those can be used in real experiments one day.

However, as explained in the Introduction, those were not our motivations. We have done this calculation as a methodical step toward understanding heavy ion collisions, in the AdS/CFT setting. One obviously needs to study one falling string before considering many. And simply adding the effect of many strings, as we did above, is not yet sufficient to understand heavy ion collisions.

As a discussion item, we would like at the end of the paper to indicate where we will go from here. What we would like to understand in general is *how and under which conditions the equilibration and entropy production happen,* so that non-hydro explosion described above becomes hydro-like. In order to derive that, one has to abandon the "probe approximation" used above, and include the gravitational impact of falling matter (strings in our setting) in the metric. Only then one may see a transition from extremal black hole (AdS metric we use) to non-extremal black hole with matter mass added and a *nonzero horizon formed*. The horizon, when present, does provide both Hawking temperature and Bekenstein entropy. We expect to use in the next paper of this series a "two-membrane paradigm", in which collision debries are represented by one (falling) membrane, and the (rising and then falling because of stretching) horizon membrane by the other. (These two membranes can be associated with the so called top-down and down-up equilibration scenarios, proposed in literature in various model settings.) When and where most of the entropy is produced is the major issue to be addressed. How that is reflected in the "hologram" observed in the gauge theory could then be calculated in the linearized approximation, as above.

Chapter 5

Gravitational collapsing shell

5.1 Introduction

Observation at RHIC of collective flows in relativistic heavy ion collisions, well described by ideal hydrodynamics [51, 52] have lead to a paradigm shift in the field toward studies of strongly coupled plasmas. AdS/CFT correspondence [1–3] is one of actively pursuit directions, both for understanding of strongly coupled gauge theories in general and properties of Quark-Gluon Plasma (QGP) in particularly: for recent review see [53].

This paper continues the line of work of our two previous papers, [54] and [57], which we will call I and II respectively below. Those papers include extensive introduction explaining our approach to the problem, which we will not repeat here. Let us just say that in those works we dealt with "elementary" collisions – calculating the shape of the falling string between two departing charges and its hologram at the boundary – which in the QCD language can be related to e^+e^- annihilation into a pair of heavy quarks or pp collisions. Thus in I and II there was no horizon on the gravity side and no temperature or entropy on the matter side. In this paper we address these issues, related with heavy ion collisions and equilibration.

Properties of equilibrium strongly coupled conformal plasma is by now well studied in significant detail in the AdS setting, in static thermal AdS-BH metric suggested by Witten. Many details about quasinormal modes of this metric and in particularly the correlators of stress tensors and their spectral densities are known, we especially recommend [59–62]. Recent developments included flowing near-equilibrium state, with slowly/gradually deformed horizons and derivation of hydrodynamics up to second order in gradients: we will not use those here, see references in a review [53].

The most challenging task of the theory now is the understanding of how

matter manages to equilibrate so rapidly in RHIC collisions, and what exactly such equilibration means microscopically. The success of hydrodynamics in describing RHIC elliptic flow data seems to suggest the thermalization time of the order of $0.5\,fm/c$, yet its mechanism remains unclear. The quest for its mechanism involves studies of various phenomenology and theoretical approaches. We will not attempt to review it and just mention one approach to ideas of which we will refer below, the "Glasma model": see Ref.[91] and references therein. It is based on classical Yang-Mills equations and starts with the so called Color Glass Condensate initial condition. While the coupling is assumed weak in this approach, strong coherent fields make its behavior nonperturbative.

Our approach also attempts to address the transition from Glasma-like initial coherent gauge fields to incoherent near-thermal QGP, but in strong coupling and thus the AdS/CFT setting. Since the vacuum corresponds to extremal black hole solution – pure AdS geometry without a horizon – while the thermal field theory is dual to AdS black hole with a horizon, the main issue is how deposition of an extra mass – from "debris" of the collision – leads to excitation of the extremal to non-extremal black hole and dynamical creation of the horizon. In simpler words, we have to follow some kind of a gravitational collapse.

In I and II we already discuss qualitatively how falling debris created in the collisions – e.g. large number of falling strings between departing charges – make a falling matter shell or membrane. While in I we studied its fall ignoring its own weight, we have to include it now, as its near-horizon breaking is entirely due to adding the mass of the shell to total gravity. We have argued in those papers that in principle one can address the problem by following the motion of *two membranes*, the *shell* and that describing *horizon* (a la "membrane paradigm" see book by Thorne and collaborators [67]).

For now we do not study motion of those two membranes in realistic geometry, for obvious reasons starting with the simplest geometry possible. We assume that the matter shell (and thus the horizon) is $flat$ – that is independent on our world 3 spatial coordinates, and moves only in the 5-th holographic direction[1]. The setup of this gravitational collapse model is described in Sec.5.2. The equation of motion for the shell is given by Israel junction condition[35] which we solve numerically. We find how its trajectory depends on the property of the shell; but in all cases the distant observer sees its slow approach to the horizon at late time.

Early works along this path include important papers [63–65] which we partly follow. They consider a collapsing shell geometry, but unlike us they use

[1]the equilibration in this setting is not due to spatial gradient as in hydrodynamics

as a probe some bulk scalar field and we don't find their boundary conditions at the shell sufficiently convincing, and we tried to improve those by using gravitons instead.

What the observer sees as the shell falls is dual to the evolution of $\mathcal{N}=4$ SYM from certain initial ensemble to the final thermal equilibrium. The insight into the problem of thermalization is thus obtained by studying various observables – the induced stress tensor and its correlation functions on the boundary – while the shell is somewhere in its process of falling. The former is given by one-point function and the metric above the shell, which in our geometry is time *independent* AdS black hole metric. Thus the "single point observer" who is only able to measure the *average density and pressure* would be driven to the conclusion that the matter is fully equilibrated at all times. More sophisticated "two point observer"– measuring the stress tensor correlation functions – would however be able to see the deviations the from the thermal ensemble. We compute those deviations in Sec. 5.3, using various components of the graviton perturbations to probe the gravitational background with a shell.

As a significant technical advance of this work, we show that unique prescription for boundary conditions for the gravity waves on the shell follows from the junction condition itself. Thus we show how correctly propagate the graviton wave across the shell, relating the obvious infalling conditions near the AdS center to what is seen on the boundary. Explicit expressions are obtained for two-point function in near equilibrium stages, when the shell is close to the horizon. We solve the wave equations both numerically and using the WKB approximation, finding good agreement between the two. Possible implications of the results are finally summarized and discussed in Sec.5.4.

5.2 Gravitationally collapsing shell in AdS

5.2.1 The background metric

Our setting includes the basic AdS background, described by the metric $ds^2 = \frac{-dt^2+d\vec{x}^2+dz^2}{z^2}$. Its holographic coordinate z is zero at the boundary (UV) and infinity at the AdS center (IR). The problem considered is a simple generalization of Israel's original problem, which was collapsing spherical shell in asymptotically flat 3d space. And it shares its main feature: although the shell is falling with its radial position time depending, the gravity both inside and outside it is time independent. Furthermore, inside a sphere there is no influence of the shell's existence at all: the famous statement going back to Newton himself. The gravity outside only knows the total shell mass.

It is not difficult to prove that the same is true for flat shell in the AdS setting as well. Starting with a generic form:

$$ds^2 = -A(z,t)dt^2 + B(z,t)d\vec{x}^2 + C(z,t)dz^2 \tag{5.1}$$

one can set $B = \frac{1}{z^2}$ by a coordinate transformation. The metric has to satisfy the vacuum Einstein equation

$$G_{\mu\nu} - \Lambda g_{\mu\nu} = 0 \tag{5.2}$$

with $\Lambda = 6$ both above[2] $z < z_m$ and below $z > z_m$ the shell's position z_m. We will also refer to those as "outside" and "inside" regions below.

The tz component tells us that $\partial_t C = 0$. The tt,zz equations are used to obtain:

$$\begin{aligned} C(z,t) &= \frac{1}{z^2(1+kz^4)} \\ A(z,t) &= F(t)\frac{1+kz^4}{z^2} \end{aligned} \tag{5.3}$$

$F(t)$ can be dropped by a rescaling in the t coordinate. Now we require the metric should reduce to the AdS form infinitely far away from the shell. as $z \to 0$, we can have $k = -\frac{1}{z_h^4}$, then outside the shell the metric is in form of translationally invariant AdS-black hole(AdS-BH). On the other hand, inside at the AdS center $z \to \infty$ we have to set $k = 0$ to suppress the z^4 term. Therefore the inside is just AdS metric.

So the background metric is the combination of AdS-BH and AdS, with the two metrics separated by a shell. We will use the metric in the usual form

$$ds^2 = \frac{R^2}{z^2}(-f(z)dt^2 + d\vec{x}^2 + dz^2/f(z)) \tag{5.4}$$

with $f = 1 - \frac{z^4}{z_h^4}$ (or $f = 1$) outside (or inside) the shell position z_m. $\vec{x}$ and z are both continuous in order for $\frac{d\vec{x}^2}{z^2}$ to match.

Note that a singularity at $z = z_h$ is outside the region where the former metric is used, as $z_m < z_h$. This does not mean that there is no horizon in the problem: in spite of pure AdS metric inside, the dynamical horizon and trapped surface (both time dependent) do exists.

---

[2]The reader is reminded that the coordinate z is inversely proportional to radial coordinate, thus somewhat counterintuitive inequalities.

5.2.2 Israel junction conditions and the falling shell

As in [54], the strings in AdS bulk were modeled by a shell (membrane), the action of which is given by:

$$S_m = -p \int d^4\sigma \sqrt{-det g_{ij}} \tag{5.5}$$

where g_{ij} is the induced metric on the shell. p is the only parameter characterizing the shell.

We use Lanczos equation to study the falling of the shell:

$$[K_{ij}] - g_{ij}[K] = -\kappa_5^2 S_{ij} \tag{5.6}$$

where $[K_{ij}] = K_{ij}^+ - K_{ij}^-$ and $K_{ij} = n_\alpha(\frac{\partial^2 x^\alpha}{\partial\xi^i\partial\xi^j} + \Gamma^\alpha_{\beta\gamma}\frac{\partial x^\beta}{\partial\xi^i}\frac{\partial x^\gamma}{\partial\xi^j})$

We parametrize the induced metric on the shell as follows:

$$ds_\Sigma^2 = -\frac{d\tau^2}{z^2} + \frac{d\vec{x}^2}{z^2} \tag{5.7}$$

We choose $\alpha = t, z, \vec{x}$ and $i = \tau, \vec{x}$ Assume the EOM is given by $z(\tau), t(\tau)$.

The norm n_α is determined from the condition $n_\alpha dx^\alpha = 0$ and $n^2 = 1$ as:

$$n_\alpha = (-\frac{\dot{z}}{z}, \vec{0}, \frac{\dot{t}}{z}) \tag{5.8}$$

Note here the norm points to the AdS center($z = \infty$). Therefore we have +:inside; −:outside

The curvature K is calculated as follows:

$$K_{\tau\tau} = \frac{\dot{t}}{z}(\frac{ff' + 2f\ddot{z}}{2(f + \dot{z}^2)} - \frac{f}{z}) \tag{5.9}$$

$$K_{xx} = \frac{\dot{t}}{z}\frac{f}{z} \tag{5.10}$$

S_{ij} is determined from the shell action: $S_{ij} = \frac{2}{\sqrt{-g}}\frac{\delta S_m}{\delta g^{ij}} = p g_{ij}$. (5.6) becomes:

$$[K_{\tau\tau} - g_{\tau\tau}K] = \frac{\kappa_5^2 p}{z^2} \tag{5.11}$$

$$[K_{xx} - g_{xx}K] = -\frac{\kappa_5^2 p}{z^2} \tag{5.12}$$

$$(5.11) \Rightarrow \sqrt{1+\dot{z}^2} - \sqrt{f+\dot{z}^2} = \frac{\kappa_5^2 p}{3} \tag{5.13}$$

$$(5.11) + (5.12) \Rightarrow [\frac{\dot{t}}{z}\frac{f f' + 2f\ddot{z}}{2(f+\dot{z}^2)}] = 0 \Rightarrow [\frac{(f'+2\ddot{z})\dot{z}}{2(f+\dot{z}^2)}] = 0$$

$$\Rightarrow [\frac{d\sqrt{f+\dot{z}^2}}{d\tau}] = 0 \tag{5.14}$$

(5.14) is solved by (5.13) with integration constant determined!

$$\dot{z} = \sqrt{(\frac{\kappa_5^2 p}{6})^2 + (\frac{3}{2\kappa_5^2 p})^2 (1-f)^2 - \frac{1+f}{2}} \tag{5.15}$$

The falling velocity seen by distant observer is given by:

$$\frac{dz}{dt} = \frac{\dot{z}}{\dot{t}} = \frac{f\sqrt{(\frac{\kappa_5^2 p}{6})^2 + (\frac{3}{2\kappa_5^2 p})^2 (1-f)^2 - \frac{1+f}{2}}}{\frac{\kappa_5^2 p}{6} + \frac{3}{2\kappa_5^2 p}(1-f)} \tag{5.16}$$

Suppose the shell starts falling at $z = z_0 > 0$ with vanishing initial velocity. The horizon radius z_h can be expressed in terms of z_0 and $\kappa_5^2 p$:

$$\frac{z_0^4}{z_h^4} = 1 - f(z_0) = 4(1 - \frac{\kappa_5^2 p}{6})\frac{\kappa_5^2 p}{6} \tag{5.17}$$

Note (5.17) implies another constraint $\kappa_5^2 p < 6$. The independent parameters z_0 and p should be estimated from the initial conditions(e.g. energy density, particle number), these will determine the equilibrium temperature of the evolution.

With chosen parameters, it is easy to integrate (5.16) to give the trajectory of the shell. We have plotted the shell trajectory in Fig.5.1. It shows three stages of falling, initial acceleration ($z = z_0 + \#t^2$), intermediate near-constant velocity fall, and the final near-horizon freezing with exponentially small deviation ($z = z_h - e^{-\#t}$).

Finally, what are the physical meaning of the parameters of our model, the initial position z_0 and the shell tension p? The wave functions of the colliding nuclei are believed to be [68] concentrated at the certain momentum scale called the "saturation scale" Q_s, which depends on collision energy and nuclei:

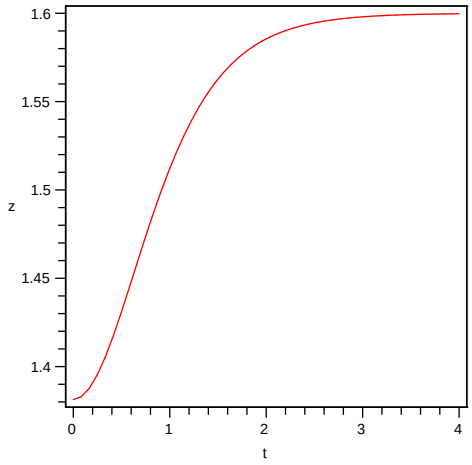

Figure 5.1: The shell trajectory as a function of time. It starts at rest at $z = z_0$ with a constant acceleration, followed by a constant falling and eventually approaches the horizon in a exponential fashion. The parameter we choose are $\kappa_5^2 p = 1$ and $z_h = 1.6$

it is about 1.5 GeV at RHIC. The holographic coordinate has the meaning of the inverse momentum scale in the renormalization group sense, thus its initial value should be identified with inverses saturation scale $z_0 = 1/Q_s$. Further "falling" corresponds to motion of the wave function into the infrared direction, till equilibrium is reached. The initial temperatures at RHIC (and thus $z_h = 1/\pi T$ are believed to be about .35 GeV, with $\pi T \approx 1.1\, GeV$: thus the expected inequality $z_h > z_0$ is satisfied.

(Physical fireballs not only equilibrate but also expand, with T decreasing by a factor 3-4 in RHIC collisions. This would correspond to a *departing* horizon toward larger z, as suggested in [23], but this feature is of course not included in the present model.)

The corresponding tension of the shell p may be calculated from (5.17). Although we do not follow this direction here, one may attempt to calculate it in a particular model of the collisions. In particular, the so called Lund model prescribe how many color strings per transverse area is created, and as the shell is but an approximation to all those strings falling together, its tension may be identified with the *sum* of the tensions of all the strings.

5.3 Correlation functions of the Gauge Theory

With the complete gravity background at hand, we are ready to study the property of the dual gauge theory under thermalization. We already commented that since the metric is asymptoticly AdS-BH, the one-point function of the stress tensor is the same as thermal SYM result. Therefore we consider the two-point functions as the expected place to find deviations from the equilibrated thermal ensemble.

The most standard way is to study a probe field in the background which is dual to some boundary operator, then use AdS/CFT prescription to find the correlation function. The simplest probe field used in early works was the bulk scalar [63–65]. However we choose to use various components of the metric field, $h_{mn}(m, n = t, \vec{x})$, which is dual to the boundary stress tensor. One obvious reason is to avoid the introduction of new field into the problem. The other reason involves the matching condition of h_{mn} on the shell, as will become clear later. Also we only probe the geometry after the creation of the shell.

Thus we solve for the metric perturbation $h_{mn}(t, x)$ propagating in the bulk specified above. This is a very difficult task in general, because the shell is always falling and thus there are time dependent boundary condition at the shell: this makes a straightforward Fourier decomposition in time impossible. However, a possible simplification can be made if the Fourier mode is much faster than the falling of shell, i.e. the condition $\omega \gg \frac{dz}{dt}$ holds, we may consider the shell as quasi-static. In this limit, we can trust the Fourier mode and study the problem in the usual way. In other words, we only trust quantities obtained for $\omega \gg \frac{dz}{dt}$. With this argument, we can in principle study two-point function in any stage provided the mode is fast enough.

5.3.1 Matching Condition on the Shell

Israel junction condition in general should be applicable for any gravity fields. Therefore, one can apply it for background plus graviton perturbation and from the latter obtain the matching condition for the graviton.

Similar as in Sec.5.2.2, we start with the Lanczos equation:

$$[K_{ij} - g_{ij}K] = -\kappa_5^2 S_{ij} = -\kappa_5^2 p g_{ij} \tag{5.18}$$

which we cast into a different form:

$$[K_{ij}] = \frac{\kappa_5^2 p}{3} g_{ij} \tag{5.19}$$

The zeroth order (in h_{mn}) Lanczos equation have already been used above, for calculation of the trajectory of the shell. Now we require vanishing of the first order terms in Lanczos equation

$$K_{ij} = n_\alpha \left(\frac{\partial^2 x^\alpha}{\partial \xi^i \partial \xi^j} + \Gamma^\alpha_{\beta\gamma} \frac{\partial x^\beta}{\partial \xi^i} \frac{\partial x^\gamma}{\partial \xi^j}\right) \tag{5.20}$$

with $\alpha = t, z, \vec{x}$ and $i = \tau, \vec{x}$. $n_\alpha = (-\frac{\dot{z}}{z}, \vec{0}, \frac{\dot{t}}{z})$ remains unchanged, so the variation of K_{ij} comes entirely from Christoffel:

$$\delta K_{ij} = n_\alpha \delta\Gamma^\alpha_{\beta\gamma} \frac{\partial x^\beta}{\partial \xi^i} \frac{\partial x^\gamma}{\partial \xi^j} \tag{5.21}$$

We choose the gauge $h_{\mu z} = 0$ and further assume $h_{mn} = h_{mn}(t, w, z)$, where $x \equiv x_1$,$y \equiv x_2$,$w \equiv x_3$. This will not affect the two-point function because the gravity background is rotationally invariant in R^3 Calculating the variation of Christoffel to the first order in h_{mn} and noting $\dot{z} = 0$,$\dot{t} = \frac{\sqrt{f+\dot{z}^2}}{f} = \frac{1}{\sqrt{f}}$ (quasi-static limit), we find the only non-vanishing components of δK_{ij} is:

$$\begin{aligned}
\delta K_{xy} &= -\frac{\sqrt{f} z}{2} \partial_z h_{xy} \\
\delta K_{\tau x} &= -\frac{z}{2} \partial_z h_{tx} \\
\delta K_{xw} &= -\frac{z\sqrt{f}}{2} \partial_z h_{xw} \\
\delta K_{\tau\tau} &= -\frac{z}{2\sqrt{f}} \partial_z h_{tt} \\
\delta K_{\tau w} &= -\frac{z}{2} \partial_z h_{tw} \\
\delta K_{xx} &= -\frac{z\sqrt{f}}{2} \partial_z h_{xx} \\
\delta K_{ww} &= -\frac{z\sqrt{f}}{2} \partial_z h_{ww}
\end{aligned}$$

We have omitted some components involving index y: those can be obtained by the substitution $x \to y$ from those listed above. Plugging to (5.19), we

have:

$$
\begin{aligned}
&\partial_z h_{xy} - \sqrt{f}\partial_z h^f_{xy} = -\frac{2\kappa_5^2 p}{3z} h_{xy} \\
&h_{xy} = h^f_{xy} \\
&\partial_z h_{tx} - \partial_z h^f_{tx} = -\frac{2\kappa_5^2 p}{3z} h_{tx} \\
&h_{tx} = h^f_{tx}\dot{t} = \frac{h^f_{tx}}{\sqrt{f}} \\
&\partial_z h_{xw} - \sqrt{f} h^f_{xw} = -\frac{2\kappa_5^2 p}{3z} h_{xw} \\
&h_{xw} = h^f_{xw} \\
&\partial_z h_{tt} - \frac{1}{\sqrt{f}}\partial_z h^f_{tt} = -\frac{2\kappa_5^2 p}{3z} h_{tt} \\
&h_{tt} = \frac{h^f_{tt}}{f} \\
&\partial_z h_{tw} - \partial_z h^f_{tw} = -\frac{2\kappa_5^2 p}{3z} h_{tw} \\
&h_{tw} = \frac{h^f_{tw}}{\sqrt{f}} \\
&\partial_z h_{xx} - \sqrt{f}\partial_z h^f_{xx} = -\frac{2\kappa_5^2 p}{3z} h_{xx} \\
&h_{xx} = h^f_{xx} \\
&\partial_z h_{ww} - \sqrt{f}\partial_z h^f_{ww} = -\frac{2}{\kappa_5^2 p} 3z h_{ww} \\
&h_{ww} = h^f_{ww}
\end{aligned}
\tag{5.22}
$$

We use from here on h_{mn} and h^f_{mn} for metric perturbations inside and outside the shell respectively. All the quantities are evaluated on the shell $z = z_m$. The other identities follow from the continuity of induced metric across the shell.

Note the jump in time coordinate, we have to do the Fourier transform in a consistent way[3]: $\int dt_{out} e^{i\omega t_{out}} = \frac{1}{\sqrt{f}} \int dt_{in} e^{i\omega/\sqrt{f} t_{in}}$, The indices "in" and "out" represent quantities inside and outside the shell. We use ω as the frequency measured by clock outside the shell, the corresponding frequency inside is given by $\frac{\omega}{\sqrt{f}}$. Thus we obtain from (5.22):

[3]The convention we use is $h_{mn}(t,w) = \int \tilde{h}_{mn}(\omega,q) e^{i\omega t - iqw} dt dw$

$$
\begin{aligned}
\tilde{h}^f_{xy} &= \frac{1}{\sqrt{f}}\tilde{h}_{xy} \\
\partial_z\tilde{h}^f_{xy} &= \frac{1}{f}(\partial_z\tilde{h}_{xy} + \frac{2\kappa_5^2 p}{3z}\tilde{h}_{xy}) \\
\tilde{h}^f_{tx} &= \tilde{h}_{tx} \\
\partial_z\tilde{h}^f_{tx} &= \frac{1}{\sqrt{f}}(\partial_z\tilde{h}_{tx} + \frac{2\kappa_5^2 p}{3z}\tilde{h}_{tx}) \\
\tilde{h}^f_{xw} &= \frac{\tilde{h}_{xw}}{\sqrt{f}} \\
\partial_z\tilde{h}^f_{xw} &= \frac{1}{f}(\partial_z\tilde{h}_{xw} + \frac{2\kappa_5^2 p}{3z}\tilde{h}_{xw}) \\
\tilde{h}^f_{tt} &= \sqrt{f}\tilde{h}_{tt} \\
\partial_z\tilde{h}^f_{tt} &= \partial_z\tilde{h}_{tt} + \frac{2\kappa_5^2 p}{3z}\tilde{h}_{tt} \\
\tilde{h}^f_{tw} &= \tilde{h}_{tw} \\
\partial_z\tilde{h}^f_{tw} &= \frac{1}{\sqrt{f}}(\partial_z\tilde{h}_{tw} + \frac{2\kappa_5^2 p}{3z}\tilde{h}_{tw}) \\
\tilde{h}^f_{xx} &= \frac{1}{\sqrt{f}}\tilde{h}_{xx} \\
\partial_z\tilde{h}^f_{xx} &= \frac{1}{f}(\partial_z\tilde{h}_{xx} + \frac{2\kappa_5^2 p}{3z}\tilde{h}_{xx}) \\
\tilde{h}^f_{ww} &= \frac{1}{\sqrt{f}}\tilde{h}_{ww} \\
\partial_z\tilde{h}^f_{ww} &= \frac{1}{f}(\partial_z\tilde{h}_{ww} + \frac{2\kappa_5^2 p}{3z}\tilde{h}_{ww})
\end{aligned}
\tag{5.23}
$$

All the quantities are evaluated on the shell $z = z_m$

From here on, we define $u = \frac{z^2}{z_h^2} = z^2(\pi T)^2$ in accordance with the literature[69]. The axial gauge is just $h_{mu} = 0$. The metric perturbations can be classified into three channels, according to [60]: scalar channel: h_{xy} shear channel: h_{tx} and h_{xw} sound channel include h_{tt}, h_{tw}, h_{ww} and $h_{aa} = h_{xx} + h_{yy}$

The metric perturbations satisfy linearized Einstein equation, and they are determined up to residual gauge transformation $h_{mn} \to h_{mn} - \nabla_m\xi_n - \nabla_n\xi_m$ where ξ_m should preserve the axial gauge chosen above. Instead of fixing the gauge, one can look for gauge invariant combination in each channel. The behavior of these gauge invariant objects encodes complete information of

retarded correlator[60, 70].[4]

The scalar channel

The gauge invariant object is simply $\phi_3^f = \tilde{h}_{xy}^f$ outside the shell and $\phi_3 = \tilde{h}_{xy}$ inside. The EOM of ϕ_3^f is given by(with $f = 1$ corresponding to ϕ_3)

$$\phi_3^{f\prime\prime} + \frac{1}{u}(3 - \frac{2}{f})\phi_3^{f\prime} + \frac{f-2}{u^2 f}\phi_3^f - \frac{q^2 f - \omega^2}{u f^2}\phi_3^f = 0 \tag{5.24}$$

The prime denote derivative with respect to u. The matching condition between ϕ_3^f and ϕ_3 can be easily obtained from (5.23):

$$\begin{aligned} \phi_3^f &= \frac{1}{\sqrt{f}}\phi_3 \\ \phi_3^{f\prime} &= \frac{1}{f}(\phi_3' + \frac{\kappa_5^2 p}{3u}\phi_3) \end{aligned} \tag{5.25}$$

Besides the matching condition (5.25), we also need boundary condition at AdS center to uniquely fix the solution of $\phi_3^f(\phi_3)$ in the bulk up to normalization. The boundary condition we use at AdS center $z = \infty$ is infalling wave or regular wave. With these conditions, we are ready to proceed. Let us start from inside the shell: ϕ_3 is given by the solution to the following equation:

$$\phi_3'' + \frac{1}{u}\phi_3' - \frac{\phi_3}{u^2} + \left(\frac{\omega^2}{f_m} - q^2\right)\frac{\phi_3}{u} = 0 \tag{5.26}$$

where $f_m = f(u_m)$. It origins from the jump of frequency across the shell. The EOM can be solved in terms of cylindrical function:

$$\phi_3 = \begin{cases} H_2^{(2)}(2\sqrt{\omega^2/f_m - q^2}\sqrt{u}) & \frac{\omega}{\sqrt{f_m}} > |q| \\ H_2^{(1)}(2\sqrt{\omega^2/f_m - q^2}\sqrt{u}) & \frac{\omega}{\sqrt{f_m}} < -|q| \\ K_2(2\sqrt{q^2 - \omega^2/f_m}\sqrt{u}) & |q| > \frac{\omega}{\sqrt{f_m}} \end{cases} \tag{5.27}$$

While outside the shell, ϕ_3^f can be written as a linear combination of two independent solutions, which we select to be the infalling wave and the outfalling

[4]there is a subtlety in the sound channel, which will be elaborated later

waves at the horizon[5]

$$\phi_3^f = c_+\phi_3^+ + c_-\phi_3^- \tag{5.28}$$

where $\phi_3^\pm$ are solutions to (5.24). If extrapolated to $u > u_m$, $\phi_3^\pm \sim (1-u)^{\pm i\omega/2}$ as $u \to 1$. (5.25) gives:

$$\frac{c_+}{c_-} = -\frac{\phi_3^- P - \phi_3^{-\prime} Q}{\phi_3^+ P - \phi_3^{+\prime} Q}|_{u=u_m} \tag{5.29}$$

where $P = \frac{1}{f}\left(\phi_3' - \frac{\kappa_5^2 p}{u}\phi_3\right)$, $Q = \frac{1}{\sqrt{f}}\phi_3$.

We expect to recover the equilibration because, as the shell approaches the "horizon", the region where geometry deviates from AdS-BH shrinks exponentially. The ratio $\frac{c_+}{c_-} \to \infty$. All deviations from equilibrium should become exponentially small as well, as we expect from any other small deviations from equilibrium.

We would like to confirm this limit by our matching/boundary condition. As the shell approaches the "horizon", $u_m \to 1$,$f_m \to 0$, we may disregard the third situation in (5.27). We want to calculate the ratio $\frac{c_+}{c_-}$ to the leading order in f_m or $(1-u_m)$. The correction to $\phi_3^\pm(u) = (1-u)^{\pm i\omega/2}$ is linear in f_m, while the correction from asymptotic expansion of Hankel function is of $\sqrt{f_m}$. Therefore we may simply use $\phi_3^\pm = (1-u)^{\pm i\omega/2}$.

Let's focus on the first situation $\phi_3 = H_2^{(2)}(2\lambda\sqrt{u})$, with $\lambda \equiv \sqrt{\frac{\omega^2}{f_m} - q^2} = \frac{\omega}{\sqrt{f_m}}(1+O(f_m))$. The correction due to q^2 can also be ignored at leading order. Using the asymptotic expansion of Hankel function, we find the leading order result cancels exactly in the denominator, while the counterpart survives in the numerator. We end up with:

$$\frac{c_+}{c_-} = (1-u_m)^{-i\omega}\frac{-i\omega}{\sqrt{f_m}}\frac{1}{1/8 - \kappa_5^2 p/6} \tag{5.30}$$

The asymptotic ratio (5.30) tends to infinity universally for any REAL ω, correctly recovering the AdS-BH limit.

[5]Note that it is just a formal basis for the solution above, we don't use it below the shell and there is no horizon singularity there.

The shear and the sound channels

The gauge invariant object in the former case is $\phi_1^f = q\tilde{h}_{tw}^f + \omega\tilde{h}_{xw}^f$ outside the shell and $\phi_1 = q\tilde{h}_{tw} + \frac{\omega}{\sqrt{f_m}}\tilde{h}_{xw}$ inside. Here again the frequency inside is scaled by $\frac{1}{\sqrt{f_m}}$. The matching condition between ϕ_1^f and ϕ_1 from (5.23) turns out to be the same as the scalar case, up to constant normalization:

$$\begin{aligned}\phi_1^f &= \phi_1 \\ \phi_1^{f\prime} &= \frac{1}{\sqrt{f}}(\phi_1' + \frac{\kappa_5^2 p}{3u}\phi_1)\end{aligned} \tag{5.31}$$

The EOM of ϕ_1^f is given by(with $f = 1$ corresponding to ϕ_1):

$$\begin{aligned}&\phi_1^{f\prime\prime} + \frac{f(3\omega^2 - q^2) - 2\omega^2}{uf(\omega^2 - q^2 f)}\phi_1^{f\prime} + \frac{(\omega^2 - q^2 f)^2 u + f^3 q^2 + f^2\omega^2 - 2f\omega^2}{u^2 f^2(\omega^2 - q^2 f)}\phi_1^f \\ &= 0\end{aligned} \tag{5.32}$$

With enough luck, we note ϕ_1 satisfies the same EOM as ϕ_3 (5.26), which combined with (5.31) guarantees the same asymptotic ratio (5.30).

Finally we consider the sound channel. The gauge invariant object is $\phi_2^f = \frac{1}{\sqrt{f_m}}\left(2q^2\tilde{h}_{tt}^f + 4\omega q\tilde{h}_{tw}^f + 2\omega^2\tilde{h}_{ww}^f + (q^2(2-f) - \omega^2)\tilde{h}_{aa}^f\right)$ outside the shell and $\phi_2 = 2q^2\tilde{h}_{tt} + \frac{4\omega q}{\sqrt{f_m}}\tilde{h}_{tw} + \frac{2\omega^2}{f_m}\tilde{h}_{ww} + (q^2 - \frac{\omega^2}{f_m})\tilde{h}_{aa}$ inside the shell.

This time we do not seem to have simple matching condition as (5.25) and (5.31). An exception is at $q = 0$, in which case, we have:

$$\begin{aligned}\phi_2^f &= \phi_2 \\ \phi_2^{f\prime} &= \frac{1}{\sqrt{f}}(\phi_2{}' + \frac{\kappa_5^2 p}{3u}\phi_2)\end{aligned} \tag{5.33}$$

For case $q \neq 0$, an easy way to avoid general discussion is to take advantage of the residue gauge. It can be shown by a proper choice of residue gauge, (5.33) still holds. The particular gauge choice of course does not shift the retarded correlator. We include a brief justification for (5.33) in Appendix.8

The EOM of ϕ_2^f is given by(with $f = 1$ corresponding to ϕ_2):

$$\phi_2^{f\prime\prime} - \frac{q^2f^2 - 8q^2f + 4q^2 + 9\omega^2 f - 6\omega^2}{uf(q^2f + 2q^2 - 3\omega^2)}\phi_2^{f\prime} - \frac{3\omega^2f^2 - 6\omega^2 f - 4q^2\omega^2 uf - 2q^2\omega^2 u + 3\omega^4 u + 2q^4 fu - q^2f^3 + q^4f^2u + 4q^2f^2}{u^2f^2(q^2f + 2q^2 - 3\omega^2)} \times \phi_2^f = 0 \tag{5.34}$$

We again find ϕ_2 satisfies the same EOM as ϕ_3 (5.26), which combined with (5.31) guarantees the same asymptotic ratio (5.30).

Summarizing the discussion above, we have found the EOM of gauge invariant objects for three channels:(5.24),(5.32) and (5.34). We also find universal matching condition for all three channels(up to a constant normalization):

$$\begin{aligned} \phi_a^f &= \phi_a \\ \phi_a^{f\prime} &= \frac{1}{\sqrt{f}}(\phi_a{}' + \frac{\kappa_5^2 p}{3u}\phi_a) \end{aligned} \tag{5.35}$$

where $a = 1, 2, 3$ and ϕ_a is given by (5.27). We may from now on forget about the geometry inside the shell and simply consider (5.35) as a boundary condition at the shell.

5.3.2 Retarded Correlators and their spectral densities

In this section, we will solve for the gauge invariant objects and extract the retarded correlator. As in [69], we switch from ϕ_a to $Z_a = u\phi_a/(\pi T)^2$, which couples to the boundary stress tensor. The equation satisfied by Z_a can be simply derived from (5.24), (5.32) and (5.34):

$$Z_3{}'' - \frac{1+u^2}{uf}Z_3{}' + \frac{\omega^2 - q^2 f}{uf^2}Z_3 = 0 \tag{5.36}$$

$$Z_1{}'' - \frac{(\omega^2 - q^2 f)f - u\omega^2 f'}{uf(\omega^2 - q^2 f)}Z_1{}' + \frac{\omega^2 - q^2 f}{uf^2}Z_1 = 0 \tag{5.37}$$

$$Z_2{}'' - \frac{3\omega^2(1+u^2) + q^2(2u^2 - 3u^4 - 3)}{uf(3\omega^2 + q^2(u^2-3))}Z_2{}' + \frac{3\omega^4 + q^4(3 - 4u^2 + u^4) + q^2(4u^2\omega^2 - 6\omega^2 - 4u^3 f)}{uf^2(3\omega^2 + q^2(u^2-3))}Z_2 = 0 \tag{5.38}$$

Without a simple analytical expression of the ratio between the infalling

and outfalling waves, we study numerically the solutions to (5.36). The boundary conditions from (5.35) are given by:

$$\begin{aligned} Z_a^f &= \frac{u}{\sqrt{f}} h \\ Z_a^{f\prime} &= \frac{u}{f} h' + \left(\frac{1}{\sqrt{f}} + \frac{\kappa_5^2 p}{3f} \right) h \end{aligned} \tag{5.39}$$

where $a = 1, 2, 3$. We have written the boundary conditions for the three channels in a uniform way. This is achieved by an appropriate scaling in Z_a and does not affect the two-point functions.

The retarded correlator are obtained according to the prescription specified in [70]:

$$G_a = -\pi^2 N_c^2 T^4 \lim_{u \to 0} \left(\frac{Z_a''}{2Z_a} - h_a \ln(u) \right) \tag{5.40}$$

where $h_a = -\frac{1}{2}(q^2 - \omega^2)^2$.

The retarded correlators are extracted from the boundary behavior of numerical solutions to (5.36). The retarded correlators correspond to some off-equilibrium state. We compare them with the counterparts in equilibrium state, which are obtained from numerical solutions to (5.36), but with infalling boundary conditions.

In particular, we study the retarded correlator of momentum density, energy density and transverse stress. They are related to the gauge invariant correlator by[60]:

$$G_{tx,tx} = \frac{1}{2} \frac{q^2}{\omega^2 - q^2} G_1 \tag{5.41}$$

$$G_{tt,tt} = \frac{2}{3} \frac{q^4}{(\omega^2 - q^2)^2} G_2 \tag{5.42}$$

$$G_{xy,xy} = \frac{1}{2} G_3 \tag{5.43}$$

We focus on the spectral density, which is defined by:

$$\chi_{\mu\nu,\rho\lambda}(\omega, q) = -2ImG_{\mu\nu,\rho\lambda}(\omega, q) \tag{5.44}$$

The spectral densities of the transverse stress are plotted at $q = 0$, $q = 1.5$

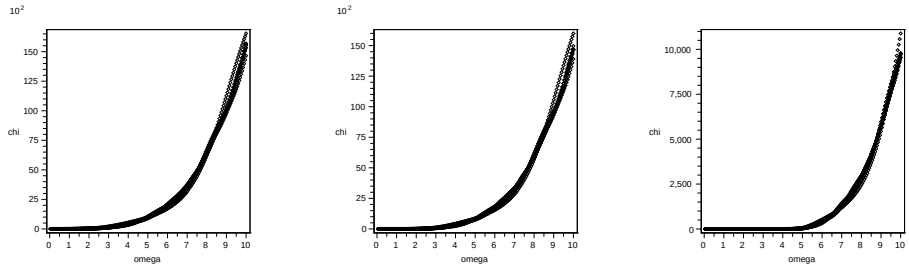

Figure 5.2: (color online)The spectral density of transverse stress $\chi_{xy,xy}$ in unit of $\pi^2 N_c^2 T^4$, at $q = 0$ left, $q = 1.5$ middle and $q = 4.5$ right. Plotted are spectral densities at different stages of thermalization: black asterisk($u_m = 0.1$), red box($u_m = 0.3$), blue circle($u_m = 0.5$), green cross($u_m = 0.7$), brown diamond($u_m = 0.9$). The thermal spectral density is also included(pink point) for comparison. The parameter we will keep using from here on is $\kappa_5^2 p = 1$

and $q = 4.5$ in Fig.5.2. Each plot includes five values of u_m, corresponding to different stage of thermalization. The thermal spectral density of the transverse stress $\chi^{th}_{xy,xy}$ is also included for comparison. All the non-thermal spectral densities can be viewed as some oscillation on top of their thermal counterpart. The first period of oscillation occurs near $\omega = q$[6]. The oscillation damps in amplitude and grows in frequency as the medium thermalizes[7], i.e. u_m approaches 1 from below. This effect is clearly illustrated in Fig.5.3, where we plot the relative deviation $R \equiv \frac{\chi_{xy,xy} - \chi^{th}_{xy,xy}}{\chi^{th}_{xy,xy}}$.

Parallel to the case of transverse stress, we also plot the spectral density of momentum density, at $q = 1.5$ and $q = 4.5$ in Fig.5.4 (The spectral density of momentum density at $q = 0$ vanishes identically). Each plot include five values of u_m, corresponding to different stage of thermalization.

The relative deviation $R \equiv \frac{\chi_{tx,tx} - \chi^{th}_{tx,tx}}{\chi^{th}_{tx,tx}}$ is plotted in Fig.5.5. We again observe the damping of amplitude and growing of frequency as the medium thermalizes.

The spectral density of energy density, at $q = 1.5$ and $q = 4.5$ are plotted in Fig.5.6. (The spectral density of energy density again vanishes). Each plot includes five values of u_m, corresponding to different stage of thermalization. The relative deviation $R \equiv \frac{\chi_{tt,tt} - \chi^{th}_{tt,tt}}{\chi^{th}_{tt,tt}}$ is plotted in Fig.5.7. We find a very sharp

[6]Similar behavior is also observed in thermal spectral density[70, 71]

[7]Here the frequency refers to the oscillation in spectral density. It is understood as the reciprocal of ω

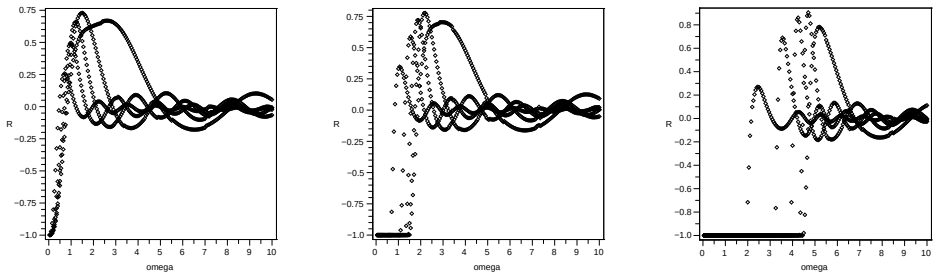

Figure 5.3: (color online)The relative deviation R at $q = 0$ left, $q = 1.5$ middle and $q = 4.5$ right. Different stages of thermalization are indicated by: black asterisk($u_m = 0.1$), red box($u_m = 0.3$), blue circle($u_m = 0.5$), green cross($u_m = 0.7$), brown diamond($u_m = 0.9$). As u_m approaches 1, i.e. the medium evolves to equilibrium, the oscillation decreases in amplitude and increases in frequency, thus the spectral density relaxes to thermal one

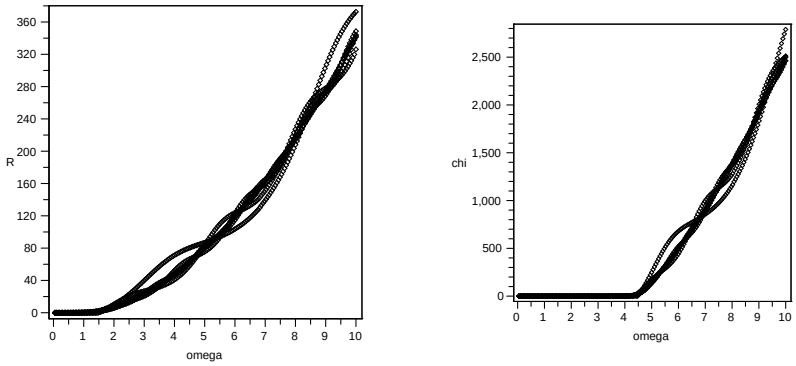

Figure 5.4: (color online)The spectral density of momentum density $\chi_{tx,tx}$ in unit of $\pi^2 N_c^2 T^4$ at $q = 1.5$ left and $q = 4.5$ right. Plotted are spectral densities at different stages of thermalization: black asterisk($u_m = 0.1$), red box($u_m = 0.3$), blue circle($u_m = 0.5$), green cross($u_m = 0.7$), brown diamond($u_m = 0.9$). The thermal spectral density is also included(pink point) for comparison

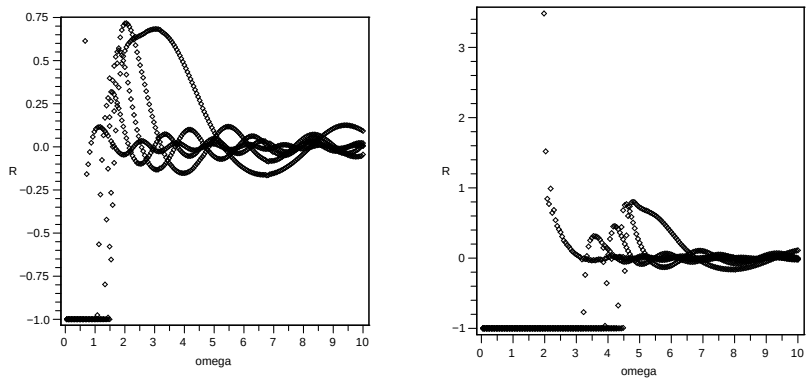

Figure 5.5: (color online)The relative deviation R at $q = 1.5$ left and $q = 4.5$ right. Different stages of thermalization are indicated by: black asterisk($u_m = 0.1$), red box($u_m = 0.3$), blue circle($u_m = 0.5$), green cross($u_m = 0.7$), brown diamond($u_m = 0.9$). As u_m approaches 1, i.e. the medium evolves to equilibrium, the oscillation decreases in amplitude and increases in frequency, thus the spectral density relaxes to thermal one

peak in the first period of oscillation, which is removed from the final plot for a better comparison. We again confirm the non-thermal spectral density relaxes to thermal one in the qualitatively the same way as described in the previous cases.

In order to explain the observed phenomenon, we would like to obtain some analytical formula for the spectral density. This is possible in the final freezing stage, where there is a simple asymptotic ratio (5.30). To the leading order in $1 - u_m$, the boundary condition as $u \to 1$ is:

$$Z_a = c_+ Z_a^+ + c_- Z_a^- \to c_+(1-u)^{\frac{i\omega}{2}} + c_-(1-u)^{\frac{-i\omega}{2}} \tag{5.45}$$

For the purpose of illuminating the problem, it is enough to focus on Z_3, the EOM of which has the simplest form. Its EOM (5.36) is solvable in terms of Heun function. However the property of Heun function is not fully understood.[8]. We have to use some approximation method, and in the regime of large ω the WKB treatment is appropriate . Following [72, 75], we obtain the expression of Z_3 near the boundary up to normalization(see Appendix.8 for details of the treatment):

[8]see [61] for a discussion

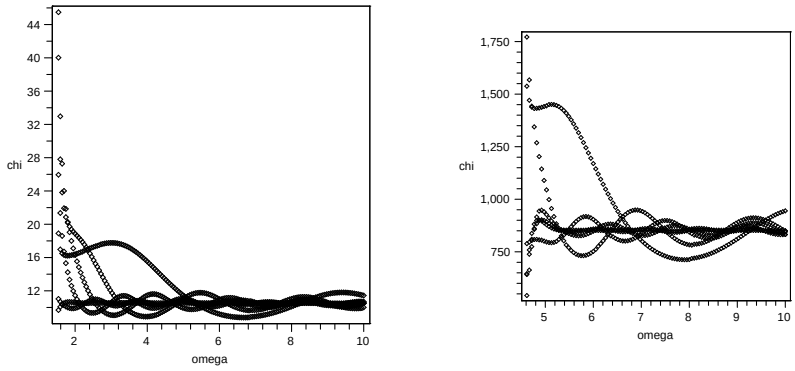

Figure 5.6: (color online)The spectral density of energy density $\chi_{tt,tt}$ in unit of $\pi^2 N_c^2 T^4$, at $q = 1.5$ left and $q = 4.5$ right. Plotted are spectral densities at different stages of thermalization: black asterisk($u_m = 0.1$), red box($u_m = 0.3$), blue circle($u_m = 0.5$), green cross($u_m = 0.7$), brown diamond($u_m = 0.9$). The thermal spectral density is also included(pink point) for comparison

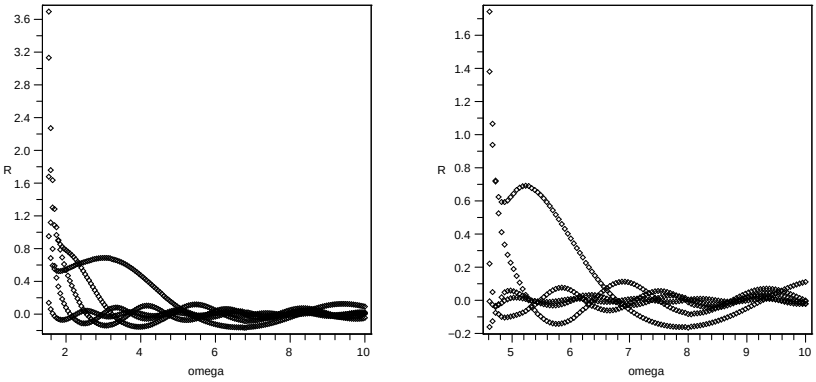

Figure 5.7: (color online)The relative deviation R at $q = 1.5$ left and $q = 4.5$ right. Different stages of thermalization are indicated by: black asterisk($u_m = 0.1$), red box($u_m = 0.3$), blue circle($u_m = 0.5$), green cross($u_m = 0.7$), brown diamond($u_m = 0.9$). As u_m approaches 1, i.e. the medium evolves to equilibrium, the oscillation decreases in amplitude and increases in frequency, thus the spectral density relaxes to thermal one

$$Z_3 = \begin{cases} \frac{u}{\sqrt{1-u^2}}\left(H_2^{(2)}(2\lambda\sqrt{u}) + \frac{ic_-}{c_+}e^{-2i\omega a_0}H_2^{(1)}(2\lambda\sqrt{u})\right) & \omega > |q| \\ \frac{u}{\sqrt{1-u^2}}\left(H_2^{(1)}(2\lambda\sqrt{u}) - \frac{ic_-}{c_+}e^{-2i\omega a_0}H_2^{(2)}(2\lambda\sqrt{u})\right) & \omega < -|q| \\ \frac{u}{\sqrt{1-u^2}}\left(1 - \frac{ic_-}{c_+}e^{-2i\omega b_0}\right)\frac{e^{\omega c_0}}{\pi}K_2(2\tilde{\lambda}\sqrt{u}) & \\ -\frac{iu}{2\sqrt{1-u^2}}\left(1 + \frac{ic_-}{c_+}e^{-2i\omega b_0}\right)e^{-\omega c_0}I_2(2\tilde{\lambda}\sqrt{u}) & 0 < \omega < |q| \\ \frac{u}{\sqrt{1-u^2}}\left(1 + \frac{ic_-}{c_+}e^{-2i\omega b_0}\right)\frac{e^{\omega c_0}}{\pi}K_2(2\tilde{\lambda}\sqrt{u}) & \\ +\frac{iu}{2\sqrt{1-u^2}}\left(1 - \frac{ic_-}{c_+}e^{-2i\omega b_0}\right)e^{-\omega c_0}I_2(2\tilde{\lambda}\sqrt{u}) & 0 > \omega > -|q| \end{cases} \tag{5.46}$$

where $\lambda = \sqrt{\omega^2 - q^2}$, $\tilde{\lambda} = \sqrt{q^2 - \omega^2}$ and the constants a_0, b_0, c_0 are defined by:

$$\begin{aligned} & lim_{u\to 1}\int_0^u du\sqrt{\frac{1-s^2(1-u^2)}{u(1-u^2)^2}} = a_0 - \frac{1}{2}ln(1-u) \\ & lim_{u\to 1}\int_{u_0}^u du\sqrt{\frac{1-s^2(1-u^2)}{u(1-u^2)^2}} = b_0 - \frac{1}{2}ln(1-u) \\ & \int_0^{u_0} du\sqrt{\frac{s^2(1-u^2)-1}{u(1-u^2)^2}} = c_0 \\ & s = |\frac{q}{\omega}| \\ & u_0 = \frac{\sqrt{s^2-1}}{s} \end{aligned} \tag{5.47}$$

The retarded correlator is calculated from the prescription (5.40). We have dropped an additional contact term: $\pi^2 N_c^2 T^4(1/2 - (\omega^2 - q^2)^2\gamma)$.

$$G^R = \begin{cases} \frac{\pi^2 N_c^2 T^4(\omega^2-q^2)^2}{4}(ln(\omega^2 - q^2) + i\epsilon\pi g(\epsilon, a_0)) & s < 1 \\ \frac{\pi^2 N_c^2 T^4(q^2-\omega^2)^2}{4}(ln(q^2 - \omega^2) + i\epsilon\pi e^{-2|\omega|c_0}g(\epsilon, b_0)) & s > 1 \end{cases} \tag{5.48}$$

where we have defined $\epsilon = sgn(\omega)$ and $g(\epsilon, c) = \frac{1+i\epsilon e^{-2i\omega c}c_-/c_+}{1-i\epsilon e^{-2i\omega c}c_-/c_+}$.

In the large ω limit, the non-logarithmic term in the second case is exponentially suppressed. Therefore the lowest order result in c_-/c_+ agrees with the zero temperature one. [72][9]. The higher order correction is due to the

[9]the imaginary part has an opposite sign, which is due to a different convention in

emergence of wave from the "horizon". The phase difference between infalling and outfalling waves gives rise to the oscillating behavior in ω. We have also calculated (5.48), with c_-/c_+ numerically obtained and restored the contact term. The result show very good agreement with retarded correlator obtained in Sec.5.3.2 in region of large ω.

The physical interpretation of (5.48) is most clear at vanishing momentum, $s = 0$. The n-th order correction appears as

$$\delta^n G^R = \frac{\pi^2 N_c^2 T^4 \omega^4}{4} 2i\pi sgn(\omega^{n+1}) \left(\frac{ic_-}{c_+} e^{-2i\omega a_0}\right)^n \tag{5.49}$$

Combined with the ratio of $\frac{c_-}{c_+}$ (5.30), the n-th order correction can be written as

$$\delta^n G^R \sim \omega^{4-n} e^{i\omega(ln(1-u_m)-2a_0)n} \tag{5.50}$$

Recall the WKB solution of the incoming wave at $s = 0$:

$$\begin{aligned} &\psi = S'^{-1/2} e^{-i\omega \int_0^u S' du + i\omega t} \\ &lim_{u\to 1} \int_0^u S' du = -\frac{1}{2} ln(1-u) + a_0 \end{aligned} \tag{5.51}$$

Taking into account the time factor $e^{i\omega t}$, we see $-(ln(1-u_m) - 2a_0)$ is just the time for the wave to travel back-and-forth in WKB potential. We define the echo time

$$t_{echo} = (-ln(1-u_m) + 2a_0) \tag{5.52}$$

in which the wave makes a roundtrip. The n'th order correction to the two-point function (spectral density) has an echo time of $n*t_{echo}$, with a suppressed amplitude, obviously the n-th echo.

This resembles the usual echo phenomenon with a sound reflected by a wall. Furthermore, the oscillations in spectral density as a function of frequency result, after the Fourier transform, in a *peak* as a function of time at the echo time. The peak is a result of many harmonics coherently added together: while smooth equilibrium spectral densities correspond to (thermally occupied) field harmonics which are completely incoherent to each other. We thus interpret

---

Fourier transform

"echo" as a partial re-appearance of coherence which was present in the original "color glass" fields at the collision moment. As the shell keeps falling toward the "horizon", $u_m \to 1$, the echo time tends to infinity and the medium loses all the coherence.

Although we derived it in near-thermal position of the shell, the echo phenomenon by itself is not restricted to the final freezing stage but exists throughout the whole process: its manifestation is in the spectral density of Fig.5.3, Fig.5.5 and Fig.5.7. Looking for "echo" in dynamical (time dependent) shell is perhaps worth addressing in later work.

5.3.3 Can the bounary observer see what happens below the shell?

In the rest of the paper we have chosen the boundary condition to correspond to the infalling wave at u-infinity (the AdS center), which leads to the solution (5.27) and its consequences discussed above. This particular choice is natural in the standard setting, when all the probes (the source and the sink) sending gravitational wave $from$ the AdS boundary $u = 0$.

Now we switch to another issue: the gravitational wave emerging from inside, below the shell, $u > u_m$. The motivation for studying this case is as follows. All stationary black hole metrics are such that no signal from the inside the horizon can propagate outside it: in particular, the geodesics do not cross horizon. But in the falling shell case we consider, the metric coincides with black hole one only above the shell, while inside it is the AdS_5 solution $without$ the horizon, since gravity of the shell produces no effect inside it. The question then is, can an observer on the boundary see what happens inside the shell?

Thus a wave sent from below would propagate all the way till the shell without any problems, and scatter on it. So we are looking now for a solution, which in the region inside the shell contains both outfalling and infalling waves, while outside ($u < u_m$) it has only outfalling wave propagating toward the boundary. At the shell the matching condition is again given by (5.23), and the precise relation between outfalling and infalling waves can be worked out parallel to what we did above. As always, a generic graviton is split into three channels, with the same eqns.

The gravitational wave outside the shell contains only the outfalling component. This is a solution in thermal-AdS metric which, if extrapolated to (non-existing) region $u_m < u < 1$ would be originating from the horizon. Thus at $u = 1$ it is $\phi_a^f \sim (1-u)^{-i\omega/2}$, it is understood as the behavior since

$u < u_m$. The wave inside the shell can be written as:

$$\phi_a = c_{in}\phi_{in} + c_{out}\phi_{out} \tag{5.53}$$

With similar argument as before, we can approximate $\phi_a^f = (1-u)^{-i\omega/2}$. Matching solutions at both sides ϕ_a^f and ϕ_a according to Israel condition (5.35), we obtain the asymptotic reflection ratio $\frac{c_{in}}{c_{out}}$

$$\frac{c_{in}}{c_{out}} = \frac{(1/8 - \kappa_5^2 p/6)\sqrt{1-u_m^2}}{\omega} exp\left(4i\omega\sqrt{\frac{u_m}{1-u_m^2}}\right) \tag{5.54}$$

which, at the shell approaching the horizon $u_m \to 1$ tends to zero. This means as the shell approaches the horizon, the portion of the wave reflected by the shell disappears, and thus all the wave emerging from below the shell is transmitted!

(To convince the reader that this conclusion is correct, here is another argument. As we have shown in the beginning of the paper, as the shell approach horizon one recovers the solution for the AdS-BH background (without any shell), with only the infalling waves on either side of the horizon without reflection (black horizon). The solution with only outfalling waves we are now describing is its complex conjugate.)

The conclusion that even at late time our collapsing shell is not that black as a horizon, as signals from inside the shell can be seen, look surprising and worrisome at first. Note however that these signals are both strongly redshifted and exponentially delayed by the warping factor $\sqrt{f(u_m)}$. As $u_m \to 1$, both effects become infinitely strong, in practical sense precluding the boundary observer from seeing what happens below the shell.

5.4 Conclusion and Outlook

Continuing the line of research started by our papers I and II, we have built a gravitational collapse scenario, describing equilibration of conformal strongly coupled plasma in the AdS/CFT setting. Using a simplified geometry we approximated falling collision debris by a single flat shell or membrane, falling from its initial position (given by the saturation scale) to its horizon (given by the equilibrium temperature). The setting itself provides inequality between the two scales, satisfied at RHIC.

The main simplification of the paper is that this shell is $flat$ - independent on our world 3 spatial coordinates. Therefore the overall solution of Einstein eqns reduces to two separate regions with well known *static* AdS-BH and AdS

metrics. The falling of the shell is time dependent, its equation of motion is determined by the Israel junction condition, which we solve and analyzed. We also determined how final temperature (horizon position) depends on initial scale and shell tension.

In statistical mechanics it is known that fluctuations at different scales are independent, and that long-range fluctuations (IR) need more time to be equilibrated than the short-range (UV) ones. With the AdS/CFT setting and our geometric simplification, this fact is taken to its perfect form. It is connected to the well known gravitational phenomenon: gravity of a sphere is independent on its size outside it, and is completely absent inside. In the equilibrating gauge theory it means that mean quantities at all scales above some $z < z_m(t)$ (corresponding to sliding position of the shell) are *exactly* as in equilibrium, while those below it are *absolutely* unaffected, being the same as in vacuum without any matter.

This is *quasiequilibrium* in the title. More specifically it means the following. In this geometry a "single point observer" – who is only able to measure the *average density and pressure* – would be driven to the conclusion that the matter is instantaneously equilibrated at *all* times. However more sophisticated "two point observer" who is able to study correlation functions of stress tensors would be able to observe deviations from the thermal case. We computed them explicitly, calculating a number of spectral densities at various positions of the shell, corresponding (in quasi-static approximation) to different stages of equilibration.

The equilibration process can roughly be divided into three stages: the initial acceleration, intermediate relativistic falling and final near-horizon freezing. By studying the graviton probes corresponding to three different combinations of h_{mn}, we calculate the retarded correlators of T_{mn} on the AdS boundary, The matching condition of h_{mn} on the shell is given by a variation of Israel junction condition. In the quasi-static limit, we study the retarded correlator of all graviton probes. We have shown that the collapsing geometry correctly reproduces the AdS-BH limit: as the shell approaches the "horizon" the ratio of the infalling wave and outfalling wave tends to infinity. We further confirmed this by numerically study the spectral density for transverse stress, momentum density and energy density, which allows us to see deviations between geometry with shell and equilibrated one (AdS BH).

We find that the main deviation between the non-thermal and equilibrium spectral densities are some oscillations. As the time goes on and the shell is at the position closer and closer to the horizon, these oscillations become exponentially smaller in amplitude and higher in frequency, eventually disappearing in the equilibrium state. In this sense we get numerical control over

the relaxation process. In the final freezing stage, when the membrane is close to the horizon, and in large ω regime, we even find analytical expressions for these deviations using the WKB method.

Oscillations in spectral densities as a function of frequency are further explained by the "echo" effect, producing peaks at certain "echo" times in the response functions. We expect at those times partial restoration of field coherence which was present at the initial time of the collision in system's wave function. For the near equilibrated medium we have the echo time analytically, from the WKB solution. The echo time tends to infinity as the medium thermalizes.

The echo phenomenon arises from the phase coherence between infalling and outfalling waves in the bulk at certain times: we expect it to exist in all gauge theory with a gravity dual. It is also interesting to extend the current study to scalar probe and vector probe. One can further study the effect of echo on electromagnetic (e^+e^-) spectral densities related to production spectra [76] which can be observable in collisions.

An attentive reader will notice that apart of small discussion of upward moving waves, we we have not yet addressed the dynamics of the horizon formation, deferred for later studies. When this paper were near-completed, we learned about an interesting work by Hubeny,Liu and Rangamani [66] who discuss certain null geodesics related observation points at the boundary. Since phases of the waves add coherently near geometric optics paths (null geodesics), this is another interesting form of coherence, although perhaps unrelated to our WKB "echos".

Finally, one may now think about relaxing our main assumption – flatness of the shell, e.g. by including first corrections resulting from slow variations of its position. In this case the metric above the shell would become time-dependent, allowing a "single point observer" to see some relaxation dynamics as well.

Chapter 6

Collision of gravitational shock waves

6.1 Introduction

The Quark Gluon Plasma(QGP) produced in Relativistic Heavy Ion Collider(RHIC) at Brookhaven National Lab is believed to be strongly coupled [8] as evidenced by its rapid equilibration, strong collective flows well reproduced by hydrodynamics, and strong jet quenching. Applications of AdS/CFT correspondence [1–3] to strongly coupled QGP has generated many fundamental results [10, 11, 13, 14] , for some further results see [53] for a recent review. However this progress so far has been mostly related either to equilibrium properties of the plasma, or to kinetics/hydrodynamics close to equilibrium.

The challenging issues related with violent initial stage of the collisions, in which the QGP is formed and equilibrated, producing most of the entropy, are not yet understood. One of them worth mentioning at the beginning is the strikingly different views on equilibration held in statistical mechanics on one hand and in AdS/CFT-based dual gravity, on the other. Statistical/kinetic approaches treat equilibration and entropy production as some gradual deformation of particle distributions, from some initial non-thermal state toward the final equilibrated one. In the dual gravity setting the source of temperature and entropy are both attributed to the gravitational horizons. Those may or may not be produced in a collision: for example decreasing the collision energy or increasing the impact parameter one may reach a point at which no horizons are formed. This implies certain singularities, or a view that switching in equilibration is similar to a phase transition rather than a gradual deformation.

Formation of a black hole in a collision, which is then is falling toward the

AdS center, was first considered in [23], with a spherical black hole. Janik and Peschanski [25] have proposed asymptotic (late-time) solution, corresponding to rapidity-independent (Bjorken) flow, see [26, 77] for most recent advances along this direction.

Grumiller and Romatschke [78] tried to describe the initial stage of high energy collisions, starting with the gravitational shock waves of certain type. In section 5 we will explore the formation of horizon in a similar setup, but taking a different point of view: the image on the boundary must be due to the source in the bulk. This will lead to a different and more consistent initial conditions, as well as subsequent evolution of matter.

A perturbative treatment of the initial conditions is discussed by Albacete, Kovchegov and Taliotis [79]. Other models of equilibration based on solutions to dynamical Einstein eqns include our previous work [80] in which a gravitationally collapsing shell of matter in AdS_5 space is considered. It sheds light on how formation of isotropic and homogeneous plasma may proceed through a very specific "quasiequilibrium" stage. We calculated the spectral densities and found they deviate from their thermal counterpart by general oscillations. Another interesting solution describing isotropization of plasma was proposed by Chesler and Yaffe [81] recently.

The issue we will address in this work is formation of trapped surfaces and entropy production in the collision of two shock waves in AdS background. The work in this direction in AdS/CFT context had started with the paper by Gubser,Pufu and Yarom [82], who considered *central* collisions of pointlike black holes in the bulk. They had located the (marginally) trapped surface at the collision moment . Its area was then used as an estimate (more accurately, the lower bound) of the entropy produced in the collision. In the limit of very large collision energy E they found that the entropy grows as $E^{2/3}$. In section 6.6 we will critically discuss how realistic are these results.

In this work we extend their work in two directions. One is the extension to collision of shock waves with a *nonzero* impact parameter. Like for shock wave collision in asymptotically flat Minkowski background [83–85], in AdS there is also an interesting jump of description: beyond certain impact parameter, the trapped surface disappears and the black hole formation no longer happens. The other direction deals with a simpler case of the so called wall-on-wall collision – collision of objects with infinite extension in transverse coordinates and nontrivial dependence in the holographic direction only, which was in a way overlooked before.

6.2 Gravitational Collisions and Trapped Surfaces

AdS/CFT approach is a duality between the $\mathcal{N}$=4 SYM theory in 3+1 dimension and string theory in $AdS_5 \times S^5$ 10-D space-time. At large number of colors the string theory is in classical (supergravity) regime. Here (and in many other related works) the angles of the sphere S^5 play no role. The 5-dim AdS_5 space has the background metric which we will write as

$$ds^2 = L^2 \frac{-dudv + (dx^1)^2 + (dx^2)^2 + dz^2}{z^2} \tag{6.1}$$

where $u = t - x^3$ and $v = t + x^3$. x^3 is longitudinal coordinate and x^1, x^2 are transverse coordinates. Effective gravity in this space (the bulk) can be related by certain rules to the $z = 0$ 4-D boundary, where the gauge theory lives. The background metric corresponds to vacuum state of the gauge theory.

The ultrarelativistic nucleus-nucleus collisions we want to model are described in the bulk as a collision of certain objects, whose hologram are the colliding nuclei. We select "longitudinal" direction to be $\pm x^3$ directions. The first step of [82] was a suggestion to model the nuclei by bulk pointlike masses. (We will return to critical discussion of this point at the end of the paper.) Their gravity field correspond to that of small black holes, and after Lorentz boost to high energy their field becomes very thin gravitational shock waves. As the shock waves approach each other, they do not interact until they meet at the collision point for causal reason. Nevertheless, the trapped surface associated with each shock wave grow as they approach the collision point, and finally merge. Note that the causality is not violated by this behavior because the trapped surface is not a physical object: in a way, it tells what happens $after$ the collision happen. The existence of trapped surface signify a black hole formation, since all matter inside it would not be able to escape.

Although in this work we would attempt to solve the Einstein eqns for times after collision, let us for completeness mention what happens next. For central collisions (or non-central ones with the impact parameter below the critical value) two colliding objects form one central black hole. Its Hawking temperature and Bekenstein entropy is perceived by the observers at the boundary $z = 0$ as the initial temperature and entropy produced in the gauge theory. When produced, the horizon of this black hole is strongly deformed, but (due to its dissipative nature) it eventually locally settles down to some stationary black hole metric. This black hole simultaneously is falling toward the AdS center ($z \to \infty$): the hologram of that is cooling and expansion of the matter produced in a collision. Since the boundary theory is conformal

and equally strongly interacting at all scales, such cooling and expansion of plasma continues indefinitely long time to arbitrarily low temperatures.

Returning to the trapped surface: its importance is in determination of what part of the system *must* end up inside the black hole. The part outside it may be carried away (as gravitational radiation) or still fall inward: thus one gets only the lower bound of the black hole mass. In this paper, we will concentrate on locating the trapped surface at the collision point and use the area of the trapped surface as a lower bound to the final black hole entropy, which by AdS/CFT sets a lower bound to the entropy production of nucleus collisions in gauge theory.

The gravitational shock waves used in [82] are written as:

$$ds^2 = L^2 \frac{-dudv + (dx^1)^2 + (dx^2)^2 + dz^2}{z^2} + L \frac{\Phi(x^1, x^2, z)}{z} \delta(u) du^2 \tag{6.2}$$

with the transverse profile $\Phi(x^1, x^2, z)$ satisfying the equation

$$\left(\Box - \frac{3}{L^2} \right) \Phi = 16\pi G_5 J_{uu} \tag{6.3}$$

with some bulk source J_{uu}, an arbitrary function. The operator $\Box$ is the the hyperbolic Laplacian on the space

$$ds^2_{H3} = L^2 \frac{(dx^1)^2 + (dx^2)^2 + dz^2}{z^2} \tag{6.4}$$

The shock wave moving in $-x^3$ direction can be obtained by the substitution $u \leftrightarrow v$ to (6.2) and (6.3).

The trapped surface is determined from the zero (non-positivity) of the so called *expansion* $\theta \leq 0$, depending on the metric. For detailed explanation of its geometric and physical meaning see e.g.[86]: it roughly corresponds to expansion or contraction of the area between two light rays (null geodesics) emitted at some small distance from each other in the same direction. Its equality to zero corresponds to the so called marginally trapped surface: these light rays neither converge nor diverge. The trapped surface is made up of two pieces: $\mathcal{S} = \mathcal{S}_1 \cup \mathcal{S}_2$. $\mathcal{S}_1(\mathcal{S}_2)$ is associated with shock wave moving in $+x^3(-x^3)$ direction before collision. An additional condition is that the outer null normal to $\mathcal{S}_1$ and $\mathcal{S}_2$ must be continuous at the intersection $\mathcal{C} = \mathcal{S}_1 \cap \mathcal{S}_2$ point $u = v = 0$ to avoid delta function in the expansion.

To find out $\mathcal{S}_1$ associated with the first shock wave,

$$ds^2 = L^2 \frac{-dudv + (dx^1)^2 + (dx^2)^2 + dz^2}{z^2} + L\frac{\Phi_1(x^1, x^2, z)}{z}\delta(u)du^2 \tag{6.5}$$

the following coordinate transformation is made to eliminate the discontinuity in geodesics:

$$v \to v + \frac{z}{L}\Phi_1\Theta(u) \tag{6.6}$$

where $\Theta(u)$ is the Heaviside step function. $\mathcal{S}_1$ is parametrized by:

$$u = 0,\ v = -\psi_1(x^1, x^2, z) \tag{6.7}$$

The expansion is defined by $\theta = h^{\mu\nu}\nabla_\mu l_\nu$, with l_ν the outer null normal to $\mathcal{S}_1$. $h^{\mu\nu}$ is the induced metric. It can be constructed from three spacelike unit vectors w_1^μ, w_2^μ, w_3^μ, which are normal to $\mathcal{S}_1$:

$$h^{\mu\nu} = w_1^\mu w_1^\nu + w_2^\mu w_2^\nu + w_3^\mu w_3^\nu \tag{6.8}$$

The vanishing of expansion corresponds to the following equation:

$$\left(\Box - \frac{3}{L^2}\right)(\Psi_1 - \Phi_1) = 0 \tag{6.9}$$

with $\Psi_1(x^1, x^2, z) = \frac{L}{z}\psi_1(x^1, x^2, z)$.

The vanishing of expansion on $\mathcal{S}_2$ associated with the second shock wave can be worked out similarly:

$$\left(\Box - \frac{3}{L^2}\right)(\Psi_2 - \Phi_2) = 0 \tag{6.10}$$

At the intersection $\mathcal{C} = \mathcal{S}_1 \cap \mathcal{S}_2$, $\mathcal{S}_1$ and $\mathcal{S}_2$ coincide, therefore $\Psi_1(x^1, x^2, z) = \Psi_2(x^1, x^2, z) = 0$. The continuity of outer null normal can be guaranteed by $\nabla\Psi_1 \cdot \nabla\Psi_2 = 4$.

In summary, the aim of finding marginally trapped surface becomes the following unusual boundary value problem:

$$\left(\Box - \frac{3}{L^2}\right)(\Psi_1 - \Phi_1) = 0$$
$$\left(\Box - \frac{3}{L^2}\right)(\Psi_2 - \Phi_2) = 0$$
$$\Psi_1|_{\mathcal{C}} = \Psi_2|_{\mathcal{C}} = 0 \tag{6.11}$$

The boundary $\mathcal{C}$ should be chosen to satisfy the constraint:

$$\nabla\Psi_1 \cdot \nabla\Psi_2|_{\mathcal{C}} = 4 \tag{6.12}$$

Note (6.11) and (6.12) are written in the form of scalar equation, invariant under coordinate transformation. For central collision, the source J_{uu} are identical for two shock waves. In [82] for simplicity they are chosen to be point-like in the bulk

$$J_{uu} = E\delta(u)\delta(z - L)\delta(x^1)\delta(x^2) \tag{6.13}$$

The solution of Φ corresponds to this source give rises to the following stress tensor on the boundary field theory:

$$T_{uu} = \frac{L^2}{4\pi G_5}\lim_{z\to 0}\frac{\Phi(x^1, x^2, z)\delta(u)}{z^3} = \frac{2L^4 E}{\pi(L^2 + (x^1)^2 + (x^2)^2)^3}\delta(u) \tag{6.14}$$

The parameters E and L can be tuned according to the energy and the transverse size of the nucleus.

The special source (6.13) preserves an $O(3)$ symmetry in H_3, which is manifest in the following coordinate system:

$$ds^2_{H3} = \frac{dr^2}{1 + r^2/L^2} + r^2\left(d\theta^2 + \sin^2\theta d\phi^2\right) \tag{6.15}$$

with the point source sitting at $r = 0$. We will elaborate the symmetry later in the context of non-central collision.

The $O(3)$ symmetry helps to solve (6.11) analytically. The area of the trapped surface can be calculated and give a lower bound to the entropy produced in the collision of shock wave, assuming the area theorem holds in AdS background.

For non-central collision, the situation is complicated by the loss of $O(3)$ symmetry. In Minkowski background, the problem of non-central collision of point shock waves in $D = 4$ was solved beautifully in [65] by conformal transformation. In $D > 4$, it was solved numerically in [84]. In all cases, a critical impact parameter was found, beyond which the trapped surface seized to exist.

In the next section, we will cast (6.11) into an integral equation, which allows us to solve (6.11) numerically.

6.3 Calculation of the Trapped Surface

Note (6.11) resembles the electrostatic problem in flat space, with Ψ being the electric potential. We are familiar with the fact that the electric potential can be expressed as an integral of surface charge density. We want to see if this can be achieved in AdS space.

Let us start with the electrostatic problem in flat space. Consider the following electrostatic problem, which is similar to (6.11):

$$\nabla^2 \Psi_i(x) = \nabla^2 \Phi_i(x) \tag{6.16}$$

$$\Psi_i(x)|_{\mathcal{C}} = 0 \tag{6.17}$$

$$\nabla \Psi_1 \cdot \nabla \Psi_2 = 4 \tag{6.18}$$

where $i = 1, 2$, ∇^2 is the Laplacian in flat space. Ψ_i is the electric potential corresponding to the source $\nabla^2 \Phi_i$, placed inside an empty chamber with conducting boundary $\mathcal{C}$. The boundary should be chosen properly such that the constraint (6.18) is also satisfied.

We want to express the electric potential by an integral of the surface charge density. This can be done with the help of the free boundary Green's function defined as the solution to:

$$\nabla^2 G(x, x') = \delta^{(3)}(\vec{x} - \vec{x}') \tag{6.19}$$

with the solution given by:

$$G(x, x') = -\frac{1}{4\pi} \frac{1}{|\vec{x} - \vec{x}'|} \tag{6.20}$$

Take (6.16) multiplied by $G(x, x')$ minus (6.19) multiplied by $\Psi_i(x)$, and

then integrate over the space inside $\mathcal{C}$, we obtain:

$$\int d^3x\big[G(x,x')\nabla^2\Psi_i(x)-\Psi_i(x)\nabla^2G(x,x')\big]=\int d^3xG(x,x')\nabla^2\Phi_i(x)-\Psi_i(x') \tag{6.21}$$

$$\int d\vec{S}\cdot\big[G(x,x')\vec{\nabla}\Psi_i(x)-\Psi_i(x)\vec{\nabla}G(x,x')\big]=\int d^3xG(x,x')\nabla^2\Phi_i(x)-\Psi_i(x') \tag{6.22}$$

Denote $B_i(x)=-\frac{\partial\Psi_i(x)}{\partial n}$(the magnitude of electric field on the boundary) and note $\Psi_i(x)$ vanishes on the boundary. With x' taken on the boundary $\mathcal{C}$, (6.22) evaluates to:

$$\int dSG(x,x')B_i(x)=\int d^3xG(x,x')\nabla^2\Phi_i(x) \tag{6.23}$$

The constraint (6.18) is simply $B_1(x)B_2(x)=4$. We have cast a problem in the volume into a problem on its boundary $\mathcal{C}$. (6.23) is a Fredholm integral equation of the first kind. We can use the following method to solve (6.16): Starting with some trial shape of $\mathcal{C}$, we can solve (6.22) to obtain $B_i(x)$ and check if (6.18) is satisfied. We can use iteration to tune the trial shape until (6.18) is satisfied.

Now we hope to apply similar method to the problem of trapped surface, the difference being the space is H_3 instead of flat.

As in case of electrostatic problem, we will keep using Green's function in AdS, defined as the solution to the following:

$$\left(\Box-\frac{3}{L^2}\right)G(x,x')=\frac{1}{\sqrt{g}}\delta^{(3)}(\vec{x}-\vec{x}') \tag{6.24}$$

where g is the metric of H_3.

The Green's function was solved in [64, 87]. We quote the result here with L dependence restored.

$$\begin{aligned}G(x,x')&=-\frac{1}{4\pi L}\frac{e^{2u}}{\sinh u}\\ \cosh u&=1+\frac{(z-z')^2+(\vec{x}_\perp-\vec{x'}_\perp)^2}{2zz'}\end{aligned} \tag{6.25}$$

where u is the invariant distance in $H_3(AdS_3)$.
It also proves useful to note another relation:

$$\begin{aligned}
&\int_M \Box f \sqrt{g} d^3x \\
&= \int_M \frac{1}{\sqrt{g}} \partial_\mu \left(\sqrt{g} g^{\mu\nu} \partial_\nu f \right) \sqrt{g} \frac{1}{3!} \epsilon_{\sigma\rho\lambda} dx^\sigma \wedge dx^\rho \wedge dx^\lambda \\
&= \int_M d(\sqrt{g} g^{\mu\nu} \partial_\nu f \epsilon_{\mu\rho\lambda} \frac{1}{2!} dx^\rho \wedge dx^\lambda)
\end{aligned} \tag{6.26}$$

where $\overline{dx}^\nu = g^{\mu\nu} \sqrt{g} \epsilon_{\mu\rho\lambda} \frac{1}{2!} dx^\rho \wedge dx^\lambda$. M is taken to be the manifold in H_3 bounded by $\mathcal{C}$, the metric g refers to H_3. f is arbitrary function of x.

With (6.26) and (6.25) at hand, we are ready to proceed:

$$\begin{cases} \left(\Box - \frac{3}{L^2}\right) \Psi_i(x) = \left(\Box - \frac{3}{L^2}\right) \Phi_i(x) \\ \left(\Box - \frac{3}{L^2}\right) G(x, x') = \frac{1}{\sqrt{g}} \delta^{(3)}(\vec{x} - \vec{x}') \end{cases} \tag{6.27}$$

with $i = 1, 2$. All the derivatives are with respect to x. The first line of (6.27) multiplied by $G(x, x')$ minus the second line of (6.27) multiplied by $\Psi_i(x)$, then integrate over M, we obtain:

$$\begin{aligned}
&\int_M \left(G(x,x') \left(\Box - \frac{3}{L^2} \right) \Psi_i(x) - \Psi_i(x) \left(\Box - \frac{3}{L^2} \right) G(x,x') \right) \sqrt{g} d^3x = \\
&\qquad \int_M G(x,x') \left(\Box - \frac{3}{L^2} \right) \Phi_i(x) \sqrt{g} d^3x - \Psi_i(x')
\end{aligned} \tag{6.28}$$

$$\begin{aligned}
&\int_M \left(G(x,x') d \left(\partial_\nu \Psi_i(x) \overline{dx}^\nu \right) - \Psi_i(x) d \left(\partial_\nu G(x,x') \overline{dx}^\nu \right) \right) = \\
&\qquad \int_M G(x,x') \left(\Box - \frac{3}{L^2} \right) \Phi_i(x) \sqrt{g} d^3x - \Psi_i(x')
\end{aligned} \tag{6.29}$$

$$\begin{aligned}
&\int_M \left(d \left(G(x,x') \partial_\nu \Psi_i(x) \overline{dx}^\nu \right) - d \left(\Psi_i(x) \partial_\nu G(x,x') \overline{dx}^\nu \right) \right) = \\
&\qquad \int_M G(x,x') \left(\Box - \frac{3}{L^2} \right) \Phi_i(x) \sqrt{g} d^3x - \Psi_i(x')
\end{aligned} \tag{6.30}$$

$$\begin{aligned}
&\int_{\partial M} \left(G(x,x') \partial_\nu \Psi_i(x) \overline{dx}^\nu - \Psi_i(x) \partial_\nu G(x,x') \overline{dx}^\nu \right) = \\
&\qquad \int_M G(x,x') \left(\Box - \frac{3}{L^2} \right) \Phi_i(x) \sqrt{g} d^3x - \Psi_i(x')
\end{aligned} \tag{6.31}$$

where in the last line we have used Stokes theorem on manifold M.

Putting x' on $\mathcal{C}$, we can simplify the above with $\Psi_i|_{\mathcal{C}} = 0$:

$$\int_{\partial M} G(x,x')\partial_\nu \Psi_i(x)\overline{dx}^\nu = \int_M G(x,x')\left(\Box - \frac{3}{L^2}\right)\Phi_i(x)\sqrt{g}d^3x \tag{6.32}$$

Furthermore, we have $\partial_\nu \psi dx^\nu = 0$ on $\mathcal{C}$ since $\Psi_i|_{\mathcal{C}} = 0$. On the other hand, $n_\nu dx^\nu|_{\mathcal{C}} = 0$, where n_ν is the unit vector normal to the boundary $\mathcal{C}$. Therefore, we may write:

$$\partial_\nu \Psi_i = -B_i n_\nu \tag{6.33}$$

With the help of (6.33), (6.32) and (6.12) can be further simplified to:

$$-\int_{\partial M} G(x,x')B_i(x)dS = \int_M G(x,x')\left(\Box - \frac{3}{L^2}\right)\Phi_i(x)\sqrt{g}d^3x \tag{6.34}$$

$$B_1(x)B_2(x) = 4 \tag{6.35}$$

where $dS \equiv n_\mu \overline{dx}^\mu$ is the area element.

Before proceeding to non-central collision, we would like to reproduce the 5-D result of [82] first. Working in spherical coordinates (6.15), the shape of $\mathcal{C}$ is parametrized by $r = \rho_0 = const.$ The simplest point shock wave corresponding to $J_{uu} = E\delta(u)\delta(z-L)\delta(x^1)\delta(x^2)$ is given by:

$$\Phi_1 = \Phi_2 = \frac{4G_5 E}{L}\frac{1 + 2(r/L)^2 - 2r/L\sqrt{1+(r/L)^2}}{r/L} \tag{6.36}$$

The Green's function (6.25) is invariant under coordinate transformation. In spherical coordinate, it is given by:

$$G(x,x') = -\frac{1}{4\pi L}\frac{e^{2u}}{\sinh u}$$
$$\cosh u = \sqrt{r^2/L^2+1}\sqrt{r'^2/L^2+1} - rr'/L^2\left[\cos\theta\cos\theta' + \sin\theta\sin\theta'\cos(\phi-\phi')\right] \tag{6.37}$$

In the presence of $O(3)$ symmetry, it is sufficient to show (6.34) holds for $\theta' = 0$, when the integral in ϕ is trivial. On the other hand, (6.35) implies $B_1 = B_2 = 2$. As a result, we only need to verify:

$$2\pi\int_0^\pi d\theta(-2)\frac{(\cosh u-\sinh u)^2}{\sinh u}\rho_0^2\sin\theta=\frac{(\sqrt{\rho_0^2+1}-\rho_0)^2}{\rho_0}(-4G_5E)4\pi$$
$$\cosh u=\rho_0^2+1-\rho_0^2\cos\theta \tag{6.38}$$

It is not difficult to complete the integral in θ, we finally arrive at $2G_5E=\sqrt{1+\rho_0^2/L^2}\rho_0^2$, which is equivalent to (115) in [82].

6.4 Colliding Point Shock Waves at nonzero Impact Parameter

6.4.1 Shock Waves in Spherical Coordinate

Consider two shock waves with impact parameter b, given by:

$$\left(\Box-\frac{3}{L^2}\right)\Psi_1=-16\pi G_5E\delta(u)\delta(z-z_0)\delta(x^1-\frac{b}{2})\delta(x^2)$$
$$\left(\Box-\frac{3}{L^2}\right)\Psi_2=-16\pi G_5E\delta(u)\delta(z-z_0)\delta(x^1+\frac{b}{2})\delta(x^2)$$

The corresponding stress energy tensor associated with two shock waves are given by:

$$T_{uu}=\frac{2L^4E}{\pi(z_0^2+(x^1-\frac{b}{2})^2+(x^2)^2)^3}\delta(u)$$
$$T_{vv}=\frac{2L^4E}{\pi(z_0^2+(x^1+\frac{b}{2})^2+(x^2)^2)^3}\delta(v)$$

Therefore z_0 characterizes the size of the nucleus. We will use spherical coordinates in solving (6.34). In case of central collision, when $b=0$. The shock wave center can be placed at the origin of spherical coordinates $r=0$. This is achieved by first going to global coordinates $Y^i(i=0,1,2,3)$:

$$
\begin{aligned}
Y^0 &= \frac{z}{2}\left(k + \frac{L^2/k + kx_\perp^2}{z^2}\right) \\
Y^3 &= \frac{z}{2}\left(-k + \frac{L^2/k - kx_\perp^2}{z^2}\right) \\
Y^1 &= L\frac{x^1}{z} \\
Y^2 &= L\frac{x^2}{z}
\end{aligned} \tag{6.39}
$$

The global coordinates link to spherical coordinates in the following way:

$$
\begin{aligned}
Y^0 &= \sqrt{r^2 + L^2} \\
Y^1 &= r\cos\theta \\
Y^2 &= r\sin\theta\cos\phi \\
Y^3 &= r\sin\theta\sin\phi
\end{aligned} \tag{6.40}
$$

When $b = 0$, the center of the shock waves can be put at the origin if we set $k = \frac{L}{z_0}$. The possibility of moving any point to the origin reflects the maximally symmetric property of AdS space.

When $b \neq 0$, we want to place the two shock waves at opposite positions with respect to the origin, so that the boundary of trapped surface $\mathcal{C}$ will have axial symmetry. Setting $1 + \frac{b^2}{4z_0^2} = \frac{L^2}{k^2 z_0^2}$, we have $Y^2 = Y^3 = 0$ and $Y^1 = \pm\frac{Lb}{2z_0}$. According to (6.40), we have the shock waves at $r = \frac{Lb}{2z_0}$, $\theta = 0$ and $\theta = \pi$. The differential equation in (6.34) becomes:

$$
\left(\Box - \frac{3}{L^2}\right)\Psi_i = -16\pi G_5 E\frac{L^3}{z_0^3}\frac{\sqrt{1 + r^2/L^2}}{r^2\sin\theta}\delta(r - r_0)\delta(\theta - \theta_i)\delta(\phi) \tag{6.41}
$$

where $r_0 = \frac{Lb}{2z_0}$, $\theta_1 = 0$, $\theta_2 = \pi$. We observe that in spherical coordinate, the trapped surface only depends on $G_5 E\frac{L^3}{z_0^3}$ and r_0. Since AdS radius is a free parameter, which will not appear alone in the final result in dual field theory, we may set $z_0 = L$ without loss of generality. As a result we have $b = 2r_0$.

6.4.2 More General Shock Waves

Before proceeding to numerical study of trapped surface, we choose to take a moment to investigate the symmetries of the problem, which will help us to study more general shock waves. To see this, we prefer to work in the differential form of the problem: (6.11) and (6.12).

As we noticed before, (6.11) and (6.12) are scalar equations. Ψ_i is a scalar. It is invariant under coordinate transformations: $x \to \tilde{x}$, $\Psi_i(x) \to \tilde{\Psi}_i(\tilde{x})$ the boundary remain the same $\mathcal{C} \to \tilde{\mathcal{C}}$, but takes a different functional form in new coordinate. As a result the third line of (6.11) and (6.12) are automatically satisfied. Suppose the transformation also preserves the form of the operator: $\Box - 3/L^2$, then $\tilde{\Psi}_i(\tilde{x})$ becomes another solution to (6.11) and (6.12). We will focus on transformations that leaves the center of the shock waves on the axis of $\theta = 0, \pi$.

To identify such a coordinate transformation, we first make a change of variable:

$$\begin{aligned} r\sin\theta &= t \\ r\cos\theta &= \sqrt{L^2+t^2}\sinh\eta \end{aligned}$$

The metric of H_3 becomes:

$$ds^2 = \frac{dt^2}{1+t^2/L^2} + (L^2+t^2)d\eta^2 + t^2 d\phi^2 \tag{6.42}$$

The metric is η independent, therefore the transformation: $\tilde{t} = t, \tilde{\phi} = \phi, \tilde{\eta} = \eta + \Delta\eta$ will not change the operator $\Box - 3/L^2$. $\tilde{t} = t$ also guarantees the center of the shock waves remain on the axis of $\theta = 0, \pi$. We have obtained the desired coordinate transformation, which is just a translation in η. It is easy to work out the corresponding transformation in spherical coordinate:

$$\begin{aligned} \tilde{r}\sin\tilde{\theta} &= r\sin\theta = t \\ \tilde{r}\cos\tilde{\theta} &= \sqrt{L^2+t^2}\sinh(\eta-\Delta\eta) \\ r\cos\theta &= \sqrt{L^2+t^2}\sinh\eta \end{aligned} \tag{6.43}$$

One can verify explicitly (6.43) preserves the form of (6.15). (6.43) moves the center of the shock waves from $Y^2 = Y^3 = 0$, $Y^1 = \pm r_0$ to $Y^2 = Y^3 = 0$, $Y^1 = \pm r_0\cosh\Delta\eta - \sqrt{L^2+r_0^2}\sinh\Delta\eta$. This means collision of shock waves

centered at $Y^2 = Y^3 = 0$, $Y^1 = \pm r_0 \cosh \Delta\eta - \sqrt{L^2 + r_0^2} \sinh \Delta\eta$ will generate the same entropy as those centered at $Y^2 = Y^3 = 0$, $Y^1 = \pm r_0$. This allows us to study the collision of more general shock waves. Let us consider the following shock waves:

$$\begin{aligned}\left(\Box - \frac{3}{L^2}\right)\Psi_1 &= -16\pi G_5 E_u \delta(u)\delta(z - z_u)\delta(x^1 - x_u)\delta(x^2) \\ \left(\Box - \frac{3}{L^2}\right)\Psi_2 &= -16\pi G_5 E_v \delta(v)\delta(z - z_v)\delta(x^1 - x_v)\delta(x^2)\end{aligned} \tag{6.44}$$

In this paper, we restrict our interest to shock waves with identical invariant energy, defined by $E_u \frac{L^3}{z_u^3} = E_v \frac{L^3}{z_v^3} \equiv E$. This keeps the mirror symmetry of the problem intact. We will see the center of the shock waves can be placed at $Y^2 = Y^3 = 0$, $Y^1 = \pm r_0 \cosh \Delta\eta - \sqrt{L^2 + r_0^2} \sinh \Delta\eta$. This is equivalent to the statement that a solution can always be found to the following equations:

$$\begin{aligned}L\frac{x_u}{z_u} &= r_0 \cosh \Delta\eta - \sqrt{L^2 + r_0^2} \sinh \Delta\eta \\ L\frac{x_v}{z_v} &= -r_0 \cosh \Delta\eta - \sqrt{L^2 + r_0^2} \sinh \Delta\eta \\ k^2\left(1 + \frac{x_u^2}{z_u^2}\right) &= \frac{L^2}{z_u^2} \\ k^2\left(1 + \frac{x_v^2}{z_v^2}\right) &= \frac{L^2}{z_v^2} \\ x_u - x_v &= \Delta x\end{aligned} \tag{6.45}$$

(6.45) can be solved easily by switching to the variable $\eta_0 = \sinh^{-1} \frac{r_0}{L}$. A solution to (6.45) always exists for any given z_u, z_v and Δx. We include the corresponding r_0 here, as it is the only relevant quantity, apart from E, for entropy calculation:

$$\frac{r_0}{L} = \sqrt{\frac{(z_u - z_v)^2 + \Delta x^2}{4 z_u z_v}} \tag{6.46}$$

In summary, we have shown that for shock waves (6.44) satisfying $E_u \frac{L^3}{z_u^3} = E_v \frac{L^3}{z_v^3} \equiv E$, the entropy is only a function of $G_5 E$ and (6.46). Note r_0 is only a function of invariant distance between the center of shock waves.

6.4.3 Numerical Solution of Trapped Surface

With all the simplification, we are ready to find the trapped surface for different impact parameter. Our procedure is as follows: Axial symmetry allows us to parametrize $\mathcal{C}$ by $r = \rho(\theta)$. Integral in ϕ on the LHS of (6.34) can be expressed in terms of elliptic integrals. (6.34) becomes essentially 1-D integral equation. We discretize the integral by 199 points, equally spaced in the full range of θ. The integral on the LHS of (6.34) is discretized accordingly, and the integral on the RHS can be expressed in terms of elementary function due to the simple form of the shock wave. We use the same sample points for θ', bringing (6.34) into a matrix form:

$$\sum_j B(\theta_j) K(\theta_j, \theta'_i) = S(\theta'_i) \tag{6.47}$$

where the indices $i, j = 1, \cdots, 199$. $K(\theta_j, \theta'_i)$ contains the Green's function and the induced metric. $S(\theta'_i)$ is from the RHS integral of shock wave.

A special treatment is needed for diagonal matrix element of $K(\theta_j, \theta'_i)$ where $\theta_j = \theta'_i$. The explicit integrand expressed in terms of elliptic integrals shows the it is logarithmically divergent in $|\theta - \theta'|$, yet the integral is convergent. The integral in this interval, represented by the diagonal matrix element, is estimated by sampling the integrand by certain number of points in the interval. The sample integrand are used to extract the coefficients of terms $\ln|\theta - \theta'|$, 1, $(\theta - \theta')\ln|\theta - \theta'|$ and $\theta - \theta'$ by method of least squares. Those coefficients are finally used for calculation of diagonal matrix elements.

The mirror symmetry of the two shock waves implies $B_2(\theta) = B_1(\pi - \theta)$. Therefore it is sufficient to calculate one of them. Given a trial shape of trapped surface $r = \rho(\theta)$, which is also necessarily symmetric under $\theta \leftrightarrow \pi - \theta$, we can solve for $B(\theta)$ from (6.47). We then evaluate $\Delta(\theta) = B_1(\theta)B_2(\theta) - 4$ and tune the shape function accordingly. We repeat the process until (6.35) is satisfied to certain accuracy. In order to assure fast convergence, we find it very helpful to calculate the gradient of $\rho(\theta)$. The gradient is the matrix form of the functional derivative: $\frac{\delta\Delta[\rho(\theta)]}{\delta\rho(\theta)}$. We parametrized $\mathcal{C}$ by: $\rho(\theta) = \sum_{n=1}^{M} a_n \cos 2(n-1)\theta$, where M is a truncation number. The same decomposition applies to $\Delta(\theta)$: $\Delta(\theta) = \sum_{n=1}^{M} b_n \cos 2(n-1)\theta$. The gradient in this representation is given by a $M \times M$ matrix: $\frac{\delta b_m}{\delta a_n}$, which again contains elliptic integrals. For a given collision energy, we can find the boundary $\mathcal{C}$ until certain critical impact parameter is reached. The critical impact parameter is located where $\frac{\partial\rho(\theta)}{\partial b}$ diverges[84]. Empirically, the gradient $\frac{\delta b_m}{\delta a_n}$ converges as $\Delta(\theta)$ reduces in the iteration, if the impact parameter is within the critical value. The gradient diverges as $\Delta(\theta)$

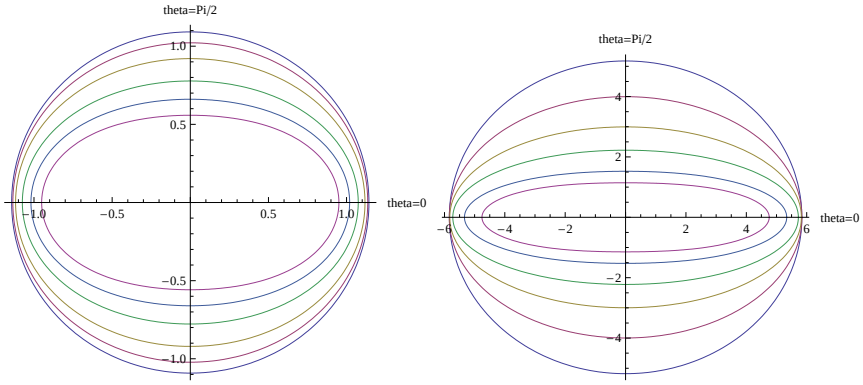

Figure 6.1: (left)The shapes of $\mathcal{C}$ (the trapped surface at $u = v = 0$) at $\frac{G_5 E}{L^2} = 1$. The impact parameters used in the plot are $0.4L$, $0.6L$, $0.8L$, $1.0L$, $1.1L$, $1.14L$ from the outer to the inner. The innermost shape being the critical trapped surface. (right)The shapes of $\mathcal{C}$ (the trapped surface at $u = v = 0$) at $\frac{G_5 E}{L^2} = 100$. The impact parameters used in the plot are $1.0L$, $2.0L$, $3.0L$, $4.0L$, $5.0L$, $5.3L$ from the outer to the inner. The innermost shape being the critical trapped surface. As collision energy grows, the trapped surface gets elongated in the axis of mismatch.

Table 6.1: critical impact parameter at different energies

$\frac{G_5 E}{L^2}$	0.1	0.5	1	4	9	12	15	50	100
$\frac{b_c}{L}$	0.40	0.86	1.14	1.90	2.50	2.74	2.94	4.28	5.30

reduces in the iteration, if the impact parameter lie beyond the critical value.

Fig.6.1 shows the shapes of trapped surface at $\frac{G_5 E}{L^2} = 1$ and $\frac{G_5 E}{L^2} = 100$ for different impact parameters. The shapes are represented in spherical coordinate. We observe the critical trapped surface does not scale with collision energy in spherical coordinate. As collision energy grows, the trapped surface gets elongated in the axis of mismatch and larger M is needed to reach prescribed accuracy.

We also obtained several critical impact parameters corresponding to different energies. The results are listed in Table.6.1

Fig.6.2 shows the log-log plot of critical impact parameter versus collision energy. It suggests a simple power law within the energy range used in the numerical study. The data are fitted with $\frac{b_c}{L} = \alpha \left(\frac{G_5 E}{L^2}\right)^{\beta}$ to give:

$$\alpha = 1.07, \quad \beta = 0.37 \tag{6.48}$$

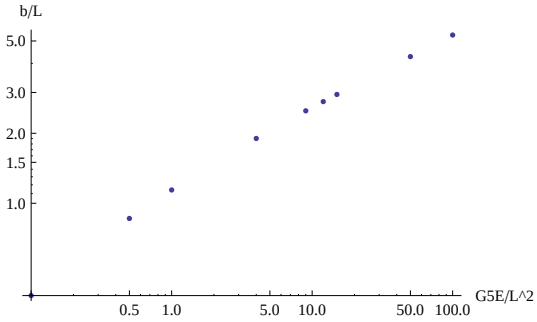

Figure 6.2: The log-log plot of critical impact parameter versus collision energy.

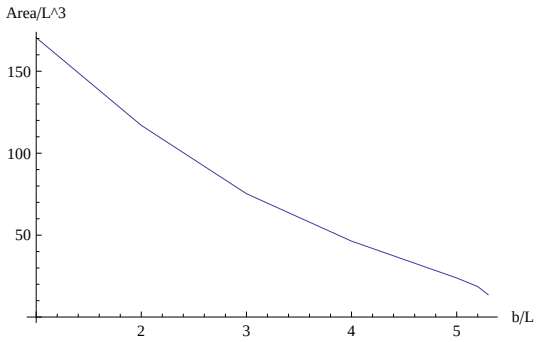

Figure 6.3: The scaled entropy $2G_5S/L^3$(the area of $\mathcal{C}$) as a function of the impact parameter scaled b/L. The energy used is $\frac{G_5E}{L^2} = 100$, where $\frac{L^3}{G_5} = \frac{2N_c^2}{\pi}$

$b \sim E^\beta L^{1-2\beta}$, the numerical value from fitting shows the critical impact parameter grows with collision energy and nucleus size.

The area of the trapped surface(twice the area of $\mathcal{C}$) sets a lower bound of the entropy produced, given as follows:

$$S_{trapped} = \frac{2A}{4G_5} = \frac{1}{2G_5}\int \sqrt{g}d^3x \tag{6.49}$$

where A is the area of the boundary $\mathcal{C}$. The prefactor is

$$\frac{L^3}{G_5} = \frac{2N_c^2}{\pi} \tag{6.50}$$

We plot the lower bound of entropy in the dual field theory for energy $\frac{G_5E}{L^2} = 100$ in Fig.6.3

6.5 Wall-on-wall collisions

In this section we address a simpler form of the shock waves, called wall-on-wall in [23], in which there is no dependence on two transverse coordinates. Grumiller and Romatschke [78] have also discussed it, using gravitational shock waves. The problem with their approach is (power) growing amplitude of the shock as a function of holographic coordinate z. If so, collision dynamics resembles the atmospheric turbulence in the sense that the largest perturbation is at the largest z – namely in the infrared modes – cascading down toward higher momenta (UV). First of all this is physically different from the heavy ion collisions, in which case the initial wave function have partons well localized near the so called "saturation scale", from which the equilibration domain (trapped surface) propagates both into small z (UV) and large z (IR) directions. Second, we think it is also inconsistent: a function growing with z cannot be considered as a small perturbation to the background metric, which is decreasing at large z as $1/z^2$. One may think that gravity near the AdS center $z=\infty$ should never be touched, as this is the original positions of the D_3 branes which gave the basis to AdS/CFT correspondence in the first place.

Our choice of the initial conditions, describing colliding walls with fixed parton density and thus fixed saturation scale is given by the following source

$$\left(\Box - \frac{3}{L^2}\right)\Phi(z) = -16\pi\frac{G_5 E}{L^2}\delta(z-z_0) \tag{6.51}$$

The corresponding solution to Einstein eqn subject to the boundary condition $\Psi(z)\to 0$ as $z\to 0$ is easily obtained:

$$\Phi(z) = \begin{cases} 4\pi G_5 E\frac{z^3}{z_0^4} & z<z_0 \\ 4\pi G_5 E\frac{1}{z} & z>z_0 \end{cases} \tag{6.52}$$

Note that it decreases in both direction from the original scale z_0: therefore (as we will see shortly) the trapped surface has finite extensions in both directions from it.

The corresponding stress energy tensor on the boundary (as seen by an observer living in dual gauge theory) is

$$T_{uu} = \frac{EL^2}{z_0^4}\delta(u) \tag{6.53}$$

The stress energy tensor is the same as that used in [78, 79], and our solution converges well as $z\to\infty$. We choose to collide states with different energy

therefore we fix z_0, but use different E. Applying the general discussion of shock wave in Sec.6.2 and noting the trapped surface only depends on z, we obtain:

$$z^2\Psi_i'' - z\Psi_i' - 3\Psi_i = -16\pi G_5 E_i \delta(z - z_0) \tag{6.54}$$
$$\Psi_i(z_a) = \Psi_i(z_b) = 0 \tag{6.55}$$

with $i = 1, 2$. Ψ_1 and Ψ_2 are shape functions corresponding to two shock waves. The trapped region at $u = v = 0$ is limited by the interval $z_a < z < z_b$. The constraint (6.35) takes a simple form:

$$\begin{aligned}\Psi_1(z_a)\Psi_2(z_a)\frac{z_a^2}{L^2} &= 4\\ \Psi_1(z_b)\Psi_2(z_b)\frac{z_b^2}{L^2} &= 4\end{aligned} \tag{6.56}$$

(6.54) is easily solved to give:

$$\begin{aligned}\Psi_i(z) &= \begin{cases} C\left(\left(\frac{z}{z_a}\right)^3 - \frac{z_a}{z}\right) & z < z_0 \\ D\left(\left(\frac{z}{z_b}\right)^3 - \frac{z_b}{z}\right) & z > z_0 \end{cases}\\ C &= -4\pi G_5 E_i \frac{\left(\frac{z_0}{z_b}\right)^3 - \frac{z_b}{z_0}}{\left(\frac{z_0}{z_a}\right)^3 z_b - \left(\frac{z_0}{z_b}\right)^3 z_a}\\ D &= -4\pi G_5 E_i \frac{\left(\frac{z_0}{z_a}\right)^3 - \frac{z_a}{z_0}}{\left(\frac{z_0}{z_a}\right)^3 z_b - \left(\frac{z_0}{z_b}\right)^3 z_a}\end{aligned} \tag{6.57}$$

Plugging (6.57) in (6.56), we obtain:

$$z_a + z_b = \frac{8\pi G_5\sqrt{E_1 E_2}}{L} \tag{6.58}$$
$$\frac{(z_a + z_b)^2 - 3z_a z_b}{(z_a z_b)^3} = \frac{L^3}{z_0^4} \tag{6.59}$$

Note E_1, E_2 appear only in the combination $\sqrt{E_1 E_2}$, This is consistent with the picture that only the center of mass contributes to the entropy. Recall the

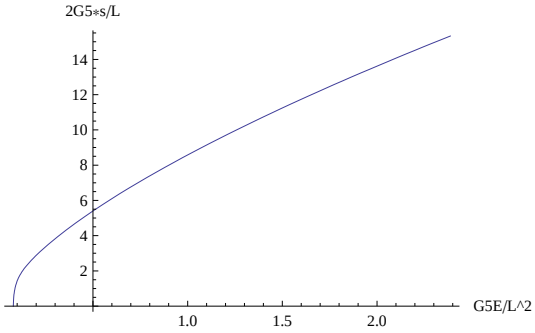

Figure 6.4: The scaled entropy per transverse area $\frac{2G_5 s}{L^2}$(the area of $\mathcal{C}$ per transverse area) as a function of scaled effective colliding energy $G_5 E/L^2$, where $\frac{L^3}{G_5} = \frac{2N_c^2}{\pi}$.

the center of mass of two massless particles with energy E_1, E_2 is $2\sqrt{E_1 E_2}$. The resulting cubic eqn (6.58) can be solved by Cardano formula, but the explicit solution is not illustrative and is not showed here. The entropy is given by:

$$\begin{aligned} S &= \frac{2A}{4G_5} = \frac{\int \sqrt{g} dz d^2x_\perp}{2G_5} \\ s &\equiv \frac{S}{\int d^2x_\perp} = \frac{L^3}{4G_5}(\frac{1}{z_a^2} - \frac{1}{z_b^2}) \end{aligned} \tag{6.60}$$

The leading behavior of entropy per transverse area s in energy is extracted:

$$s \sim \frac{4L^2}{z_0^4}(\pi G_5 \sqrt{E_1 E_2} z_0^2)^{\frac{2}{3}} \tag{6.61}$$

The power 2/3 is the same as point shock wave obtained in [82]. There is also an obvious lower bound of the energy for the formation of trapped surface:

$$4\pi G_5 E \geq z_0 L \tag{6.62}$$

The equality is reached at $z_a = z_b$, when the $\mathcal{C}$ has vanishing volume. For general energy, s is evaluated as a function of effective colliding energy $E = \sqrt{E_1 E_2}$. We again set $z_0 = L$. Fig.6.4 shows the entropy as a function of effective colliding energy.

6.6 Matching gravitational and heavy ion collisions

As the reader who came to this point of the paper knows, this is up to now a purely theoretical work devoted to solving well-posed mathematical problems, defined in terms of (the AdS/CFT correspondence) gravity framework. Now, near the end of this work, we would like to address wider issues of the limitations of such an approach, as well as the best strategies to put it for practical use.

Gubser et al [82] have applied the gravitational collision scenario *literally*, selecting initial conditions at time long before nuclei collide. More specifically, they have (i) tuned the scale L or z_0 of the bulk colliding object to the size of the nucleus R and (ii) have used the realistic CM gamma factor of the colliding nuclei $E/m = \gamma \sim 100$. The result of such choice is a *rather unrealistic* fireball produced, in spite of a reasonable entropy. Indeed, the size of the trapped surface [82] is huge, about $300fm$, which is very large compared to colliding nuclei. In real heavy ion collisions the produced fireball has the same size as the nuclei, with the radius about $6fm$. The initial temperature – as estimated by $z_{min} \sim 1/\pi T_i$ where z_{min} is the minimal distance of the trapped surface to the AdS boundary – is however way too high. So, what can be wrong with this approach?

The answer to this question is in fact well known: initial formation of the partonic wave function, describing nuclei at the collision moment, can *not* be adequately described by the dual gravity. We know from experiment that growing partonic density makes hadrons and nuclei blacker and of larger size, as the collision energy grows. This is phenomenologically described by a Pomeron, a power fit to rizing cross section $\sim s^{\alpha(t)-1}$. Although qualitatively similar to what happens in gravitational collisions, this growth is very compared to that predicted in dual gravity. Indeed, the observed Pomeron intercept $\alpha(t=0)-1 \sim 0.1$ while in the AdS/CFT world the Pomeron intercept $\alpha(t=0)-1 = 1$[21] . Thus the effective size of objects in gravitational collision grows with energy with an exponent ten times that in the real QCD. In view of this, one should clearly give up the idea to tune the scale L or z_0 of the bulk colliding object to the size of the nucleus, and tune it perhaps to the parton density ("saturation scale" Q_s in the "color glass" models) of the corresponding nuclear wave function.

More generally, we are dealing with a complicated problem in QCD, in which the effective coupling runs, from higher scale to lower as the collisions progress from initial violent partonic stage toward equilibration, expansion and cooling. So in principle, it would be logic to switch – as smoothly as possible –

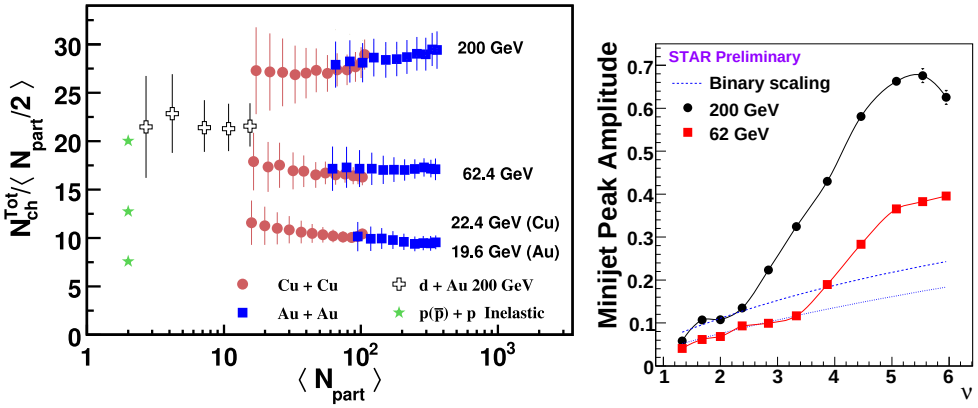

Figure 6.5: (left) PHOBOS data [88] on integrated number of charged particles, scaled by $N_{part}/2$, in p+p, d+Au, Cu+Cu and Au+Au collisions as a function of centrality. The uncertainty of N_{part} has been included in the error bars. (right) The height of the ridge as a function of the number of mean binary collisions per nucleon. The data are from STAR collaboration [90, 91] at two collision energies shown in the figure.

from the weak-coupling based methods (such as classical Yang-Mills) to strong coupling ones (such as AdS/CFT) at certain proper time τ_{switch} appropriately chosen by the evolution of the coupling[1].

Therefore one should not try to tune the parameters of the gravitational collision model neither to initial nuclei, at $\tau = -\infty$, nor to "decoherent" partons at the collision moment, at $\tau = 0$, but at the later time τ_{switch}.[2] Although we at the moment do not understand the evolution of appropriate coupling quantitatively enough, one may always treat it as a parameter. The practical utility of the AdS/CFT approach at later time $\tau > \tau_{switch}$ still remains significant: namely one can use much more fundamental dual gravity description instead of its near-equilibrium approximation, the hydrodynamics, currently used.

[1]The so called AdS/QCD approach (see e.g.[92, 93]) tries to incorporate the running coupling into the gravitational framework. A particularly simple example of that is a jump of the coupling at certain "domain wall" scale proposed in [34].

[2]It is proposed in [79] that one may choose to collide some special unphysical shock waves

6.7 Are there critical impact parameters in heavy ion collisions?

Summarizing our findings in one sentence, there exists a discontinuity in grazing gravitational collisions in the AdS space. As one smoothly increases the impact parameter b, the trapped surface and black hole formation disappear suddenly, at certain critical impact parameter $b_c(E)$ depending the collision energy E. The reason for this seems quite general: increasing b one increases the angular momentum of the system while at the same time *decrease* the mass which can be stopped, and at some moment – as one knows from Kerr solution for rotating black holes – black hole formation becomes impossible.

Suppose the AdS gravitational shock waves can describe the strongly coupled plasma in heavy ion collisions: then one would expect similar behavior in heavy ion experiments. We have looked at the data and found that indeed there are experimental indications that relatively rapid switch of the underlying dynamics at some $b_c(E)$ seem to exist.

The most straightforward observable is entropy, related to the particle multiplicity versus the impact parameter. In Fig.6.5(left) from [88] we show some data plotted as a function of the number of participants N_{part}. The right end of the figure corresponds to all nucleons participating, or central collisions: toward the left end are peripheral collisions. There are indeed two values of multiplicity per participant observed, one for small systems, pp and dAu collisions (stars and crosses) and one for "large" systems, CuCu and AuAu (circles and squares). There must be a transition between them somewhere, but, unfortunately, the experimental multiplicity measurements for "grazing" collisions are not available yet [3]. So, unfortunately, we do not yet know how exactly transition from one regime to another happens and what is $b_c(E)$, if it can be defined.

However some other observables associated with collective flows of excited matter do show rapid changes at certain $b_c(E)$ seems to be there. Some evidence for that were seen in the elliptic flow measurements, as deviations from the hydrodynamical predictions for very peripheral collisions. Even more clearly those are seen in the centrality dependence of the so called "ridge" phenomenon (see its relation to flow in [89, 91]) which we show in Fig.6.5(right).

Admittedly, these rapid change of the dynamics have not been systematically studied yet, neither experimentally nor theoretically. The naive explanation often given to it attribute the change to the fact that it happens when

[3]Small multiplicity collisions are detected for all systems, but their accurate separation from beam-residual gas collisions has not yet been systematically resolved.

overlap system gets "too small" in terms of participating nucleons N_p, causing large enough fluctuations $O(1/\sqrt{N_p})$. However, if this would be the reason, one would expect this jump to be dependent on N_p and *independent* on the collision energy. Furthermore, the gravitational collisions do not have any discrete elements at all, while predicting $b_c(E)$ growing with E, as observed in Fig.6.5. We therefore suggest that angular momentum may also be important: this issue clearly deserves to be studied further.

6.8 Conclusions

In this work we have developed a method to solve for the shape of the trapped surface based on an analogy to electrostatic problem in flat space: its main idea is to proceed from differential to integral form of the equation. We used the method to obtain the shape of trapped surface at different impact parameters and collision energy. We observe a critical impact parameter within the range of energy we explored. The phenomenon is analogous to the the critical behavior found in flat space[65, 84, 85], the difference being the critical trapped surface depends both on the collision energy and the nucleus size. We found the dependence is approximately given by a power law. Furthermore, the shape of the critical trapped surface gets elongated in spherical coordinate as the collision energy grows. We also discussed in the preceding subsection that grazing heavy ion collisions also seem to suggest a rapid switch to another dynamics, without equilibration. The exact cause of this jump is to be clarified in further studies.

We also studies wall-to-wall collision of shock waves as a simple version of the problem. The wall is sourced by a delta function at certain initial scale z_0. We believe it is more reasonable initial conditions than those used by Grumiller and Romatschke [78], to be used in future following their method to study the initial stage.

The applicability and limitation of this approach is discussed. We claim it is more realistic to adopt partonic picture in initial stage and only switch to effective gravity treatment at some time $after$ collision, when the coupling becomes strong enough. However, we argue that the observed critical phenomenon is still relevant for heavy ion collisions, where there also seems to be rapid change of collision regime as a function of impact parameter.

Finally we would like to mention very recent work by Alvarez-Gaume et al[94] who discussed another extension of the problem. They considered central collision of shock waves sourced by certain nontrivial matter distribution in the transverse space. They in particularly discuss critical phenomenon occurring as the shock wave reaches some diluteness limit and the formation of the

trapped surface is no longer possible. It would obviously be interesting to study how the two forms of critical phenomenon are related.

Chapter 7

Shock wave collisions: sourceful vs sourceless

7.1 Introduction

The problem of understanding the physics behind thermalization of the medium produced in ultrarelativistic heavy ion collisions is one of the main open questions in heavy ion theory. It has become especially important in recent years after hydrodynamic simulations indicated that a very short thermalization time of the order of 1 fm/c is required to describe RHIC data [51, 98]. Lately the problem of thermalization has been studied in the strong coupling framework of the Anti-de Sitter space/conformal field theory (AdS/CFT) correspondence [1–3] with the goal of learning about the dynamics of the strongly-coupled QCD medium by studying the strongly coupled medium in $\mathcal{N} = 4$ super-Yang-Mills (SYM) theory [25, 78, 79, 82, 94, 96, 97, 99, 100].

The 5-dimensional gravity dual of a shock wave (ultrarelativistic nucleus) in our 4-dimensional space-time was first constructed in [25]. The AdS_5 shock wave metrics are shown below in Eqs. (7.1) and (7.2). These metrics are solutions of Einstein equations in the AdS_5 bulk without sources. In four dimensions they correspond to nuclei of infinite transverse extent with a uniform distribution of matter in the transverse plane. Collisions of shock waves in Eqs. (7.1) and (7.2) have been studied in [78, 79, 99, 101] with the goal of explicitly constructing the metric after the collision. While the shock wave collisions in AdS_3 allowed for an exact solution of the problem [99], it turned out to be significantly harder in AdS_5, allowing only for a perturbative solution of Einstein equations in graviton exchanges [78, 79]. While all-order graviton exchanges with one of the shock waves (corresponding to proton-nucleus collisions) were resummed exactly in [101], the full problem of nucleus-nucleus

collisions involving all-order graviton exchanges with *both* nuclei still remains unsolved in AdS_5.

In [82] an alternative to the exact solution of Einstein equations was proposed: the authors of [82] constructed a trapped surface for a head-on collision of two shock waves with sources in the AdS bulk following [83, 102]. Sources in the bulk lead to the nuclei in the boundary theory having some transverse coordinate dependence in their matter distributions. Formation of a trapped surface before the collision indicates that a black hole will be formed in the future, after the collision. Thus the authors of [82] have proven that black hole is formed in a collision of two shock waves with point sources in the bulk. Generalizations of [82] to the case of nuclear collisions with non-zero impact parameter were presented in [97, 100]. Also a trapped surface was found in [100] for an important case of collision of two shock waves with extended (not point-like) bulk sources.

However, the exact implications of a source in the bulk for the boundary theory are still not entirely clear. The same energy-momentum tensor of the boundary theory can be given by metrics with extended sources at different bulk locations. It is possible that the sources would manifest themselves in fluctuations of the metric, but more research is needed to understand which bulk source gives the "right" fluctuations most accurately describing real-life heavy ion collisions. In [100] it was suggested that the position of the source in the bulk is related to the saturation scale of the shock wave. Initial steps on determination of saturation scale in shock waves were done in [103–105]. It appears more work is needed to clarify the complete impact of the bulk source on the boundary gauge theory.

Interestingly the trapped surfaces found in [82, 97, 100] are always formed around the source in the bulk. One may therefore wonder whether the source is required for the trapped surface to form. No trapped surface analysis has been performed to date for the sourceless shock waves of Eqs. (7.1) and (7.2) to answer this question.

Here we perform a trapped surface analysis for a collision of two sourceless shock waves from Eqs. (7.1) and (7.2). We first consider the trapped surface obtained in [100] for a collision of two shock waves with extended sources in the bulk, and then take the limit in which the sources are moved to the deep infrared (IR) while keeping the energies of the shock waves in the boundary gauge theory fixed. Interestingly enough, the trapped surface does not disappear in this source-free limit, its lower boundary remains at finite value of the 5th dimension coordinate z with its finite area giving a finite expression for the produced entropy. We argue that collisions of two shock waves with sources in the deep IR (at $z = \infty$) are indistinguishable from collisions of two shock

waves without bulk sources by performing a perturbative solution of Einstein equations for the shock wave with sources in the bulk and taking the sources to $z = \infty$. We also note that the trapped surface which remains after we send the sources to $z = \infty$ does not depend on how the limit was taken and on which sources were sent to infinity: the remaining trapped surface is the same for extended and point-like sources sent to the IR.

We therefore conclude that a collisions of two sourceless shock waves in AdS_5 leads to creation of a black hole in the bulk. The absence of bulk sources leaves no uncertainty in the interpretation of the physics and makes application of AdS/CFT correspondence better justified. For the boundary theory this result proves that thermalized quark-gluon plasma is produced in heavy ion collisions at strong coupling.

The paper is structured as follows. In Sect. 7.2 we present the problem at hand and describe how the limit of sending the sources to the IR should be taken without changing the bulk physics. In Sect. 7.3 we present a lowest-order perturbative solution of Einstein equations for a collision of two shock waves with sources along the lines of a similar calculation for the sourceless shock waves in [79]. We take the limit of the shock waves sources going to the IR and show that our solution exactly maps onto the metric produced in a collision of two sourceless shock waves found in [79]. This provides a strong argument that the shock waves with sources at $z = \infty$ collide in the same way as the shocks without any sources. In Sect. 7.4 we perform the trapped surface analysis and demonstrate that the trapped surface does not disappear when the sources are send to the deep IR. Thus we obtain the trapped surface for the collision of two sourceless shock waves. In Sect. 7.5 we conclude by presenting a guess for the thermalization time inspired by our analysis (see also [78]). We argue that thermalization proper time is likely to be parametrically shorter than the light-cone stopping time for shock waves found in [79, 101], which indicates that our conclusions may be applied to real-life heavy ion collisions at least at the qualitative level. We note however that the numbers generated by our approximate thermalization time estimate are too short to describe RHIC physics.

7.2 The Problem

High energy heavy ion collision can be realistically modeled by a collision of two ultrarelativistic shock waves. In [25], using the holographic correspondence [106], the geometry in AdS_5 dual to each one of the nuclei in the boundary

theory is given by the following metric

$$ds^2 \;=\; \frac{L^2}{z^2}\,\left\{-2\,dx^+\,dx^- + t_1(x^-)\,z^4\,dx^{-\,2} + dx_\perp^2 + dz^2\right\} \tag{7.1}$$

for nucleus 1 and by

$$ds^2 \;=\; \frac{L^2}{z^2}\,\left\{-2\,dx^+\,dx^- + t_2(x^+)\,z^4\,dx^{+\,2} + dx_\perp^2 + dz^2\right\} \tag{7.2}$$

for nucleus 2. Here $dx_\perp^2 = (dx^1)^2 + (dx^2)^2$ is the transverse metric and $x^\pm = (x^0 \pm x^3)/\sqrt{2}$ where x^3 is the collision axis. L is the radius of S_5 and z is the coordinate describing the 5th dimension with the boundary of AdS_5 at $z = 0$. We have also defined

$$t_1(x^-) \;\equiv\; \frac{2\,\pi^2}{N_c^2}\,\langle T_{1\,--}(x^-)\rangle,\;\; t_2(x^+) \;\equiv\; \frac{2\,\pi^2}{N_c^2}\,\langle T_{2\,++}(x^+)\rangle \tag{7.3}$$

in accordance with the prescription of holographic renormalization [106]. Here $\langle T_{1\,--}(x^-)\rangle$ and $\langle T_{2\,++}(x^+)\rangle$ are the energy-momentum tensors of the two shock waves in the gauge theory. We assume that the nuclei are so large and homogeneous that one can neglect transverse coordinate dependence in $\langle T_{1\,--}(x^-)\rangle$ and $\langle T_{2\,++}(x^+)\rangle$. Following [25] we take

$$\langle T_{1\,--}(x^-)\rangle \;=\; \mu_1\,\delta(x^-),\;\; \langle T_{2\,++}(x^+)\rangle \;=\; \mu_2\,\delta(x^+). \tag{7.4}$$

For simplicity we also put $\mu_1 = \mu_2 = \mu$.

The metrics in Eqs. (7.1) and (7.2) solve Einstein equations in the empty AdS_5 space:

$$R_{\mu\nu} - \frac{1}{2}\,g_{\mu\nu}\,R - \frac{6}{L^2}\,g_{\mu\nu} \;=\; 0. \tag{7.5}$$

However, as we will see below, it is hard to perform the trapped surface analysis with the sourceless shock waves. To this end, as we have mentioned above, it will be more convenient to represent sourceless shock waves as limiting cases of the shock waves with sources, when the sources are sent to $z = \infty$ while keeping energy-momentum tensor of the nuclei in the boundary theory intact.

We therefore need to construct shock waves with sources in the bulk, which we will do following [82, 100]. We need to satisfy Einstein equations in AdS_5 with sources in the bulk

$$R_{\mu\nu} - \frac{1}{2}\,g_{\mu\nu}\,R - \frac{6}{L^2}\,g_{\mu\nu} \;=\; 8\,\pi\,G_5\,J_{\mu\nu} \tag{7.6}$$

where $J_{\mu\nu}$ is the energy momentum tensor for bulk sources. We will not specify what fields contribute to create non-zero $J_{\mu\nu}$ in the bulk: as for us the source will serve as an IR regulator we do not need to know the origin of $J_{\mu\nu}$ in detail. The 5-dimensional Newton constant is

$$G_5 = \frac{\pi\, L^3}{2\, N_c^2}. \tag{7.7}$$

Eq. (7.6) can be rewritten as

$$R_{\mu\nu} + \frac{4}{L^2}\, g_{\mu\nu} \;=\; 8\,\pi\, G_5 \left(J_{\mu\nu} - \frac{1}{3}\, g_{\mu\nu}\, J \right) \tag{7.8}$$

with

$$J \;=\; J_\mu^{\ \mu} \;=\; J_{\mu\nu}\, g^{\mu\nu}. \tag{7.9}$$

Following [100] for one shock wave we will consider a source without any transverse (x^1, x^2) coordinate dependence, with the only non-zero component of the energy-momentum tensor

$$J^{(0)}_{--} \;=\; \frac{E}{z_0\, L}\, \delta(x^-)\, \delta(z - z_0). \tag{7.10}$$

The source is located at $z = z_0$ and $x^- = 0$, spans the transverse directions and moves along the x^+ axis. E is a yet unspecified parameter with dimension of energy. To find the metric of the shock wave satisfying Eq. (7.8) with the source (7.10) we look for it in the following form generalizing Eq. (7.1)

$$ds^2 \;=\; \frac{L^2}{z^2} \left\{ -2\, dx^+\, dx^- + \phi(z)\, \delta(x^-)\, {dx^-}^2 + dx_\perp^2 + dz^2 \right\}. \tag{7.11}$$

Plugging Eqs. (7.11) and (7.10) into Eq. (7.8) we get the following equation for the "$--$" component of Einstein equations [100]

$$\frac{3}{2\, z}\, \phi'(z) - \frac{1}{2}\, \phi''(z) \;=\; 8\,\pi\, G_5\, \frac{E}{z_0\, L}\, \delta(z - z_0). \tag{7.12}$$

When solving this equation we require that $\phi(z) \to 0$ as $z \to 0$ and that $\phi(z)$ is regular as $z \to +\infty$. The latter condition is needed to avoid the singular behavior of metrics (7.1) and (7.2) in the IR. While the singularity of metrics (7.1) and (7.2) does not affect curvature invariants and is thus not unphysical, it is easier to perform trapped surface analysis which we intend to do below on a metric with is regular in the IR.

Solving Eq. (7.12) with the boundary condition that $\phi(z) \to 0$ as $z \to 0$ and $\phi(z)$ is regular at $z \to +\infty$ yields [100]

$$\phi(z) \,=\, \frac{4\,\pi\,G_5\,E}{L}\,\begin{cases} \frac{z^4}{z_0^4}, & z \leq z_0 \\ \\ 1, & z > z_0. \end{cases} \tag{7.13}$$

Eqs. (7.13) and (7.11) give us the metric of a single shock wave with the bulk source (7.10).

Using holographic renormalization [106] (see e.g. Eq. (7.3) above) we conclude that the energy-momentum tensor corresponding to the metric (7.11) has only one non-zero component [100]

$$\langle T_{--} \rangle \,=\, \frac{L^3}{4\,\pi\,G_5}\,\delta(x^-)\,\lim_{z\to 0}\frac{\phi(z)}{z^4} \,=\, \frac{E\,L^2}{z_0^4}\,\delta(x^-). \tag{7.14}$$

It is clear that this energy-momentum tensor would be the same as for the sourceless shock wave (7.1) given by Eq. (7.4) if we identify

$$\mu \,=\, \frac{E\,L^2}{z_0^4} \tag{7.15}$$

obtaining

$$\langle T_{--} \rangle \,=\, \mu\,\delta(x^-). \tag{7.16}$$

The difference between the metrics for the shock wave with source in Eqs. (7.13) and (7.11) and the sourceless shock wave in Eq. (7.1) is that the source regulates the metric in the IR. It is important to note that if we take $z_0 \to \infty$ limit of the metric in Eqs. (7.11) and (7.13) keeping E/z_0^4 (and therefore μ in Eq. (7.15) fixed) we would recover the metric in Eq. (7.1) without modifying the energy-momentum tensor of the gauge theory given by (7.16). At any finite z the metric of Eqs. (7.11) and (7.13) becomes equivalent to (7.1) in this limit, which sends the source at z_0 to the IR infinity. The question arises whether the metric (7.1) is equivalent to the $z_0 \to \infty$, $E/z_0^4 = const$ limit of the metric in Eqs. (7.11) and (7.13). In other words, is having the sources at infinity identical to having no sources at all?

We are interested in the answer to this question in the context of collisions of two shock waves. The question then becomes whether colliding shock waves from Eqs. (7.1) and (7.2) are identical to colliding the shock wave in Eqs. (7.11) and (7.13) with its counterpart with $x^+ \leftrightarrow x^-$ in the limit $z_0 \to \infty$, $E/z_0^4 = const$ of the resulting post-collision metric?

The intuitive answer to the this question is "yes". Indeed it is highly unlikely that sources at $z_0 = \infty$ would affect any physics at finite z. Even in empty AdS_5 space light propagates with velocity 1 along the z-direction. It would take light an infinite time to travel to any finite z from $z_0 = \infty$ after the collision. The metric modification in the collision is only likely to lower the light velocity in the z-direction: in the "extreme" case when a black hole is created no signal from $z = \infty$ would be able to propagate outside of the horizon. Even more minor modifications of the metric are likely to only change the speed of light in z-direction leaving it finite and not changing the above arguments. Hence any modification of sources at $z_0 = \infty$ in the collision is not going to affect the physics at finite z. Hence the collision of two shock waves with sources at $z_0 = \infty$ should be indistinguishable from the collision of two sourceless shock waves in Eqs. (7.1) and (7.2).

One may also think of a source at z_0 as providing an (externally imposed) infrared cutoff $1/z_0$ on the transverse momenta k_T of the partons inside the shock wave in the boundary gauge theory (see [100]). With this interpretation the limit of $z_0 \to \infty$, $E/z_0^4 = const$ can be interpreted in the boundary theory as removing the IR cutoff on the transverse momenta of the partons while keeping the energy of the shock wave fixed. The shock waves without sources would then correspond to nuclei without an ad hoc IR cutoff on the transverse momenta of their partons in the boundary theory. Hence, from the standpoint of the boundary theory, the $z_0 \to \infty$ limit imposed on the four-dimensional shock waves dual to the shocks with sources in the bulk would simply remove the IR cutoff on partons' k_T. This would make the boundary theory shock waves identical to those dual to the sourceless shock waves in the bulk. Therefore, with the IR k_T-cutoff interpretation of $1/z_0$ [100] the $z_0 \to \infty$ limit also appears to be a justified way of obtaining duals of sourceless bulk shock waves in the boundary theory.

To verify the above arguments we will perform a perturbative solution of Einstein equations for a collision of two shock waves with sources in the next Section. We will explicitly demonstrate that taking the $z_0 \to \infty$, $E/z_0^4 = const$ limit of the obtained metric produced in the collision would simply reduce it to the metric produced in the collision of two sourceless shock waves found previously in [78, 79], thus substantiating our intuitive argument above.

7.3 Perturbative Solution of Einstein Equations for Colliding Shock Waves with Bulk Sources

Consider a collision of two shock waves with sources like the one given in Eq. (7.10). The general metric for such a collision could be written as

$$ds^2 = \frac{L^2}{z^2}\Big\{ -\big[2+g(x^+,x^-,z)\big]\,dx^+\,dx^- + \big[\phi(z)\,\delta(x^-)+f(x^+,x^-,z)\big]\,dx^{-\,2} + \Big[\phi(z)\,\delta(x^+)+\tilde{f}(x^+,x^-,z)\Big]\,dx^{+\,2} + \big[1+h(x^+,x^-,z)\big]\,dx_\perp^2 + dz^2\Big\}. \tag{7.17}$$

The functions f, $\tilde{f}$, g, and h are non-zero only for $x^+ \geq 0$, $x^- \geq 0$. Before the collision (for $x^- < 0$ and $x^+ < 0$) the superposition of the metrics of colliding shocks (the terms with ϕ's above) solves Einstein equations (7.8) exactly.

We will follow [78, 79, 101] and find the functions f, $\tilde{f}$, g, and h perturbatively at the lowest order treating the shock waves as perturbations of the empty AdS_5 space. As $\phi(z) \sim \mu$ one can argue that f, $\tilde{f}$, g, and h start at order μ^2 [79, 101]. Our strategy is to expand Einstein equations to the order linear in f, $\tilde{f}$, g, and h and quadratic in ϕ. This is the same procedure as used in [79, 101] for a collision of two sourceless shock waves.

The main difference in the case at hand is that the shock waves now have sources. The energy-momentum tensors of the sources, given by the following non-vanishing components before the collision (order μ, see Eqs. (7.15 and (7.10))))

$$J^{(0)}_{--} = \mu\,\frac{z_0^3}{L^3}\,\delta(x^-)\,\delta(z-z_0), \quad J^{(0)}_{++} = \mu\,\frac{z_0^3}{L^3}\,\delta(x^+)\,\delta(z-z_0) \tag{7.18}$$

get modified in the collision. In principle to understand modifications of the bulk source one needs to know the field content of the source and the corresponding equations of motion for the fields. However, it turns out that this is not really necessary. Following a similar procedure for perturbative construction of classical Yang-Mills fields in nuclear collisions [107] we note that Einstein equations (7.6) imply

$$\nabla_\mu\, J^{\mu\nu} = 0 \tag{7.19}$$

where ∇_μ is the covariant derivative. Imposing causality and using Eq. (7.19)

along with Einstein equations one can perturbatively construct the bulk energy-momentum tensor order-by-order in μ. Using the symmetries of the problem one can argue that it is unlikely that colliding sources would recoil in the transverse or z directions. This limits the non-zero contributions to the bulk energy-momentum tensor to J_{++}, J_{--} and $J_{+-} = J_{-+}$. Note that to find $J^{\mu\nu}$ at order μ^2 one only need the metric (7.17) at order μ. This means one does not yet need to know the functions f, $\tilde{f}$, g, and h. It is then not too hard to infer the sources up to order μ^2: the non-vanishing components of the bulk energy-momentum tensor are

$$J_{++} = \mu \frac{z_0^3}{L^3} \delta(z - z_0) \left[\delta(x^+) + \frac{1}{2} \theta(x^-) \delta'(x^+) \left[z \phi'(z) - \phi(z) \right] + \dots \right] \tag{7.20a}$$

$$J_{--} = \mu \frac{z_0^3}{L^3} \delta(z - z_0) \left[\delta(x^-) + \frac{1}{2} \theta(x^+) \delta'(x^-) \left[z \phi'(z) - \phi(z) \right] + \dots \right] \tag{7.20b}$$

$$J_{+-} = J_{-+} = -\mu \frac{z_0^3}{L^3} \delta(z - z_0) \delta(x^+) \delta(x^-) \left[\phi(z) + \frac{1}{2} z \phi'(z) \right] + \dots . \tag{7.20c}$$

Plugging Eqs. (7.17) and (7.20) into (7.8) and expanding the result in powers of μ we obtain at order μ^2 the following expressions for the "$\perp\perp$" and the "zz" components of Einstein equations

$$(\perp\perp) \quad g_z + 5 h_z - z h_{z z} + 2 z h_{x^+ x^-} = 2 \delta(x^+) \delta(x^-) \phi(z) \phi'(z)$$
$$- \frac{16 \pi}{3} \frac{G_5}{L^3} z_0^5 \mu \delta(x^+) \delta(x^-) \delta(z - z_0) \phi'(z) \tag{7.21a}$$

$$(zz) \quad g_z + 2 h_z - z g_{z z} - 2 z h_{z z} = -\delta(x^+) \delta(x^-) \left[-2 \phi(z) \phi'(z) + z (\phi'(z))^2 \right.$$
$$\left. + 2 z \phi(z) \phi''(z) \right] - \frac{16 \pi}{3} \frac{G_5}{L^3} z_0^5 \mu \delta(x^+) \delta(x^-) \delta(z - z_0) \phi'(z). \tag{7.21b}$$

Here the subscripts indicate partial derivatives. Solving Eq. (7.21a) for g_z and substituting the result into Eq. (7.21b) yields

$$-3 h_z + 3 z h_{z z} - z^2 h_{z z z} + 2 z^2 h_{x^+ x^- z} = \delta(x^+) \delta(x^-)$$
$$\times \left[z [\phi'(z)]^2 - \frac{16 \pi}{3} \frac{G_5}{L^3} z_0^5 \mu z \left[\delta'(z - z_0) \phi'(z) + \delta(z - z_0) \phi''(z) \right] \right] . \tag{7.22}$$

Eq. (7.22) can be rewritten as

$$z^2\,\partial_z\left[\frac{3}{z}\,h_z - h_{z\,z} + 2\,h_{x^+\,x^-}\right] \;=\; \delta(x^+)\,\delta(x^-)$$
$$\times\left[z\,[\phi'(z)]^2 - \frac{16\,\pi}{3}\,\frac{G_5}{L^3}\,z_0^5\,\mu\,z\;[\delta'(z-z_0)\,\phi'(z) + \delta(z-z_0)\,\phi''(z)]\right]. \quad (7.23)$$

We can now substitute $\phi(z)$ from Eq. (7.13) into Eq. (7.23). There is a small subtlety: the derivative of $\phi(z)$ is discontinuous at $z = z_0$. It is therefore not clear which value of the derivative to choose, the one at $z - z_0 \to 0^+$ or the one at $z - z_0 \to 0^-$. As for $z > z_0$ all derivatives of $\phi(z)$ are zero, plugging the derivatives at $z - z_0 \to 0^+$ into Eq. (7.23) would simply eliminate all bulk source effects. It therefore seems more physical to use the derivatives at $z - z_0 \to 0^-$. This gives

$$\frac{3}{z}\,h_z - h_{z\,z} + 2\,h_{x^+\,x^-} \;=\; \frac{1}{3}\left(\frac{16\,\pi\,G_5\,\mu}{L^3}\right)^2\,\delta(x^+)\,\delta(x^-)\,\big[\frac{z^6}{2}\,\theta(z_0 - z)$$
$$-\,\frac{z_0^6}{2}\,\theta(z - z_0) - z_0^7\,\delta(z - z_0)\big]. \quad (7.24)$$

Eq. (7.24) is easy to solve as the Green function for the operator on its left hand side was found in [39, 101]. Defining the Green function by

$$\left[\frac{3}{z}\partial_z - \partial_z^2 + 2\partial_+\partial_-\right]G(x^+, x^-, z; x'^+, x'^-, z') = \delta(x^+ - x'^+)\delta(x^- - x'^-)\delta(z - z') \quad (7.25)$$

one can find an integral expression [39, 101]

$$G(x^+, x^-, z; x'^+, x'^-, z') \;=\; \frac{1}{2}\,\theta(x^+ - x'^+)\,\theta(x^- - x'^-)\,\frac{z^2}{z'}\int_0^\infty dm$$
$$\times\; m\,J_0\left(m\,\sqrt{2\,(x^+ - x'^+)\,(x^- - x'^-)}\right)\,J_2(m\,z)\,J_2(m\,z') \quad (7.26)$$

which can be integrated to give

$$G(x^+, x^-, z; x'^+, x'^-, z') \;=\; \frac{1}{2\,\pi}\,\theta(x^+ - x'^+)\,\theta(x^- - x'^-)\theta(s)\,\theta(2 - s)\,\frac{z}{z'^2}$$
$$\times\,\frac{1 + 2\,s\,(s-2)}{\sqrt{s\,(2-s)}} \quad (7.27)$$

with

$$s \equiv \frac{2\,(x^+ - x'^+)\,(x^- - x'^-) - (z - z')^2}{2\,z\,z'}. \tag{7.28}$$

With the help of Eq. (7.26) we solve Eq. (7.24) and write

$$\begin{aligned} h(x^+, x^-, z) = \frac{1}{3}\left(\frac{16\,\pi\,G_5\,\mu}{L^3}\right)^2 \int_{-\infty}^{x^+} dx'^+ \int_{-\infty}^{x^-} dx'^- \int_0^\infty dz' \frac{z^2}{2\,z'} \int_0^\infty dm\, m \\ \times\, J_0\left(m\sqrt{2(x^+ - x'^+)(x^- - x'^-)}\right) J_2(m\,z) J_2(m\,z')\delta(x'^+)\,\delta(x'^-) \\ \left[\frac{z'^6}{2}\,\theta(z_0 - z') - \frac{z_0^6}{2}\,\theta(z' - z_0) - z_0^7\,\delta(z' - z_0)\right]. \end{aligned} \tag{7.29}$$

Integrating over x'^+ and x'^- trivially yields

$$\begin{aligned} h(x^+, x^-, z) = \frac{1}{3}\left(\frac{16\,\pi\,G_5\,\mu}{L^3}\right)^2 \theta(x^+)\,\theta(x^-) \int_0^\infty dz' \frac{z^2}{2\,z'} \int_0^\infty dm\, m\, J_0\,(m\,\tau) \\ \times\, J_2(m\,z) J_2(m\,z') \left[\frac{z'^6}{2}\,\theta(z_0 - z') - \frac{z_0^6}{2}\,\theta(z' - z_0) - z_0^7\,\delta(z' - z_0)\right] \end{aligned} \tag{7.30}$$

where we defined the proper time

$$\tau \;=\; \sqrt{2\,x^+\,x^-}. \tag{7.31}$$

Let us evaluate the three terms in the brackets in Eq. (7.30) separately. Start with the last term: it is proportional to

$$\begin{aligned} &\int_0^\infty dz' \frac{z^2}{2\,z'} \int_0^\infty dm\, m\, J_0\,(m\,\tau)\, J_2(m\,z) J_2(m\,z')\, z_0^7\,\delta(z' - z_0) \\ &= \frac{z^2}{2}\, z_0^6 \int_0^\infty dm\, m\, J_0\,(m\,\tau)\, J_2(m\,z) J_2(m\,z_0) \\ &= \frac{z^2}{2\,\pi}\, z_0^6\,\theta(s_0)\,\theta(2 - s_0)\,\frac{1 + 2\,s_0\,(s_0 - 2)}{\sqrt{s_0\,(2 - s_0)}} \end{aligned} \tag{7.32}$$

with

$$s_0 = \frac{\tau^2 - (z - z_0)^2}{2\, z\, z_0}. \tag{7.33}$$

We see that taking $z_0 \to \infty$ and keeping μ fixed gives $s_0 \approx -z_0/(2\, z)$ such that the expression in Eq. (7.32) becomes zero due to $\theta(s_0)$. Hence the last term in the brackets of Eq. (7.30) does not contribute in the $z_0 \to \infty$ limit.

The second term in the brackets of Eq. (7.30) is proportional to

$$\begin{aligned} &\int_{z_0}^{\infty} dz' \frac{1}{z'} \int_0^{\infty} dm\, m\, J_0\left(m\,\tau\right) J_2(m\, z) J_2(m\, z') \\ &= \frac{1}{z_0} \int_0^{\infty} dm\, J_0\left(m\,\tau\right) J_2(m\, z) J_1(m\, z_0) \;=\; 0 \end{aligned} \tag{7.34}$$

with the last step being valid for $z_0 > z + \tau$, i.e., for the large z_0 we are interested in.

We are left with the first term in the brackets of Eq. (7.30). Hence at large z_0 we have

$$\begin{aligned} h(x^+, x^-, z) =& \frac{1}{3} \left(\frac{8\,\pi\, G_5\, \mu}{L^3}\right)^2 \theta(x^+)\, \theta(x^-)\, z^2 \int_0^{z_0} dz' z'^5 \int_0^{\infty} dm\, m\, J_0\left(m\,\tau\right) \\ &\times J_2(m\, z) J_2(m\, z') \\ =& \frac{1}{3} \left(\frac{8\,\pi\, G_5\, \mu}{L^3}\right)^2 \theta(x^+)\, \theta(x^-)\, z^2\, z_0^4 \int_0^{\infty} \frac{dm}{m} J_0\left(m\,\tau\right) J_2(m\, z) \\ &\times \left[6\, J_4(m z_0) - m z_0\, J_5(m z_0)\right] \\ =& \left(\frac{8\,\pi\, G_5\, \mu}{L^3}\right)^2 \theta(x^+)\, \theta(x^-)\, z^4 \left[\tau^2 + \frac{1}{3}\, z^2\right]. \end{aligned} \tag{7.35}$$

This is exactly the solution found for sourceless shock waves in [79]! Using h from Eq. (7.35) in Eq. (7.21a) one would obtain function g, which, for $z_0 \to \infty$ would also be z_0-independent and would also correspond to that found for sourceless shock waves in [79]. Similarly one can show that f and $\tilde{f}$ would also reduce to the ones from [79] in the $z_0 \to \infty$ limit. We conclude that, at least at this lowest non-trivial order in μ, colliding shock waves with sources gives a metric which in the limit of $z_0 \to \infty$ (keeping μ fixed) reduces to that produced in the collision of two shock waves without sources. This presents a

strong argument supporting our earlier assertion that collisions of the shock waves with sources at $z_0 = \infty$ are equivalent to collisions of the shock waves without the sources.

7.4 Trapped Surface Analysis

Below we will present trapped surface analysis for a collision of two shock waves without bulk sources. We will begin by outlining general concepts of the trapped surface analysis and will present a naive attempt to find the trapped surface for a collision of shock waves from Eqs. (7.1) and (7.2). We will then obtain the trapped surface for a collision of two shock waves with bulk sources and take the limit of $z_0 \to \infty$, deriving the trapped surface for a collision of sourceless shock waves. We will solidify our above conclusion of the equivalence between the sourceless shock wave and the one with sources at $z = \infty$ by taking the limit of sources going to the IR for a collision of two different shock waves with extended sources at z_1 and z_2 and showing that the limiting trapped surface is the same as obtained before.

7.4.1 Generalities

Let us start with outlining some generalities of trapped surface. Consider the collision of two shock waves given by the following metric before the collision:

$$ds^2 = \frac{L^2}{z^2}\left\{-2\,dx^+dx^- + dx_\perp^2 + dz^2\right\} + \frac{L}{z}\,\Phi_1(x_\perp, z)\,\delta(x^+)\,dx^{+2} + \frac{L}{z}\,\Phi_2(x_\perp, z)\,\delta(x^-)\,dx^{-2} \tag{7.36}$$

where (cf. Eq. (7.17))

$$\Phi_i(x_\perp, z) = \frac{L}{z}\,\phi_i(x_\perp, z), \quad i = 1, 2. \tag{7.37}$$

The marginally trapped surface is found from the condition of vanishing of expansion θ[86]. The trapped surface is made up of two pieces: $\mathcal{S} = \mathcal{S}_1 \cup \mathcal{S}_2$. $\mathcal{S}_1(\mathcal{S}_2)$ is associated with shock wave at $x^+ = 0$ ($x^- = 0$) before the collision. An additional condition is imposed requiring that the outer null normal to $\mathcal{S}_1$ and $\mathcal{S}_2$ must be continuous at the intersection $\mathcal{C} = \mathcal{S}_1 \cap \mathcal{S}_2$ point $x^+ = x^- = 0$ to avoid delta function in the expansion.

To calculate the trapped surface associated with shock wave at $x^+ = 0$, we

use the following coordinate transformation [82, 83]:

$$x^- \to x^- + \frac{\phi_1(x_\perp, z)}{2}\,\theta(x^+) \tag{7.38}$$

to eliminate the delta-function discontinuity at $x^+ = 0$.[1] The trapped surface $\mathcal{S}_1$ can then be parametrized by [83]

$$x^+ = 0,\;\; x^- = -\frac{\psi_1(x_\perp, z)}{2}. \tag{7.39}$$

The condition of marginally trapped surface is the vanishing of expansion $\theta \equiv h^{\mu\nu}\nabla_\mu\, l_\nu$, with $h^{\mu\nu}$ the induced metric and l_ν the outer null normal to the trapped surface. Similarly to [82, 97, 100], the condition gives rise to

$$\left(\Box - \frac{3}{L^2}\right)\,\left[\Psi_1(x_\perp, z) - \Phi_1(x_\perp, z)\right] \;=\; 0 \tag{7.40}$$

with $\Psi_1(x_\perp, z) \;=\; \frac{L}{z}\psi_1(x_\perp, z)$ and the Laplacian is defined with respect to Euclidean AdS_3 space

$$ds^2 \;=\; \frac{L^2}{z^2}\,\left\{dx_\perp^2 + dz^2\right\}. \tag{7.41}$$

By analogy, we have the condition defining the trapped surface $\mathcal{S}_2$:

$$\left(\Box - \frac{3}{L^2}\right)\,\left[\Psi_2(x_\perp, z) - \Phi_2(x_\perp, z)\right] \;=\; 0. \tag{7.42}$$

The continuity of trapped surface $\mathcal{S}_1$ and $\mathcal{S}_2$ and their outer null normal on the cusp of the light-cone $x^+ = x^- = 0$ reduce to the boundary conditions

$$\Psi_1(x_\perp, z)|_{\mathcal{C}} \;=\; \Psi_2(x_\perp, z)|_{\mathcal{C}} \;=\; 0 \tag{7.43a}$$
$$\nabla\Psi_1(x_\perp, z)\cdot\nabla\Psi_2(x_\perp, z)|_{\mathcal{C}} \;=\; 8 \tag{7.43b}$$

where the boundary $\mathcal{C}$ is to be determined from Eq. (7.43). The covariant derivative ∇ is again defined with respect to Eq. (7.41).

Having the equations for the trapped surface with arbitrary shock wave (7.40), (7.42) and (7.43) at hand, we are ready to apply them to the collision of source-free shock waves (7.1) and (7.2). With the symmetry $\phi_1(z) = \phi_2(z) \equiv$

[1] Note a different definition for the light-cone coordinates used in [82, 83].

$\phi(z)$ (and thus $\psi_1(z) = \psi_2(z) \equiv \psi(z)$), they take a particularly simple form

$$z^2\,\Psi''(z) - z\,\Psi'(z) - 3\,\Psi(z) \;=\; 0 \tag{7.44a}$$

$$\Psi(z_a) \;=\; \Psi(z_b) \;=\; 0 \tag{7.44b}$$

$$\frac{z_a^2}{L^2}\,\Psi'(z_a)^2 \;=\; \frac{z_b^2}{L^2}\,\Psi'(z_b)^2 \;=\; 8. \tag{7.44c}$$

The boundary $\mathcal{C}$ in this case is given by $z_a < z < z_b$, as there is no dependence on transverse coordinates. Eq. (7.44) is easily solved by

$$\Psi(z) \;=\; C_1\,z^3 + \frac{C_2}{z} \tag{7.45}$$

with C_1 and C_2 arbitrary constants.

Obviously we cannot have $C_1 = C_2 = 0$ because of Eq. (7.44c). It is easy to see then Eq. (7.44b) would immediately require $z_a = z_b$. Similar phenomenon of no trapped surface was observed in [83] for collisions of gravitational shock waves in asymptotically Minkowskian 4-dimensional space-time. One may be tempted to conclude that trapped surface formation is not possible in collisions of source-free shock waves. Before accepting such conclusion, let us point out that the reason we choose $\mathcal{C}$ to be bounded by $z_a < z < z_b$ from both sides in the bulk is because the trapped surface has to be closed. However, AdS_5 is different from asymptotically Minkowskian spaces: it appears not quite clear whether the requirement of a closed trapped surface necessarily implies finite z_b.[2] If one searches for the trapped surface with $z_b = \infty$, i.e., with $z > z_a$ constraint only, such that conditions in Eqs. (7.44) are imposed only at z_a, one gets

$$\Psi(z) \;=\; \frac{L}{\sqrt{2}}\left[\frac{z^3}{z_a^3} - \frac{z_a}{z}\right] \tag{7.46}$$

giving

$$\psi(z) \;=\; \frac{1}{z_a^3\,\sqrt{2}}\left[z^4 - z_a^4\right]. \tag{7.47}$$

Unfortunately the conditions in Eqs. (7.44) are insufficient to fix z_a uniquely.

However, z_a in Eq. (7.46) can be fixed if we choose to study a closely relevant situation. Let us consider the trapped surface formation in the collision

[2]Requirement that the trapped surface has to be closed appears to stem from the cosmic censorship conjecture, which we assume to be true in $AdS_5 \times S_5$: the issue of whether trapped surfaces in AdS_5 necessarily have to be closed may require further investigation.

of two sourced shock waves

$$ds^2 \;=\; \frac{L^2}{z^2}\,\Big\{-2\,dx^+\,dx^- + \phi_1(z)\,\delta(x^-)\,dx^{-\,2} + dx_\perp^2 + dz^2\Big\} \tag{7.48a}$$

$$ds^2 \;=\; \frac{L^2}{z^2}\,\Big\{-2\,dx^+\,dx^- + \phi_2(z)\,\delta(x^+)\,dx^{+\,2} + dx_\perp^2 + dz^2\Big\} \tag{7.48b}$$

with the sources $J_{++} = \frac{E_1}{z_1 L}\,\delta(x^+)\,\delta(z-z_1)$ and $J_{--} = \frac{E_2}{z_2 L}\,\delta(x^-)\,\delta(z-z_2)$ corresponding to each of the shock waves. As discussed in the previous sections, we keep $\frac{E_1\,L^2}{z_1^4} = \frac{E_2\,L^2}{z_2^4} = \mu$ such that the nuclei on the boundary have the same energy density.

The equations (7.44) for the trapped surface now take the following form:

$$z^2\Psi_i''(z) - z\,\Psi_i'(z) - 3\,\Psi_i \;=\; -16\,\pi\,G_5\,E_i\,\delta(z-z_i) \tag{7.49a}$$

$$\Psi_i(z_a) \;=\; \Psi_i(z_b) \;=\; 0 \tag{7.49b}$$

$$\frac{z_a^2}{L^2}\,\Psi_1'(z_a)\,\Psi_2'(z_a) \;=\; \frac{z_b^2}{L^2}\,\Psi_1'(z_b)\,\Psi_2'(z_b) \;=\; 8 \tag{7.49c}$$

where the boundary $\mathcal{C}$ is again $z_a < z < z_b$ and $i = 1, 2$. Eq. (7.49) is solved by

$$\Psi_i = \begin{cases} C_i\,\left(\frac{z^3}{z_a^3} - \frac{z_a}{z}\right), & z < z_i \\ \\ D_i\,\left(\frac{z^3}{z_b^3} - \frac{z_b}{z}\right), & z > z_i \end{cases} \tag{7.50}$$

with the constants

$$\begin{cases} C_i = \frac{-4\pi G_5 E_i}{z_i^4}\,\frac{\left(\frac{z_i^4}{z_b^4}-1\right) z_b}{\frac{z_b^4 - z_a^4}{z_a^3 z_b^3}} \\ \\ D_i = \frac{-4\pi G_5 E_i}{z_i^4}\,\frac{\left(\frac{z_i^4}{z_a^4}-1\right) z_a}{\frac{z_b^4 - z_a^4}{z_a^3 z_b^3}}. \end{cases} \tag{7.51}$$

The third equation in (7.49) gives the following simple relations:

$$C_1\,C_2 \;=\; D_1\,D_2 \;=\; \frac{L^2}{2}. \tag{7.52}$$

7.4.2 Shock Waves with Identical Sources

It is instructive to first consider a collision of identical shock waves in AdS_5. Putting $z_1 = z_2 = z_0$ and $E_1 = E_2 = E$ in Eqs. (7.50) and (7.51) above we obtain from Eq. (7.52) [100]

$$\begin{cases} z_a + z_b \;=\; \frac{4\sqrt{2}\,\pi\,G_5}{L}\,E \\ \\ \frac{(z_a+z_b)^2-3\,z_a\,z_b}{z_a^3\,z_b^3} \;=\; \frac{1}{z_0^4}. \end{cases} \tag{7.53}$$

We want to take $z_0 \to \infty$ limit while keeping the energy of the shock wave in the boundary theory fixed. That is we want to hold

$$\mu \;=\; \frac{E\,L^2}{z_0^4} \tag{7.54}$$

fixed. We rewrite Eq. (7.53) in terms of μ as

$$\begin{cases} z_a + z_b \;=\; \frac{2\sqrt{2}\,\pi^2}{N_c^2}\,\mu\,z_0^4 \\ \\ \frac{(z_a+z_b)^2-3\,z_a\,z_b}{z_a^3\,z_b^3} \;=\; \frac{1}{z_0^4} \end{cases} \tag{7.55}$$

where we have replaced $G_5 = \pi\,L^3/2\,N_c^2$. Now, taking $z_0 \to \infty$ keeping μ fixed we can easily infer the asymptotics of z_a and z_b. First one can consider the case that in this limit z_a and z_b are of the same order, $z_a \sim z_b$. In such case the first equation in (7.55) gives $z_a \sim z_b \sim z_0^4$, which can not satisfy the second equation in (7.55). As $z_a < z_b$ by definition, we are left to consider the case when, in the $z_0 \to \infty$ limit one has $z_a \ll z_b$. Then the first equation in (7.55) yields

$$z_b \;\approx\; \frac{2\sqrt{2}\,\pi^2}{N_c^2}\,\mu\,z_0^4 \tag{7.56}$$

which, when plugged into the second equation in (7.55) along with the assumption that $z_a \ll z_b$ gives

$$z_a \;\approx\; \frac{1}{\left(\frac{2\sqrt{2}\,\pi^2}{N_c^2}\,\mu\right)^{\frac{1}{3}}} \;\equiv\; z_a^*. \tag{7.57}$$

The values of z_a and z_b given by Eqs. (7.57) and (7.56) satisfy $z_a \ll z_b$ condition when z_0 is large, which confirms that they give the correct asymptotics.

In the strict $z_0 \to \infty$ limit we see that $z_b \to \infty$, but z_a remains finite given by Eq. (7.57). Indeed Eqs. (7.57) and (7.56) can also be obtained by solving Eqs. (7.55) explicitly and taking the $z_0 \to \infty$ limit: the exact solution of Eq. (7.55) giving real z_a and z_b is

$$z_a = \frac{\tilde{\mu}\, z_0^4}{2} - \frac{1}{4\,\xi}\sqrt{2^{11/3}\,\xi^3 - 2^{13/3}\,z_0^4\,\xi + 4\,z_0^8\,\tilde{\mu}^2\,\xi^2} \tag{7.58a}$$

$$z_b = \frac{\tilde{\mu}\, z_0^4}{2} + \frac{1}{4\,\xi}\sqrt{2^{11/3}\,\xi^3 - 2^{13/3}\,z_0^4\,\xi + 4\,z_0^8\,\tilde{\mu}^2\,\xi^2} \tag{7.58b}$$

where

$$\tilde{\mu} = \frac{2\sqrt{2}\,\pi^2}{N_c^2}\,\mu \tag{7.59}$$

and

$$\xi = \left(z_0^6\sqrt{4 + z_0^{12}\,\tilde{\mu}^4} - z_0^{12}\,\tilde{\mu}^2\right)^{1/3}. \tag{7.60}$$

One can readily check that the $z_0 \to \infty$ asymptotics of Eqs. (7.58a) and (7.58b) is given by Eqs. (7.57) and (7.56).[3]

Taking the $z_0 \to \infty$ limit in Eq. (7.50) one can see that the trapped surface is described by

$$\psi(z) = \frac{2\,\pi^2}{N_c^2}\,\mu\,\left[z^4 - z_a^{*\,4}\right] = \frac{\tilde{\mu}}{\sqrt{2}}\,\left[z^4 - \tilde{\mu}^{-4/3}\right], \tag{7.61}$$

which is exactly Eq. (7.47) with z_a now fixed by Eq. (7.57). We see that introducing bulk source as a regulator of the metric in the IR and then taking $z_0 \to \infty$ limit allows one to fix z_a and hence determines the trapped surface uniquely.

Now let us verify that the obtained value of z_a in Eq. (7.57) is independent of the way we take the limit of sending the bulk sources to infinite IR. Let us show that the same trapped surface arises in a more general case when the two shock waves are different from each other.

[3]Note that for $z_0 < (2/\tilde{\mu})^{1/3}$ both z_a and z_b from Eqs. (7.58a) and (7.58b) become complex and trapped surface ceases to exist: however this small-z_0 limit is the exact opposite of the $z_0 \to \infty$ case we would like to consider here.

7.4.3 Shock Waves with Sources at Different Bulk Locations

We consider a collision of shock waves with sources at different locations and with different E_i's: now we have $z_1 \neq z_2$ and $E_1 \neq E_2$ but with $\frac{E_1\,L^2}{z_1^4} = \frac{E_2\,L^2}{z_2^4} = \mu$. It proves useful to set $\frac{z_1^4}{z_a^2 z_b^2} = \lambda_1$, $\frac{z_2^4}{z_a^2 z_b^2} = \lambda_2$ and rewrite Eq. (7.52) as

$$\begin{cases} \frac{z_a^2}{z_b^2} + \frac{z_b^2}{z_a^2} + 1 = \frac{\lambda_1+\lambda_2+1}{\lambda_1\lambda_2} \\ \\ (z_a z_b)^3 \frac{\frac{z_a}{z_b}+\frac{z_b}{z_a}}{\left(\frac{z_a^2}{z_b^2}-\frac{z_b^2}{z_a^2}\right)^2} = \left(\frac{N_c^2}{2\pi^2\mu}\right)^2 \frac{1}{2(1-\lambda_1\lambda_2)} \end{cases} \tag{7.62}$$

eliminating z_1 and z_2. Finding solution for z_a and z_b seems to be a hard task. We instead first solve the first equation in (7.62) for z_a/z_b and use the obtained ratio in the second equation in (7.62) to find $z_a\,z_b$. Using the product $z_a\,z_b$ in $\frac{z_1^4}{z_a^2 z_b^2} = \lambda_1$, $\frac{z_2^4}{z_a^2 z_b^2} = \lambda_2$ we can write z_1 and z_2 as $(i = 1, 2)$

$$z_i^4 \;=\; \lambda_i \left(\frac{N_c^2}{2\,\pi^2\,\mu}\right)^{4/3} \left[\frac{\lambda_1+\lambda_2+1-3\,\lambda_1\,\lambda_2}{2\,(1-\lambda_1\,\lambda_2)}\right]^{2/3} \frac{[(\lambda_1+1)\,(\lambda_2+1)]^{1/3}}{\lambda_1\,\lambda_2}. \tag{7.63}$$

Again we have replaced $G_5 = \pi\,L^3/2\,N_c^2$. We are interested in the limit $z_1, z_2 \to \infty$ while keeping $r_{12} = \frac{z_1}{z_2} =$ finite and μ is fixed. It is not difficult to see that the limit can be achieved by taking $\lambda_1, \lambda_2 \to 0$. In this limit Eq. (7.63) takes a very simple form:

$$z_1^4 \;=\; \frac{1}{4\,\lambda_2} \left(\frac{N_c^2}{\pi^2\,\mu}\right)^{4/3} \tag{7.64a}$$

$$z_2^4 \;=\; \frac{1}{4\,\lambda_1} \left(\frac{N_c^2}{\pi^2\,\mu}\right)^{4/3}. \tag{7.64b}$$

As $z_b > z_a$, the first equation in (7.62) gives in the $\lambda_1, \lambda_2 \to 0$ limit that $z_b \gg z_a$. Solving the second equation in (7.62) for $z_b \gg z_a$ one obtains z_a asymptotics. Using the result in $\frac{z_1^4}{z_a^2 z_b^2} = \lambda_1$ along with the first equation in

(7.62) yields

$$z_a \approx \left(\frac{N_c^2}{2\sqrt{2}\,\pi^2\,\mu}\right)^{1/3} \equiv z_a^* \tag{7.65a}$$

$$z_b \approx (z_1 z_2)^2 \left(\frac{N_c^2}{2\sqrt{2}\pi^2\mu}\right)^{-1} \to \infty. \tag{7.65b}$$

These equations are completely analogous to Eqs. (7.57) and (7.56) above. Therefore the trapped surface is independent of the way one send the bulk sources to the IR infinity: the sources do not have to be at the same bulk location to obtain the same answer as we had in the previous Subsection. To further test the independence of taking the limit of sources going to infinite IR bulk, we have also taken a similar limit for the point-like sources, first advocated in [82]: the trapped surface found in [82] again reduced to the trapped surface found in this work above.

This completes our analysis of trapped surface in the collision of two shock waves with sources infinitely deep in the bulk. We note unlike source in finite depth[100], no critical value for the energy density is found in the limit. The formation of the trapped surface is always guaranteed. The trapped surface is even independent of the ratio $r_{12} = \frac{z_1}{z_2}$, i.e. the details of the limit! It is important to stress that the trapped surface does not disappear with the removal of the sources in the bulk, which can be viewed as IR regulators. In all the examples of scattering of shock waves with bulk sources the trapped surface always appears to be more or less centered around the source in the $x_\perp, z$ space. One was tempted to conjecture therefore that the trapped surface is an inherent property of non-zero bulk energy-momentum tensor. Our result proves otherwise, giving an example of the source-free shock waves collision with a well defined trapped surface.

7.4.4 Limiting Trapped Surface

To summarize our trapped surface analysis let us re-state that the profiles of the trapped surface are given by

$$\Psi_i(z) = \frac{2\,\pi^2\,L\,\mu}{N_c^2}\,z_a^{*\,3}\left(\frac{z^3}{z_a^{*\,3}} - \frac{z_a^*}{z}\right) \tag{7.66}$$

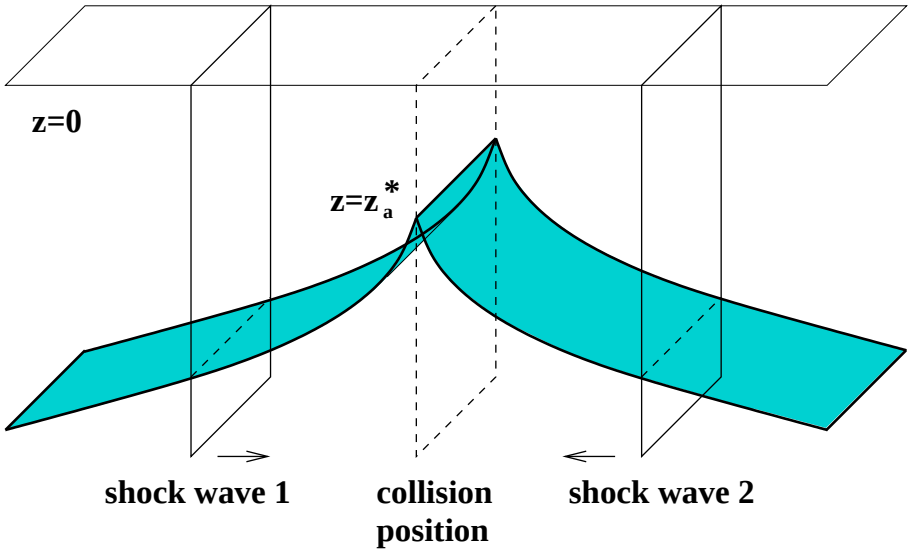

Figure 7.1: An illustration of the trapped surface in the collision of two source-less shock waves. Vertical axis is the bulk z-direction, the horizontal left-right axis can be thought of either as the collision axis or as the time direction. The trapped surface is shaded.

which is exactly Eq. (7.46) with z_a^* from Eq. (7.57). In the transformed light cone coordinates (see Eq. (7.38)) the trapped surface is then determined by

$$x^+ = 0,\ x^- = -\frac{\pi^2}{N_c^2}\,\mu\,\left[z^4 - z_a^{*\,4}\right] = -\frac{\tilde{\mu}}{2\sqrt{2}}\,\left[z^4 - \tilde{\mu}^{-4/3}\right] \tag{7.67}$$

with an analogous expression for the other shock wave obtained by interchanging $x^+ \leftrightarrow x^-$ in Eq. (7.67).

The trapped surface for a collision of source-free shock waves from Eq. (7.67) is illustrated in Fig. 7.1. One can clearly see that the trapped surface is present at all times before the collision and rises from the deep IR toward finite values of z. Similar behavior was observed for the trapped surface in the numerical model of heavy ion collision involving gravitational perturbations in the 4-dimensional world in [81, 108]. A horizon rising from the deep IR was also deduced in [109] for a model of heavy ion collision involving a rapidity-independent matter distribution after the collision.

It is interesting to point out that the obtained shape of the trapped surface appears to imply that the black hole produced in the collision would have a singularity at $z = \infty$ with the horizon independent of the transverse coordinates $x_\perp$. This is indeed very similar to the black hole dual to Bjorken

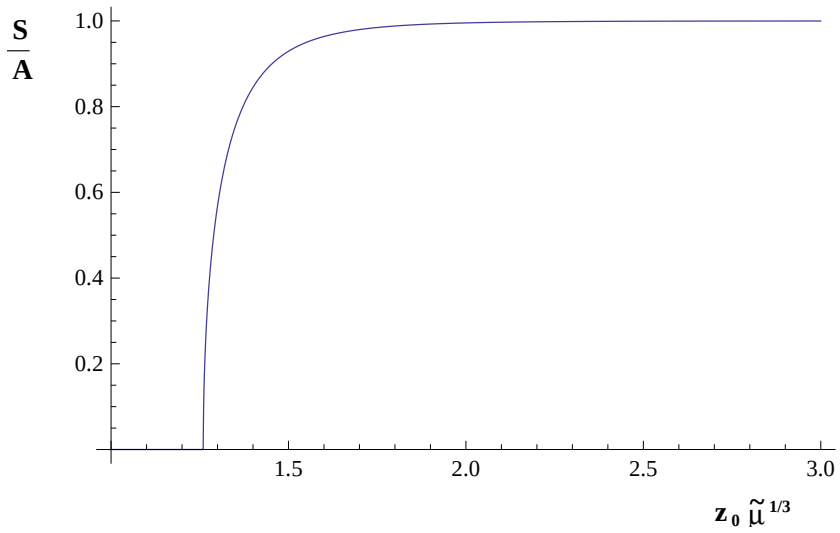

Figure 7.2: The (lower bound on the) Entropy density produced in the collision of two identical shock waves with sources as a function of the source position z_0 in units of $\tilde{\mu}^{-1/3}$. The entropy density is in arbitrary units.

hydrodynamics constructed in [25]. The main difference is that in our case the metric (and the energy-momentum tensor in the gauge theory) are rapidity-dependent, as follows from explicit calculations of the metric produced in shock wave collisions [78, 79, 101].

Our estimate for the produced entropy per unit transverse area $A_\perp$ for a collision of two shock waves with the sources at z_0 is [100]

$$\frac{S}{A_\perp} = \frac{N_c^2}{2\,\pi}\left[\frac{1}{z_a^2} - \frac{1}{z_b^2}\right]. \tag{7.68}$$

Using Eqs. (7.57) and (7.56) we obtain for $z_0 \to \infty$

$$\frac{S}{A_\perp} = \left[\pi\, N_c^2\, \mu^2\right]^{1/3}. \tag{7.69}$$

As $\mu^2 \sim s$ with s the center of mass energy of the collision, we get

$$\frac{S}{A_\perp} \propto s^{1/3} \tag{7.70}$$

in agreement with the result obtained in [82].

The entropy from Eq. (7.68) is plotted in Fig. 7.2 in arbitrary units as a function of the bulk source location z_0 (for a collision of two identical shock

waves). Fig. 7.2 demonstrated that produced entropy becomes practically independent of the bulk source position rather fast, approaching its asymptotic value well before $z_0\,\tilde{\mu}^{1/3}$ becomes large.

As we noted above, for $z_0\,\tilde{\mu}^{1/3} < 2^{1/3}$ both z_a and z_b given by Eqs. (7.58a) and (7.58b) become complex and the trapped surface ceases to exist (see also [94] for a similar result). This likely implies that no black hole is formed in collisions of such shock waves. To understand this result from the boundary gauge theory perspective one has to have a rigorous interpretation of what shock wave sources in the bulk are dual to in the gauge theory. Such interpretation is missing at the moment, which inspired our present investigation of collisions of the sourceless shock waves. We may speculate though: following [100] we may assume that the inverse position of the source in the bulk $1/z_0$ provides an IR cutoff on the transverse momenta of the partons in the shock waves' wave functions in the boundary theory. Reducing z_0 would increase the cutoff $1/z_0$ thus decreasing the number of partons: this is likely to lower the number of degrees of freedom produced in the collision, leading to the reduction of the entropy density with decreasing z_0 in Fig. 7.2. Still it is not entirely clear why the trapped surface disappears completely at a finite small z_0 forcing the estimate for produced entropy to go to zero. Indeed our delta-function shock waves are described by a single dimensionful parameter $\tilde{\mu}$ (or μ): the largest momentum scale in the problem is therefore $\tilde{\mu}^{1/3}$. If $1/z_0$ is the IR cutoff, then clearly it can not exceed the largest momentum scale: hence $1/z_0 \lesssim \tilde{\mu}^{1/3}$. This, however, can not explain why the trapped surface vanishes entirely at $z_0 = 2^{1/3}\,\tilde{\mu}^{-1/3}$. Besides nothing pathological seems to happen in the perturbative solution presented in Sect. 7.3 for small finite z_0. In this work we are interested in the large-z_0 asymptotics: Fig. 7.2 demonstrates that the produced entropy density does not seem to change much between having sources at finite large $z_0 > 2^{1/3}\,\tilde{\mu}^{-1/3}$ and having no sources at all, which seems to agree with the IR cutoff interpretation of the sources and, more importantly, shows that the entropy is "well-behaved" in the $z_0 \to \infty$ limit we are taking. We leave the detailed study of the small-z_0 regime for future work.

7.5 Thermalization Time Estimate and Conclusions

The result fixing z_a^* in Eq. (7.57) could be predicted if one realizes that in the limit of delta-function shock waves the problem has only one dimensionful parameter $\tilde{\mu}$ which has dimensions of mass cubed. If a non-vanishing trapped surface is created in such collisions it has to be proportional to the only distance

scale in the problem: $1/\tilde{\mu}^{1/3}$. Stretching this analogy further one should expect that the proper time of thermalization (the time of black hole formation) is

$$\tau_{therm} \sim \frac{1}{\tilde{\mu}^{1/3}}, \tag{7.71}$$

as was originally suggested in [78].

An interesting question is the relation between this thermalization time and the time it takes for the shock waves to stop. It was argued in [79, 101] that colliding shock waves come to a complete stop shortly after the collision. One can argue that $\mu \sim p^+ \Lambda^2 A^{1/3}$ [79], where p^+ is the large longitudinal momentum of a "nucleon" in the shock wave, Λ is the typical transverse momentum scale in the shock, and A is the atomic number of the nucleus we model by the shock wave. The characteristic light-cone stopping time for a shock wave moving in the light-cone "plus" direction is given by [79, 101]

$$x^+_{stop} \sim \frac{1}{\Lambda A^{1/3}}. \tag{7.72}$$

This is of course parametrically much longer than

$$\tau_{therm} \sim \frac{1}{\tilde{\mu}^{1/3}} \sim \frac{1}{(p^+ \Lambda^2 A^{1/3})^{1/3}}. \tag{7.73}$$

Hence, if one assumes that thermalization happens at mid-rapidity first, then, as near mid-rapidity $t \approx \tau$, the time of thermalization is $t_{therm} \approx \tau_{therm} \ll t_{stop} = x^+_{stop}/\sqrt{2}$. It is therefore likely that thermalization happens at times which are parametrically earlier than the stopping time. If our guess of thermalization time is correct, this would imply that the shock waves still move along their light cones when thermalization happens, justifying an assumption commonly used in hydrodynamic simulations of heavy ion collisions. Note also that the thermalization time in Eq. (7.73) is very short, and decreases with center-of-mass energy of the collision. (In fact, as was noticed in [78] this thermalization time is too short: if one plugs in $p^+ = 100$ GeV, $\Lambda = 0.2$ GeV and $A = 196$ into the parametric estimate (7.73) one would obtain $\tau_{therm} \approx 0.07$ fm/c for RHIC, which is far too short for agreement with hydrodynamic simulations [51, 98]. Indeed the thermalization time estimate of Eq. (7.71) is too crude for 0.07 fm/c to be taken literally, and a numerical coefficient in front of the estimate (7.71), if it results from a more exact calculation and from a more realistic model of colliding nuclei, may significantly change this number.)

It is important to stress the difference between the mathematical limit of delta-function shock waves ($a \to 0$ with a being the x^--width of the smeared non-delta-function shock wave [79, 101] moving in the x^+ direction or vice versa) and the physical high energy limit of $p^+ \gg \Lambda$ for nuclei. While in the former limit $\tilde{\mu}$ is the only non-vanishing dimensionful parameter in the problem, the latter limit has another non-vanishing dimensionful scale $\tilde{\mu}\, a$, which in fact gives the stopping time (7.72), $x^+_{stop} \sim 1/\sqrt{\tilde{\mu}\, a}$ [79, 101]. (As one can easily see $a \sim A^{1/3}/p^+$ in the center-of-mass frame, such that $\tilde{\mu}\, a \sim \Lambda^2\, A^{2/3}$ is independent of p^+ [79, 101].) With the presence of two momentum scales in the problem the validity of the thermalization time estimate of [78] shown here in Eq. (7.71) becomes less apparent. Our trapped surface analysis resulting in Eq. (7.57) appears to indicate that it is the momentum scale which depend only on $\tilde{\mu}$ and not on a that matters for thermalization, thus providing new evidence to support the estimate in Eq. (7.71). In other words we show that if one neglects the smaller second momentum scale $\tilde{\mu}\, a$ and approximates the shock wave profiles by delta-functions, thermalization is achieved in the collisions at the time given in Eq. (7.71). If one treats the problem more carefully and includes the scale $\tilde{\mu}\, a$ by considering shock waves of finite longitudinal spread [79, 101], Eq. (7.71) is likely to get corrections with the relative suppression factor being some positive power of $\tilde{\mu}\, a/\tilde{\mu}^{2/3}$, which is very small for high energy collisions, thus leaving the estimate in Eq. (7.71) practically unchanged.

One may argue that the strongly-coupled dynamics of the $\mathcal{N} = 4$ SYM medium produced in shock wave collisions may be similar to that of strongly-coupled QCD medium. Then our conclusion of rapid thermalization may be applicable to soft (non-perturbative, $k_T \sim \Lambda_{QCD}$) modes in heavy ion collisions, which would thermalize very quickly. Harder (perturbative) modes may then thermalize through interactions with the soft non-perturbative thermal bath, though more work is needed to justify such thermalization scenario and to modify the thermalization time estimate (7.73) to take into account perturbative dynamics.

Another interesting question would concern understanding the relation between the rather quick thermalization in heavy ion collisions for the theory at strong coupling argued here and the impossibility of thermalization at weak coupling suggested in [110] by one of the authors.[4] While further research is needed to clarify this problem, the solution may have already been suggested in [114, 115], where the authors argue that it is possible that there is a critical value λ_c of 't Hooft coupling λ. For $\lambda > \lambda_c$ black hole formation is likely in high energy collisions. At the same time, for $\lambda < \lambda_c$ the black hole is *not*

[4]Note that perturbative thermalization scenarios have been advocated in [111–113].

formed in high energy collisions [114, 115], corresponding to no thermalization in the boundary theory. Indeed in the case of real-life heavy ion collisions, due to the running of the strong coupling constant, the coupling assumes a wide range of values in a single collision. The coupling is always large for soft transverse modes, making thermalization due to large coupling effects likely in light of our above results.

To conclude let us point out once more that we have obtained a trapped surface for a collision of two sourceless shock waves in AdS_5. The shape of the trapped surface is given by Eq. (7.67) and is illustrated in Fig. 7.1. Existence of this trapped surface proves that a black hole is created in the bulk for a collision of two sourceless shock waves, corresponding to creation of thermalized medium (quark-gluon plasma) in the boundary gauge theory.

Chapter 8

Summary

The thermalization of gauge fields at strong coupling can be interpreted as the formation of black hole horizon in the dual gravitational theory. We have studied three scenarios of thermalization of gauge fields in this dissertation. In the first scenario, the stringy debris created by heavy ion collisions fall in the AdS background. The black hole is expected to form as a consequence of the merging of debris. We solved the hologram of separate debris, which corresponds to the stress energy tensor of the gauge fields, but found no signature of thermalization. This is because we ignored the interaction among the debris. In the second scenario, we restore the interaction by modeling the debris as a shell, which undergoes a gravitational collapse. The formation of an isotropic horizon is realized in this model. The shell state gives the same energy and pressure as a thermal plasma. We characterized its deviation from thermal equilibrium by spectral densities and found a universal behavior of the spectral densities as the equilibrium is approached. The third scenario is a gravitational shock wave collision model. It is more close to real world heavy ion collisions. We explicitly constructed the apparent horizon, which signals the formation of a black hole at later time. This corresponds to the equilibration of matter and formation of Quark Gluon Plasma. We found strikingly the apparent horizon disappears as the impact parameter exceeds certain critical value. We discussed its relevancy to experiments of heavy ion collisions.

The first scenario is based on a gravity model dual to heavy ion collisions in [23]. We have solved the falling of various stringy debris in the AdS background in the probe limit. We found an analytic scaling solution corresponding to an open string whose ends are attached to quark and antiquark moving with $\pm v$. In the slow moving limit, we have derived a velocity dependent potential, which is an analog of Ampere's law at strong coupling. We found an instability of the string solution as v grows. At large v, we solved the falling of the string numerically and observed a universal asymptotic behavior. Going

beyond the probe limit, we restored the backreaction of the stringy debris by solving linearized Einstein equation in the AdS background. We extracted the stress energy tensor on the boundary from the metric correction due to the stringy source. We obtained interesting results for the stress energy tensor due to the scaling string, which is close to the situation of proton-proton collision. In contrast to perturbative QCD expectation, the result contains no jet-like structure and shows a near spherical distribution of matter. It is a consequence of the strong coupling nature of the dual field theory. Moreover, we have showed the stress energy tensor is incompatible with hydrodynamical parametrization, which implies equilibrium is not reached in proton-proton collision and indicates the necessity to include nonlinear terms in Einstein equation for the study of thermalization.

In the second scenario, we solved the falling of the shell by Israel junction condition and probed the collapsing geometry with gravitational waves, from which we extract the spectral function of the stress energy tensor. We calculated the spectral functions for all three channels of stress energy tensors at different stages of equilibration. The results showed a universal behavior: They differ from their thermal counterpart by general oscillations. The oscillations always damp in amplitude and grow in frequency, corresponding to the damping of non thermal mode and divergence of coherence time.

In the third scenario, we obtained a lower bound for the entropy production with a gravitational shock wave collision model, following [82]. We constructed the apparent horizon from past infinity to the collision moment. The area of the apparent horizon at the collision moment sets a lower bound for entropy production in nucleus collisions according to the duality. We obtained the area of apparent horizon as a function of the impact parameter and collision energy. We observed a critical impact parameter, beyond which apparent horizon does not exist. Furthermore, the entropy production does not vanish at critical impact parameter, indicating a first order transition. The dependence of the critical impact parameter on the collision energy is examined numerically and a leading power law is found, with the obtained power in good agreement with [97]. Despite of the interesting phenomena we found in gravitational shock wave collision, we critically argued its limitation in modeling nucleus collisions and proposed more realistic model. The model includes a saturation scale but discard the nucleus size. We discussed the physical origin of the critical phenomenon and demonstrated an equivalence of collision of gravitational shock wave without source and with source at infinite IR limit.

More fascinating issues are expected to be resolved in the post collision domain, where gravitational field of the shock waves interact strongly. Solving the metric explicitly in this domain remains an open question. The strong

gravitational effect makes the problem more technically challenging, however at large distance, the metric can be solved perturbatively, with the leading order giving the gravitational radiation. The solution of the gravitational radiation carries information on the loss of energy and angular momentum. These will give further constraint on the formation of black hole in the collision, and we will obtain further understanding of equilibration process of strongly coupled gauge theory.

Bibliography

[1] J. M. Maldacena, Adv. Theor. Math. Phys. **2**, 231 (1998) [Int. J. Theor. Phys. **38**, 1113 (1999)] [arXiv:hep-th/9711200].

[2] E. Witten, Adv. Theor. Math. Phys. **2**, 253 (1998) [arXiv:hep-th/9802150].

[3] S. S. Gubser, I. R. Klebanov and A. M. Polyakov, Phys. Lett. B **428**, 105 (1998) [arXiv:hep-th/9802109].

[4] G. 't Hooft, arXiv:gr-qc/9310026.

[5] E. Witten, Adv. Theor. Math. Phys. **2**, 505 (1998) [arXiv:hep-th/9803131].

[6] S. S. Gubser, Nucl. Phys. A **830**, 657C (2009) [arXiv:0907.4808 [hep-th]].

[7] E. V. Shuryak, Phys. Rept. **61**, 71 (1980).

[8] E.V.Shuryak, Prog. Part. Nucl. Phys. **53**, 273 (2004) [hep-ph/0312227]. E.V.Shuryak and I. Zahed, `hep-ph/0307267`, Phys. Rev. C **70**, 021901 (2004) Phys. Rev. D **69** (2004) 014011. [hep-th/0308073].

[9] J. Liao and E. Shuryak, Phys. Rev. C **75**, 054907 (2007) [arXiv:hep-ph/0611131].

[10] S. S. Gubser, I. R. Klebanov and A. A. Tseytlin, Nucl. Phys. B **534**, 202 (1998) [arXiv:hep-th/9805156].

[11] G. Policastro, D. T. Son and A. O. Starinets, Phys. Rev. Lett. **87**, 081601 (2001) [arXiv:hep-th/0104066].

[12] P. Kovtun, D. T. Son and A. O. Starinets, Phys. Rev. Lett. **94**, 111601 (2005) [arXiv:hep-th/0405231].

[13] J. Casalderrey-Solana and D. Teaney, hep-ph/0605199.

[14] H. Liu, K. Rajagopal, and U. A. Wiedemann, Phys. Rev. Lett. **97**, 182301 (2006) [arXiv:hep-ph/0605178].
A. Buchel, Phys. Rev. D **74**, 046006 (2006) [arXiv:hep-th/0605178].
C. P. Herzog, A. Karch, P. Kovtun, C. Kozcaz, and L. G. Yaffe, JHEP **0607**, 013 (2006) [arXiv:hep-th/0605158].
S. S. Gubser, Phys. Rev. D **74**, 126005 (2006) [arXiv:hep-th/0605182].

[15] E. V. Shuryak, "Strongly coupled quark-gluon plasma: The status report," arXiv:hep-ph/0608177. "Electric-Magnetic Struggle in QGP, Deconfinement and Baryons," arXiv:0709.2175 [hep-ph].

[16] J. Casalderrey-Solana, E. V. Shuryak and D. Teaney, "Conical flow induced by quenched QCD jets," hep-ph/0411315. arXiv:hep-ph/0602183. H. Stoecker, "Collective Flow signals the Quark Gluon Plasma," Nucl. Phys. A **750**, 121 (2005) [arXiv:nucl-th/0406018].

[17] J. J. Friess, S. S. Gubser and G. Michalogiorgakis, JHEP **0609**, 072 (2006) [arXiv:hep-th/0605292].

[18] P. M. Chesler and L. G. Yaffe, Phys. Rev. Lett. **99**, 152001 (2007) [arXiv:0706.0368 [hep-th]].

[19] P. Romatschke and U. Romatschke, "How perfect is the RHIC fluid?," arXiv:0706.1522 [nucl-th]. H. Song and U. W. Heinz, "Suppression of elliptic flow in a minimally viscous quark-gluon plasma," arXiv:0709.0742 [nucl-th]. K. Dusling and D. Teaney, "Simulating elliptic flow with viscous hydrodynamics," arXiv:0710.5932 [nucl-th].

[20] M. Lublinsky and E. Shuryak, Phys. Rev. C **76**, 021901 (2007) [arXiv:0704.1647 [hep-ph]].

[21] J. Polchinski and M. J. Strassler, Phys. Rev. Lett. **88**, 031601 (2002) [arXiv:hep-th/0109174].

[22] S. B. Giddings, Phys. Rev. D **67**, 126001 (2003) [arXiv:hep-th/0203004].

[23] E. Shuryak, S. J. Sin and I. Zahed, arXiv:hep-th/0511199.

[24] J.D. Bjorken, Phys.Rev.**D27** (1983) 140.

[25] R. A. Janik and R. Peschanski, Phys. Rev. D **73**, 045013 (2006) arXiv:hep-th/0512162, arXiv:hep-th/0606149.

[26] S. Nakamura and S. J. Sin, arXiv:hep-th/0607123.

[27] M. P. Heller and R. A. Janik, Phys. Rev. D **76**, 025027 (2007) [arXiv:hep-th/0703243].

[28] K. Kajantie, J. Louko and T. Tahkokallio, arXiv:0705.1791 [hep-th].

[29] P. Benincasa, A. Buchel, M. P. Heller and R. A. Janik, arXiv:0712.2025 [hep-th].

[30] B. Andersson, G. Gustafson, G. Ingelman and T. Sjostrand, Phys. Rept. **97**, 31 (1983).

[31] S. J. Brodsky and G. F. de Teramond, arXiv:0709.2072 [hep-ph].

[32] L. D. McLerran and R. Venugopalan, Phys. Rev. D **49**, 2233 (1994) [arXiv:hep-ph/9309289].

[33] A. Krasnitz, Y. Nara and R. Venugopalan, Nucl. Phys. A **727**, 427 (2003) [arXiv:hep-ph/0305112].

[34] E. Shuryak, arXiv:0711.0004 [hep-ph].

[35] W. Israel, Nuovo Cim. B **44S10**, 1 (1966) [Erratum-ibid. B **48**, 463 (1967 NUCIA,B44,1.1966)].

[36] O. Aharony, S. Minwalla and T. Wiseman, "Plasma-balls in large N gauge theories and localized black holes," `hep-th/0507219`.

[37] J. M. Maldacena, Phys. Rev. Lett. **80**, 4859 (1998) [arXiv:hep-th/9803002]. S. J. Rey and J. T. Yee, Eur. Phys. J. C **22**, 379 (2001) [arXiv:hep-th/9803001].

[38] D. J. Gross, A. Mikhailov and R. Roiban, Annals Phys. **301**, 31 (2002) [arXiv:hep-th/0205066]. Y. Makeenko, P. Olesen and G. W. Semenoff, Nucl. Phys. B **748**, 170 (2006) [arXiv:hep-th/0602100].

[39] U. H. Danielsson, E. Keski-Vakkuri and M. Kruczenski, JHEP **9901**, 002 (1999) [arXiv:hep-th/9812007].

[40] E. V. Shuryak and I. Zahed, Phys. Lett. B **608**, 258 (2005) [arXiv:hep-th/0310031].

[41] J. A. Minahan, Adv. Theor. Math. Phys. **2**, 559 (1998) [arXiv:hep-th/9803111].

[42] O. Kaczmarek and F. Zantow, PoS **LAT2005**, 192 (2006) [arXiv:hep-lat/0510094].

[43] J. Liao and E. Shuryak, arXiv:0706.4465 [hep-ph].

[44] M. N. Chernodub and V. I. Zakharov, Phys. Rev. Lett. **98**, 082002 (2007) [arXiv:hep-ph/0611228].

[45] G. W. Semenoff and K. Zarembo, Nucl. Phys. Proc. Suppl. **108**, 106 (2002) [arXiv:hep-th/0202156].

[46] C. G. . Callan and A. Guijosa, Nucl. Phys. B **565**, 157 (2000) [arXiv:hep-th/9906153].

[47] E. Shuryak and I. Zahed, Phys. Rev. D **69**, 046005 (2004) [arXiv:hep-th/0308073].

[48] I. R. Klebanov, J. M. Maldacena and C. B. . Thorn, JHEP **0604**, 024 (2006) [arXiv:hep-th/0602255].

[49] B. A. Gelman, E. V. Shuryak and I. Zahed, Phys.Rev.C, in press, arXiv:nucl-th/0601029, nucl-th/0605046.

[50] J. Liao and E. V. Shuryak, Nucl. Phys. A **775**, 224 (2006) [arXiv:hep-ph/0508035].

[51] D. Teaney, J. Lauret and E. V. Shuryak, arXiv:nucl-th/0110037.

[52] P. F. Kolb and U. W. Heinz, arXiv:nucl-th/0305084.

[53] E. Shuryak, arXiv:0807.3033 [hep-ph].

[54] S. Lin and E. Shuryak, Phys. Rev. D **77**, 085013 (2008) [arXiv:hep-ph/0610168].

[55] T. Han, Z. Si, K. M. Zurek and M. J. Strassler, JHEP **0807**, 008 (2008) [arXiv:0712.2041 [hep-ph]].

[56] S. Lin and E. Shuryak, Phys. Rev. D **76**, 085014 (2007) [arXiv:0707.3135 [hep-th]].

[57] S. Lin and E. Shuryak, Phys. Rev. D **77**, 085014 (2008) [arXiv:0711.0736 [hep-th]].

[58] R. Venugopalan, arXiv:0806.1356 [hep-ph].

[59] G. T. Horowitz and V. E. Hubeny, Phys. Rev. D **62**, 024027 (2000) [arXiv:hep-th/9909056].

[60] P. K. Kovtun and A. O. Starinets, Phys. Rev. D **72**, 086009 (2005) [arXiv:hep-th/0506184].

[61] A. Nunez and A. O. Starinets, Phys. Rev. D **67**, 124013 (2003) [arXiv:hep-th/0302026].

[62] A. O. Starinets, Phys. Rev. D **66**, 124013 (2002) [arXiv:hep-th/0207133].

[63] U. H. Danielsson, E. Keski-Vakkuri and M. Kruczenski, Nucl. Phys. B **563**, 279 (1999) [arXiv:hep-th/9905227].

[64] U. H. Danielsson, E. Keski-Vakkuri and M. Kruczenski, JHEP **0002**, 039 (2000) [arXiv:hep-th/9912209].

[65] S. B. Giddings and A. Nudelman, JHEP **0202**, 003 (2002) [arXiv:hep-th/0112099].

[66] V. E. Hubeny, H. Liu and M. Rangamani, JHEP **0701**, 009 (2007) [arXiv:hep-th/0610041].

[67] K. S. . Thorne, R. H. . Price and D. A. . Macdonald, "BLACK HOLES: THE MEMBRANE PARADIGM," *NEW HAVEN, USA: YALE UNIV. PR. (1986) 367p*

[68] R. Venugopalan, Eur. Phys. J. C **43**, 337 (2005) [arXiv:hep-ph/0502190].

[69] G. Policastro, D. T. Son and A. O. Starinets, JHEP **0209**, 043 (2002) [arXiv:hep-th/0205052].

[70] P. Kovtun and A. Starinets, Phys. Rev. Lett. **96**, 131601 (2006) [arXiv:hep-th/0602059].

[71] S. A. Hartnoll and S. Prem Kumar, JHEP **0512**, 036 (2005) [arXiv:hep-th/0508092].

[72] D. T. Son and A. O. Starinets, JHEP **0209**, 042 (2002) [arXiv:hep-th/0205051].

[73] G. Policastro, D. T. Son and A. O. Starinets, JHEP **0212**, 054 (2002) [arXiv:hep-th/0210220].

[74] D. Z. Freedman, S. D. Mathur, A. Matusis and L. Rastelli, Nucl. Phys. B **546**, 96 (1999) [arXiv:hep-th/9804058].

[75] D. Teaney, Phys. Rev. D **74**, 045025 (2006) [arXiv:hep-ph/0602044].

[76] S. Caron-Huot, P. Kovtun, G. D. Moore, A. Starinets and L. G. Yaffe, JHEP **0612**, 015 (2006) [arXiv:hep-th/0607237].

[77] M. P. Heller, R. A. Janik and R. Peschanski, Acta Phys. Polon. B **39**, 3183 (2008) [arXiv:0811.3113 [hep-th]].

[78] D. Grumiller and P. Romatschke, JHEP **0808**, 027 (2008) [arXiv:0803.3226 [hep-th]].

[79] J. L. Albacete, Y. V. Kovchegov and A. Taliotis, JHEP **0807**, 100 (2008) [arXiv:0805.2927 [hep-th]].

[80] S. Lin and E. Shuryak, Phys. Rev. D **78**, 125018 (2008) [arXiv:0808.0910 [hep-th]].

[81] P. M. Chesler and L. G. Yaffe, arXiv:0812.2053 [hep-th].

[82] S. S. Gubser, S. S. Pufu and A. Yarom, Phys. Rev. D **78**, 066014 (2008) [arXiv:0805.1551 [hep-th]].

[83] D. M. Eardley and S. B. Giddings, Phys. Rev. D **66**, 044011 (2002) [arXiv:gr-qc/0201034].

[84] H. Yoshino and Y. Nambu, Phys. Rev. D **67**, 024009 (2003) [arXiv:gr-qc/0209003].

[85] E. Kohlprath and G. Veneziano, JHEP **0206**, 057 (2002) [arXiv:gr-qc/0203093].

[86] S. W. Hawking and R. Penrose, Proc. Roy. Soc. Lond. A **314**, 529 (1970).

[87] D. E. Berenstein, R. Corrado, W. Fischler and J. M. Maldacena, Phys. Rev. D **59**, 105023 (1999) [arXiv:hep-th/9809188].

[88] G. I. Veres *et al.* [PHOBOS Collaboration], arXiv:0806.2803 [nucl-ex].

[89] E. V. Shuryak, Phys. Rev. C **76**, 047901 (2007) [arXiv:0706.3531 [nucl-th]].

[90] M. Daugherity [STAR Collaboration], J. Phys. G **35**, 104090 (2008) [arXiv:0806.2121 [nucl-ex]].

[91] A. Dumitru, F. Gelis, L. McLerran and R. Venugopalan, Nucl. Phys. A **810**, 91 (2008) [arXiv:0804.3858 [hep-ph]].

[92] U. Gursoy and E. Kiritsis, JHEP **0802**, 032 (2008) [arXiv:0707.1324 [hep-th]].

[93] U. Gursoy, E. Kiritsis and F. Nitti, JHEP **0802**, 019 (2008) [arXiv:0707.1349 [hep-th]].

[94] L. Alvarez-Gaume, C. Gomez, A. S. Vera, A. Tavanfar and M. A. Vazquez-Mozo, arXiv:0811.3969 [hep-th].

[95] K. Kang and H. Nastase, Phys. Rev. D **72**, 106003 (2005) [arXiv:hep-th/0410173].

[96] H. Nastase, Prog. Theor. Phys. Suppl. **174**, 274 (2008) [arXiv:0805.3579 [hep-th]].

[97] S. S. Gubser, S. S. Pufu and A. Yarom, arXiv:0902.4062 [hep-th].

[98] P. Huovinen, P. F. Kolb, U. W. Heinz, P. V. Ruuskanen and S. A. Voloshin, Phys. Lett. B **503**, 58 (2001) [arXiv:hep-ph/0101136].

[99] K. Kajantie, J. Louko and T. Tahkokallio, Phys. Rev. D **77**, 066001 (2008) [arXiv:0801.0198 [hep-th]].

[100] S. Lin and E. Shuryak, Phys. Rev. D **79**, 124015 (2009) [arXiv:0902.1508 [hep-th]].

[101] J. L. Albacete, Y. V. Kovchegov and A. Taliotis, JHEP **0905**, 060 (2009) [arXiv:0902.3046 [hep-th]].

[102] R. Penrose, unpublished (1974)

[103] J. L. Albacete, Y. V. Kovchegov and A. Taliotis, JHEP **0807**, 074 (2008) [arXiv:0806.1484 [hep-th]].

[104] A. H. Mueller, A. I. Shoshi and B. W. Xiao, Nucl. Phys. A **822**, 20 (2009) [arXiv:0812.2897 [hep-th]].

[105] E. Avsar, E. Iancu, L. McLerran and D. N. Triantafyllopoulos, JHEP **0911**, 105 (2009) [arXiv:0907.4604 [hep-th]].

[106] S. de Haro, S. N. Solodukhin and K. Skenderis, Commun. Math. Phys. **217**, 595 (2001) [arXiv:hep-th/0002230].

[107] Y. V. Kovchegov and D. H. Rischke, Phys. Rev. C **56**, 1084 (1997) [arXiv:hep-ph/9704201].

[108] P. M. Chesler and L. G. Yaffe, arXiv:0906.4426 [hep-th].

[109] G. Beuf, M. P. Heller, R. A. Janik and R. Peschanski, JHEP **0910**, 043 (2009) [arXiv:0906.4423 [hep-th]].

[110] Y. V. Kovchegov, Nucl. Phys. A **762**, 298 (2005) [arXiv:hep-ph/0503038].

[111] R. Baier, A. H. Mueller, D. Schiff and D. T. Son, Phys. Lett. B **502**, 51 (2001) [arXiv:hep-ph/0009237].

[112] S. Mrowczynski, Phys. Lett. B **214**, 587 (1988) [Erratum-ibid. B **656**, 273 (2007)].

[113] P. Arnold, J. Lenaghan and G. D. Moore, JHEP **0308**, 002 (2003) [arXiv:hep-ph/0307325].

[114] L. Cornalba, M. S. Costa and J. Penedones, arXiv:0911.0043 [hep-th].

[115] O. Aharony, S. Minwalla and T. Wiseman, Class. Quant. Grav. **23**, 2171 (2006) [arXiv:hep-th/0507219].

Appendices

A Linearization of Ricci tensor

We may start with the following relations:

$$\delta R_{\mu\nu} = \delta\Gamma^{\lambda}_{\mu\lambda;\nu} - \delta\Gamma^{\lambda}_{\mu\nu;\lambda}$$
$$\delta\Gamma^{\lambda}_{\mu\nu} = \frac{1}{2}g^{\lambda\sigma}(\delta g_{\sigma\mu;\nu} + \delta g_{\sigma\nu;\mu} - \delta g_{\mu\nu;\sigma})$$

Since the covariant derivative on the metric vanishes, $g^{\lambda\sigma}_{;\mu} = 0$, the metric commutes with the covariant derivative. $\delta R_{\mu\nu}$ can be further simplified.

$$\begin{aligned}\delta R_{\mu\nu} &= \frac{1}{2}g^{\lambda\sigma}(-h_{\sigma\mu;\nu;\lambda} - h_{\sigma\nu;\mu;\lambda} + h_{\sigma\lambda;\mu;\nu} + h_{\mu\nu;\sigma;\lambda}) \\ &= -\frac{1}{2}g^{\lambda\sigma}(h_{\sigma\mu;\nu;\lambda} + h_{\sigma\nu;\mu;\lambda}) + \frac{1}{2}h_{;\mu;\nu} + \frac{1}{2}g^{\lambda\sigma}h_{\mu\nu;\sigma;\lambda} \qquad (1)\end{aligned}$$

with $h_{\mu\nu} = \delta g_{\mu\nu}$ $h = g^{\lambda\sigma}h_{\lambda\sigma}$.

We choose to work in Poincare coordinate, the only nonvanishing Christoffels of which are:

$$\Gamma^{z}_{tt} = \Gamma^{z}_{zz} = -\frac{1}{z},\ \Gamma^{z}_{x^i x^i} = \frac{1}{z},\ \Gamma^{t}_{tz} = \Gamma^{x^i}_{x^i z} = -\frac{1}{z} \qquad (2)$$

We calculate the components δR_{zz},δR_{zm},δR_{mn} separately. Through tedious algebra, we arrive at:

$$\delta R_{zz} = \frac{1}{2}h_{,z,z} - \frac{1}{2z}h_{,z} \qquad (3)$$
$$\delta R_{zm} = \frac{1}{2}\left(h_{,m} - h_{m}\right)_{,z} \qquad (4)$$
$$\delta R_{mn} = \frac{1}{2}\Box h_{mn} + 2h_{mn} + \frac{z}{2}h_{mn,z} - \frac{1}{2}\left(h_{m,n} + h_{n,m}\right) + \frac{1}{2}(h_{,m,n} - \Gamma^{z}_{mn}h_{,z}) \qquad (5)$$

with $h_m = g^{\lambda\sigma} h_{\lambda m,\sigma}$

B Inverse Fourier Transform of Green's function

Let us recall the expression of Green's function in momentum space:

$$G(z,z') = \{ \begin{array}{ll} -\frac{2}{z'} I_2(i\lambda z_<) K_2(i\lambda z >) & \omega > 0, |\omega| > k ① \\ -\frac{2}{z'} I_2(-i\lambda z_<) K_2(-i\lambda z >) & \omega < 0, |\omega| > k ② \\ -\frac{2}{z'} I_2(\tilde{\lambda} z_<) K_2(\tilde{\lambda} z >) & |\omega| < k ③ \end{array} \tag{6}$$

We will use ①,②,③ to refer to the three cases as indicated above. In order to do the inverse Fourier transform: $\frac{1}{(2\pi)^4} \int G(z,z') e^{i\omega t - i\vec{k}\vec{x}} d\omega d^3k$, we make the change of variable for each case:

$$\begin{aligned} &① : \omega = \sqrt{k^2+\lambda^2} \frac{1}{(2\pi)^4} \int G(z,z') e^{i\omega t - i\vec{k}\vec{x}} d\omega d^3k \\ &= \frac{1}{(2\pi)^3} \int G(z,z') e^{i\sqrt{k^2+\lambda^2}t} \frac{2sin(kr)}{kr} k^2 dk \frac{\lambda d\lambda}{\sqrt{k^2+\lambda^2}} \\ &② : \omega = -\sqrt{k^2+\lambda^2} \frac{1}{(2\pi)^4} \int G(z,z') e^{i\omega t - i\vec{k}\vec{x}} d\omega d^3k \\ &= \frac{1}{(2\pi)^3} \int G(z,z') e^{-i\sqrt{k^2+\lambda^2}t} \frac{2sin(kr)}{kr} k^2 dk \frac{\lambda d\lambda}{\sqrt{k^2+\lambda^2}} \\ &③ : \omega = \pm\sqrt{k^2-\tilde{\lambda}^2} \frac{1}{(2\pi)^4} \int G(z,z') e^{i\omega t - i\vec{k}\vec{x}} d\omega d^3k \\ &= \frac{1}{(2\pi)^3} \int G(z,z') 2cos\sqrt{k^2-\tilde{\lambda}^2}t \frac{2sin(kr)}{kr} k^2 dk \\ &\times \frac{\lambda d\lambda}{\sqrt{k^2-\tilde{\lambda}^2}} \end{aligned} \tag{7}$$

We use the following formulas to evaluate the k-integrals:

$$2\int_0^\infty \frac{cos(b\sqrt{x^2+a^2})}{\sqrt{x^2+a^2}} sin(\xi x)xdx = \pi Y_0'(a\sqrt{b^2-\xi^2}) \times$$
$$\frac{-a\xi}{\sqrt{b^2-\xi^2}}\theta(b-\xi) - 2K_0'(a\sqrt{\xi^2-b^2})\frac{a\xi}{\sqrt{\xi^2-b^2}}\theta(\xi-b)$$
$$2\int_0^\infty \frac{cos(b\sqrt{x^2-a^2})}{\sqrt{x^2-a^2}} sin(\xi x)xdx = -2K_0'(a\sqrt{b^2-\xi^2}) \times$$
$$\frac{-a\xi}{\sqrt{b^2-\xi^2}}\theta(b-\xi) + \pi Y_0'(a\sqrt{\xi^2-b^2})\frac{a\xi}{\sqrt{\xi^2-b^2}}\theta(\xi-b)$$
$$2\int_0^\infty \frac{sin(b\sqrt{x^2+a^2})}{\sqrt{x^2+a^2}} sin(\xi x)xdx = -\pi J_0'(a\sqrt{b^2-\xi^2})$$
$$\times\frac{-a\xi}{\sqrt{b^2-\xi^2}}\theta(b-\xi) + \pi\delta(b-\xi) \tag{8}$$

with $a, b, \xi > 0$

These formulas are obtained by differentiating with respect ξ the cosine-transform of $\frac{cos(b\sqrt{x^2+a^2})}{\sqrt{x^2+a^2}}$, $\frac{cos(b\sqrt{x^2-a^2})}{\sqrt{x^2-a^2}}$ and $\frac{sin(b\sqrt{x^2+a^2})}{\sqrt{x^2+a^2}}$

Let's focus on the case $t > 0$ at the moment. With the help of 8, 7 becomes:

$$①: \int -\frac{2}{z'} I_2(i\lambda z_<)K_2(i\lambda z_>)\frac{\lambda d\lambda}{(2\pi)^3}\left[\pi Y_0'(\lambda\sqrt{t^2-r^2})\right.$$
$$\times\frac{-\lambda}{\sqrt{t^2-r^2}}\theta(t-r) - 2K_0'(\lambda\sqrt{r^2-t^2})\frac{\lambda}{\sqrt{r^2-t^2}}\theta(r-t)$$
$$\left.-i\pi J_0'(\lambda\sqrt{t^2-r^2})\frac{-\lambda}{\sqrt{t^2-r^2}}\theta(t-r) + i\pi\frac{\delta(t-r)}{r}\right]$$
$$②: \int -2\frac{2}{z'} I_2(-i\lambda z_<)K_2(-i\lambda z_>)\frac{\lambda d\lambda}{(2\pi)^3}\left[\pi Y_0'(\lambda\sqrt{t^2-r^2})\right.$$
$$\times\frac{-\lambda}{\sqrt{t^2-r^2}}\theta(t-r) - 2K_0'(\lambda\sqrt{r^2-t^2})\frac{\lambda}{\sqrt{r^2-t^2}}\theta(r-t)$$
$$\left.+i\pi J_0'(\lambda\sqrt{t^2-r^2})\frac{-\lambda}{\sqrt{t^2-r^2}}\theta(t-r) - i\pi\frac{\delta(t-r)}{r}\right]$$
$$③: 2\int -\frac{2}{z'} I_2(\lambda z_<)K_2(\lambda z_>)\frac{\lambda d\lambda}{(2\pi)^3}\left[-2K_0'(\lambda\sqrt{t^2-r^2})\right.$$
$$\left.\times\frac{-\lambda}{\sqrt{t^2-r^2}}\theta(t-r) + \pi Y_0'(\lambda\sqrt{r^2-t^2}\frac{\lambda}{\sqrt{r^2-t^2}}\theta(r-t))\right] \tag{9}$$

Suppose we replace $z_>$ by $z_> - i\epsilon$, convergence of the integral enables us to rotate the contour of ③ and ①:

$$\int -\frac{2}{z'} I_2(\lambda z_<) K_2(\lambda z_>) \frac{\lambda d\lambda}{(2\pi)^3} \left[-2K_0'(\lambda\sqrt{t^2-r^2}) \right.$$
$$\left. \times \frac{-\lambda}{\sqrt{t^2-r^2}} \theta(t-r) \right] = \int -\frac{2}{z'} I_2(i\lambda z_<) K_2(i\lambda z_>) \frac{\lambda d\lambda}{(2\pi)^3} \times$$
$$\left[(-\pi Y_0'(\lambda\sqrt{t^2-r^2}) - i\pi J_0'(\lambda\sqrt{t^2-r^2})) \frac{-\lambda}{\sqrt{t^2-r^2}} \theta(t-r) \right]$$
$$\int -\frac{2}{z'} I_2(i\lambda z_<) K_2(i\lambda z_>) \frac{\lambda d\lambda}{(2\pi)^3} \left[-2K_0'(\lambda\sqrt{r^2-t^2}) \right.$$
$$\left. \times \frac{\lambda}{\sqrt{r^2-t^2}} \theta(r-t) \right] = \int -\frac{2}{z'} I_2(\lambda z_<) K_2(\lambda z_>) \frac{\lambda d\lambda}{(2\pi)^3} \times$$
$$\left[(-\pi Y_0'(\lambda\sqrt{r^2-t^2}) + i\pi J_0'(\lambda\sqrt{r^2-t^2})) \frac{\lambda}{\sqrt{r^2-t^2}} \theta(r-t) \right] \tag{10}$$

Similarly, suppose $z_> \to z_> + i\epsilon$, we can rotate the contour of ③ and ②:

$$\int -\frac{2}{z'} I_2(\lambda z_<) K_2(\lambda z_>) \frac{\lambda d\lambda}{(2\pi)^3} \left[-2K_0'(\lambda\sqrt{t^2-r^2}) \times \right.$$
$$\left. \frac{-\lambda}{\sqrt{t^2-r^2}} \theta(t-r) \right] = \int -\frac{2}{z'} I_2(-i\lambda z_<) K_2(-i\lambda z_>) \frac{\lambda d\lambda}{(2\pi)^3} \times$$
$$\left[(-\pi Y_0'(\lambda\sqrt{t^2-r^2}) + i\pi J_0'(\lambda\sqrt{t^2-r^2})) \frac{-\lambda}{\sqrt{t^2-r^2}} \theta(t-r) \right]$$
$$\int -\frac{2}{z'} I_2(-i\lambda z_<) K_2(-i\lambda z_>) \frac{\lambda d\lambda}{(2\pi)^3} \left[-2K_0'(\lambda\sqrt{r^2-t^2}) \times \right.$$
$$\left. \frac{\lambda}{\sqrt{r^2-t^2}} \theta(r-t) \right] = \int -\frac{2}{z'} I_2(\lambda z_<) K_2(\lambda z_>) \frac{\lambda d\lambda}{(2\pi)^3} \times$$
$$\left[(-\pi Y_0'(\lambda\sqrt{r^2-t^2}) - i\pi J_0'(\lambda\sqrt{r^2-t^2})) \frac{\lambda}{\sqrt{r^2-t^2}} \theta(r-t) \right] \tag{11}$$

Summing up piece ①,② and ③, we find various terms cancel against each other. We are left with:

$$
\begin{aligned}
&z_> \to z_> - i\epsilon : \\
&\int -\frac{2}{z'} I_2(i\lambda z_<) K_2(i\lambda z_>) \frac{\lambda d\lambda}{(2\pi)^3} \left[-2\pi i J_0'(\lambda\sqrt{t^2-r^2}) \right. \\
&\left. \times \frac{-\lambda}{\sqrt{t^2-r^2}} \theta(t-r) + \pi i \frac{\delta(t-r)}{r} \right] + \int -\frac{2}{z'} I_2(\lambda z_<) K_2(\lambda z_>) \\
&\times \frac{\lambda d\lambda}{(2\pi)^3} \left[\pi i J_0'(\lambda\sqrt{r^2-t^2}) \frac{\lambda}{\sqrt{r^2-t^2}} \theta(r-t) \right] \\
&z_> \to z_> + i\epsilon : \\
&\int -\frac{2}{z'} I_2(-i\lambda z_<) K_2(-i\lambda z_>) \frac{\lambda d\lambda}{(2\pi)^3} \left[2\pi i J_0'(\lambda\sqrt{t^2-r^2}) \right. \\
&\left. \times \frac{-\lambda}{\sqrt{t^2-r^2}} \theta(t-r) - \pi i \frac{\delta(t-r)}{r} \right] + \int -\frac{2}{z'} I_2(\lambda z_<) K_2(\lambda z_>) \\
&\times \frac{\lambda d\lambda}{(2\pi)^3} \left[-\pi i J_0'(\lambda\sqrt{r^2-t^2}) \frac{\lambda}{\sqrt{r^2-t^2}} \theta(r-t) \right]
\end{aligned}
\tag{12}
$$

If we are only interested in the coefficient of the $z_<^2$ term[1], we may make the following substitution: $I_2(\pm i\lambda z_<) \to -\frac{1}{8}\lambda^2$,$I_2(\lambda z_<) \to \frac{1}{8}\lambda^2$,$z_> \to z'$

Further evaluation of the integral involves the two formulas:

$$
\begin{aligned}
&\int_0^\infty x^{\mu+\nu+1} J_\mu(ax) K_\nu(bx) dx = 2^{\mu+\nu} a^\mu b^\nu \frac{\Gamma(\mu+\nu+1)}{(a^2+b^2)^{\mu+\nu+1}} \\
&\int_0^\infty x^\mu K_\nu(ax) dx = 2^{\mu-1} a^{-\mu-1} \Gamma(\frac{1+\mu+\nu}{2}) \Gamma(\frac{1+\mu-\nu}{2})
\end{aligned}
\tag{13}
$$

It is easy to find $\int \lambda^3 d\lambda K_2(\pm i\lambda z_>)$ and $\int \lambda^4 d\lambda K_2(\lambda z_>) J_1(\lambda\sqrt{r^2-t^2})\theta(r-t)$ contain no singularity in $z_>$, thus the contribution from $z_> \pm i\epsilon$ cancel each other. We end up with:

[1]By analyzing the small z expansion of $h_{mn}(z) = \int G(z,z') s_{mn}(z') dz' d^4x$, one can show the coefficient of z^2 term equals that of $z_<^2$ term, provided that $s_{mn}(z')$ contains no z'^0 and z'^2 terms. The latter condition is satisfied by the sources considered in this paper

$$\int -\frac{2}{z'}\frac{-\lambda^2}{8}K_2(i\lambda z_>)\frac{\lambda d\lambda}{(2\pi)^3}(-2\pi i)J_1(\lambda\sqrt{t^2-r^2})$$
$$\times\frac{\lambda}{\sqrt{t^2-r^2}}\theta(t-r)\Big|_{z_>\to z_>-i\epsilon}+\int -\frac{2}{z'}\frac{-\lambda^2}{8}K_2(-i\lambda z_>)$$
$$\times\frac{\lambda d\lambda}{(2\pi)^3}2\pi i J_1(\lambda\sqrt{t^2-r^2})\frac{\lambda}{\sqrt{t^2-r^2}}\theta(t-r)\Big|_{z_>\to z_>+i\epsilon}$$
$$=\frac{12iz'}{(2\pi)^2}\left[\frac{1}{(t^2-r^2-z'^2+i\epsilon)^4}-\frac{1}{(t^2-r^2-z'^2-i\epsilon)^4}\right]$$
$$\times\theta(t-r) \tag{14}$$

For $t<0$, similar procedure leads to a vanishing result. Therefore the $z_<^2$ term of the Green's function in coordinate space, which is exactly the propagator we are looking for, can be expressed as [2]:

$$P_R=\frac{12iz'}{(2\pi)^2}\left[\frac{1}{(t^2-r^2-z'^2+i\epsilon)^4}-\right.$$
$$\left.\frac{1}{(t^2-r^2-z'^2-i\epsilon)^4}\right]\theta(t-r) \tag{15}$$

C Extract Energy Density in Comoving Frame

The aim is to kill the $(0,i)$ components(momentum density) by local Lorentz transformation: $T'=STS^T$, where

$$T'=T'_{\alpha\beta}\ ,T=T_{\mu\nu}\ ,S_{\alpha\mu}=\frac{\partial x^\mu}{\partial x^\alpha} \tag{16}$$

Local Lorentz transformation matrix is a product of matrices, which are either rotations,e.g.① or boosts,e.g.②. This is a consequence of the fact:

[2]the $t>0$ condition is included in the theta function

$SgS^T = g$, where $g = diag(-1, 1, 1, 1)$ is the Minkowski metric.

$$
\begin{aligned}
&① \begin{pmatrix} 1 & & & \\ & \cos(\theta) & \sin(\theta) & \\ & -\sin(\theta) & \cos(\theta) & \\ & & & 1 \end{pmatrix} \\
&② \begin{pmatrix} chy & shy & & \\ shy & chy & & \\ & & 1 & \\ & & & 1 \end{pmatrix}
\end{aligned}
\tag{17}
$$

A nice property of g is: $g = g^T = g^{-1}$, therefore gT' and Tg are related by similarity transformation:

$$gT' = gSTgg^TS^T = gS(Tg)(gS)^{-1} \tag{18}$$

Since gT' does not alter the zero entries of T', now the problem becomes to kill the $(0, i)$ components of Tg by similarity transformation. The original matrix Tg can be viewed as an operator L acting on a set of basis, while the similarity transformation is just a change of basis:

$$
\begin{aligned}
(Tg)_{mn} &= (e_n, Le_m) \\
(gT')_{mn} &= (e'_n, Le'_m) \\
e'_n &= (gS)_{nm} e_m
\end{aligned}
\tag{19}
$$

We want to find a basis e'_0 such that $Le'_0 = \lambda e'_0$ with $\lambda = (gT')_{00}$. Denote $e'_0 = x_m e_m$, it is easy to show $x_m(Tg)_{mn} = \lambda x_n$ This is exactly an eigenvalue problem for matrix $(Tg)^T$. The restriction in transformation matrix is translated to: $x_0^2 - x_1^2 - x_2^2 - x_3^2 > 0$. It turns out this condition is just enough to determine a unique eigenvalue out of four possible eigenvalues. The energy density is given by $\epsilon = -\lambda$.

D WKB treatment of (5.36)

In order to apply WKB method to (5.36), we need to convert it Schrodinger-type equation. Introducing a new field $\psi = \sqrt{\frac{1-u^2}{u}} Z_3$, (5.36) becomes:

$$\psi'' + \frac{\omega^2(1-s^2(1-u^2))}{u(1-u^2)^2}\psi + \frac{-3+6u^2+u^4}{4u^2(1-u^2)^2}\psi = 0 \tag{20}$$

with $s = |\frac{q}{\omega}| \approx 1$. ω is a large parameter to justify WKB. There are two singularities in (20): $u = 0$,$u = 1$. The term proportional to ω^2 may vanish at $u_0 = \frac{\sqrt{s^2-1}}{s}$ if $s > 1$. We discuss two cases separately: I $s < 1$, II $s > 1$ and focus on $\omega > 0$ only. The solution for $\omega < 0$ can be obtained easily from the solution for $\omega > 0$ by the substitution $c_+ \leftrightarrow c_-$.

Case I $s < 1$: Away from the singularities, the WKB solution to (20) is given as:

$$\psi_\pm = S'^{-1/2} e^{\pm i\omega \int_0^u S' du} \tag{21}$$

with $S' = \sqrt{\frac{1-s^2(1-u^2)}{u(1-u^2)^2}}$

Near the singularities, (20) becomes:

$$\begin{aligned}
&u \to 0 \\
&\psi'' + \frac{\omega^2(1-s^2)}{u}\psi - \frac{3}{4u^2}\psi = 0 \Rightarrow \psi = \sqrt{u} H_2^{(1),(2)}(2\omega\sqrt{1-s^2}\sqrt{u}) \\
&u \to 1 \\
&\psi'' + \frac{1+\omega^2}{4(1-u)^2}\psi = 0 \Rightarrow \psi = (1-u)^{\frac{1\pm i\omega}{2}}
\end{aligned} \tag{22}$$

On the other hand, we have:

$$\begin{aligned}
u \to 0 \quad S' \to \sqrt{\frac{1-s^2}{u}} \int_0^u S' du = 2\sqrt{u}\sqrt{1-s^2} \\
u \to 1 \quad S' \to \frac{1}{2(1-u)} \int_0^u S' du = a_0 - \frac{1}{2} ln(1-u)
\end{aligned} \tag{23}$$

Matching the WKB solution with the approximate solutions near the singularities (using asymptotic expansion of Hankel function), we obtain:

$$
\begin{aligned}
&\psi = c_+(1-u)^{\frac{1+i\omega}{2}} + c_-(1-u)^{\frac{1-i\omega}{2}} \\
&\sim c_+ e^{i\omega a_0}\psi_- + c_- e^{-i\omega a_0}\psi_+ \\
&\sim c_+ e^{i(\omega a_0 - \frac{5\pi}{4})}\sqrt{u}H_2^{(2)}(2\omega\sqrt{1-s^2}\sqrt{u}) + c_- e^{-i(\omega a_0 - \frac{5\pi}{4})}\sqrt{u}H_2^{(1)}(2\omega\sqrt{1-s^2}\sqrt{u}) \\
&\sim \sqrt{u}\left(H_2^{(2)}(2\omega\sqrt{1-s^2}\sqrt{u}) + \frac{ic_-}{c_+}e^{-2i\omega a_0}H_2^{(1)}(2\omega\sqrt{1-s^2}\sqrt{u}\right)
\end{aligned} \tag{24}
$$

Case.II $s > 1$: This case is a little more complicated because WKB approximation breaks down near $u = u_0$. Away from $u = 0, 1, u_0$, we have the following WKB solutions:

$$
\begin{aligned}
u > u_0 \quad \psi_\pm^> &= S'^{-1/2} e^{\pm i\omega \int_{u_0}^{u} S' du} \\
u < u_0 \quad \psi_\pm^< &= S'^{-1/2} e^{\pm\omega \int_{u}^{u_0} \bar{S}' du}
\end{aligned} \tag{25}
$$

where $S' = \sqrt{\frac{1-s^2(1-u^2)}{u(1-u^2)^2}}, \bar{S}' = \sqrt{\frac{s^2(1-u^2)-1}{u(1-u^2)^2}}$.
We first match WKB solutions at $u = u_0$. Near $u = u_0$, (20) becomes:

$$
\psi'' + \omega^2 a(u-u_0)\psi + b\psi = 0 \tag{26}
$$

where $a = \frac{2s^2 u_0}{u_0(1-u_0^2)^2}, b = \frac{-3+6u_0^2+u_0^4}{4u_0^2(1-u_0^2)^2}$
(26) can be solved by Airy functions:

$$
\begin{aligned}
\psi &= Ai(-\frac{\omega^2 a(u-u_0)+b}{(\omega^2 a)^{2/3}}) \\
\psi &= Bi(-\frac{\omega^2 a(u-u_0)+b}{(\omega^2 a)^{2/3}})
\end{aligned} \tag{27}
$$

Using the asymptotic expansion of Airy functions:($x > 0$)

$$
\begin{aligned}
Ai(x) &\sim \frac{e^{-\frac{2}{3}x^{3/2}}}{2\sqrt{\pi}x^{1/4}} \\
Bi(x) &\sim \frac{e^{\frac{2}{3}x^{3/2}}}{\sqrt{\pi}x^{1/4}} \\
Ai(-x) &\sim \frac{sin(\frac{2}{3}x^{3/2}+\frac{1}{4}\pi)}{\sqrt{\pi}x^{1/4}} \\
Bi(x) &\sim \frac{cos(\frac{2}{3}x^{3/2}+\frac{1}{4}\pi)}{\sqrt{\pi}x^{1/4}}
\end{aligned} \tag{28}
$$

We obtain the following match between WKB solutions:

$$
\frac{C}{2}(\psi_+^> + \psi_-^>) + \frac{D}{2i}(\psi_+^> - \psi_-^>) \sim \frac{C-D}{2}\psi_+^< + \frac{C+D}{4}\psi_-^< \tag{29}
$$

Next we match WKB solutions with approximate solutions near singularities similarly as case I. Finally we have:

$$
\begin{aligned}
&\psi = c_+(1-u)^{\frac{1+i\omega}{2}} + c_-(1-u)^{\frac{1-i\omega}{2}} \\
&\sim \left(c_+e^{i\omega b_0} - ic_-e^{-i\omega b_0}\right)\frac{e^{\omega c_0}}{\pi}\sqrt{u}K_2(2\omega\sqrt{s^2-1}\sqrt{u}) \\
&+\frac{1}{2}\left(-ic_+e^{i\omega b_0} + c_-e^{-i\omega b_0}\right)e^{-\omega c_0}\sqrt{u}I_2(2\omega\sqrt{s^2-1}\sqrt{u}) \\
&\sim \sqrt{u}\left(1 - \frac{ic_-}{c_+}e^{-2i\omega b_0}\right)\frac{e^{\omega c_0}}{\pi}K_2(2\omega\sqrt{s^2-1}\sqrt{u}) \\
&-\frac{i\sqrt{u}}{2}\left(1 + \frac{ic_-}{c_+}e^{-2i\omega b_0}\right)e^{-\omega c_0}I_2(2\omega\sqrt{s^2-1}\sqrt{u})
\end{aligned} \tag{30}
$$

with $lim_{u\to 1}\int_{u_0}^{u} S'du = b_0 - \frac{1}{2}ln(1-u)$,$\int_0^{u_0}\bar{S}'du = c_0$
Summarizing all cases, we have:

$$\psi = \begin{cases} \sqrt{u}\left(H_2^{(2)}(2\lambda\sqrt{u}) + \frac{ic_-}{c_+}e^{-2i\omega a_0}H_2^{(1)}(2\lambda\sqrt{u})\right) & \omega > |q| \\ \sqrt{u}\left(H_2^{(1)}(2\lambda\sqrt{u}) - \frac{ic_-}{c_+}e^{-2i\omega a_0}H_2^{(2)}(2\lambda\sqrt{u})\right) & \omega < -|q| \\ \sqrt{u}\left(1 - \frac{ic_-}{c_+}e^{-2i\omega b_0}\right)\frac{e^{\omega c_0}}{\pi}K_2(2\tilde{\lambda}\sqrt{u}) & \\ -\frac{i\sqrt{u}}{2}\left(1 + \frac{ic_-}{c_+}e^{-2i\omega b_0}\right)e^{-\omega c_0}I_2(2\tilde{\lambda}\sqrt{u}) & 0 < \omega < |q| \\ \sqrt{u}\left(1 + \frac{ic_-}{c_+}e^{-2i\omega b_0}\right)\frac{e^{\omega c_0}}{\pi}K_2(2\tilde{\lambda}\sqrt{u}) & \\ +\frac{i\sqrt{u}}{2}\left(1 - \frac{ic_-}{c_+}e^{-2i\omega b_0}\right)e^{-\omega c_0}I_2(2\tilde{\lambda}\sqrt{u}) & 0 > \omega > -|q| \end{cases} \tag{31}$$

with $\lambda = \sqrt{\omega^2 - q^2}$, $\tilde{\lambda} = \sqrt{q^2 - \omega^2}$

E Gauge Choice for the Sound Channel

The aim of the section is to show it is possible render the following matching condition by a proper choice of gauge:

$$\begin{aligned} \phi_2^f &= \phi_2 \\ \phi_2^{f\prime} &= \frac{1}{\sqrt{f}}\phi_2{}' + \frac{\kappa_5^2 p}{3u}\frac{\phi_2{}'}{\sqrt{f}} \end{aligned} \tag{32}$$

With the help of (5.23), (32) can be simplified to:

$$\begin{aligned} &\tilde{h}_{aa} - \frac{2-f}{\sqrt{f}}h_{aa}^f = 0 \\ &\tilde{h}_{aa}{}' + \frac{\kappa_5^2 p}{3u}\tilde{h}_{aa} - (2-f)\tilde{h}_{aa}^f{}' + f' h_{aa}^f = 0 \end{aligned} \tag{33}$$

where all the quantities are evaluated at $u = u_m$.

We note the residue gauge degree of freedom implies that it is sufficient to satisfy (5.23) up to a gauge choice. In particular, we could add pure gauge solution to the sound channel: h^{gauge} inside the shell and $h^{gauge,f}$ outside. According to [73], the only pure gauge solution that touch h_{aa}^f(h_{aa} with $f = 1$) is:

$$
\begin{aligned}
h_{tt}^{gauge,f} &= \frac{\sqrt{f}(1+u^2+2\omega^2 u)}{u} \\
h_{tw}^{gauge,f} &= \frac{-q\omega \arcsin u - q\omega u\sqrt{f}}{u} \\
h_{aa}^{gauge,f} &= -\frac{2\sqrt{f}}{u} \\
h_{ww}^{gauge,f} &= \frac{2q^2 \arcsin u - \sqrt{f}}{u}
\end{aligned} \tag{34}
$$

Now, it is enough to satisfy:

$$
\begin{aligned}
&\bar{h}_{aa} - \frac{2-f}{\sqrt{f}}\bar{h}^f_{aa} = 0 \\
&\bar{h}'_{aa} + \frac{\kappa_5^2 p}{3u}\bar{h}_{aa} - (2-f)\bar{h}^f_{aa}{}' + f'\bar{h}^f_{aa} = 0
\end{aligned} \tag{35}
$$

where $\bar{h}_{aa} = \tilde{h}_{aa} + \frac{A}{u}$ and $\bar{h}^f_{aa} = \tilde{h}^f_{aa} + \frac{B\sqrt{f}}{u}$. It is easy to see it is always possible to satisfy (35) with a proper choice of constants A and B.